THE JOURNAL OF
PHYSICAL CHEMISTRY

Volume 74, Number 18 September 3, 1970

AUTHOR INDEX

THE JOURNAL OF
PHYSICAL CHEMISTRY

VOLUME 74, NUMBER 18 SEPTEMBER 3, 1970

The Absolute Rate of Association of Borane Molecules[1]

by G. W. Mappes,[2] S. A. Fridmann, and T. P. Fehlner

Department of Chemistry and Radiation Laboratory,[3] University of Notre Dame, Notre Dame, Indiana 46556
(Received April 9, 1970)

The absolute rate of the reaction of two borane molecules, BH_3, to form diborane, B_2H_6, has been directly measured. Both the loss of BH_3 and the formation of B_2H_6 have been followed. At 545°K and 5 Torr total pressure of helium, the rate constant for this reaction is 2×10^9 l./(mol sec). The activation energy for this reaction is 0 ± 2 kcal/mol. The collisional efficiency at higher total pressures is estimated to be equal to or higher than that for radical–radical reactions. The implications of these measurements are discussed in terms of the absolute rate theory.

The association reactions of unstable molecular fragments have attracted the interest and attention of numerous research groups.[4] The primary aim of these studies is to correlate electronic structure and reactivity, and the association of the borane species, BH_3, is of significant interest for this reason. However, the characterization of active intermediates is also a major source of illumination of the mechanisms of complex reactions. In this regard, the association of borane is of particular interest because considerable indirect evidence exists for the participation of BH_3 as an active intermediate in many reactions involving boron hydrides.[5] Generally the self-association reaction is an intimate part of the mechanisms postulated. The existence of BH_3 as an intermediate has been established by the work of a number of groups.[6-16] To date no successful structural studies of BH_3 have been published, and our only information concerning this aspect of BH_3 comes from calculations.[17] There has been some speculation on the magnitude of the rate constant for the self-association of BH_3,[18,19] and there has been a suggestion that this process might involve a significant activation energy.[20] Indeed, one can argue reasonably either for low efficiency with or without activation energy or for high efficiency. Therefore, the objective of this work was to obtain some quantitative information on the rate of the self-association of borane.

To obtain information of this type it is necessary to have an intense source of BH_3 and a suitable system in which to carry out the rate measurements. We have

(1) Supported in major part by the National Science Foundation under Grant No. GP 10199.

(2) National Science Foundation predoctoral fellow.

(3) The Radiation Laboratory is operated by the University of Notre Dame under contract with the Atomic Energy Commission. This is AEC Document No. COO-38-706.

(4) See, for example, F. W. Dalby, *J. Chem. Phys.*, **41**, 2297 (1964).

(5) R. L. Hughes, I. C. Smith, and E. W. Lawless, "Production of the Boranes and Related Research," R. T. Holzmann, Ed., Academic Press, New York, N. Y., 1967.

(6) T. P. Fehlner and W. S. Koski, *J. Amer. Chem. Soc.*, **86**, 2733 (1964).

(7) E. J. Sinke, G. A. Pressley, Jr., A. B. Baylis, and F. E. Stafford, *J. Chem. Phys.*, **41**, 2207 (1964).

(8) T. P. Fehlner and W. S. Koski, *J. Amer. Chem. Soc.*, **87**, 409 (1965).

(9) A. B. Baylis, G. A. Pressley, Jr., and F. E. Stafford, *ibid.*, **88**, 2428 (1966).

(10) J. Grotewald, E. A. Lissi, and A. E. Villa, *J. Chem. Soc. A*, 1038 (1966).

(11) J. H. Wilson and H. A. McGee, Jr., *J. Chem. Phys.*, **46**, 1444 (1967).

(12) P. S. Ganguli and H. A. McGee, Jr., *ibid.*, **50**, 4658 (1969).

(13) T. P. Fehlner and G. W. Mappes, *J. Phys. Chem.*, **73**, 873 (1969).

(14) S. J. Steck, G. A. Pressley, Jr., and F. E. Stafford, *ibid.*, **73**, 1000 (1969).

(15) O. Herstad, G. A. Pressley, Jr., and F. E. Stafford, *ibid.*, **74**, 874 (1970).

recently reported in detail a kinetically clean source of free borane.[21] The development of this source proceeded logically from our previous work on the production of borane in low-pressure pyrolytic systems.[8,13] Specifically, we observed that the major loss of BH_3 in these systems, with the exception of dimerization, is the destruction of BH_3 on the surface of the reactor. We have also observed that borane carbonyl decomposes thermally to yield BH_3 and CO by both homogeneous and heterogeneous pathways of comparable rates. Our technique, then, is based on increasing the production of BH_3 by enhancing the conditions for homogeneous reaction compared to those of heterogeneous reaction. In addition, as the decomposition of BH_3 on the wall has an activation energy,[22] the products of the pyrolysis of BH_3CO are rapidly transferred to a lower temperature container thereby decreasing the wall destruction even further. In this fashion, yields of BH_3 as high as 65% have been observed and partial pressures of BH_3 up to 0.08 Torr at purities of 80% (based on total boron hydrides) have been produced. We report below the first measurements of the absolute rate of the self-association of borane to form diborane.[23] As will be seen, this reaction proceeds at high efficiency and requires no activation energy.

Experimental Section

The rationale of these experiments is illustrated with Figure 1. The tubular flow reactor,[21,24] shown schematically at the bottom of the figure, is constructed with 20 individually controlled heating coils in an 8-cm length of reactor. This heating arrangement allows temperature profiles, such as the two illustrated, to be set up in the reactor. These hot zones are used to produce BH_3 from the thermal decomposition of BH_3CO at various distances from the downstream end of the reactor. The borane carbonyl is introduced at low concentration in the inert carrier gas upstream of the heated zone, and analysis is carried out mass spectrometrically at the position designated "leak" in Figure 1. Temperature profiles for the decomposition of BH_3CO are chosen such that better than 90% of the BH_3CO has decomposed, and these profiles are set up such that their shape is independent of the distance from the analysis point. A typical measurement involves setting up two preparation zones such as those illustrated in Figure 1 and measuring the product concentration distributions $(P)_1$ and $(P)_2$. The difference between $(P)_1$ and $(P)_2$ may be attributed to reaction taking place in the shaded region of length $l_{1,2}$ (hereafter called the recombination zone). There are two major advantages to this experimental procedure. First, measurements on reactions occurring in the recombination zone do not depend on knowledge of the reactions occurring in the preparation zone. Second, the recombination zone has a well-defined time associated with it. One disadvantage of this procedure is that the subtraction process increases

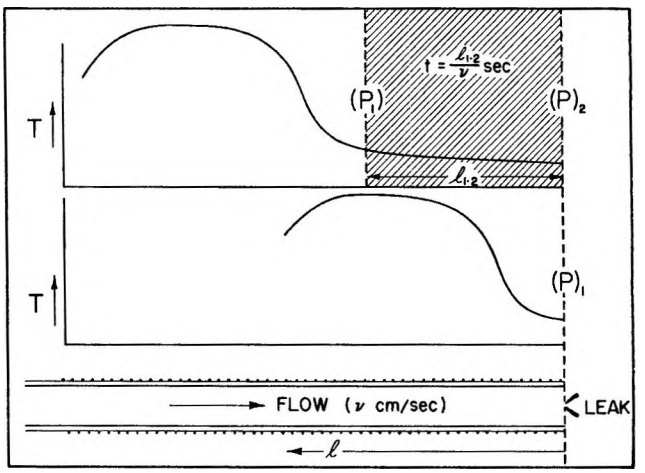

Figure 1. Schematic drawing of the reactor showing typical temperature profiles for this study. Temperature profiles were measured along the cylindrical axis of the reactor. (P) refers to a measured product distribution.

the scatter in the analytical data. Another disadvantage is that at higher carrier pressures the temperature profile distorts in the downstream direction and the temperature of the recombination zone increases. Therefore, the effect of a variation of the total pressure could not be carried out. The primary data obtained in these experiments are the product concentration distributions $(P)_1$ and $(P)_2$ as a function of borane concentration, recombination zone time, and recombination zone temperature. A more detailed description of the experimental measurements follows.

Analysis. The composition of the gas exiting the tubular reactor was determined by sampling with a minimum sampling time of 5×10^{-5} sec through a small thin-edged orifice situated 5 mm downstream of the last reactor coil into a mass spectrometer system utilizing modulated molecular beam sampling. The latter system operates by collimating the efflux of the sampling orifice into a molecular beam using a three-stage differentially pumped system and crossing this molecular beam with an electron beam. The resulting

(16) It appears that BH_3 has been successfully isolated in a low-temperature argon matrix. A. Kaldor and R. F. Porter, private communication.

(17) See, for example, W. E. Palke and W. N. Lipscomb, *J. Chem. Phys.*, **45**, 3948 (1966).

(18) S. H. Bauer, A. Shepp, and R. E. McCoy, *J. Amer. Chem. Soc.*, **75**, 1003 (1953).

(19) S. H. Bauer, *ibid.*, **78**, 5775 (1956).

(20) W. C. Kreye and R. A. Marcus, *J. Chem. Phys.*, **37**, 419 (1962).

(21) G. W. Mappes and T. P. Fehlner, *J. Amer. Chem. Soc.*, **92**, 1562 (1970).

(22) S. A. Fridmann and T. P. Fehlner, Abstracts, Third Great Lakes Regional Meeting of the American Chemical Society, DeKalb, Ill., June 1969, p 44; *Inorg. Chem.*, in press.

(23) Presented at the 158th National Meeting of the American Chemical Society, New York, N. Y., Sept 1969, Phys. 71.

(24) Similar to one described by I. P. Fisher, J. B. Homer, B. Roberts, and F. P. Lossing, *Can. J. Chem.*, **44**, 2205 (1966).

Table I: Partial Pressures of Product Distributions in mTorr at a Total Pressure of 5.0 Torr at the Lower Temperatures

Expt	$10^{-3}V$, cm/sec	$10^{4}\Delta t_r$, sec	T_r, °K	Sensitivity	$(BH_3CO)_0$	$(BH_3)_S$	$(BH_3)_L$	$(B_2H_6)_S$	$(B_2H_6)_L$	$\frac{\Delta(BH_3) - 2\Delta(B_2H_6)}{(BH_3)_S}$
3211	7.69	3.12	540	3.99	17	6.5	3.9			
					36	11.0	5.2	4.1	5.6	0.29
					62	13.1	9.5	7.5	9.2	0.02
					89	19.5	11.7	10.9	14.1	0.07
					120	21.6	14.6	15.3	17.9	0.07
3212	7.69	3.12	540	3.99	17	5.6	3.9	2.0	2.2	0.23
					36	9.1	5.2	2.9	5.6	−0.16
					62	15.7	9.5	4.8	9.2	−0.17
					89	20.8	11.7	8.9	14.1	−0.06
					120	25.6	14.6	10.8	17.9	−0.12
3301	8.63	2.78	560	2.45	18	7.6	4.0	1.1	2.3	0.16
					35	8.5	6.5	1.6	3.6	−0.23
					49	14.6	9.1	4.0	4.5	0.31
					75	20.3	9.5	5.4	9.2	0.16
					107	23.9	14.0	7.0	12.2	−0.02
					124	24.1	13.1	9.5	16.0	−0.08
					144	32.5	13.0	11.3	19.0	0.13
3061[a]	7.76	3.09	543	1.00	41[b]	12.4[b]	11.2[b]	2.9[b]	7.1[b]	−0.58[b]
					73	27.0	12.7	6.9	12.4	0.12
					109	31.5	16.4	7.8	20.4	−0.32
					177	46.3	20.8	14.4	27.0	0.01
					227	53.8	19.8	14.8	36.2	−0.16
3161[a]	8.41	2.85	540	1.59	42	12.8	8.7			
					73	23.5	10.9			
					112	32.3	12.3			
					131	42.1	18.5			
					187	46.6	19.6			
3081	4.37	7.32	503	0.65	49	20.6	2.7			
					112	30.8	2.7			
					183	34.4	11.8			
					221	44.9	10.8			
					323	31.1	7.0			

[a] Linear correction applied, see text. [b] This point not used in rate constant calculations.

ions are accelerated, mass analyzed, and detected utilizing an electron multiplier. The molecular beam is modulated at 160 Hz, and the signal from the electron multiplier is fed to a narrow-band amplifier which is locked into the frequency and phase of the modulation device. This type of system is very convenient in that it discriminates strongly against steady-state background, various extraneous ion source processes, and beam molecules that have suffered collisions. Details of this type of sampling system may be found elsewhere.[25] Calibration of the mass spectrometer system for the stable species under flow conditions and for various temperatures has been described previously.[21] Products were identified by their mass spectra[26] and the dependence of these spectra on the reactor parameters. The only species observed were BH_3CO, B_2H_6, BH_3, CO, and H_2 (the last is deduced indirectly from our previous experiments[13] and the formation of solid boron in this reactor). The formation of other products containing more than 5% of the BH_3CO decomposed are excluded by our measurements. The determination of the sensitivity for BH_3 has also been described in detail.[21] Briefly, upper and lower limits on the sensitivity were established from a mass balance and the yield of diborane in the recombination zone. An absolute value of the sensitivity was obtained by noting that (at constant total pressure) the loss of BH_3CO, at a chosen decomposition temperature and partial pressure, and the loss of BH_3 at the same temperature are predominantly first order in BH_3CO and BH_3, respectively (note that the latter holds only at the relatively high decomposition temperatures). For a number of pro-

(25) T. P. Fehlner, *J. Amer. Chem. Soc.*, **90**, 4817 (1968); S. N. Foner, "Advances in Atomic and Molecular Physics," Vol. 2, D. R. Bates and Immanuel Estermann, Ed., Academic Press, New York, N. Y., 1966, p 385.

(26) Our mass spectrum for BH_3CO (ref 21) corresponds closely to that presented in ref 14. We can complete the table in the latter by reporting that the relative intensity of CO^+ (m/e 28) is 10% of m/e 40 while BH_3^+ (m/e 14) is 0.4% of m/e 40 in the spectrum of BH_3CO containing boron in normal isotopic abundance.

files at the same temperature but differing times, a simple kinetic relation involving the respective decomposition constants and the borane carbonyl and borane concentrations may be derived provided that each molecule of borane carbonyl decomposed yields one molecule of borane. The only unknown is the relative sensitivities of BH_3 and BH_3CO. The stoichiometry of the BH_3CO decomposition was proved by examining the formation of B_2H_6 at a number of temperatures. The sensitivity of BH_3 relative to that for BH_3CO used in this work in terms of ion current per unit pressure is 0.7 ± 0.2 using the m/e 13 and 40 ions to measure BH_3 and BH_3CO, respectively. The variation in the sensitivity of BH_3 due to changes in the reactor temperature and flow velocity were assumed to be the same as those for butane.

BH_3CO was injected into the flow stream by using a calibrated variable leak attached to the BH_3CO container held at a constant temperature of 174°K. This procedure was reproducible within 4%. The maximum partial pressure of BH_3CO used in an experiment was 6.5% of the total pressure (*i.e.*, 93.5% He, 6.5% BH_3CO). This corresponds to a mass flow of 0.7 Torr l./sec at 5 Torr total pressure. To minimize consumption of BH_3CO (and thus minimize plug-up of the sampling orifice) and to maximize the signal to noise ratio, the spectrometer was focused individually on each ion of interest. The BH_3CO mass flow was then initiated, and measurements of approximately 1 min duration were made.

There were several major sources of noise in these analytical measurements. Fluctuations in the spectrometer sensitivities were estimated as less than 10% as were statistical fluctuations of the ion current. Small differences between the temperature profiles could have resulted in a 5–10% change in the BH_3 partial pressure produced in the decomposition zone. This was minimized by keeping the extent of decomposition of BH_3CO high in the decomposition zone. In addition, errors of this type appear in opposite directions in the BH_3 and B_2H_6 measurements. From the mass balances contained in Table I in the results we estimate the overall analytical error as 15%. Because of the considerable noise in the analysis, the change in BH_3 between the two profiles was made quite large, being on the average 50%. To establish the reaction order the partial pressure of BH_3 was varied by a factor of 8 and the overall recombination time by a factor of 2.5. In addition, where possible, both the loss of BH_3 and the formation of B_2H_6 were followed. Finally, each point in the tables is the average of several measurements.

Flow System and Time. The flow system was capable of giving flow velocities of up to 10^5 cm/sec. Variation in flow velocity was accomplished by adding carrier gas (helium) downstream of the reactor and thereby changing the effective pumping speed at the reactor. The carrier gas was metered to the flow system with a servo-driven leak controlled by a differential capacitance manometer. Additional stability was obtained by connecting two 300-l. tanks in the pumping line. These served both to dampen fluctuations in the pumping speed of the pump and also to allow the accurate measurement of the pumping speed of the mechanical pump. This was simply accomplished by measuring the tank volume and the time required to pump down a given pressure differential. These measurements were carried out for a range of pressures. The volumetric flow rate through the reactor was calculated from a measurement of the total mass flow rate, and the mass flow rate of carrier gas which was added downstream of the reactor. The linear flow velocity was then obtained from the cross-sectional area of the reactor. The value used in calculating the time was corrected for the higher temperature of the reactor by the factor $T/297$, where T is the mean recombination zone temperature. As the reactor coils were accurately wound and the spacing was known, the time was simply calculated from the difference in the number of coils away from the analysis point for the two profiles. The times involved in these studies were in the range of 0.1–0.7 msec. The pressure upstream and downstream of the reactor was measured utilizing a Wallace–Tiernan gauge. The calculated pressure drop across the reactor was 7%. The mean pressure is reported here.

Under typical conditions the Reynolds number of the gas in the reactor is about 20.[27] This is below the minimum value for turbulent flow in a smooth tube; however, the presence of the thermocouple probe with guide wires and rough boron on the tube walls probably causes the flow to be turbulent in nature. In any case, the fact that at higher temperatures BH_3 reaches the wall to decompose into boron and hydrogen indicates that there is radial mixing. Therefore the reactor is treated as a case of plug flow. We estimate the error in time as 20% mainly due to an uncertainty in the recombination zone temperature.

Temperature. The temperature of the gases in the reactor was measured with a thermocouple probe (0.005 in. chromel and constantan) that could be scanned on the center axis along the length of the reactor during normal operation. One use of this probe was to measure the temperature profiles discussed above. This allowed small adjustments to be made in the heating coils so that the profiles for a given decomposition zone (see Figure 1) could be made as identical as possible. The other use of this probe was to obtain a temperature for the recombination zone. There is some question whether this probe measures the actual gas temperature. It appears that in a similar reactor the gas temperature is close to that measured with a somewhat finer thermocouple.[24] Of more concern is the change in temperature

(27) S. Dushman and J. M. Lafferty, Ed., "Scientific Foundations of Vacuum Techniques," 2nd ed, Wiley, New York, N. Y., 1952, p 85.

Table II: Partial Pressures of Product Distributions in mTorr at a Total Pressure of 5.0 Torr at the Higher Temperatures

Expt	$10^{-3}V$, cm/sec	$10^{4}\Delta t_r$, sec	T_r, °K	Sensitivity	$(BH_3CO)_0$	$(BH_3)_S$	$(BH_3)_L$	$(B_2H_6)_S$	$(B_2H_6)_L$	$\frac{\Delta(BH_3) - 2\Delta(B_2H_6)}{(BH_3)_S}$
0071	12.2	2.95	610	5.1	28	13.1	6.5	1.6	5.5	−0.09
					57	30.1	16.5	3.1	8.6	0.09
					95	42.5	24.0	3.9	12.3	0.04
					134	58.0	32.0	7.3	18.3	0.07
0081	11.7	3.07	640	3.8	24	16.0	8.3	2.7	4.4	0.27
					46	29.8	12.4	4.4	7.8	0.36
					72	38.1	23.6	6.3	13.4	0.01
					129	76.2	29.3	10.8	21.3	0.34
0091[a]	14.0	2.57	630	5.0	8	4.0	3.2	0.7		
					19	14.2	3.9	1.8	2.7	0.60
					37	26.7	15.0	2.7	3.9	0.35
					70	37.8	23.6	8.0	7.6	0.39
0092[a]	14.1	2.55	636	3.1	8	7.0	4.9			
					19	18.5	14.5			
					37	34.8	20.3	4.4	10.3	0.08
					70	59.0	29.4			
3271	10.4	2.30	700	2.8	23	13	6.6			
					39	21	6.6			
					61	28	14			
					80	38	19			
					111	46	26			
0041	13.9	1.72	706	5.5	14	5.8	3.3			
					28	12.5	8.6			
					59	23.4	17.9			
					95	39.7	29.6			
2991	11.5	1.39	720	1.8	27	7.2	4.3			
					49	14.2	9.0			
					86	19.4	11.1			
					136	23.8	12.6			

[a] Linear correction applied, see text.

over the recombination zone. The temperature downstream of the decomposition zone has a considerable gradient, and the lowest mean recombination temperature available is 540°K for typical pressures and decomposition zone temperatures. Ideally one could minimize the temperature change in the recombination zones by moving the decomposition zone in small steps. However, because maximum analytical precision was required (see above), these steps had to be made quite long. As the reactions of interest have small temperature coefficients, the increased analytical precision was more important than good temperature resolution. For a typical recombination zone of 3 cm with a midpoint temperature of 540°K, the temperature at the upstream edge of the zone was 559°K and that at the analysis point was 514°K. This temperature difference disappeared when the recombination zone had the same temperature as the decomposition zone. To minimize systematic error due to small differences in the profiles, the order of setting up profiles at differing distances from the analysis point was varied.

Results

The primary data of these experiments are contained in Tables I and II. The temperatures listed are the mean recombination zone temperatures. Each time given corresponds to the difference in the times between decomposition and analysis for the two given profiles. Initial partial pressures of BH_3CO are tabulated for reference. The partial pressures of borane and diborane are given for two profiles, where profile L is further removed in time from the analysis point than is profile S. The raw ion intensities were treated in the following way. The contribution to m/e 13 from B_2H_6 and small amounts of BH_3CO was removed. This was typically 15% of the original m/e 13 ion intensity for profile S. No significant change in the fragmentation pattern of diborane or BH_3CO with temperature over the temperature range employed here has been observed,[6-14] and they were assumed constant in these calculations. The relative sensitivities of BH_3 and B_2H_6 with respect to butane and the absolute sensitivity of butane under flow conditions at the temperature of

the sampling orifice were used to convert the data into the partial pressures shown in the tables. For the data in Table I the difference in the sampling orifice temperature for the two profiles was typically 40°. To maximize the BH_3 pressure, the data for the first four runs in Table II were obtained with the decomposition profile *S* as close to the sampling orifice as possible. Thus the difference in sampling orifice temperature was more like 100° which involved a change in sensitivity of *ca.* 5%. In the three runs with the recombination zone temperature equal to the decomposition zone temperature, the temperature of the sampling orifice was the same for the two profiles. A relative sensitivity for each experiment is listed, and the analytical precision is proportional to these numbers. In the experiments indicated, a small correction was applied to account for the change in sensitivity due to sampling orifice plug-up over the course of an experiment. This correction was assumed to be linear in time and changed the concentrations by less than 6%. A number of runs were discarded as this correction was too large. The last column contains the deviation in the mass balances for each run, and for the lower temperature runs (Table I) it shows that in the recombination zone the stoichiometry is $2BH_3 = B_2H_6$. The average deviation at 545°K is 16%. The poor mass balances at the highest temperatures (Table II) are due to decomposition of BH_3 on the wall and some decomposition of the product of recombination, B_2H_6. In a separate experiment using pure diborane diluted with helium it was found that diborane is *ca.* 30% decomposed at 750°K with a decomposition time of 8.5×10^{-5} sec.

A number of rate laws were investigated assuming plug flow (see above). Figure 2 shows plots of first- and second-order rate constants as a function of initial BH_3 partial pressure for run 3301. Clearly the reaction is not simply first order and may not be simply second order. The last entry in Table I (run 3081) is data for a run using a recombination zone time better than double that of the other runs. The average second-order rate constant for this run is 1.3 times that for run 3301 while the average first-order rate constant for run 3081 is 2.6 times that of 3301. This also indicates that the reaction is mainly second order in BH_3. Data at long recombination times were not used in the final calculations because of the poor precision in measuring $(BH_3)_L$ for long times. Simple plots of $[(BH_3)_S - (BH_3)_L]/(BH_3)_{av}\Delta t$ *vs.* $(BH_3)_{av}$ yield curves of positive slope and nonzero intercept. Therefore the rate law indicated is

$$\text{rate} = -{}^1/_2 d(BH_3)/dt = [k_1 + k_2(BH_3)](BH_3)$$

where k_1 and k_2 are first- and second-order rate constants, respectively. This rate law may be integrated to yield

$$(BH_3)_S[1 + k_2(BH_3)_L/k_1]/(BH_3)_L[1 + k_2(BH_3)_S/k_1] = \exp(2k_1t)$$

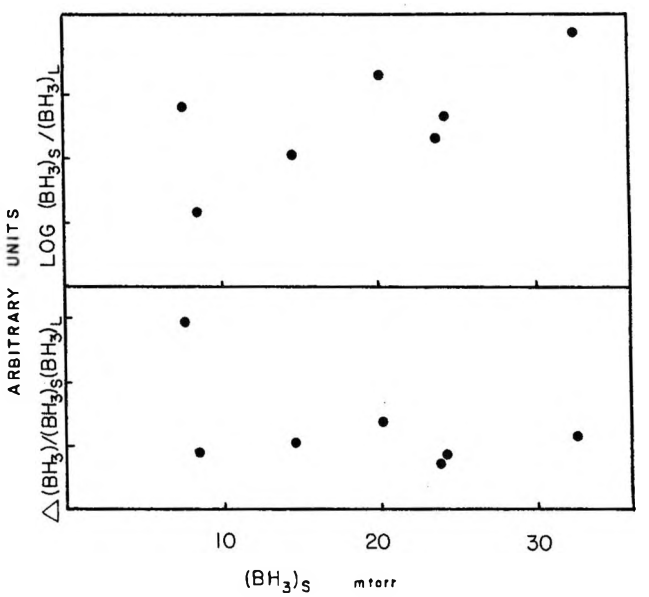

Figure 2. A plot of the rate constant times time for first-order kinetics (top) and second-order kinetics (bottom) *vs.* the borane partial pressure for the short profile.

where *t* is the reaction time in the recombination zone. The rate constants k_1 and k_2 were evaluated from the data contained in Tables I and II in the following manner. The integrated equation may be written

$$\log\{(BH_3)_S/(BH_3)_L\} = \log\{[1 + k_2(BH_3)_S/k_1]/[1 + k_2(BH_3)_L/k_1]\} + 2k_1t/2.303$$

The ratio k_2/k_1 was then varied until the unweighted least-squares slope of a plot of $\log (BH_3)_S/(BH_3)_L$ *vs.* $\log [1 + k_2 (BH_3)_S/k_1]/[1 + k_2(BH_3)_L/k_1]$ was equal to 1.00. The intercept of this plot is equal to $2k_1t/2.303$. An example of this plot for the loss of BH_3 at 545°K is shown in Figure 3. The length of the vertical bar is twice the root-mean-square error of the first-order least-squares fit. By utilizing the known stoichiometry, the data on the formation of B_2H_6 yield an independent determination of k_1 and k_2. As above, the ratio k_2/k_1 was varied until the unweighted least-squares slope of a plot of $\log [1 + 2\Delta \cdot (B_2H_6)]/(BH_3)_L$ *vs.* $\log [1 + k_2(BH_3)_S/k_1]/[1 + k_2 \cdot (BH_3)_L/k_1]$ was equal to 1.00. Once again the intercept of this plot is equal to $2k_1t/2.303$. An example of this plot for the formation of B_2H_6 at 545°K is shown in Figure 4. The calculated rate constants are summarized in Table III. The data on the loss of BH_3 gave good straight line plots at 545 and 629°K as illustrated in Figure 3. The data on BH_3 loss at 709°K had roughly twice the scatter of the data on formation of B_2H_6 at 545°K (see Figure 4) which in turn has about twice the scatter of the BH_3 data at the lower temperatures. It should be noted that the most badly scattered points in Figure 3 are high while in Figure 4 they are low. The data on the formation of B_2H_6 at 629°K

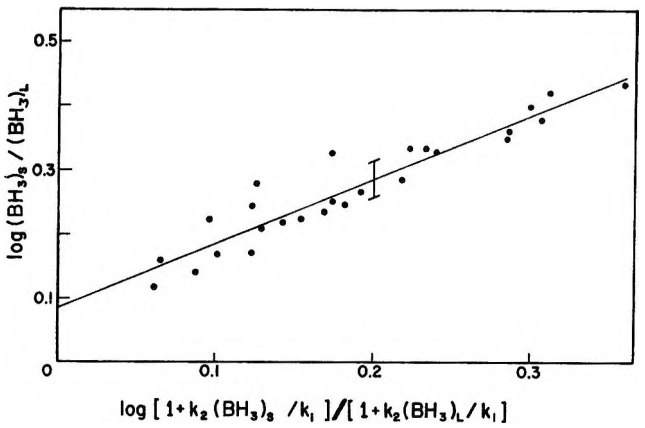

Figure 3. A plot of log $(BH_3)_S/(BH_3)_L$ *vs.* log $[1 + k_2(BH_3)_S/k_1]/[1 + k_2(BH_3)_L/k_1]$ at a mean recombination zone temperature of 545°K and a total pressure of 5.0 Torr of helium.

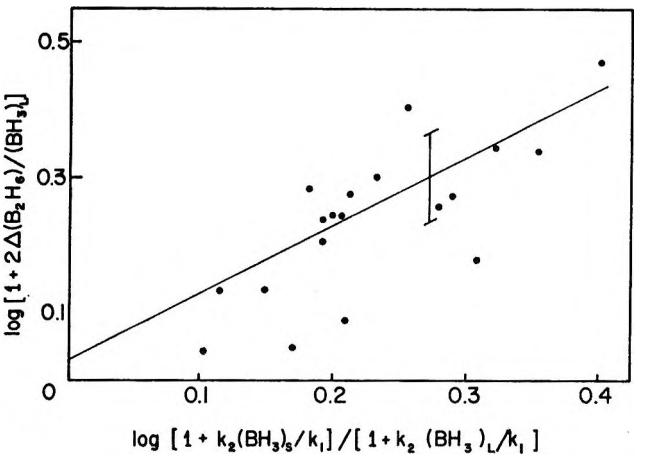

Figure 4. A plot of log $[1 + 2\Delta(B_2H_6)]/(BH_3)_L$ *vs.* log $[1 + k_2(BH_3)_S/k_1]/[1 + k_2(BH_3)_S/k_1]$ at a mean recombination zone temperature of 545°K and a total pressure of 5.0 Torr of helium.

Table III: First- and Second-Order Rate Constants for the Loss of BH_3 and the Formation of B_2H_6 at 5 Torr

$k_2 \times 10^{-9}$, l./(mol sec)	$k_1 \times 10^{-2}$, sec^{-1}	Species measured	Av temp, °K	No. of points
1.7 ± 0.3	3.3 ± 2	BH_3	545	26
1.5 ± 0.6	1.1 ± 3	B_2H_6	545	20
1.5 ± 0.3	2.6 ± 2	BH_3	629	15
(0.4 ± 1)	(2.6)	B_2H_6	629	10
1.3 ± 1	12 ± 5	BH_3	708	13

were few and badly scattered. Consequently, the value of k_2 given in Table III for these runs was calculated by fixing the intercept at the value obtained for the BH_3 data. The rate constant obtained is consistent with the other values but was used for no other purpose than this comparison. The precision listed in Table III was estimated by removing one of the most scattered points and recalculating k_2 and k_1. The accuracy of the rate constant at 545° is estimated[28] to be ±50%. The error is mainly analytical in nature.

A plot of log k_2 *vs.* $1/T$ and log k_1 *vs.* $1/T$, roughly weighted according to the analytical precision and temperature spread of the recombination zone, yielded activation energies of −1 and 5 kcal, respectively. Although there is considerable uncertainty in the actual temperature in the recombination zone, it is clear that the temperature of the run designated 709°K is higher than 629°K and likewise 629°K is higher than 545°K. Therefore, even though the numerical values of the activation energies are not too meaningful, it is certainly true that the activation energy associated with the second-order rate constant is very close to zero. We estimate the uncertainty in this activation energy as 2 kcal. Once again, despite the large uncertainty in temperature the error is mainly analytical.[28]

Discussion

The results presented in the previous section may be summarized as follows. In the lowest temperature recombination zone, BH_3 is lost by first- and second-order parallel reaction paths that produce diborane exclusively. At the highest temperatures BH_3 is lost by an additional first-order path that does not produce diborane. The second-order rate constant is 2×10^9 l./(mol sec) at 545°K, and the activation energy associated with this rate constant is 0 ± 2 kcal and probably negative. The first-order rate constant is about 3×10^2 sec^{-1} at 545°K and has an apparent activation energy of 5 kcal. We now discuss the two reaction paths individually.

The First-Order Path. Consider the first-order path at 545° where diborane is the exclusive product of borane loss. The mechanism of the reaction $2BH_3 = B_2H_6$ yielding the first-order term must involve the surface in some fashion. This interaction probably takes place in the following specific way.

$$BH_3 + S \rightleftharpoons BH_3\text{–}S \qquad K$$

$$BH_3\text{–}S + BH_3 \longrightarrow B_2H_6 + S \qquad k_s$$

where S represents a surface site; BH_3–S, adsorbed borane; and BH_3, gaseous borane. This Rideal mechanism yields a rate law

$$R = k_sKL(BH_3)^2/[1 + (BH_3)K]$$

where k_s is the rate constant for the reaction of free BH_3 with adsorbed BH_3, K is the adsorption equilibrium constant for BH_3, and L is the total number of sites. This expression assumes an idealized type of adsorption.[29] If $(BH_3)K \gg 1$

$$R = k_sL(BH_3)$$

(28) S. W. Benson, "The Foundations of Chemical Kinetics," McGraw-Hill, New York, N. Y., 1960, pp 86–94.

(29) K. J. Laidler, "Chemical Kinetics," McGraw-Hill, New York, N. Y., 1965, Chapter 6.

and k_sL would be identified with our measured Vk_1/S at 545°K where S/V is the surface-to-volume ratio of our reactor. The expression k_sL can be estimated from an equation developed by applying the absolute rate theory to this type reaction.[29] The result is

$$k_1(\text{calcd}) = (LS/V)(kT/h)(f^{\ddagger}/Ff_s)\exp(-E_0/kT)$$

where $f^{\ddagger}$ is the partition function of the adsorbed activated complex, F is the partition function of free BH_3, f_s is the partition function of the surface site, E_0 is the activation energy for the process, k is Boltzmann's constant, T is the absolute temperature, and h is Planck's constant. Using $L = 10^{15}$ cm^{-2}, $f^{\ddagger}/f_s = 1$, $kT/h = 10^{13}$ sec^{-1}, $S/V = 5$ cm^{-1}, $T = 545$°K, and $F = 5 \times 10^{26}$ cc^{-1} we obtain

$$k_1(\text{calcd}) = 10^2\exp(-E_0/kT)\ \text{sec}^{-1}$$

Therefore, we can account for our observed rate constant (3×10^2 sec^{-1}) only if $E_0 = 0$. This is the only mechanism involving the surface that will yield a specific rate as large as the observed value.

This mechanism is also consistent with the information available on the surface recombination of methyl radical. The first-order rate constant for the association of methyl radicals measured at 551°K under conditions similar to ours has a reported value of 3.2×10^2 sec^{-1}. A Rideal mechanism has been established for this reaction, and again this is the only mechanism that can account for the large rate constant. Finally, we have already reported in an independent experiment the similarity of the heterogeneous collision yields of BH_3 to give B_2H_6 and CH_3 to give C_2H_6.[13]

At higher temperatures the extent of reactions *via* the first-order path increases. This is due to the opening of another reaction channel for the loss of BH_3 at increased temperatures, namely

$$BH_3 \xrightarrow{\text{surface}} B(s) + {}^3/_2H_2$$

The occurrence of this reaction has been reported previously.[13,22] Indeed the rate constant of this reaction reported previously in the study on the low-pressure pyrolysis of BH_3CO,[13] the rate constant of the same reaction obtained from the low-pressure pyrolysis of B_2H_6,[22] and the first-order rate constant measured here at 709°K correlate very well if the activation energy of the process is about 10 kcal. Note that the apparent activation energy of the first-order process measured here is only a minimum value for the process of BH_3 yielding boron and H_2. The fact that the apparent activation energy measured here is less than 10 kcal indicates that the surface decomposition of BH_3 to yield boron and hydrogen is negligible at 545°K. This is in accord with our measured stoichiometry at 545°K.

The Second-Order Path. As noted in the last section the large specific rate constant for the first-order path places rather strict restraints on any mechanism. Now note that k_2 (BH_3) is several times larger than k_1 and that a Rideal mechanism involving a partially saturated surface requires that $k_2(BH_3)$ be less than k_1. So if both our first- and second-order data are to be explained by such a mechanism, the actual limiting k_1 must be very much larger than the apparent k_1 that we observed. However, a rate constant very much larger than the one we observed is totally unreasonable and we discard this hypothesis. All possible explanations of the observed second-order rate involving surface interactions can be ruled out by the incompatibility of the magnitude of the observed rate and the requirements of such interactions. In essence, our argument can be stated as follows. The binding of an activated complex on the surface in some fashion involves the loss of translational degrees of freedom. This results in a large factor favoring the gas-phase reaction. If the activation energy of the process is very low, both in the gas phase and on the surface, then for the concentrations of reactants and concentrations of sites employed here, the gas-phase reaction is favored over the surface reaction. It is just possible to explain the large magnitude of the rate of the first-order path by invoking one bound species and therefore reactions involving two bound species cannot contribute significantly to the second-order rate. The observed second-order rate constant must be attributed to the reaction

$$BH_3 + BH_3 \longrightarrow B_2H_6 \qquad k_2$$

occurring in the gas phase, and our measured k_2 is equal the rate constant for this elementary reaction.

One implication of our measurement becomes clear if we examine it in light of the overall entropy change for the reaction

$$B_2H_6 = 2BH_3$$

From Shepp and Bauer's calculation of the entropy change for this reaction,[30] we know that $\log A_d = \log A_2 + 5.7$ at 300°K where A_d is the frequency factor for the dissociation reaction, A_2 is the frequency factor for the association reaction, and the standard state is 1 mol/l. As the activation energy for the association reaction is very small A_d must be at least $10^{15.0}$ sec^{-1}. This is a reasonable value for the frequency factor for the dissociation of this molecule.[31]

It appears, however, that the value of the rate constant we have measured is not the high-pressure limiting value. As "fall-off" behavior is crudely dependent on molecular size, it is instructive to consider the association of methyl radicals to yield ethane—a system of the same molecular complexity as that studied here. The methyl–ethane system has been extensively studied,[32] and the fall-off behavior has been measured.[33]

(30) A. Shepp and S. H. Bauer, *J. Amer. Chem. Soc.*, 76, 265 (1954).
(31) S. W. Benson, "Thermochemical Kinetics," Wiley, New York, N. Y., 1968, Chapter III.

In addition this reaction has been studied under conditions similar to ours.[34] The high-pressure value of the rate constant for the association of methyl radicals obtained by Gomer and Kistiakowsky[32] and corrected by Shepp[35] is 2.2×10^{10} l./(mol sec). The value obtained by Ingold and Lossing at 551°K and a pressure of 5.0 Torr helium is 6.5×10^{9} l./(mol sec).[34] In addition a small negative activation energy was observed. So it is very likely that our rate constant for the borane–diborane system is not the high-pressure limiting value. Unfortunately, because of the experimental difficulties mentioned above, we were unable to study the rate of association of BH_3 as a function of total pressure. The probable negative activation energy does suggest that our measurements were made in the fall-off region but yields no measure of the extent of falloff. It is possible to estimate the order of magnitude of the falloff in several ways. We choose to do this semiempirically by correcting the observed falloff in the methyl–ethane system under conditions identical with ours for the gross differences between it and the borane–diborane system. These differences appear in E_0/RT and A_d where E_0 is the dissociation energy and A_d is defined above. It is sufficient for our purposes to use the Slater formulation of the fall-off equation.[36] Using $E_0 = 35.5$ kcal/mol and $A_d = 10^{16}$ sec^{-1} for the borane–diborane system and varying the value of m in Slater's equation from 3 to 7 yielded a ratio of the pressure-dependent rate to pressure-independent rate in the borane–diborane system ranging from 0.1 to 0.02.[37] Therefore, the high-pressure rate constant for the association of borane is estimated to be given by $k_\infty(\text{est}) = 10^{10.6 \pm 0.4}$ l./(mol sec)—a value as large as or larger than that for the association of methyl radicals. This in turn means that the frequency factor for the dissociation of B_2H_6 is given by $A_d = 10^{16.3 \pm 0.4}$.

Very fast association reactions have been the subject of considerable theoretical discussion.[38] The high efficiency of these reactions, which is coupled to a large frequency factor for the reverse reaction (dissociation), has been explained by introducing the so-called loose structure model of the activated complex into the absolute rate theory.[39] In this model, the reactant species, *e.g.*, CH_3, rotate as freely as if they were separated from each other. A problem in this interpretation has been to account for the orientation-independent interaction between the unpaired electrons of the two radicals at relatively large distances. van der Waals forces between the radicals have been suggested as responsible for the bonding but this explanation has been criticized as being too weak. Thus Rice[40] has suggested two-electron, three-center bonds involving carbon–hydrogen–carbon nuclei while Benson[38] suggests partial ionic bonding with and without bridging hydrogens.

It appears that the collision efficiency for the reaction $2BH_3 \rightarrow B_2H$ lies between 1 in 2 to 1 in 10 gas kinetic collisions. Again, this high efficiency requires

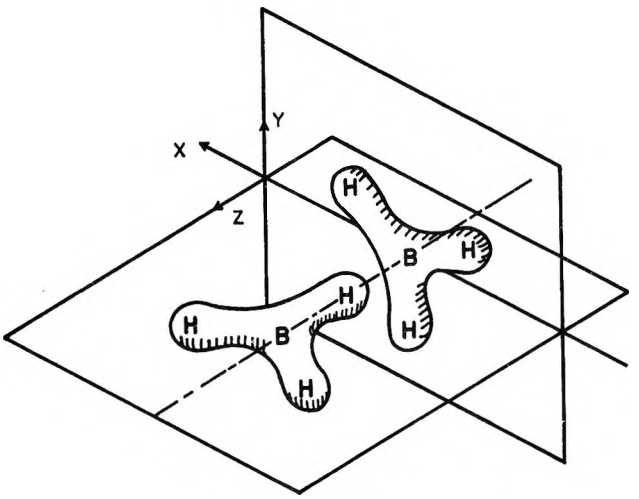

Figure 5. Schematic representation of an orientation of two borane molecules in the activated complex for the association reaction.

that bending vibrations be loosened to rotations in the activated complex. For this reason it is very unlikely that the activated complex looks anything like "normal" doubly bridge-bonded diborane. One possible "loose" structure for the activated complex that accommodates both bonding and "free tumbling" involves the formation of one boron to hydrogen bridge bond as

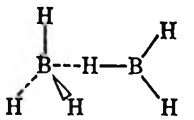

We know from molecular orbital calculations of the electronic structure of BH_3[17] that the lowest-lying unfilled orbital is a p_z orbital perpendicular to the plane of the four atoms. In the suggested activated complex the empty p_z orbital of one BH_3 molecule overlaps with the B–H bonding orbital of a second BH_3 molecule to form a new bonding orbital. In Figure 5 we picture a cross section of the activated complex before bond formation in terms of total (90%) electron density contours for

(32) R. Gomer and G. B. Kistiakowsky, *J. Chem. Phys.*, 19, 85 (1951).

(33) G. B. Kistiakowsky and E. K. Roberts, *ibid.*, 21, 1637 (1953).

(34) K. U. Ingold and F. P. Lossing, *ibid.*, 21, 1135 (1953); K. U. Ingold, I. H. S. Henderson, and F. P. Lossing, *ibid.*, 21, 2239 (1953).

(35) A. Shepp, *ibid.*, 24, 939 (1956).

(36) N. B. Slater, "Theory of Unimolecular Reactions," Cornell University Press, Ithaca, N. Y., 1959.

(37) Although this treatment is very approximate it is entirely sufficient simply because without any calculation at all one knows that the falloff must lie between 1 and 10^{-2}.

(38) S. W. Benson and W. B. DeMore in "Annual Review of Physical Chemistry," Vol. 16, H. Eyring, C. J. Christensen, and H. S. Johnston, Ed., Annual Reviews Inc., Palo Alto, Calif., 1965, pp 410–413.

(39) T. S. Ree, T. Ree, H. Eyring, and T. Fueno, *J. Chem. Phys.*, 36, 281 (1962).

(40) O. K. Rice, *J. Phys. Chem.*, 65, 1588 (1961).

BH_3.[17] It is of interest that this picture of the activated complex is similar to that proposed for the association of singlet methylene.[41]

Conclusions

The absolute rate of the association reaction $BH_3 + BH_3 \rightarrow B_2H_6$ has been measured. At a total pressure of 5 Torr helium and low partial pressures of reactants, the reaction proceeds at every hundredth gas kinetic collision and requires no activation energy. It is estimated that at higher pressures the efficiency approaches 1 in 10 to 1 in 2 gas kinetic collisions. From the very high rates we conclude that the association of BH_3 to yield diborane must be considered as of the same reaction type as radical association and ion–molecule reactions. This means that BH_3, which is neither radical nor ion, can form activated complexes with structures loose enough to permit rotation, yet sufficiently bound to restrict independent translation. It appears that the mechanism for the binding in these complexes may involve interactions of the two-electron, three-center type.

The results presented here have some more general implications with respect to the field of boron hydrides. It now is established that borane exists and has a reactivity with respect to association that is entirely equivalent to that of free radicals. The reactivity of borane with respect to other species remains to be established. However, it is almost certain that borane is an active species in boron hydride systems. This orbitally unsaturated species (or fragment as it has been called by others) may well have higher homologs just as there are higher homologs of the methyl radical. If so, the explanation of the reactions of the boron hydrides will probably be heavily based on the presence of these species as intermediates. In fact, such an explanation has already been put forth,[42] and it is supported by these measurements.

(41) R. Hoffmann, R. Gleiter, and F. B. Mallory, *J. Amer. Chem. Soc.*, **92**, 1460 (1970).

(42) J. Plesek, S. Hermanek, B. Stibr, and F. Hanousek, *Collect. Czeck. Chem. Commun.*, **32**, 1095 (1968).

The Catalytic Effect of Metal Oxides on Thermal Decomposition Reactions. II. The Catalytic Effect of Metal Oxides on the Thermal Decomposition of Potassium Chlorate and Potassium Perchlorate as Detected byThermal Analysis Methods

by Winfried K. Rudloff and Eli S. Freeman

IIT Research Institute, Chicago, Illinois 60616 *(Received March 27, 1969)*

The catalytic activity of a series of metal oxides on the thermal decomposition of potassium chlorate and its intermediate decomposition product, potassium perchlorate, was investigated. Thermal analytical methods and electrical conductivity experiments were used to investigate correlations between catalytic activity and electrical properties of the oxides. It was found that oxides of the transition elements were the most reactive. Interpretations of the data in terms of the mechanisms of catalysis are discussed.

Introduction

The thermal decomposition of potassium chlorate ($KClO_3$), which was described in the first paper of this series,[1] is catalyzed by many metal oxides.[2-9]

The catalytic activity of manganese dioxide (MnO_2) and ferric oxide (Fe_2O_3) on the decomposition of $KClO_3$ has been investigated extensively.[2-8] Others[10-12] found that MnO_2 and MgO also catalyze the intermediate decomposition product of $KClO_3$, potassium perchlorate, $KClO_4$.

A systematic study of the relationship between defect structure of metal oxides and their catalytic activity is not evident in the many investigations dealing with the catalytic activity of the oxides on the decompositions of $KClO_3$ and $KClO_4$.

Some correlation has been found between the electronic defect structure of metal oxides and their catalytic activity on the decomposition of nitrous oxide (N_2O).[13,14] An apparent increase in catalytic activity of the oxides with respect to N_2O decomposition was observed in p-semiconductive oxides, less increase in insulator oxides, and the least increase in n-semiconductive oxides. Only a fragmentary attempt was made to correlate electronic defects of oxides to their catalytic activity with respect to the thermal decomposition of $KClO_3$.[9]

This second paper in the series is concerned with a systematic investigation of the catalytic activity of metal oxides on the thermal decomposition of $KClO_3$ and its intermediate decomposition product $KClO_4$. For this investigation a series of metal oxides was selected in which the p-semiconductive character decreases from left to right: Cu_2O, CoO, NiO, CuO, MgO, Al_2O_3, ZnO, TiO_2, Fe_2O_3.[15] The catalytic activity with respect to N_2O also decreases in this order. We considered, however, that methods of preparation, impurities, and defect structure of the oxides can significantly influence the semiconducting character of the oxides.[16] We found that the order of catalytic activity of the selected reagent grade oxides on the decomposition of $KClO_3$ and $KClO_4$ differed somewhat from the order reported for N_2O decomposition. Additional oxides in our series included Cr_2O_3, Co_3O_4, MnO_2, and Ag_2O.

This second paper is mainly phenomenological in nature; however, some interpretation of the results is given. Correlations between electronic and possibly

(1) W. K. Rudloff and E. S. Freeman, *J. Phys. Chem.*, **73**, 1209 (1969).

(2) H. A. Neville, *J. Amer. Chem. Soc.*, **45**, 2330 (1923).

(3) F. E. Brown, J. A. Burrows, and H. M. McLaughlin, *ibid.*, **45**, 1343 (1923).

(4) J. A. Burrows and F. E. Brown, *ibid.*, **48**, 1790 (1926).

(5) H. M. McLaughlin and F. E. Brown, *ibid.*, **50**, 782 (1928).

(6) S. S. Bhatnagar, B. Prakash, and J. Singh, *J. Ind. Chem. Soc.*, **17**, 125 (1939).

(7) F. E. Brown and J. D. Woods, *Proc. Iowa Acad. Sci.*, **63**, 410 (1956).

(8) J. M. Gaidis and E. G. Rochow, *J. Chem. Educ.*, **40**, 78 (1963).

(9) F. Solymosi and N. Krix, *Acta Chim. Acad. Sci. Hung.*, **34**, 241 (1962).

(10) C. E. Otto and H. S. Fry, *J. Amer. Chem. Soc.*, **45**, 1134 (1923).

(11) E. S. Freeman and D. A. Anderson, *Nature*, **206**, 378 (1965).

(12) M. M. Markowitz and D. A. Boryta, *J. Phys. Chem.*, **69**, 1114 (1965).

(13) G. M. Schwab and H. Schultes, *Z. Phys. Chem.*, **B9**, 265 (1930); G. M. Schwab, R. Staeger, and H. H. von Baumbach, **B21**, 65 (1933); G. M. Schwab and H. Schultes, **B25**, 411 (1934).

(14) G. Schmid and N. Keller, *Naturwissenschaften*, **37**, 43 (1950).

(15) W. E. Garner, "Chemistry of the Solid State," Butterworths, London, 1955, p 395.

(16) Reference 15, p 123.

ionic defect structure and catalytic activity of the metal oxides will be more thoroughly discussed in a subsequent paper covering an investigation in which the induced semiconductive characteristics and catalytic effects of a few selected representative oxides were investigated in more detail.

Experimental Section

Preparation and Standardization of Samples. The preparation and standardization of reagent grade $KClO_3$ and $KClO_4$ have already been described.[1]

Reagent grade metal oxides were thoroughly sieved; the sieve fractions between 53 and 63 μ were dried and stored in a desiccator and were used in differential thermal analysis (dta), thermogravimetric analysis (tga), and differential thermogravimetric analysis (dtga) experiments. The oxides had the following purity specifications: nickel oxide (NiO), B&A reagent grade, Code 2012, assay of Ni minimum 77.0%; cuprous oxide (Cu_2O), B&A reagent grade, Code 1661, assay as Cu_2O minimum 97.0%; cupric oxide (CuO), B&A reagent grade, Code 1645, assay as CuO minimum 99.0%; manganese dioxide (MnO_2), B&A reagent grade, Code 1948, assay as MnO_2 minimum 99.5%; ferric oxide (Fe_2O_3), B&A reagent grade, Code 1741, assay as Fe_2O_3 minimum 99.0%; aluminum oxide (Al_2O_3), B&A reagent grade, Code 1236; titanic oxide (TiO_2), Fisher reagent grade, less than 0.013% impurities; cobalt-(II,III) oxide (Co_3O_4), B&A reagent grade, Code 1590, assay as Co minimum 70%; magnesium oxide (MgO), B&A reagent grade, Code 1917, assay as MgO (after ignition) minimum 99.0%; zinc oxide (ZnO), USP, Code 2451, no purity specifications listed; silver oxide (Ag_2O), Goldsmith Brothers, Division of National Lead Co., no purity specifications listed; chromium(III) oxide (Cr_2O_3), B&A purified, Code 1581.

All oxides were mixed with similar sieve fractions of $KClO_3$ and/or $KClO_4$ in a mole ratio that corresponded to a ratio of one oxide cation to five potassium cations in the chlorate and/or perchlorate. The mixtures were shaken for several hours to provide for intimate mixing. The mixtures were stored in a desiccator for later use in the dta–tga experiments. The sample sizes for the thermal analysis experiments were approximately 200 mg of $KClO_3$ plus the corresponding amount of metal oxide. The heating rates were nominally 10°/min, and the thermal analysis was performed in air.

The Combined Differential Thermal Analysis–Thermogravimetric Analysis Apparatus. A Chevenard thermobalance was modified to permit the simultaneous recording of differential temperature, weight loss, and sample temperature (Figure 1). The sample vessel, a quartz crucible, is divided into two compartments. The first contains the sample under investigation, and the second contains a corresponding amount of Al_2O_3 reference material. The thermocouple wires are led through a four-hole ceramic rod that is connected to the

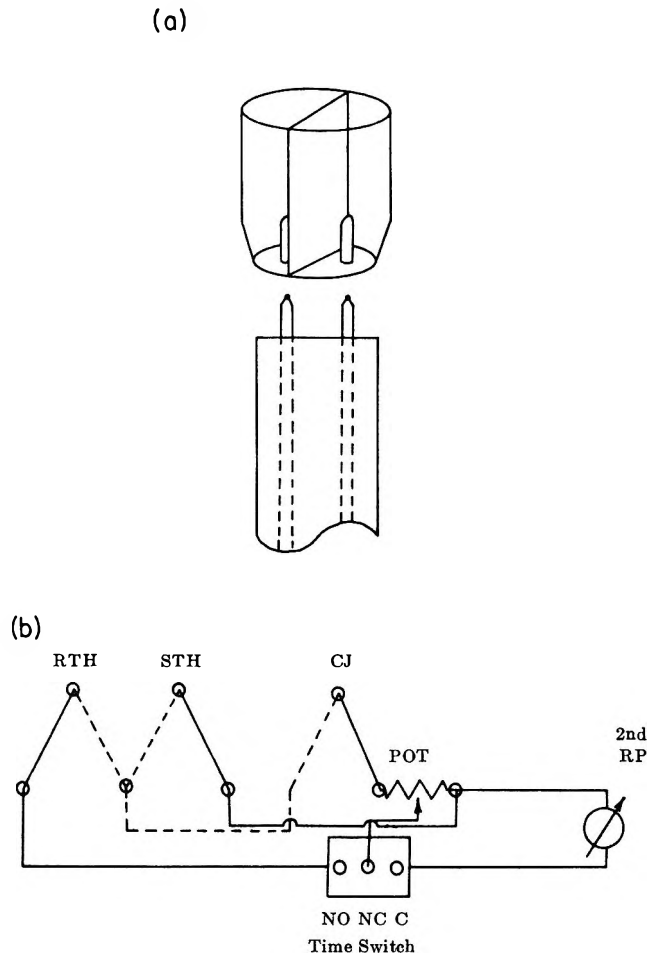

Figure 1. (a) Schematics of the combined dta–tga apparatus; crucible for the apparatus. (b) Schematics of the combined dta–tga apparatus; electrical wiring for the second recorder pen for recording ΔT and T: (RTH) reference thermocouple, (STH) sample thermocouple, (CJ) cold junction, (POT) 10,000 potentiometer, (RP) recorder pen, (NO) normally open, (NC) normally closed, (C) common.

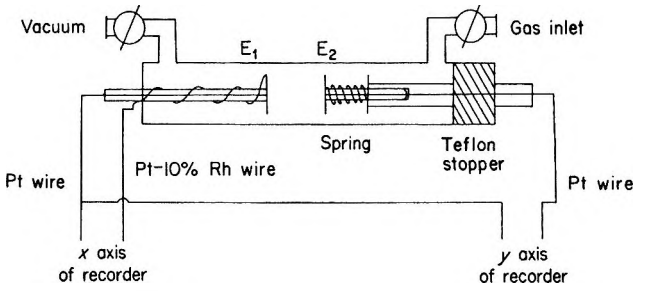

Figure 2. Electrical conductivity apparatus.

Chevenard balance beam. The crucible is held on top of the rod by the thermocouples.

The weight changes during reaction are recorded by the motion of a metal rod that hangs on the opposite side of the balance rod. This metal rod moves up and down in a spool when the sample holder moves down and up. The motions of the metal rod within the spool

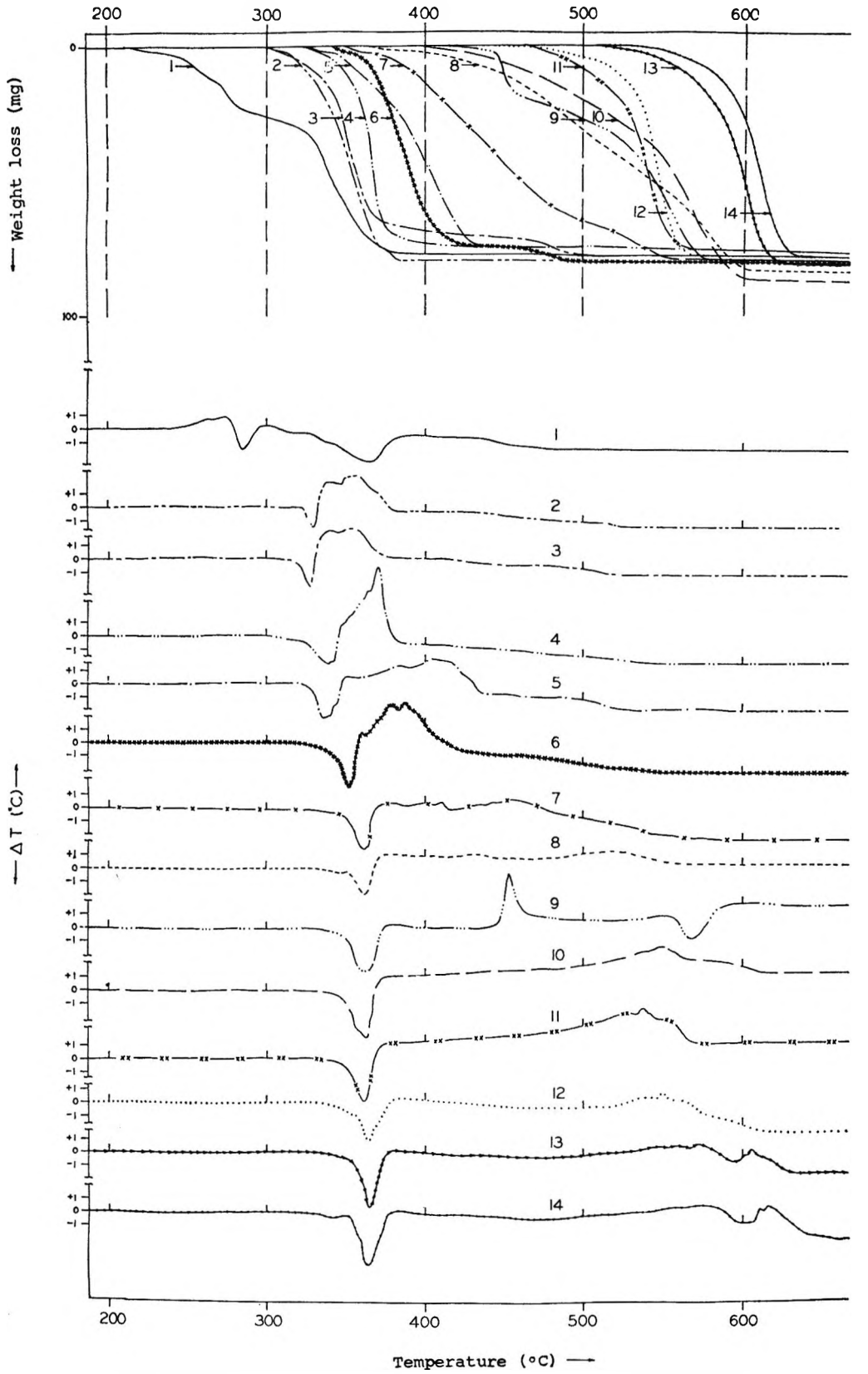

Figure 3. Thermogravimetric analysis and differential thermal analysis of the catalytic activity of metal oxides on the decomposition of $KClO_3$: (1) Cr_2O_3, (2) CoO, (3) Co_3O_4, (4) Fe_2O_3, (5) MnO_2, (6) Cu_2O, (7) CuO, (8) NiO, (9) Ag_2O, (10) ZnO, (11) MgO, (12) TiO_2, (13) Al_2O_3, (14) no catalyst.

create changes in the electromagnetic field that are recorded with one pen of a Bristol two-pen recorder. The second pen in connection with a time switch permits almost simultaneous recording of the differential temperature, ΔT, and the sample temperature, T.

The Stone–Cahn Tga–Dtga Apparatus. A Stone–Cahn thermobalance with a derivative computer was used in some typical runs to obtain simultaneous traces of tga and dtga. These experiments were designed to obtain a more quantitative insight into the complex mechanism of the catalyzed decomposition of $KClO_3$.

Electrical Conductivity Measurements. Electrical conductivity of the oxides was measured in the apparatus pictured in Figure 2. Single-crystal material, such as MgO, was platinum (Pt) coated *in vacuo* on two opposite sides to obtain intimate electrical contact between the oxide and Pt electrodes. Powders were pressed at 30,000 psig into cylindrical pellets, cut to similar size, and pressed between electrodes E_1 and E_2.

Electrode E_1, inside of a flow tube of Vycor glass, is mounted on a glass disk that is fused to a sturdy glass capillary fixed at one side of the flow tube. Electrode E_2 is fixed on a similar disk–capillary combination. The glass capillary is led through a special Teflon stopper, to provide adjustable distances between the electrodes. In addition, a spring provides adequate pressure of the electrodes to the single crystal or powder pellets for good electrical contact. The flow tube is placed in a tube furnace, which is heated at a nominally constant rate. A wire of Pt–10% Rh is fused to one Pt electrode, and this junction serves as a thermocouple junction. Thus, simultaneously with the recording of electrical conductivity (as the y axis on a Moseley x–y recorder), the temperature can be recorded (as x axis on the x–y recorder). Gas inlets and outlets provide for a proper flow or nonflow atmosphere. The conductance (or rather resistance) is measured with a General Radio electrometer, which is connected to the y axis of the recorder. During operation the whole system must be shielded very carefully because of noise pickup from the surroundings. This pickup mainly occurs if high resistances are involved.

Results

In Figure 3 the differential temperature, ΔT, and the weight loss are plotted as functions of temperature (average reference temperature) for the decomposition of $KClO_3$ in intimate contact with various metal oxides. The curves are listed in approximate order of catalytic activity of the oxides. In Figure 4 the melting temperature and temperatures at different stages of decomposition of $KClO_3$ are plotted in the approximate order of catalytic oxide activity. In some cases, error limits (standard deviations from the mean) are listed.

Figure 4 indicates that the initial decomposition temperatures of $KClO_3$ in mixtures with oxides increase in the order Cr_2O_3, Co_3O_4, CoO, MnO_2, Fe_2O_3, Cu_2O, CuO,

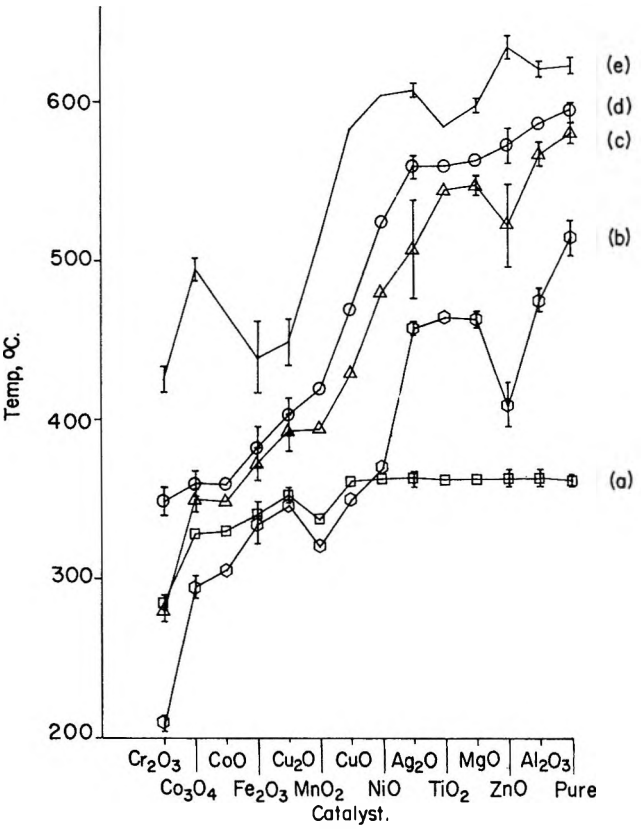

Figure 4. Decomposition and melting temperature of $KClO_3$ in mixtures with oxide catalysts: (a) melting point, (b) initial decomposition, (c) 25% decomposition, (e) 50% decomposition, (e) final decomposition.

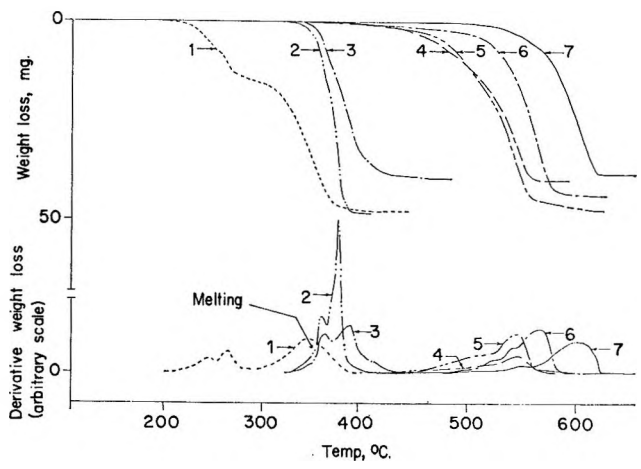

Figure 5. Thermogravimetric and derivative thermogravimetric analysis of the catalytic effect of (1) Cr_2O_3, (2) Fe_2O_3, (3) Cu_2O, (4) Al_2O_3, (5) MgO, (6) TiO_2, (7) no catalyst on the $KClO_3$ decomposition.

NiO, ZnO, Ag_2O, MgO, TiO_2, Al_2O_3, no catalyst. At 25 and 50% decomposition the order is slightly different: Cr_2O_3, CoO, Co_3O_4, Fe_2O_3, Cu_2O, MnO_2, CuO, NiO, Ag_2O, ZnO, MgO, TiO_2, Al_2O_3, no catalyst.

The melting temperature of $KClO_3$ is reduced when the oxides Cr_2O_3, Co_3O_4, CoO, Fe_2O_3, MnO_2, Cu_2O, and

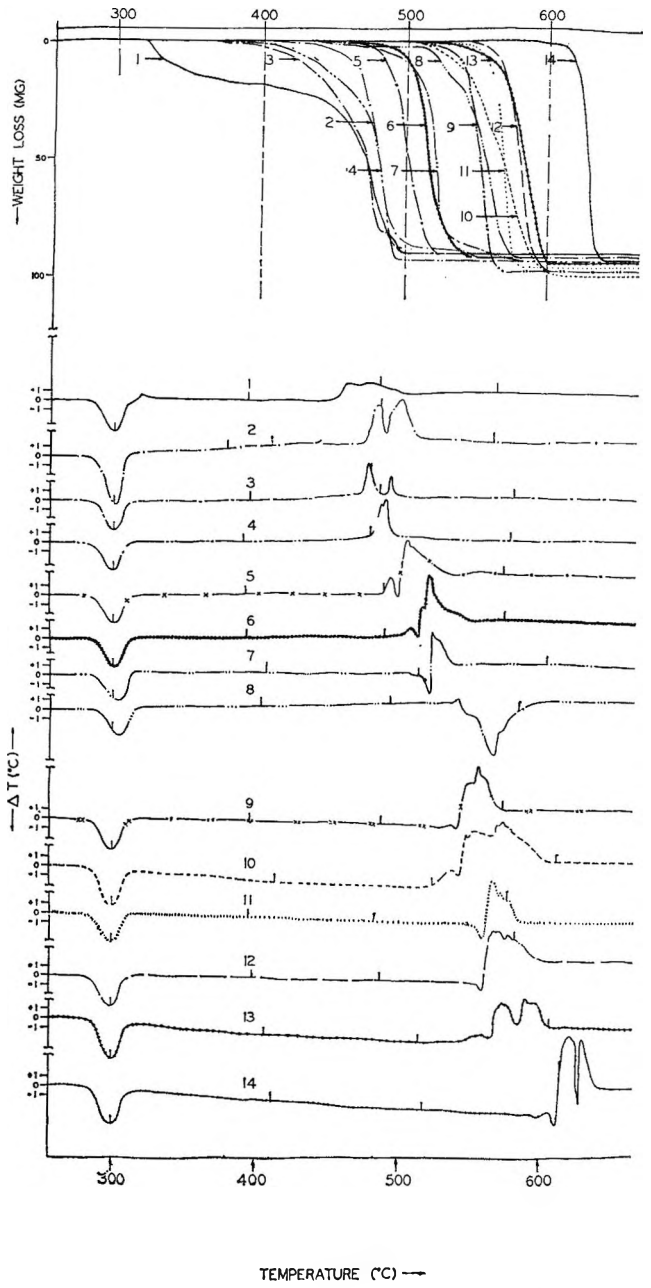

Figure 6. Thermogravimetric analysis and differential thermal analysis of the catalytic activity of metal oxides on the decomposition of $KClO_3$: (1) Cr_2O_3, (2) Cu_2O, (3) Co_3O_4, (4) CoO, (5) CuO, (6) MnO_2, (7) Fe_2O_3, (8) Ag_2O, (9) MgO, (10) NiO, (11) TiO_2, (12) ZnO, (13) Al_2O_3, (14) no catalyst.

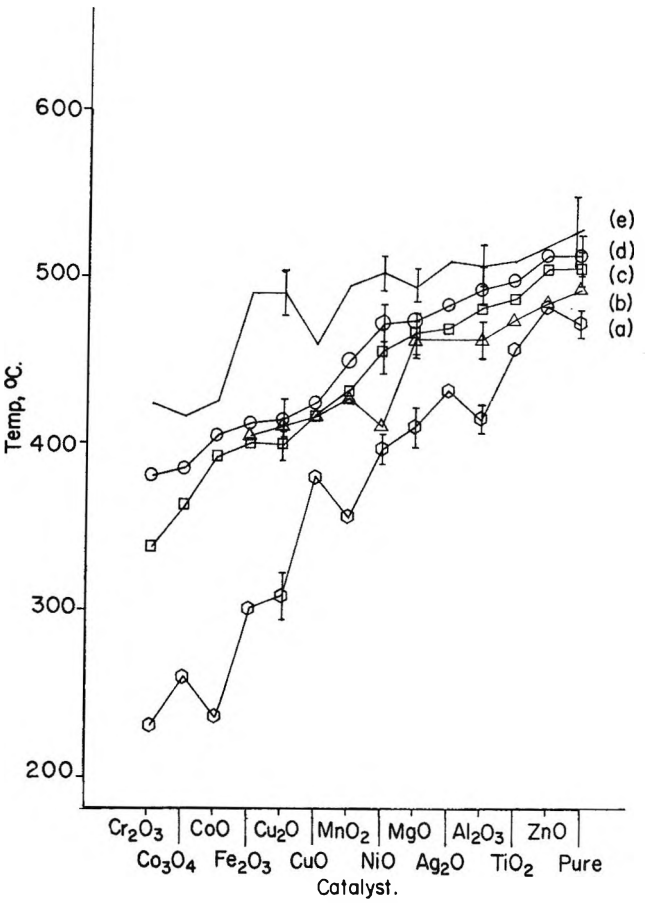

Figure 7. Decomposition temperatures of $KClO_4$ in mixtures with oxide catalysts: (a) initial decomposition, (b) melting point, (c) 25% decomposition, (d) 50% decomposition, (e) final decomposition.

CuO are present. It stays constant, within error limits, when the other oxides are present. In the first series, decomposition already begins in the solid phase. In most cases two or more decomposition steps are observable in the tga curves. These observations are even more obvious in Figure 5 in which tga and dtga curves of some selected oxide catalysts are plotted *vs.* temperature. In some cases, such as CuO, NiO, and ZnO, decomposition occurs over a wider temperature range. Cr_2O_3 and Ag_2O each show a distinct decomposition step at relatively low temperatures. Co_3O_4, MnO_2, and Cu_2O each show a small decomposition step at higher temperatures.

In Figure 6 the simultaneous tga and dta curves of $KClO_4$–oxide mixtures are plotted, and the corresponding melting and decomposition temperatures at various stages are plotted in Figure 7. (Temperature pips on the dta curves, Figure 6, indicate the hundreds degrees of the actual sample temperatures.)

There are essentially two endothermal reactions occurring in the $KClO_4$–metal oxide mixture: a solid phase transition of the perchlorate at around 300° and melting. The melting endotherm is sometimes embedded in the exotherm of the decomposition and occurs frequently after an initial rise of the differential temperature. In some cases this initial rise is apparently so slow that it does not show in the dta curves. However, the initial decomposition temperatures as taken from the tga curves clearly indicate that the reaction proceeds already in the solid phase. In a few representative cases melting was checked visually and found to coincide approximately with the second endotherms in the dta curves.

The phase transition endotherm of $KClO_4$ is only slightly affected by the oxide catalysts, while the melt-

ing point is apparently influenced by the oxides or by possible reaction products formed during the initial solid-state decomposition of $KClO_4$. In all cases decomposition begins below the apparent melting endotherm. The sequence of catalytic activity of the oxides is somewhat similar to the chlorate activity. Again several steps of decomposition are apparent.

In Table I the differences in temperature at decomposition stages of 25 and 50% are listed for the oxides with $KClO_3$ and $KClO_4$. A distinct separation into two groups of oxides is apparent, one in which the differences are above 100° and a second in which they are well below 100°.

Table I: Temperature Differences between Decomposition Temperature of $KClO_3$ and $KClO_4$ at 25 and 50% Decomposition

Oxide	ΔT at 25% decomposition	ΔT at 50% decomposition
Cr_2O_3	158 ± 6	141
Co_3O_4	113 ± 7	125
CoO	114	145
MnO_2	137	128
Fe_2O_3	127 ± 10	112 ± 22
Cu_2O	105 ± 20	130
CuO	87	60
NiO	76 ± 13	47
ZnO	82	25
Ag_2O	62 ± 31	38
MgO	23 ± 18	12
TiO_2	42	42
Al_2O_3	14 ± 17	8 ± 14
....	25 ± 16	19 ± 16

In Figure 8 electrical conductivities of various representative oxide pellets in air are semilogarithmically plotted *vs.* temperature. The electrical conductivities of the oxides approximately follow the order Cr_2O_3, Fe_2O_3, TiO_2, MgO. TiO_2 and MgO exhibit a crossover in the electrical conductivity at about 400°. The slope for MgO is less steep, however.

Discussion

A distinct difference exists in catalytic activity between two apparent oxide groups—n-semiconductive oxides and p-semiconductive oxides. Oxides in the p-semiconductive group—Cr_2O_3, CoO, Co_3O_4, MnO_2, CuO, and perhaps NiO—show relatively high catalytic activity. [The classification of MnO_2 is somewhat questionable; some authors[17] classify it to be p-semiconductive, while it is classified by Kubaschewski[18] as n-semiconductive.] The catalyzed decomposition of $KClO_3$ in mixtures with these oxides begins in the solid phase. These oxides appear to reduce the melting point of the chlorate. (Melting is indicated by the endothermal change between 300 and 400°.) Metal oxides that are generally considered to be p-semi-

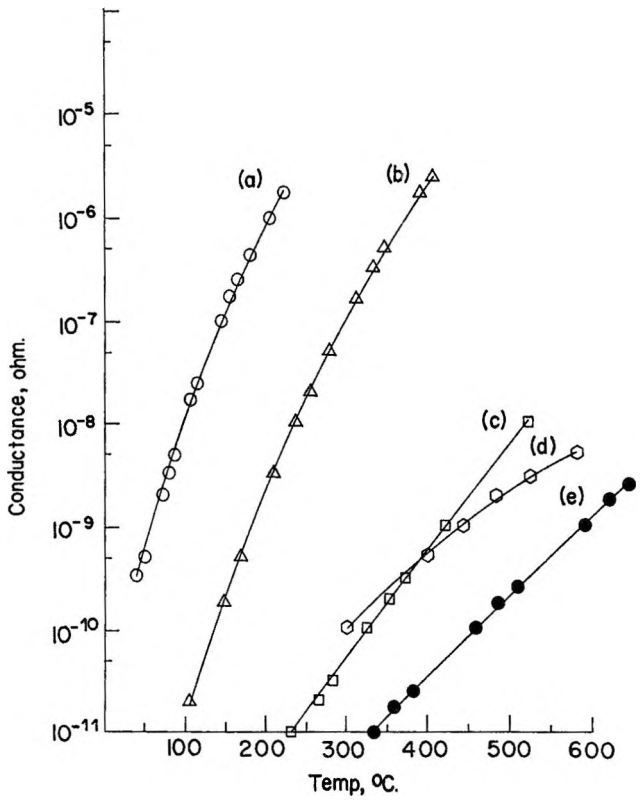

Figure 8. Electrical conductance of oxide pellets as a function of temperature: (a) Cr_2O_3, (b) Fe_2O_3, (c) TiO_2, (d) MgO pellet, and (e) MgO single crystal.

conductors[17] (or intrinsic semiconductors forming positive holes at higher temperatures) are the most active catalysts in the thermal decomposition reactions of $KClO_3$ and $KClO_4$. The exception is perhaps Fe_2O_3, which is considered to be an n-conductor.

Oxides classified as n-semiconductive, the second group, barely influence the melting temperature of $KClO_3$ (again, melting is indicated by the endothermal change between 300 and 400°). These oxides only initiate decomposition in the molten phase, in which the chlorate ions are very mobile. (The curves in Figure 4 representing melting and initial decomposition temperatures cross over.)

In the first step of decomposition (initial shoulder in curve 2 of Figure 5), the decomposition rate is relatively slow, and this step appears to be mainly governed by the charge mobility within the solid chlorate, since at this stage the chlorate has not yet become molten. After the melting has occurred the decomposition accelerates, and the decomposition rate passes through a maximum. Another, higher maximum appears at higher temperatures. An approximate weight ratio of 1:2 for the small and large peaks is obtained when this

(17) Reference 15, p 397; see also K. Hauffe, *Advan. Catal.*, **7**, 213 (1955).

(18) O. Kubaschewski and B. E. Hopkins, "Oxidation of Metals and Alloys," Butterworths, Washington, D. C., and London, 2nd ed, 1962, p 24.

ratio is geometrically analyzed in agreement with the two-step disproportionation mechanism previously postulated for the uncatalyzed reaction.[1]

$$2KClO_3 \longrightarrow KCl + KClO_4 + O_2 \quad (1)$$

$$KClO_4 \longrightarrow KCl + 2O_2 \quad (2)$$

It may be speculated that a bimolecular chlorate anion adsorbs on the surface of the apparent p-semiconductive oxide with a partial and/or total electron transfer to the positive holes in the valence band (VB) and forms the surface complex

$$\oplus VB + \begin{bmatrix} O & & O \\ Cl & O & Cl & O \\ O & & O \end{bmatrix}^{-2} \longrightarrow$$

$$\oplus VB\text{—}\begin{bmatrix} O & & O \\ Cl & O & Cl & O \\ O & & O \end{bmatrix}^{-x} \quad (x < 2) \quad (3)$$

Consequently, the Cl–O bonds of the anion become less stable, and disproportionation occurs at much lower temperatures than without the catalyst

$$\oplus VB\text{—}\begin{bmatrix} O & & O \\ Cl & O & Cl & O \\ O & & O \end{bmatrix}^{-(x)} \longrightarrow$$

$$\oplus VB\text{—}\begin{bmatrix} O \\ Cl \\ O \end{bmatrix}^{-(x-1)} + \begin{bmatrix} & O & \\ O & Cl & O \\ & O & \end{bmatrix}^{-1} \quad (4)$$

Subsequently, the adsorbed, rather unstable $ClO_2^{-(x-1)}$ surface anion further decomposes and desorbs as Cl^- and O_2 where the Cl^- ion takes along the electron partially donated to the valence band. The more stable ClO_4^- anion then decomposes at much higher temperatures. It is interesting to note that differences between the temperatures at 25 and 50% decomposition of $KClO_4$ (Table I) significantly decrease if apparent n-semiconductive oxides are present, indicating perhaps different mechanisms by which the catalytic effect of the oxides on the decomposition of $KClO_3$ approaches that on the decomposition of $KClO_4$

$$\theta_{BC} + \begin{bmatrix} & O & & O \\ O & Cl & O & Cl \\ & O & & O \end{bmatrix}^{-2} \longrightarrow$$

$$\theta_{CB}\text{—}\begin{bmatrix} & O & & O \\ O & Cl & O & Cl \\ & O & & O \end{bmatrix}^{-x} \xrightarrow[-Cl^- - O_2]{(x>2)}$$

$$\theta_{CB}\text{—}\begin{bmatrix} & O & \\ O & Cl & O \\ & O & \end{bmatrix}^{-(x-1)} \longrightarrow \theta_{CB} + Cl^- + 2O_2 \quad (5)$$

The possible electrical nature of the catalytic decomposition reaction of both chlorate and perchlorate may be demonstrated when Figures 3 to 7 are correlated to Figure 8. The higher the apparent conductivity (the easier a charge transfer from or to the oxide), the higher the catalytic activity appears to be—the electrical conductivities of both MgO and TiO_2 appear to be of similar order of magnitude and so do the catalytic activities as reflected in the thermal analysis curves of $KClO_3$ and $KClO_4$.

There is some evidence that the charge-transfer mechanism, at least where the oxides of the transition elements are involved, is not entirely electronic, and ionic and/or vacancy diffusion through the oxide catalyst may be indicated.

Fe_2O_3 and more so Cr_2O_3 show much higher electrical conductivities corresponding to higher catalytic activities. In the cases of Cr_2O_3 and perhaps of MnO_2,[7] however, a partial or complete electron transfer results in an apparent irreversible change in oxidation state of the metal ion—the water-insoluble Cr_2O_3, which is by itself stable at higher temperatures, is oxidized by the chlorate to chromate and/or bichromate. This oxidized state is indicated by the residue of a thermal analysis of a Cr_2O_3–$KClO_3$ mixture turning yellow and becoming completely soluble in water. (The pseudocatalytic nature of different chromium compounds on the thermal decomposition of $KClO_3$ will be discussed in more detail in a subsequent paper.) Literature data indicate that MnO_2 changes also to a limited degree to a higher oxidation state of the cation.[7] Cu_2O is also oxidized to its higher state CuO, as apparently indicated by a change in color from red to black. Furthermore, the apparent activation energies of the charge-transfer process as obtained from an Arrhenius plot of the conductance are between 10 and 20 kcal/mol. This is much higher than usually found, if the mechanism were purely electronic.[19]

On the other hand, recent evidence indicates that Fe_2O_3 is not altered after the reaction. Mössbauer spectroscopy of the oxide before and after the catalytic reaction shows identical Fe_2O_3 spectra indicating that no irreversible change has taken place during the reaction. (A more detailed study on this will be published in a subsequent paper.)

Ag_2O appears to be rather peculiar. Under normal conditions it decomposes at relatively low temperatures, ~300°.[20] The presence of the highly oxidizing chlorate and/or perchlorate appears, however, to stabilize the oxide. The first exothermal decomposition step in the mixture with chlorate occurs at around 450° and is rather well defined. It may be speculated that ClO_3^- and/or ClO_4^- anions form complexes with the silver cations on the surface of the oxide, thus stabilizing the oxide. The first decomposition step does not correspond to the stoichiometry pertaining the 1:2 ratio of the normal chlorate disproportionation reaction.

(19) P. Zirkind and E. S. Freeman, *J. Chem. Phys.*, **41**, 906 (1964).

(20) R. C. Weast, S. M. Selby, and C. D. Hodgman, "Handbook of Chemistry and Physics," Chemical Rubber Publishing Co., Cleveland, Ohio, 46th ed, 1965, p B220.

In Table II the differences in heat of oxide formation per mole of metal ion are listed for selected metal oxides of various valence states. The ease with which the valence state of the transition element oxides changes can thus be correlated to their catalytic activity as is apparent from this table.

Table II: Heats of Formation of Some Metal Oxides

Reaction	ΔH_f,[a] kcal/mol
$^1/_2Cr_2O_3 + {}^3/_4O_2 \rightarrow CrO_3$	−2.3
$^1/_3Fe_3O_4 + {}^1/_6O_2 \rightarrow {}^1/_2Fe_2O_3$	−9
$^1/_2Mn_2O_3 + {}^1/_4O_2 \rightarrow MnO_2$	−11.1
$CoO + {}^1/_6O_2 \rightarrow {}^1/_3Co_3O_4$	−13.0
$^1/_2Cu_2O + {}^1/_4O_2 \rightarrow CuO$	−17.2
$^1/_3Ti_3O_5 + {}^1/_6O_2 \rightarrow TiO_2$	−32.4

[a] ΔH_f = heat of reaction per mole of metal ion in lower valent oxide.

A final comment on the apparent melting point depression should be added. It may be argued that lowering of the melting point is only consistent with a diffusion of catalyst ionic components into the chlorate lattice to form impurity centers (polarization centers), but the reaction products formed at the oxide surfaces may have a similar influence.[21] The lowering of the melting point can be interpreted as resulting from the formation of reaction products at low temperatures due to catalysis.[22] The reaction rate may be expected to be further enhanced by the formation of the molten phase. Only in the case of Cr_2O_3 is it evident that Cr(VI) ions penetrate into the chlorate phase. The Cr(VI) ions are formed by oxidation of the Cr(III) ions.

Conclusions

The results in the present paper lead to the conclusion that transition metal oxides are the most reactive catalysts investigated in this work on the thermal decomposition of $KClO_3$ and its intermediate decomposition product $KClO_4$. This may be correlated to the "p" semiconduction nature of these oxides. Except for Fe_2O_3, the apparent n-semiconductive oxides are less catalytically active than p-semiconductors. The disproportionation reaction step is generally preserved during the catalytic decomposition.

Electrical conductivity measurements on some selected oxides indicate the electrical nature of the catalytic action. In some cases, such as with Cr_2O_3, a complete charge transfer is apparent, and the oxide itself is irreversibly changed to a higher oxidation state. This and the additional evidence that the activation energies for the electrical conduction process in the oxides are relatively high suggest that the charge-transfer mechanism during catalysis may be at least in part ionic.

Acknowledgment. This work was supported by the U. S. Army Edgewood Arsenal under Project No. DA-18-035-AMC-341(A). The authors are grateful to Mr. B. Zeffert and Mr. Harry A. Brown for valuable discussions and useful suggestions. The authors also wish to acknowledge Brent Boldt for the laboratory work which he conducted on this program.

(21) W. K. Rudloff and E. S. Freeman, to be published.

(22) A. D. Anderson and E. S. Freeman, *J. Inorg. Nucl. Chem.*, **27**, 1471 (1965).

Gas-Phase Radiolysis of Toluene

by Yukio Yamamoto, Setsuo Takamuku, and Hiroshi Sakurai

The Radiation Laboratory, The Institute of Scientific and Industrial Research, Osaka University, Suita, Osaka, Japan *(Received December 31, 1969)*

The γ radiolysis of toluene in the gas phase was studied at room temperature as a function of pressure (1.5–18 mm) and added NO and N_2O. The G values obtained at 10.7 mm and a total dose of 1.9×10^{19} eV are hydrogen, 0.36; methane, 0.15; ethane, 0.07; acetylene, 0.41; benzene, 0.18; ethylbenzene, 0.05; xylenes, 0.05; 2-methyldiphenylmethane (MDPM), 0.05; 3-MDPM, 0.34; 4-MDPM, 0.05; and bibenzyl, 0.03. The effect of added NO indicates that ethane, ethylbenzene, xylenes, bibenzyl, and some of the benzene are formed by radical reactions but not acetylene and MDPMs. The product formation was compared with that of the γ radiolysis in the liquid phase and the mercury-sensitized photolysis in the gas phase which was reinvestigated in this study. The basic difference between these studies is due to the different reactive species formed by the β-bond fissions; in the gas-phase radiolysis $C_7H_7^+$ ions are formed and produce three isomers of MDPM, while in the photolysis and liquid phase radiolysis benzyl radicals, producing predominantly bibenzyl, are formed. The addition of N_2O results in the considerable increase of MDPMs and bibenzyl yields, which can be attributed to the additional formation of benzyl and tolyl radicals.

Introduction

Many papers have been published on the radiolysis of toluene in the liquid phase. In some detailed studies the yields of a number of products, gases and liquids including dimers, were determined, and their formation has been attributed to the reactions through excited molecules.[1,2] However, little attention has been paid to the radiolysis of toluene in the gas phase[3] where ionic reactions are expected to constitute a significant segment of the overall reaction. For the gas-phase radiolysis of simple alkylbenzenes such as toluene, ethylbenzene, and xylenes, of interest is the product formation by the reactions of $C_7H_7^+$ ion, which is the most abundant ion in the mass spectra of these alkylbenzenes and whose structure and formation process have been extensively investigated mass spectrometrically.[4,5] In the previous paper[6] we reported that in the gas-phase radiolysis of toluene, ethylbenzene, and *m*-xylene the corresponding benzylated alkylbenzenes, alkyldiphenylmethanes, were formed as the main products in all cases, and their formation was suggested to be due to an ion–molecule reaction of the $C_7H_7^+$ ion.

In the present study of the gas-phase radiolysis of toluene, the formation of methyldiphenylmethanes (MDPM's) by the reaction of the $C_7H_7^+$ ion and that of other products were investigated in some detail. The mercury-photosensitized decomposition of gaseous toluene is included in this study for comparison with the radiolysis.

Experimental Section

Materials. Toluene was obtained from Wako Pure Chemical Industrial Co. and purified by the usual method. After the extensive distillations using a 1-m column packed with stainless helices, the purity determined chromatographically by flame-ionization detection was more than 99.99%. The purified toluene was dried over sodium, degassed, and stored in a high-vacuum line. Nitric oxide and nitrous oxide, both obtained from Takachiho Shoji Co., were purified by several low-pressure distillations.

Procedures. The irradiation cells were Pyrex cylinders of approximately 120-ml volume, and each cell was fitted with a break-seal. After the cells were evacuated at a pressure of 10^{-6} mm for ~10 hr with periodic heating by a hand torch, the toluene vapor from the storage was extensively dried by passing through a sodium mirror, degassed, and then introduced into the cells. The pressure of the samples was measured by a mercury manometer.

Samples were irradiated with γ rays from a 5000-Ci ^{60}Co source at room temperature. The dose rate to toluene was determined by ethylene dosimetry, using a G value of 1.28 for hydrogen formation[7] and correcting for the electron density of toluene relative to ethylene. The irradiations were carried out at a constant dose

(1) (a) J. Hoigne and T. Gaumann, *Helv. Chim. Acta*, **44**, 2141 (1961); (b) J. Hoigne and T. Gaumann, *ibid.*, **46**, 365 (1963); (c) J. Hoigne, W. G. Burns, W. R. Marsh, and T. Gaumann, *ibid.*, **47**, 247 (1964).

(2) J. Weiss and C. H. Collins, *Radiat. Res.*, **28**, 1 (1966).

(3) The G values of the radiolysis products in the gas phase including some discussion are reported by K. E. Wilzbach and L. Kaplan, Advances in Chemistry Series, No. 82, American Chemical Society, Washington, D. C., 1968, p 134.

(4) H. M. Grubb and S. Meyerson in "Mass Spectrometry of Organic Ions," F. W. McLafferty, Ed., Academic Press, New York, N. Y., 1963, p 453.

(5) A recent study is, for example, K. L. Rinehart, Jr., A. C. Buchholz, G. E. Van Lear, and H. L. Cantrill, *J. Amer. Chem. Soc.*, **90**, 2983 (1968).

(6) Y. Yamamoto, S. Takamuku, and H. Sakurai, *ibid.*, **91**, 7192 (1969).

(7) R. A. Back, T. W. Woodward, and K. A. McLauchlan, *Can. J. Chem.*, **40**, 1380 (1962).

Table I: Yields in the γ Radiolysis and Hg-Sensitized Photolysis of Toluene Vapor, and Comparison with Reported Yields in the Radiolysis

	Radiolysis			Hg-sensitized photolysis	
	Temp, °C				
	25	30[a]	50[b]	25	25
	Pressure, mm				
	10.7	7.5	Liquid	5.5	16.0
Products	G value			μmol	
H_2	0.36	0.47	0.14	0.034	0.097
CH_4	0.15	0.15	0.012	0.034	0.023
C_2H_2	0.41	0.64	0.002	n.d.[c]	n.d.
C_2H_4	Trace	0.10	0.0003	n.d.	n.d.
C_2H_6	0.07	0.06	...	0.017	0.006
Benzene	0.18	0.20	0.0188	0.137	0.101
Ethylbenzene	0.05	0.07	0.0012	0.079	0.066
o-Xylene	0.05[a]	0.02	0.0009	<0.01[d]	<0.01[d]
m-Xylene		0.06	0.0015		
p-Xylene		0.007	0.0010		
2-MDPM	0.05	...	...	*e*	*e*
3-MDPM	0.34	...	0.0097	*e*	*e*
4-MDPM	0.05	...	0.0102	*e*	*e*
Bibenzyl	0.03	...	0.0715	0.181	0.254

[a] Data of Wiltzbach and Kaplan (ref 3). [b] Data of Weiss and Collins (ref 2). In their work many other product yields are determined such as: G(methylcyclohexadiene), 62.30×10^{-3}; G(dimethylcyclohexenes), 8.90×10^{-3}; G(benzylmethylcyclohexadiene), 23.9×10^{-3}; G(2,3-dimethylbiphenyl), 43.2×10^{-3}. [c] Not detectable. [d] In this work three isomers of xylene were not separated. [e] In the photolysis several dimeric products other than bibenzyl were formed but in much smaller yields.

rate of 3.91×10^{15} eV/(hr μmol) for toluene. After irradiation, the cell was sealed to a high-vacuum line, and the break-seal was ruptured after evacuation. The gases volatile at −196°, hydrogen and methane, were collected with a standard Toepler pump and analyzed by measurement of the volumes with a gas buret before and after removing hydrogen through a palladium thimble heated up to 300°. The residual products were analyzed with a gas chromatograph using a flame-ionization detector. The gas fraction volatile at −120° containing C_2 to C_4 hydrocarbons and the liquid products except dimers were analyzed with 3-m silica gel and Apiezon L columns, respectively, at 100°. For the analysis of dimers, a 6-m mixed nitrate column[8] was used with temperature programming from 60 to 120°, and the retention times of the dimers, 2-, 3-, 4-MDPM, and bibenzyl, were 31, 33, 34, and 38 min, respectively. The yields of the gaseous and liquid products were determined by comparison of peak areas with those for known amounts of propane and benzene, respectively, which were submitted to gas chromatography before each analysis. The calibration for flame-ionization detection was carried out using known amounts of authentic gases and propane or standard mixtures of authentic liquids and benzene.

The authentic samples, 2- and 4-MDPM were prepared by Friedel–Crafts benzylation of toluene according to the experiment of Olah, Kuhn, and Flood.[9] Authentic 3-MDPM was also prepared under the same condition by Friedel–Crafts substitution of benzene with *m*-xylyl chloride which was prepared by the method of Kharasch and Brown.[10]

The mercury-photosensitized decomposition of gaseous toluene was carried out in a cylindrical quartz cell (5 cm in diameter and 5 cm long) with a low-pressure mercury lamp at room temperature. The procedures of sampling and analysis were the same as those in the radiolytic study.

Results

The G values of the products in the gas-phase radiolysis of toluene at 10.7 mm and a dose of 1.9×10^{19} eV are presented in Table I with the results of previous studies both in the gas and liquid phase. At 10.7 mm of toluene pressure the G values were also obtained at the doses of 1.2×10^{19} and 2.4×10^{19} eV, and the dose effect was not observed for all products. The mercury-photosensitized decomposition of gaseous toluene was investigated over the pressure range from 2 to 19 mm, and the results at the two pressures are also presented in the table. The photolysis is thought to be initiated by the 2537-Å irradiation, and some features of the decomposition are in agreement with those of the direct photolysis previously reported, where dimeric products are not analyzed.[11,12]

(8) W. W. Hanneman, C. F. Spencer, and J. F. Johnson, *Anal. Chem.*, **32**, 1386 (1960).

(9) G. A. Olah, S. J. Kuhn, and S. H. Flood, *J. Amer. Chem. Soc.*, **84**, 1688 (1962).

(10) M. S. Kharasch and H. C. Brown, *ibid.*, **61**, 2142 (1939).

(11) K. E. Wilzbach and L. Kaplan, *ibid.*, **86**, 2307 (1964).

(12) As previously indicated by Hentz and Burton (see ref 14), the irradiations of the mixtures of toluene and mercury vapors with 2537 Å may result in competitive absorptions by toluene molecules and mercury atoms, and both the direct and mercury-sensitized photolysis could occur.

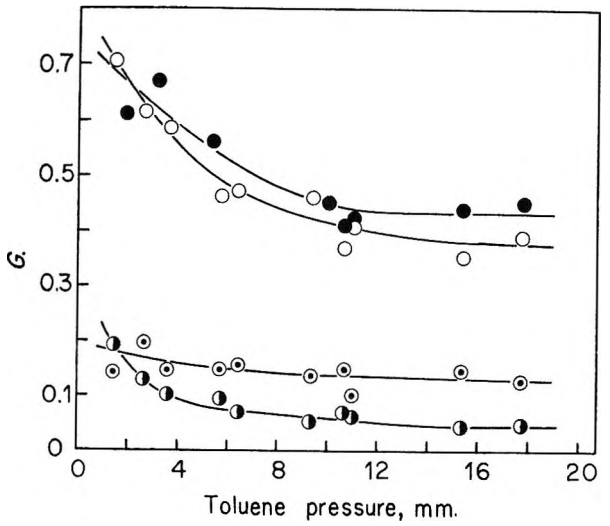

Figure 1. The pressure dependence of the gaseous product yields in the radiolysis of toluene vapor: ○, $G(H_2)$; ⊙, $G(CH_4)$; ◑, $G(C_2H_6)$; ●, $G(C_2H_2)$.

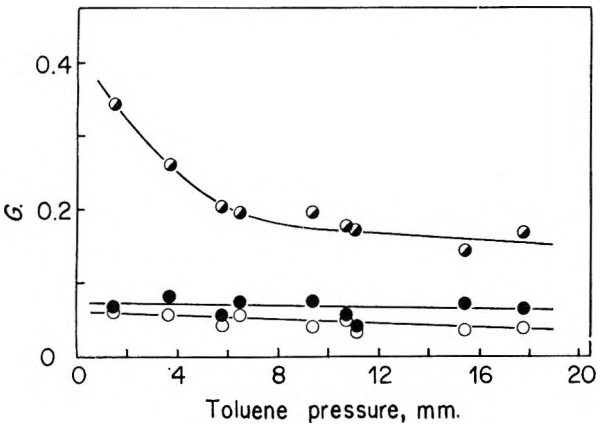

Figure 2. The pressure dependence of the liquid product yields in the radiolysis of toluene vapor: ◒, G(benzene); ●, G(xylenes); ○, G(ethylbenzene).

As also indicated previously by Wilzbach and Kaplan,[3] the yields of all products in the gas-phase radiolysis were greater than those in the liquid-phase radiolysis. The dimeric product with the greatest G value was 3-MDPM, while the most abundant product was bibenzyl in the liquid-phase radiolysis as well as in the gas-phase photolysis. Another notable discrepancy is the formation of various kinds of monomeric and dimeric products with partially hydrogenated rings in the liquid-phase radiolysis[13] with contrast to in the gas-phase radiolysis, indicating that the addition of hydrogen atoms to aromatic rings is important in the liquid phase but not in the gas phase.

Figures 1, 2, and 3 show the pressure dependence of the product yields at a dose of 2.8×10^{17} eV/μmol for toluene. The yield of 4-MDPM, the minor dimeric product, was almost the same as that of 2-MDPM at all the pressures studied and was excluded in the figure.

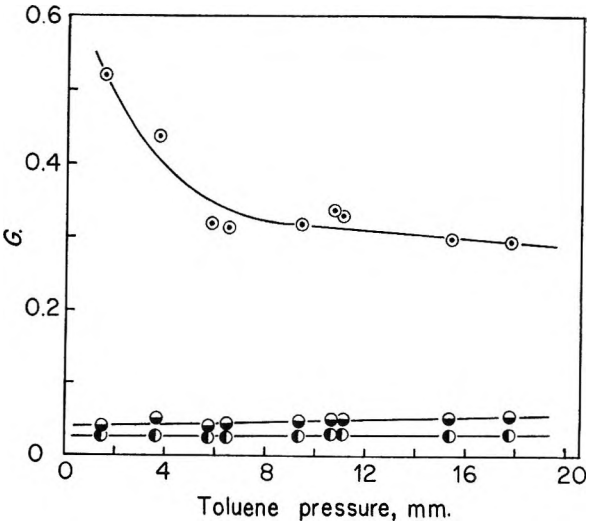

Figure 3. The pressure dependence of the dimeric product yields in the radiolysis of toluene vapor: ◒, G(2-MDPM); ⊙, G(3-MDPM); ◐, G(bibenzyl).

The effects of nitric oxide and nitrous oxide added as radical and electron scavengers, respectively, were studied at a dose of 1.9×10^{19} eV and at 11 mm of toluene pressure. At the minimum concentration of added NO (2.6 mol %), ethane, ethylbenzene, xylenes, and bibenzyl disappeared and, as is shown in Figure 4, benzene was reduced to a constant G value, 0.10. On the other hand, three isomers of MDPM were not appreciably affected with the addition of NO and acetylene increased slightly with increasing NO concentration as shown in the figure.

When 8.1 mol % NO was added in the mercury-photosensitized decomposition of toluene at a pressure of 12 mm, the yields of ethane, benzene, ethylbenzene, and bibenzyl decreased by 46, 7, 77, and 54%, respectively. In the photolysis all the products are considered to be formed through radicals as noted in the Discussion. Hence the observed lower efficiency of radical scavenging by added NO in the photolysis than that in the radiolysis is attributable to the facts that the photolysis occurs in the limited region close to the window faced to the lamp and the only limited amount of added NO contributes to the reaction, and that the yield of radicals is much more in the photolysis than that in the radiolysis.

When N_2O was added, the most apparent effect on the product yields was the increase of the dimers, MDPM's and bibenzyl, as shown with solid lines in Figure 5. The other effects of added N_2O were the slight increases of ethylbenzene and acetylene and the slight decreases of ethane and benzene.

When two sets of scavengers, different amounts of N_2O and 10 mol % NO, were added, MDPM's did not

(13) The yields of these products are not presented in Table I, but some of those are shown in the footnote *b* in the table.

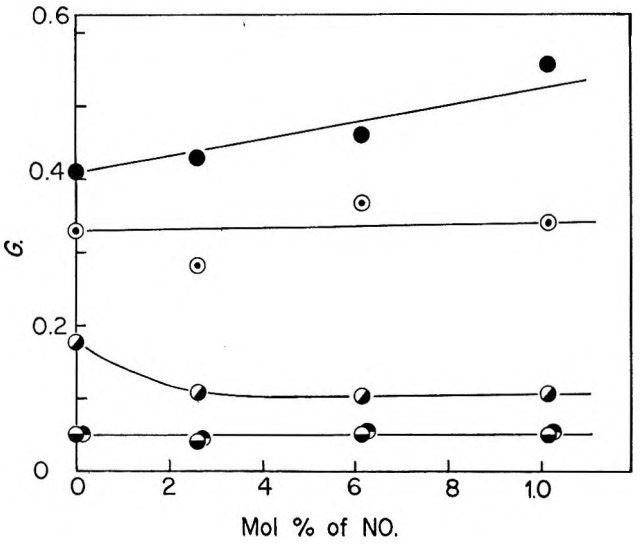

Figure 4. The effect of added NO in the radiolysis of toluene vapor (11 mm): ●, $G(C_2H_2)$; ◕, G(benzene); ◒, G(2-MDPM); ⊙, G(3-MDPM); ◓, G(4-MDPM).

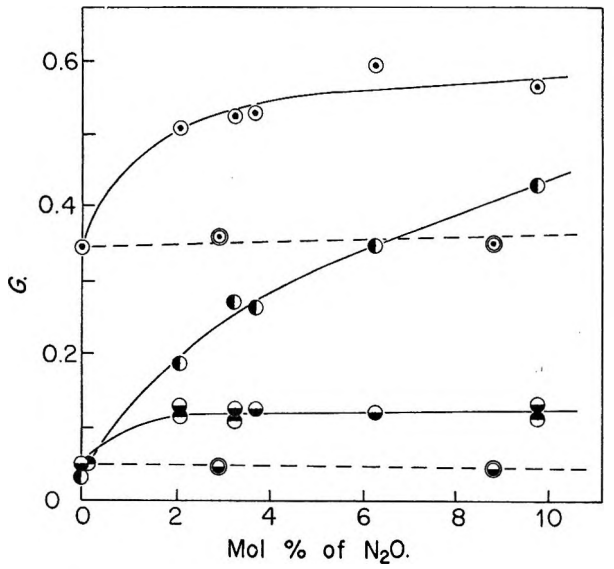

Figure 5. The effects of added N_2O and N_2O–NO in the radiolysis of toluene vapor (11 mm): ◒, G(2-MDPM); ⊙, G(3-MDPM); ◓, G(4-MDPM); ◐, G(bibenzyl); ⊜, G(3-MDPM), N_2O–10 mol % NO; ◒, G(2-MDPM) and G(4-MDPM), N_2O–10 mol % NO.

increase but showed the same yield as that observed in the case of pure toluene, as shown with dotted lines in Figure 5, and dibenzyl disappeared. The yields of other products when these sets of scavengers were added were almost the same as those when 10 mol % NO was added alone (Figure 4).

When these additives were added, the yields of hydrogen and methane were not determined because of the interference of the additives with an accurate determination.

Discussion

Comparison of Photolysis and Radiolysis. The direct and mercury-sensitized photolysis at 2537 Å of gaseous toluene have been investigated by several workers[11,14,15] and the main bond fissions are known to occur at the C–H bond β to the ring and the C–C bond α to the ring. In our study the observed product formation can be attributed to the reactions of the radicals produced by such bond fissions, *i.e.*, combinations, and hydrogen abstractions from toluene molecules

$$C_6H_5CH_3 \xrightarrow[Hg]{h\nu} C_6H_5CH_3^* \quad (1)$$

$$C_6H_5CH_3^* \longrightarrow C_6H_5CH_2\cdot + H \quad (2)$$

$$C_6H_5CH_3^* \longrightarrow C_6H_5\cdot + CH_3\cdot \quad (3)$$

$$R\cdot + C_6H_5CH_3 \longrightarrow RH + C_6H_5CH_2\cdot \quad (4)$$

$$R\cdot + R\cdot \longrightarrow R{-}R \quad (5)$$

where R· represents any radical produced in the primary processes or by hydrogen abstraction from toluene. The low relative yield of xylenes, thought to be formed by the combination of methyl and tolyl radicals, indicates that the formation of tolyl radical is not important or tolyl radical readily changes to benzyl radical by hydrogen abstraction from toluene.

If it is assumed that hydrogen, methane, and benzene are formed only by hydrogen abstraction reaction (4) and the consumption of the radicals by the formation of higher polymers is neglected, the yields of the radicals produced in the primary processes (reactions 2 and 3) are obtained by eq 6–8. Such yields of the radicals

$$[C_6H_5CH_2\cdot] = 2[\text{bibenzyl}] + [\text{ethylbenzene}] - \{[H_2] + [CH_4] + [\text{benzene}]\} \quad (6)$$

$$[C_6H_5\cdot] = [\text{benzene}] \quad (7)$$

$$[CH_3\cdot] = [CH_4] + 2[C_2H_6] + [\text{ethylbenzene}] \quad (8)$$

were obtained over the pressure range from 2 to 19 mm and plotted in Figure 6. As shown in this figure the pressure dependence of the yield of benzyl radical is different from that of methyl and phenyl radicals, which are almost equivalent over the entire pressure range studied. Although the above equations are based on the assumptions mentioned, such a result is considered to support the suggestion of Sehon and Darwent[15] that different excited states contribute to the primary processes 2 and 3. On the other hand, in the gas-phase radiolysis of toluene, ethane, ethylbenzene, xylenes, bibenzyl, and some benzene were shown to be formed through radical reactions with the effect of added NO. The processes of the formation of these products and the precursors of the radicals,

(14) R. R. Hentz and M. Burton, *J. Amer. Chem. Soc.*, **73**, 532 (1951).

(15) A. H. Sehon and B. deB. Darwent, *J. Chem. Phys.*, **23**, 822 (1955).

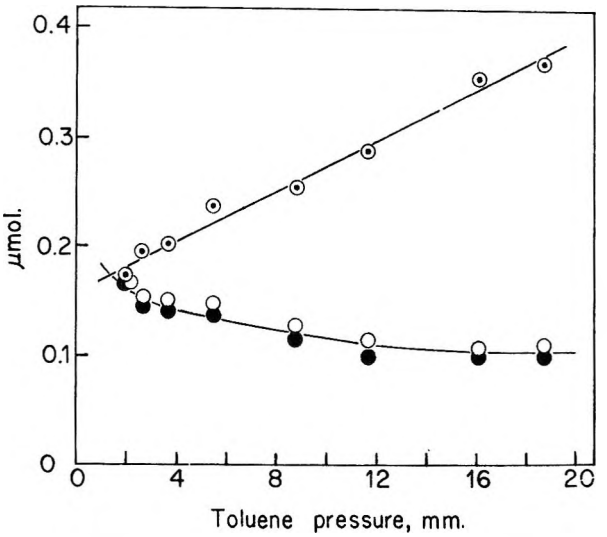

Figure 6. The pressure dependence of the radical yields in the primary process of the Hg-sensitized photolysis: ⊙, $[C_6H_5CH_2\cdot]$; ●, $[C_6H_5\cdot]$; ○, $[CH_3\cdot]$.

i.e., excited molecules, are considered to be the same as those in the photolysis. The relative yields of ethylbenzene and bibenzyl, which are formed through benzyl radicals, were much smaller than those in the photolysis. This fact indicates that the benzyl radical formation in the primary process is only minor in the radiolysis, while it is considered to be major in the photolysis from the result shown in Figure 6.

The formation of acetylene and MDPM's, which were not detected in the photolysis, is attributable to nonradical processes on the basis of the effect of added NO (Figure 4).

Nonradical Processes in the Gas-Phase Radiolysis of Toluene. Mass spectrometric studies are one of the important sources of information relating to the ionic processes in the gas-phase radiolysis. In the mass spectrum of toluene it is well known that $C_7H_7^+$ ion is the most abundant ion and partially decomposes to $C_5H_5^+$ ion and C_2H_2.[4] Furthermore, on the basis of the isotope randomization observed in the mass spectra of labeled toluenes, the $C_7H_7^+$ and $C_5H_5^+$ ions have been suggested to be tropylium and cyclopentadienyl ions, respectively, as shown in eq 9.[4,5]

$$+ \; C_2H_2 \qquad (9)$$

On the other hand, in the recent studies of ion–molecule reactions of gaseous aromatic hydrocarbons by high-pressure mass spectrometry[16,17] it is reported that the dominant product ions are dimeric ions at higher pressure, and for toluene such dimeric ions are $C_{14}H_{15}^+$ and $C_{14}H_{16}^+$ formed by the addition of the $C_7H_7^+$ and $C_7H_8^+$ ions to toluene, respectively. In the gas-phase radiolysis of toluene, which is carried out at much higher pressures than mass spectrometry, these dimeric ions are expected to contribute to the product formation. We suggested in the previous paper[6] that MDPM's are formed *via* the $C_{14}H_{15}^+$ ions, *i.e.*, through an electrophilic substitution reaction by the $C_7H_7^+$ ions, on the basis of the following observations. (1) The G values of MDPM's were not affected with nitric oxide added as a radical scavenger. (2) The analogous benzylation reactions leading to the formation of alkyldiphenylmethanes were also observed in the radiolysis of ethylbenzene and *m*-xylene, which are known to produce the $C_7H_7^+$ ions in the mass spectra as well as toluene.[4,18]

The formation of MDPM's *via* the $C_{14}H_{16}^+$ ions, formed by the addition of the parent ions to toluene molecules, may be neglected considering the results of ethylbenzene and *m*-xylene radiolysis, where C_{16} hydrocarbons were minor products.[19] In this regard, the study by Field, Hamlet, and Libby on the temperature effect in the high-pressure mass spectrometries of benzene and of benzene–toluene mixtures is instructive.[20] They reported that the rise of temperature results in an increase of the relative intensity of $C_6H_6^+$ ion and a decrease of that of the dimeric ion, $(C_6H_6)_2^+$, and that similar temperature dependences of the relative intensities of monomeric and dimeric ions are also observed in the case of toluene molecular ion and the dimeric ion, $(C_7H_8)_2^+$. On the basis of such observations they suggested that these monomeric and dimeric ions are in equilibrium, for example

$$C_6H_6^+ + C_6H_6 \rightleftarrows (C_6H_6)_2^+ \qquad (10)$$

with contrast to $C_6H_5^+$ and $C_6H_6\cdot C_6H_5^+$ ions, whose relative intensities are almost independent of temperature. In view of the above data it seems reasonable to assume that such dimeric ions, formed from aromatic molecular ions, produce no dimer in the gas-phase radiolysis because these are the loosely bonded π complexes, which may not be transformed into σ complexes.[21] On the other hand, one might think that

(16) S. Wexler and R. P. Clow, *J. Amer. Chem. Soc.*, **90**, 3940 (1968).

(17) A. Giardini-Guidoni and F. Zocchi, *Trans. Faraday Soc.*, **64**, 2342 (1968).

(18) Other evidences for this suggestion were also obtained. (i) In the rare gas-sensitized radiolysis of gaseous toluene the sensitizing effect on the formation of MDPM's was observed to decrease in the order Ar > Kr > Xe, suggesting that the precursor of MDPM's is a fragment ion but not an excited molecule or the parent ion. (ii) In the gas-phase radiolysis of the mixture of toluene-d_8 and cycloheptatriene-h_8, which is also known to produce the $C_7H_7^+$ ion in the mass spectrum, $CD_3C_6D_4CH_2C_6H_5$ was formed as well as $CD_3C_6D_4CD_2C_6D_5$. These investigations are to be published in separate papers.

(19) In the high-pressure mass spectra of xylenes (ref 17), the dominant ions at higher pressure are also C_{15} and C_{16} ions formed from the $C_7H_7^+$ and parent ions, respectively, and a similar result is to be expected for ethylbenzene though the data are lacking.

(20) F. H. Field, P. Hamlet, and W. F. Libby, *J. Amer. Chem. Soc.*, **91**, 2839 (1969).

(21) In the gas-phase radiolysis of benzene [R. R. Hentz and S. J. Rzad, *J. Phys. Chem.*, **72**, 1027 (1968)] the G value of the dimeric product, biphenyl, is relatively small when NO is added, in spite of the large relative intensity of the $(C_6H_6)_2^+$ ion (see ref 16, 17, and 20), suggesting that the $(C_6H_6)_2^+$ ion does not contribute to the formation of biphenyl.

carbonium ions such as $C_6H_5^+$ and $C_7H_7^+$ add to aromatic rings to form σ complexes leading to the formation of substitution products.

In the previous paper[6] the isomer distribution of MDPM's was discussed and accounted for by the isomerization of the σ complexes, $C_{14}H_{15}^+$, from Ia and Ib to Id as shown with the following scheme.

Scheme I

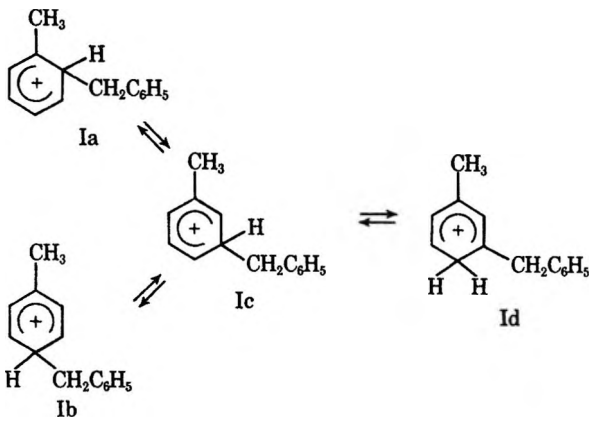

where the stabilities of these complexes, I, increase in the order Id > Ia ≃ Ib > Ic. The yield of 3-MDPM decreased with increasing pressure, while those of other two isomers were almost independent of pressure (Figure 3). Such a result suggests that the reactivities of the complexes I depend on the structures or the magnitudes of the excess energies of I. On this basis, the possible mode of the formation of MDPMs is considered as

$$C_7H_7^+ + C_6H_5CH_3 \rightleftarrows (C_{14}H_{15}^+)^* \quad (11)$$
$$\text{I}^*$$

$$\text{I}^* + C_6H_5CH_3 \longrightarrow$$

$$\text{MDPM} + C_7H_9^+ \quad \text{(minor)} \quad (12)$$

$$\longrightarrow \text{I} + C_6H_5CH_3 \quad \text{(major)} \quad (13)$$

$$\text{Ia, b, c} \longrightarrow \text{Id} \quad (14)$$

$$\text{Id} + C_6H_5CH_3 \longrightarrow \text{3-MDPM} + C_6H_9^+ \quad (15)$$

$$\rightleftarrows (C_{21}H_{23}^+)^* \quad (16)$$

$$(C_{21}H_{23}^+)^* + C_6H_5CH_3 \longrightarrow C_{21}H_{22} + C_7H_9^+ \quad (17)$$

$$\longrightarrow C_{21}H_{23}^+ + C_6H_5CH_3 \quad (18)$$

Thus, the highly excited complexes, I*, produce three isomers of MDPM by the proton-transfer process 12, which is analogous to that reported in the study of the reactions of toluene with He^3H^+ ions,[22] but not trimeric ions. On the other hand, the complexes I, having less excess energies, isomerize to the most stable one, Id, which produces 3-MDPM or a trimeric ion. The proton transfer reaction (15) is thought to be somewhat endothermic, and it is required for Id to have some excess energies which are less than the activation energy of the isomerization process (Scheme I). Considering the effect of added N_2O–NO mixtures, indicating that the yields of MDPMs are not affected with electron captures by N_2O as discussed below, the proton-transfer reaction 15 seemed probable for the process of the formation of 3-MDPM from Id. However, the $C_{14}H_{15}^+$ ions are considered to be rather stable and relatively long-lived species as previously reported,[16] and if the anions such as O^- and OH^-, formed by the reactions 22 and reactions 24 and 26, respectively, described below, might contribute to ion neutralizations in the presence of N_2O instead of electrons, the following processes could not be neglected. On this problem further investigations are required.

$$C_{14}H_{15}^+ + e \longrightarrow \text{MDPM} + H \quad (19)$$

$$C_{14}H_{15}^+ \longrightarrow C_{14}H_{14}^+ + H \quad (20)$$

$$C_{14}H_{14}^+ + e \longrightarrow \text{MDPM} \quad (21)$$

Generally a great number of investigations have been undertaken on the electrophilic substitution reactions of aromatic compounds in solutions, but little attention has been paid to those in the gas phase. The radiolysis is felt to be a useful tool in the investigations of such ionic reactions in the gas phase.[23]

Hentz and Rzad reported mechanisms for acetylene formation in the gas-phase radiolysis of benzene[21] by comparison with the vacuum ultraviolet photolysis with the Xe and Kr resonance lamps.[24] They concluded that acetylene is formed from either superexcited molecules or ion–molecule reactions of $C_6H_5^+$ with C_6H_6 or both. In the radiolysis of toluene the same processes may contribute to the acetylene formation as well as reaction 9.

The mechanism of the formation of benzene unscavengeable by added NO is not clear, but the possible processes are thought to involve hot radicals or $C_6H_5^+$ ions, known to be the product ions in the mass spectrum of toluene.[4]

The Effect of Added N_2O. When N_2O was added, MDPM's and bibenzyl showed a marked increase (Figure 5). To investigate the processes of the additional formation of these dimers, 10 mol % NO was added to the toluene–N_2O mixtures. In such mixtures no increase of MDPM's was seen and bibenzyl disappeared. Such a result indicates that these additional dimer formation is due to radical reactions. The considerable increase of the bibenzyl yield with increasing N_2O concentration suggests that benzyl radicals are formed in a large yield in the presence of N_2O.

(22) F. Cacace and S. Caronna, *J. Amer. Chem. Soc.*, 89, 6848 (1967).

(23) In our laboratory the propylations of aromatic hydrocarbons with propyl cations in the gas-phase radiolysis of the mixtures of propane with aromatic hydrocarbons are under investigation, and the results are to be published.

(24) R. R. Hentz and S. J. Rzad, *J. Phys. Chem.*, 71, 4096 (1967).

On the other hand, the yields of MDPM's are not appreciably affected by N_2O concentrations above about 3 mol %, and such a dependence on N_2O concentration is different from that of bibenzyl. Thus, the additional formation of MDPM's is thought to be due to the combination of benzyl and tolyl radicals but not due to the reaction of benzyl radicals and toluene molecules.[25] It is also observed that ethylbenzene slightly increased while the yield of xylenes, formed by the combination of tolyl and methyl radicals, did not vary. On the basis of the above results, tolyl radicals may also be formed in the presence of N_2O as well as benzyl radicals but in a limited amount.

In the gas-phase radiolysis of hydrocarbons N_2O has been generally used as an electron scavenger, but the observed effects are often complicated because of reactions subsequent to electron capture by N_2O, which have been attributed to the O^- ions formed as[21,26-28]

$$e + N_2O \longrightarrow N_2 + O^- \qquad (22)$$

For aromatic hydrocarbons Hentz and Rzad[21] reported the formation of large yields of nitrogen and phenol in the radiolysis of the benzene–N_2O mixtures, and Rzad and Warman[26] in a further investigation of the mechanism of the formation of these products proposed a short-chain mechanism including the O^- ions.

In the radiolysis of the toluene–N_2O mixtures it seems also reasonable to conclude that benzyl and tolyl radicals are formed by reactions of the O^- ions with toluene molecules.

The plot of $1/G(N_2)$ *vs.* $1/[N_2O]$ gives a good straight line as shown in Figure 7, indicating that the formation of N_2 involves a competition between electron capture (22) and ion neutralization (23).[26,28] Values of $Gm(N_2)$,

$$e + M^+ \longrightarrow M^* \qquad (23)$$

the yield of nitrogen when all the electrons are captured by N_2O, and $\sqrt{k_{23}/k_{22}}$ are obtainable from the values of the slope and intercept of this plot,[26,28] and these values obtained in this study were 6.3 and 1.6 $\times$ 10^{11} (molecule cm^{-3} $sec)^{1/2}$, respectively, using 27 for the value of W, the energy in electron volts required to form one ion pair. In the radiolysis of the benzene–N_2O mixtures[21] it is reported that $Gm(N_2)$ is 29, indicating a short-chain mechanism for the formation of N_2, and the value of $\sqrt{k_{23}/k_{22}}$ is 3.6 $\times$ 10^{11}.

Of interest is the difference of the effect of added N_2O in the radiolysis of benzene and of toluene, and it may be attributed to the inductive effect of the methyl group in the toluene molecule resulting in a higher electron density of the aromatic ring.

The possible mechanism of the reactions of the O^- ions with toluene molecules leading to the formation of benzyl and tolyl radicals is thought to be

$$O^- + C_6H_5CH_3 \longrightarrow (OC_6H_5CH_3^-) \longrightarrow \cdot C_6H_4CH_3 + OH^- \qquad (24)$$

(II)

$$\cdot C_6H_4CH_3 + C_6H_5CH_3 \longrightarrow C_6H_5CH_3 + C_6H_5CH_2\cdot \qquad (25)$$

$$O^- + C_6H_5CH_3 \longrightarrow C_6H_5CH_2\cdot + OH^- \qquad (26)$$

Thus, the O^- ion is considered to attack the electron-deficient methyl group of toluene as well as the aromatic ring.[29] The anion II is an unstable intermediate and readily decomposes to tolyl radical and OH^- because of the higher electron density of the ring of toluene. On the other hand, in the radiolysis of the benzene–N_2O mixtures the corresponding anion, $C_6H_6O^-$, is more stable and reacts with N_2O to form phenol and initiate a chain process.[26]

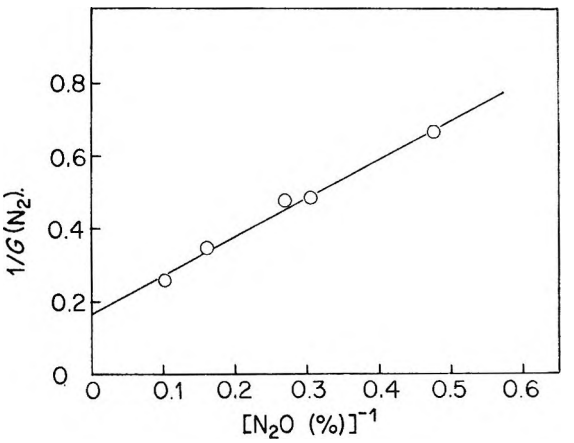

Figure 7. Kinetic plots of $G(N_2)$ in the radiolysis of toluene vapor with N_2O.

The yields of MDPM's did not vary when a set of scavengers, N_2O and NO, indicating that the yields of the MDPM's formed from the $C_7H_7^+$ ions are not affected with electron capture by N_2O.

As previously mentioned, the $C_7H_7^+$ ions from toluene are suggested to be tropylium ions in the mass spectrometric studies.[4,5] However, in the present study of the gas-phase radiolysis of toluene any evidence to support such a suggestion was not obtained, while it has been found that the $C_7H_7^+$ ions react with toluene

(25) This idea is probable considering the result of the photolysis, where MDPMs yields were negligible while benzyl radicals, producing ethylbenzene and bibenzyl, were formed in a large yield.

(26) S. J. Rzad and J. M. Warman, *J. Phys. Chem.*, 72, 3013 (1968).

(27) (a) W. J. Holtslander and G. R. Freeman, *Can. J. Chem.*, 45, 1661 (1967); (b) W. J. Holtslander and G. R. Freeman, *J. Phys. Chem.*, 71, 2562 (1967).

(28) (a) G. R. A. Johnson and J. M. Warman, *Trans. Faraday Soc.*, 61, 1709 (1965); (b) J. M. Warman, *Nature*, 213, 381 (1967); (c) J. M. Warman, *J. Phys. Chem.*, 71, 4066 (1967).

(29) The analogous reaction, the hydrogen abstraction from aliphatic hydrocarbon molecules by the O^- ions, is reported in ref 27.

molecules to form MDPM's. We are further investigating the structure of the $C_7H_7^+$ ions in the gas-phase radiolysis.

Acknowledgment. We thank Mr. Tamotsu Yamamoto and Mr. Tomikazu Sawai in the Radiation Laboratory for assistance in the γ irradiations.

On the Photoreduction of Acetophenone

by Frederick D. Lewis

Department of Chemistry, Northwestern University, Evanston, Illinois 60201 *(Received April 23, 1970)*

The photoreduction of acetophenone in 2-propanol–benzene solution has been reexamined. The effect of 2-propanol concentration on quantum yields and apparent triplet decay rate constants is attributed to the presence of a quenching impurity in commercial 2-propanol. The value for the triplet decay rate constant in 0.1 *M* 2-propanol, 3.4×10^5 sec^{-1}, is in accord with values obtained by phosphorescence decay studies and is similar to the limiting value for benzophenone triplet decay in benzene solution.

The photoreduction of aromatic ketones with 2-propanol is one of the most intensely studied areas of solution photochemistry. Kinetic studies and quantum yield determinations have provided information about the reactivity and lifetime of the triplet states of benzophenone,[1-10] acetophenone,[11-14] and their derivatives. However, several types of evidence have been reported which indicate that the mechanism of these photoreduction reactions is far from simple.[15,16] First, the quantum yield for disappearance of acetophenone[12] or benzophenone[11] is reported to increase with 2-propanol concentration at low concentrations, but to decrease at high ($\gtrsim 1$ *M*) concentrations of 2-propanol. This phenomenon has been related[12] to the observation of highly absorbing and/or quenching by-products or intermediates formed in the photoreduction reactions of acetophenone[12] and benzophenone[1,6-9] in concentrated 2-propanol solutions. Second, values for triplet decay rate constants (*vide infra*) determined in 2 *M* 2-propanol–benzene for acetophenone (1.6×10^6 sec^{-1})[14] and benzophenone (7.3×10^5 sec^{-1})[10] are disturbingly greater than values obtained in recent phosphorescent decay studies (3.0×10^6 sec^{-1} for acetophenone and 1.9×10^5 sec^{-1} for benzophenone).[17] Using benzhydrol as the hydrogen donor for benzophenone photoreduction a value of 3×10^5 sec^{-1} is obtained.[16] Finally, there is no *a priori* reason to expect the triplet decay rate constant for acetophenone to be substantially greater than that for benzophenone.

We wish to present evidence obtained from a detailed reinvestigation of acetophenone photoreduction that both the anomalous quantum yields and rate constants are due to a quenching impurity in commercial 2-propanol.

The generally accepted mechanism for reduction of acetophenone (A) by 2-propanol (RH) in the presence of a quencher (Q) can be described by the following equations.

$$A \xrightarrow{h\nu} A^1 \xrightarrow{k_{ST}} A^3 \qquad (1)$$

$$A^3 \xrightarrow{k_d} A \qquad (2)$$

(1) J. N. Pitts, R. L. Letsinger, R. P. Taylor, J. M. Patterson, G. Recktenwald, and R. B. Martin, *J. Amer. Chem. Soc.*, **81**, 1068 (1959).

(2) J. N. Pitts, W. H. Johnson, and T. Kuwana, *J. Phys. Chem.*, **66**, 2456 (1962).

(3) A. Beckett and G. Porter, *Trans. Faraday Soc.*, **59**, 2051 (1963).

(4) W. M. Moore and M. D. Ketchum, *J. Phys. Chem.*, **68**, 214 (1964).

(5) S. G. Cohen and R. J. Baumgarten, *J. Amer. Chem. Soc.*, **89**, 3471 (1967).

(6) S. G. Cohen and J. I. Cohen, *Tetrahedron Lett.*, 4823 (1968); *Israel J. Chem.*, **6**, 757 (1968).

(7) H. J. L. Bäckström, K. L. Appelgren, and R. J. V. Niclasson, *Acta Chem. Scand.*, **19**, 1555 (1965).

(8) G. O. Schenck, M. Cziesla, K. Eppinger, G. Matthias, and M. Pape, *Tetrahedron Lett.*, 193 (1967).

(9) N. Filipescu and F. L. Minn, *J. Amer. Chem. Soc.*, **90**, 1544 (1968); *J. Chem. Soc., B*, 84 (1969).

(10) N. C. Yang and R. L. Dusenbery, *Molecular Photochem.*, **1**, 159 (1969).

(11) S. G. Cohen, D. A. Lanfer, and W. V. Sherman, *J. Amer. Chem. Soc.*, **86**, 3060 (1964).

(12) S. G. Cohen and B. Green, *ibid.*, **91**, 6824 (1969).

(13) N. C. Yang, D. S. McClure, S. L. Murov, J. J. Houser, and R. Dusenbery, *ibid.*, **89**, 5466 (1967).

(14) N. C. Yang and R. L. Dusenbery, *ibid.*, **90**, 5899 (1968).

(15) Similar observations have recently been made in the case of benzophenone photoreductions.[16]

(16) P. J. Wagner, *Molecular Photochem.*, **1**, 71 (1969).

(17) W. C. K. Clark, A. D. Litt, and C. Steel, *Chem. Commun.*, 1087 (1969).

$$A^3 + Q \xrightarrow{k_q} A + Q^3 \quad (3)$$

$$A^3 + RH \xrightarrow{k_r} Ph\overset{OH}{\underset{}{C}}(CH_3)\dot{} + (CH_3)_2\dot{C}OH \quad (4)$$

$$(CH_3)_2\dot{C}OH + A \xrightarrow{k_i} Ph\overset{OH}{\underset{}{C}}(CH_3)\dot{} + (CH_3)_2CO \quad (5)$$

$$2Ph\overset{OH}{\underset{}{C}}(CH_3)\dot{} \xrightarrow{k_t} \text{pinacol} \quad (6)$$

Assuming that the initially formed radicals (step 4) all proceed to products, the usual Stern–Volmer eq 7 and 8 are derived in the absence and presence of quencher, respectively.

$$\frac{1}{\varphi} = 1 + \frac{k_d}{k_r[RH]} \quad (7)$$

$$\frac{1}{\varphi} = \frac{k_r[RH] + k_d}{k_r[RH]} + \frac{k_q[Q]}{k_r[RH]} \quad (8)$$

The variation in quantum yield with 2-propanol concentration in degassed benzene solution[18] was determined for acetone and pinacol formation and for loss of acetophenone using purified reagent grade 2-propanol. Acetone formation could be followed at low conversion (<5%) by gas chromatography, whereas higher conversions (<20%) were necessary for determination of the loss of acetophenone. Although the absolute quantum yields given in Table I may be in error by ±5%, the relative quantum yields for acetone formation are considerably more accurate (±2%). The data in Table I are in accord with steps 1–6 in the general mechanism which require that $\Phi_{acetone} = \Phi_{pinacol} = {}^1/_2\Phi_{-acetophenone}$. The quantum yield for acetone formation as a function of 2-propanol concentration was also determined using 2-propanol prepared by lithium aluminum hydride reduction of Spectrograde acetone.[19] The results are included in the last column of Table I.

Table I: Quantum Yields of the Photoreduction of Acetophenone in 2-Propanol–Benzene Solutions

2-Propanol, *M*	Φ^a Acetone	Φ^b Pinacol	Φ^b −Acetophenone	Φ^c Acetone
0.10	0.166	...	...	0.167
0.125	0.202	0.16	0.32	0.202
0.167	0.259	0.19	0.43	0.260
0.20	0.276	...	...	...
0.25	0.348	0.30	0.63	0.324
0.50	0.356	0.36	0.71	0.376
1.0	0.354	0.38	0.75	0.410
1.5	0.360	...	...	...
2.0	0.376	0.37	0.74	0.456
3.0	0.371	...	...	...
4.0	0.386	...	...	0.465
12.8	...	...	...	0.483

[a] Quantum yield in commercial 2-propanol at <5% conversion ±2% relative accuracy. [b] Quantum yield in commercial 2-propanol at <20% conversion ±5% relative accuracy. [c] Quantum yield in synthetic 2-propanol at <5% conversion ±2% relative accuracy.

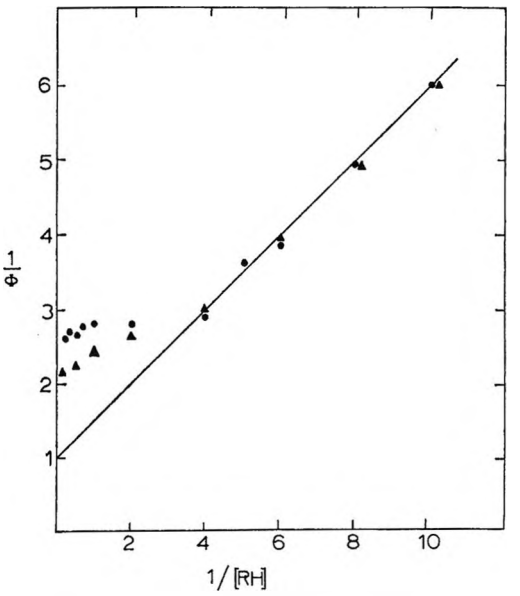

Figure 1. Dependence of quantum yield for photoreduction of acetophenone upon 2-propanol concentration for commercial (●) and synthetic (▲) 2-propanol.

A plot of $1/\varphi_{acetone}$ *vs.* $1/[RH]$ (Figure 1) is linear for concentrations of 2-propanol less than 0.25 *M*. The slope (k_d/k_r) is equal to 0.50 and the extrapolated intercept is 1.0 as required by the assumed mechanism (eq 7). Any intercept other than 1.0 (or 0.5 for loss of acetophenone[20]) demands that either the mechanism or the experimental data be incorrect. At concentrations of 2-propanol less than 0.25 *M* the plot of $1/\varphi$ *vs.* $1/[RH]$ levels off; however, more noticeably so for the commercial 2-propanol samples than for the 2-propanol obtained by reduction of acetone. In neither case was a decrease in quantum yield observed in concentrated 2-propanol solutions as reported by Cohen and Green.[12]

Several explanations can be advanced for the variation of quantum yield with 2-propanol concentration. An increase in 2-propanol concentration could lower the quantum yield by directly effecting the carbonyl excited state. Since alcohols do not decrease the reactivity of aryl alkyl ketones toward type II elimina-

(18) Failure to rigorously degas samples results in lowered and eratic quantum yields.

(19) As commercial acetone is prepared by oxidation of 2-propanol, trace impurities in the latter may persist in the former.

(20) Cohen and Green[12] report an intercept of 0.83 for loss of acetophenone.

tion[21] and should not substantially alter the n, π^* character of the lowest triplet state of acetophenone,[22] such an effect seems unlikely. Evidence has been presented that a transient light-absorbing intermediate is formed to a greater extent in more concentrated 2-propanol solutions.[12] Such an intermediate could lower the quantum yield either by quenching of triplet acetophenone and/or by competitive absorption. Quenching by an intermediate should increase with the extent of reaction[6] and the light intensity.[23] The low conversions and light intensities used in the present study should minimize formation of the transient intermediate and thus may account for the lack of upward curvature in Figure 1. In order to access the importance of quenching by an intermediate, the dependence of the quantum yield for disappearance of 0.1 *M* acetophenone in 2 *M* 2-propanol–benzene upon the extent of conversion was examined. The results given in Table II were obtained by measurement of aceto-

Table II: Quantum Yields for Disappearance of Acetophenone as a Function of Extent of Reaction

% reaction	Φ	% reaction	Φ
2.9	0.74	21.5	0.69
5.8	0.74	26.0	0.64
11.4	0.73	29.7	0.64
18.3	0.70		

phenone absorbance at the wavelength of irradiation (3130 Å) after varying time intervals. This procedure allowed observation of the decay of the absorbing transient. The small decrease in quantum yield observed over the first 30% reaction is qualitatively consistent with increased competitive absorption by the intermediate. However, since there is no decrease in quantum yield over the first 10% reaction, the intermediate cannot account for the low quantum yields observed at low conversion in concentrated 2-propanol–benzene solutions (Figure 1).

An alternative explanation for the variation in quantum yield with 2-propanol concentration is that a small amount of quenching impurity is present initially in the 2-propanol. The observation that synthetic 2-propanol gives higher quantum yields at high concentrations than commercial 2-propanol suggests that at least part of the observed effect is due to solvent impurities. Analytical gas chromatography showed that several minor impurities (<0.05%) were present in both samples of 2-propanol. The extremely low concentration of these impurities precluded attempts to isolate and identify them. The uv spectrum of neat 2-propanol shows a low-intensity maximum at 3100 Å ($\epsilon = 1 \times 10^{-3}$) thus providing further evidence for the presence of a trace impurity capable of acting as an

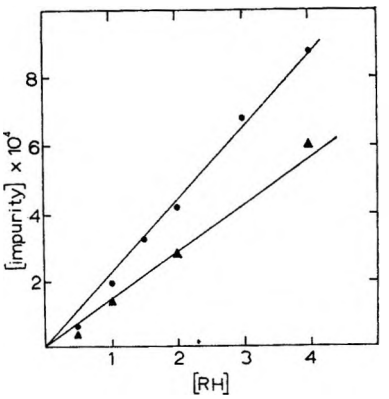

Figure 2. Calculated amount of quenching impurity as a function of 2-propanol concentration for commercial (●) and synthetic (▲) 2-propanol.

efficient quencher of triplet acetophenone. Furthermore, by using eq 8, the kinetic data described below, the measured and extrapolated quantum yields (Figure 1), and assuming diffusion-controlled quenching, the amount of quenching impurity at each concentration can be calculated. Such a treatment leads to linear plots shown in Figure 2 of calculated impurity *vs.* 2-propanol concentration with the amount of impurity being 0.021% and 0.015% for the two samples of 2-propanol. It is hard to conceive of any explanation other than impurity quenching which would show a precise linear dependence upon 2-propanol concentration.

A small amount of quenching impurity in 2-propanol will alter the intercept of a Stern–Volmer quenching plot (eq 8) by changing the effective quencher concentration and thus alter the calculated value k_d, the rate constant for unimolecular triplet decay. However, the ratio k_q/k_r obtained from the slope should remain constant. Linear Stern–Volmer plots (Figure 3) were obtained for 0.1 *M* solutions of acetophenone in 2.0, 0.5, and 0.1 *M* 2-propanol–benzene using 3×10^{-4} to 3×10^{-3} *M* *trans*-piperylene as the triplet quencher. The value of k_q, the diffusion-controlled rate constant for triplet quenching, is assumed to be the same for all 2-propanol–benzene solutions as the viscosity changes are small. Knowing the approximate amount of quenching impurity in the 2-propanol (Figure 2), the kinetic data in 0.5 and 2.0 *M* 2-propanol solution can be corrected to give k_d values in better agreement with that determined in 0.1 *M* 2-propanol. As further verification of the kinetic data obtained in 0.1 *M* 2-propanol, the ratio k_d/k_r determined from the data in Table III agrees exactly with the value obtained from the slope of Figure 1 at low 2-propanol concentrations.

The kinetic data given in Table III display several

(21) P. J. Wagner, *J. Amer. Chem. Soc.*, **89**, 5898 (1967).
(22) A. A. Lamola, *J. Chem. Phys.*, **47**, 4810 (1967).
(23) N. C. Yang and S. Murov, *J. Amer. Chem. Soc.*, **88**, 2852 (1966).

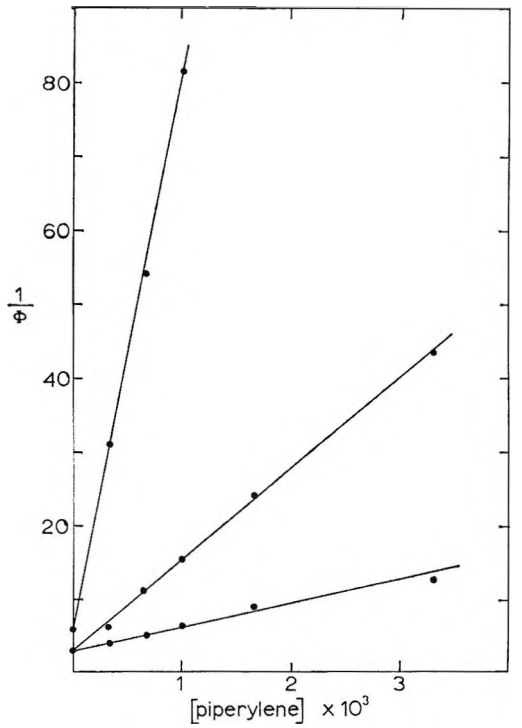

Figure 3. Stern–Volmer plots for piperylene quenching of acetone formation from acetophenone photoreduction in 0.1, 0.5, and 2.0 *M* 2-propanol–benzene in order of decreasing slope.

Table III: Kinetic Data for Photoreduction of Acetophenone in 2-Propanol–Benzene[a]

2-Propanol, *M*	$k_r \times 10^5$, M^{-1} sec^{-1} [b]	$k_d \times 10^5$, sec^{-1} [c]	$\tau \times 10^6$, sec[d]
2.0	7.5	28	0.23
0.5	7.5	6.8	0.65
0.1	6.8	3.4	2.4

[a] Limits of error for kinetic data = ±10%. [b] Rate constant for hydrogen abstraction obtained from the slope of linear Stern–Volmer plots using *trans*-1,3-pentadiene as a quencher of acetone formation. k_q was taken as 5×10^9 M^{-1} sec^{-1}. [c] Apparent rate constant for triplet decay obtained from the intercept of linear Stern–Volmer plots. [d] Calculated from $\tau = (k_r[\mathrm{RH}] + k_d)^{-1}$.

notable features. First, the rate constant for hydrogen abstraction, k_r, remains essentially constant as the concentration of 2-propanol is decreased. Second, the apparent rate constant for triplet decay, k_d, decreases by nearly an order of magnitude in going from 2.0 to 0.1 *M* 2-propanol. The calculated value for τ, the triplet lifetime [$\tau = (k_r[\mathrm{RH}] + k_d)^{-1}$], shows a related increase. The value of k_d in 0.1 *M* 2-propanol (3.4×10^5 sec^{-1}) is in good accord with the value obtained by the phosphorescence decay method (3.0×10^5 sec^{-1}).[17] As has been pointed out,[17] such results are apparent triplet decay rate constants observed in purified benzene solution and may not be indicative of the inherent triplet lifetime of acetophenone. Wagner[16] has suggested that the rate of decay of all triplet species is the same under a given set of conditions, being determined by a low steady-state concentration of a quenching species. The value obtained for benzophenone in benzene solution is 3×10^5 sec^{-1}.[16] Our result for acetophenone agrees with Wagner's value for benzophenone and thus obviates explanation of the different rate constants for acetophenone and benzophenone previously reported.[10]

In conclusion, many of the anomalous data observed in the photoreduction of acetophenone in 2-propanol may be attributed to a trace of quenching impurity in the 2-propanol. Related observations for benzophenone photoreduction in 2-propanol (*e.g.*, short lifetimes, upward curvature of $1/\varphi$ *vs.* $1/[\mathrm{RH}]$ plots) suggest a similar conclusion may be arrived at for these systems.[24] Whether the 2-propanol impurity is in some way related to the formation of the transients observed in acetophenone and benzophenone photoreductions in 2-propanol remains to be investigated. It is clear that the use of concentrated 2-propanol leads to anomalous kinetic results and that published results obtained in such solutions must be regarded with reserve.

Experimental Section

Solvents and Materials. Acetophenone (Eastman) was purified by recrystallization from ethanol–water and from petroleum ether and then distilled. Benzene was Spectrograde refluxed twice over fresh phosphorus pentoxide and fractionated, the middle 70% being retained. Matheson Coleman and Bell 2-propanol was distilled from calcium hydride, the middle fraction being retained. Spectrograde acetone was reduced with lithium aluminum hydride and distilled from calcium hydride through a 1-m column of glass helices. Analysis of both samples of 2-propanol on a 12 ft × 1/8-in. column of 20% Carbowax 20 *M* on Chromosorb P showed several trace impurities ($\lesssim 10^{-4}$ of 2-propanol). Viscosities of benzene–2-propanol solutions were measured with an Ostwald viscosimeter.

Quantum Yields. Solutions of 0.1 *M* acetophenone 2-propanol–benzene mixtures were sealed under vacuum in 13-mm o.d. Pyrex tubes after four freeze–pump–thaw cycles at a vacuum of less than 1 Torr. Samples were irradiated in parallel on a merry-go-round apparatus at 25 ± 1° using a filter solution of potassium chromate to isolate the 3130-Å irradiation from a Hanovia 450-W medium pressure lamp. Light intensities measured by simultaneous irradiation of benzophenone–benzhydrol actinometer solutions[25] were approximately 5×10^{-6} Einstein l.$^{-1}$ sec^{-1}. Samples

(24) As the rate constant for hydrogen abstraction by benzophenone is greater than that for acetophenone,[10] the presence of a quenching impurity will have less of an effect on the benzophenone kinetics.

(25) W. M. Moore and M. Ketchum, *J. Amer. Chem. Soc.*, **84**, 1368 (1962).

were analyzed for acetone formation on a calibrated 12 ft × 1/8-in. column of 20% Carbowax 20 *M* on Chromosorb G at 60°. Loss of acetophenone and pinacol formation were determined on a calibrated 5 ft × 1/8-in. column of 4% QF 1 and 1% Carbowax 20 *M* on Chromosorb G using tetradecane as an internal standard. Analyses were performed on a Hewlett–Packard 5750 dual flame gas chromatograph. Quantum yields for loss of acetophenone as a function of extent reaction were determined by measuring the absorbance at 3130 Å using a Beckman DU spectrophotometer with a Gilford attachment Model 222. Absorbances were measured immediately after photolysis and were monitored until a constant value was attained.

Quenching Studies. Samples were prepared and analyzed as for quantum yield determination except that varying amounts of *trans*-piperylene (Chemical Samples) were added to the acetophenone solutions. Five concentrations of piperylene, in addition to blanks containing no piperylene, were used for each Stern–Volmer plot.

Acknowledgments. The author wishes to thank the donors of the Petroleum Research Fund, administered by the American Chemical Society, the Research Corp., and the Merck Foundation for support of this research and Dr. Richard Hautala for helpful discussions.

Paramagnetic Resonance Study of Liquids during Photolysis.

IX. Oxalic Acid and Its Esters[1,2]

by Henry Zeldes* and Ralph Livingston

Chemistry Division, Oak Ridge National Laboratory, Oak Ridge, Tennessee 37830 *(Received April 9, 1970)*

Epr spectra of aliphatic radicals produced from oxalic acid and its mono- and diesters following electron capture from donor radicals were studied in solutions during photolysis. Radical production is greatly increased by the presence of water. Aqueous solutions were studied for a range of acid concentrations. Cis and trans isomers were found for radicals, ROOCĊ(OH)OR and ROOCCOOR·⁻, derived from ethyl and methyl diesters. The neutral cis isomer undergoes fast exchange making all alkyl protons equivalent in isopropyl alcohol solution. This is attributed to intramolecular hydroxyl proton transfer. The neutral trans isomer undergoes exchange between tautomeric forms by an acid-catalyzed mechanism. Only a single line was seen for reduced oxalic acid. Splittings from ^{13}C were not seen for reduced oxalic acid in a number of solutions for which the signal was strong enough to see unbroadened lines. This may be due to electron exchange between oxalic acid and an anion form of reduced oxalic acid. Spectra with anomalous relative line strengths and even emission lines were found for electron-donor radicals in the presence of a high enough concentration of oxalic acid which shortens the lifetime of the donor radicals. Apparently the radicals are generated with nonequilibrium distribution of spins; for at least some of the nuclear spin states there are more radicals generated in the upper electron spin state.

We wish to report electron paramagnetic resonance (epr) spectra of radicals derived from oxalic acid and its esters observed during the photolysis of various solutions. These solutions were chosen to give high concentrations of aliphatic radicals having the unpaired electron on a carbon atom bonded to a hydroxyl group. Radicals of this kind are known to be good electron donors.[3,4] The addition of oxalic acid and its esters to these solutions gave new radicals resulting from the one-electron reduction of oxalic acid and its esters

$$R'OOCCOOR + \dot{D} \longrightarrow R'OOCCOOR\cdot^- + D^+$$

$$R'OOCCOOR\cdot^- + H_3O^+ \rightleftharpoons R'OOC\dot{C}(OH)OR + H_2O \quad (1)$$

where R as well as R′ may be an alkyl group or H. This reduction is not surprising, as aliphatic α-di-

* To whom correspondence should be addressed.

(1) Research sponsored by the U. S. Atomic Energy Commission under contract with Union Carbide Corporation.

(2) The preceding paper of this series is by R. Livingston and H. Zeldes, *J. Chem. Phys.*, in press.

(3) A. L. Buley and R. O. C. Norman, *Proc. Chem. Soc.*, 225 (1964).

(4) R. O. C. Norman and R. J. Pritchett, *J. Chem. Soc. B*, 378 (1967).

ketones which are structurally similar have also been reduced in this way[4] to form semidione, $RCOCOR\cdot^-$, and monoprotonated semidione, $RCO\dot{C}(OH)R$, radicals.

The radicals made by reduction of the diesters reported here are expected to show similarities to the semidione or monoprotonated semidione radicals which result from reduction of symmetrical aliphatic α-diketones. Semidione radicalsh ave been studied[4-6] extensively. Monoprotonated semidione radicals, particularly the radical derived from biacetyl, have been studied[4,7,8] in isopropyl alcohol, in acidic aqueous, and in acidic isopropyl alcohol solutions. Cis and trans isomers of the semidiones have been prepared by disproportionation of acyloins in basic dimethyl sulfoxide solution and identified by Russell and Stephens.[5] Norman and Pritchett[4] produced the semidione and the monoprotonated semidione radicals in aqueous solution in two ways using the rapid mixing method. One way involved reduction of α-diketones as stated earlier, and the other involved oxidation of acyloins. They found for pH >5 that the trans semidione radical is made by the reduction method and that both semidione isomers are made by the oxidation method. At lower pH they found different spectra and determined that the trans monoprotonated isomer is formed by the reduction method and that both monoprotonated isomers are formed by the oxidation method. The existence of cis and trans isomers requires that there be enough double-bond character in the bond joining the two carbonyl groups to prevent rapid rotation about this bond. Semidione and monoprotonated semidione radicals derived from biacetyl have also been prepared photolytically and studied[7] by epr. The radicals were generated in aqueous and in isopropyl alcohol solution by the reaction of photolytically excited biacetyl with good H atom donors such as isopropyl alcohol. Only one isomer was reported in this work, and this may be identified[4,5] as trans. For an isopropyl alcohol solution containing 2% biacetyl, photolysis gives[7] a sharp-lined spectrum from the trans monoprotonated semidione with hyperfine splittings from all protons. The two methyl groups have very different couplings. Upon adding acid, very large line-shape effects due to chemical exchange were seen and studied. These acid-catalyzed exchange effects were also studied by Norman and Pritchett[4] and by Pritchett[8] in aqueous solution. With sufficient acid present (pH of 0.5 for an aqueous solution[4]) the protons of the two methyl groups give equal splittings and there is no splitting from the hydroxyl proton. This is a consequence of rapid acid-catalyzed interchange between tautomeric forms

$$CH_3\dot{C}(OH)COCH_3 \overset{H^+}{\rightleftharpoons} CH_3CO\dot{C}(OH)CH_3 \quad (2)$$

which interchanges coupling values for the two methyl groups and also causes reversals in the magnetic spin state for the hydroxyl proton.

It is apparent that radicals produced by reduction of oxalic acid and its esters may have cis and trans isomers, protonated and unprotonated forms, and tautomeric forms which undergo acid-catalyzed exchange. For this reason, the acid concentration was varied, and both aqueous and nonaqueous solutions were investigated.

Very strong spectra of the donor radicals could be obtained in the absence of oxalic acid or oxalate. Upon the addition of oxalic acid, these spectra became weaker and the intensities of their hyperfine components became anomalous. A number of these anomalous spectra will be discussed.

Experimental Section

The microwave spectrometer operated at about 9.5 GHz and used 100-kHz field modulation. The experimental arrangement was described[9] earlier, and the same methods were used for making measurements and calculating g values and hyperfine couplings. The estimated error limits are ± 0.00004 for g and ± 0.02 G for the couplings unless indicated otherwise. The sample handling system has also been described.[9b] The solutions were freed of molecular oxygen by purging with gaseous helium. Photolysis then took place in a flat silica cell in the microwave cavity as the solution flowed through it at about 1 ml/min. The inside cross section of the cell was 0.4 mm thick (optical path length) by 9 mm wide. Temperatures are given for the solutions shortly after leaving the cavity. All chemicals were used as purchased except where otherwise noted. The diethyl oxalate (bp 72–74° (10 mm)), n-propyl alcohol (bp 96–98°), and acetaldehyde (bp 20–22°) were from Matheson Coleman and Bell. All other chemicals were reagent quality.

Results and Discussion

Reduction by Electron-Donor Radicals. Epr spectra were not seen during photolysis of aqueous solutions containing just oxalic acid, or oxalic acid and H_2O_2, or oxalic acid and isopropyl alcohol. However, when an aqueous solution contained oxalic acid, H_2O_2, and isopropyl alcohol, a very strong sharp line with a g value of 2.00403 was seen. In the absence of oxalic acid this solution[9a] gives a strong seven-line spectrum due to $(CH_3)_2\dot{C}OH$. Upon adding oxalic acid the spectrum from $(CH_3)_2\dot{C}OH$ became progressively weaker and the single sharp line grew stronger. From these observations and the knowledge[3,4] that certain organic radicals having the unpaired electron on a carbon atom bonded to a hydroxyl or alkoxyl group are good electron donors,

(5) G. A. Russell and R. D. Stephens, *J. Phys. Chem.*, **70**, 1320 (1966).

(6) See also references contained in ref 4 and 5.

(7) H. Zeldes and R. Livingston, *J. Chem. Phys.*, **47**, 1465 (1967).

(8) R. J. Pritchett, *Mol. Phys.*, **12**, 481 (1967).

(9) (a) R. Livingston and H. Zeldes, *J. Amer. Chem. Soc.*, **88**, 4333 (1966); (b) R. Livingston and H. Zeldes, *J. Chem. Phys.*, **44**, 1245 (1966).

Table I: Values of g and Couplings ($a(n)$) (in Gauss for n Equivalent Protons) for Reduced Dimethyl and Monomethyl Oxalate

Compn of soln (per l.)	Medium	pH	g	$a(n)$	n	Radical
30 g of dimethyl oxalate and 100 ml of acetone at 32°	2-Propanol	(Slightly acid)	2.00418	1.87	6	*cis*-$CH_3O_2C\dot{C}(OH)OCH_3$
			2.00414	2.015	3	
				1.55	3	*trans*-$CH_3O_2C\dot{C}(OH)OCH_3$
				0.71	1	
20.4 g of dimethyl oxalate, 102 ml of acetone, 102 ml of 2-propanol, and 19 g of sodium acetate at 34°	Aqueous	5.1	2.00424 ± 0.00015[a]	1.70 ± 0.05[a]	6	$CH_3O_2CCO_2CH_3\cdot^-$
			2.00437	1.39	3	Anion[b]
			2.00440 ± 0.00010[c]	1.59 ± 0.05[c]	3[c]	Anion[b]
20.4 g of dimethyl oxalate, 102 ml of acetone, and 102 ml of 2-propanol at 33°	Aqueous	1.9	2.00413[a]	1.89 ± 0.03[a]	6	$CH_3O_2C\dot{C}(OH)OCH_3$
			2.00406	1.77	3	$CH_3O_2C\dot{C}(OH)_2$[d]
Above solution after adding concd HCl at 34°	Aqueous	(0.39 *N* HCl)	2.00410[a]	1.93[a]	6	$CH_3O_2C\dot{C}(OH)OCH_3$
			2.00406	1.79	3	$CH_3O_2C\dot{C}(OH)_2$[d]

[a] Mean value for 2 isomers with unresolved lines. [b] Possible radicals are $CH_3O(OH)\dot{C}CO_2^-$, $CH_3O_2CCO_2H\cdot^-$, and $CH_3O_2CCO_2\cdot^{2-}$. [c] Parameters uncertain as it is not definite that this is a 1–3–3–1 spectrum. This spectrum is weaker than the other 1–3–3–1 spectrum. [d] Rapidly exchanging reduced monoester radicals: $CH_3O_2C\dot{C}(OH)_2 \rightleftharpoons CH_3O(OH)\dot{C}CO_2H$.

we conclude that the one-line spectrum results from the one-electron reduction of oxalic acid by $(CH_3)_2\dot{C}OH$ to form $HOOCCOOH\cdot^-$ or its protonated form $HOOC\dot{C}(OH)_2$.

Oxalic acid was reduced in aqueous solutions using donor radicals made[7,9,10] by photolysis of isopropyl alcohol and H_2O_2 to form $(CH_3)_2\dot{C}OH$, ethyl alcohol and H_2O_2 to form $CH_3\dot{C}HOH$, acetone and isopropyl alcohol to form $(CH_3)_2\dot{C}OH$, acetone and ethyl alcohol to form a mixture of $(CH_3)_2\dot{C}OH$ and $CH_3\dot{C}HOH$, acetaldehyde and ethyl alcohol to form $CH_3\dot{C}HOH$, *n*-propyl alcohol and acetone to form a mixture of $CH_3CH_2\dot{C}HOH$ and $(CH_3)_2\dot{C}OH$, and ethylene glycol and acetone to form a mixture of $HOCH_2\dot{C}HOH$ and $(CH_3)_2\dot{C}OH$. From solutions containing both $(CH_3)_2\dot{C}OH$ and $CH_3\dot{C}HOH$ it was apparent that $(CH_3)_2\dot{C}OH$ is the better electron donor. Oxalic acid in an aqueous solution was also exposed to the radical (Å) which is formed from *p*-dioxane by loss of a hydrogen atom. This radical, which has been studied[10,11] by epr, was made by photolysis of *p*-dioxane and H_2O_2. It was seen that very much less reduction of oxalic acid occurred using Å than the other radicals. This is consistent with the report[4] that Å is ineffective as an electron donor in reducing biacetyl, whereas $\dot{C}H_2OH$ and $CH_3\dot{C}HOH$ as well as radicals derived from several ethers are effective.

Water was needed to obtain a strong line from reduced oxalic acid. In a solution containing 5.4 g of oxalic acid dihydrate and 160 ml of acetone per liter of isopropyl alcohol solution, the line was very weak. Upon adding water to bring the water content to 115 ml per liter, the line became about 6 times stronger. By adding more water the line-strength could be further increased by more than a factor of 10.

The methyl and ethyl diesters of oxalic acid and a number of monoesters were also found to react with

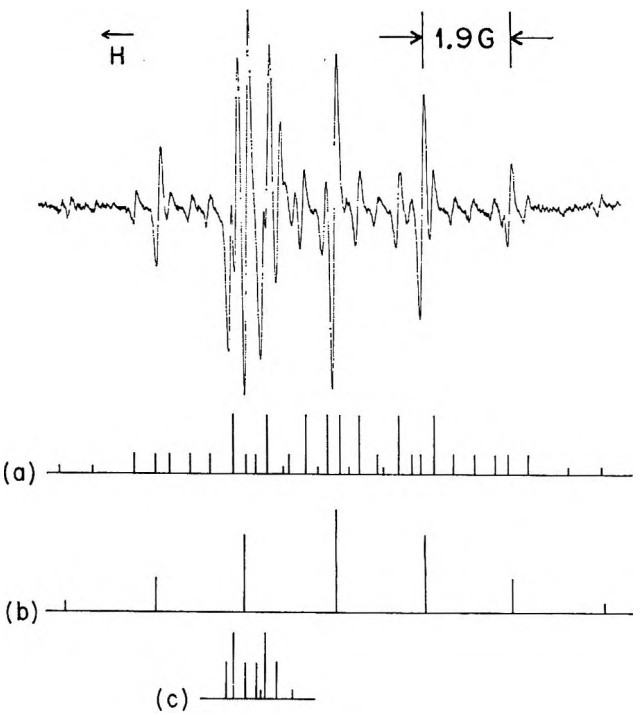

Figure 1. Spectrum during photolysis of an isopropyl alcohol solution containing 30 g of dimethyl oxalate and 100 ml of acetone per liter at 33°. Stick spectra (a) and (b) identify lines of two reduced dimethyl oxalate radicals. Stick spectrum (c) identifies components from the central (20-strength) line of $(CH_3)_2\dot{C}OH$.

good electron donor radicals to form radical reduction products. The diesters too gave much higher radical yields when the solutions contained water. Unfortunately, the diesters were hydrolyzing during the observations in water solution. This made it difficult to

(10) H. Zeldes and R. Livingston, *J. Chem. Phys.*, 45, 1946 (1966).
(11) W. T. Dixon and R. O. C. Norman, *J. Chem. Soc.*, 4850 (1964).

study the reduced diesters. Their concentrations were changing during the observations, and radicals from monoesters were being produced. Another problem was that the pH, an important parameter, was changing rapidly.

Reduced Dimethyl Oxalate. Figure 1 shows the spectrum for an isopropyl alcohol solution containing dimethyl oxalate and acetone at 33°. Lines from three radicals are identified by the stick spectra. Nineteen of the 32 lines from spectrum (a) were resolved and measured. These well overdetermined this spectrum, a (1-3-3-1) (1-3-3-1) (1-1) pattern of lines due to protons from two nonequivalent methyl groups and one other proton. This radical is undoubtedly $CH_3O_2C\dot{C}(OH)OCH_3$, the neutral, monoprotonated one-electron reduction product of dimethyl oxalate. The presence of a small amount of acid due to hydrolysis from water as an impurity could be an important factor in causing protonation. Radical (b) which has a (1-6-15-20-15-6-1) pattern of lines from six equivalent methyl protons was also measured. We identify radicals (a) and (b) as trans and cis neutral isomers, respectively. The cis isomer is presumed to give equivalent splittings for the two methyl groups because of fast interchange between tautomers (cis-1) and (cis-2) which results from intramolecular proton-transfer

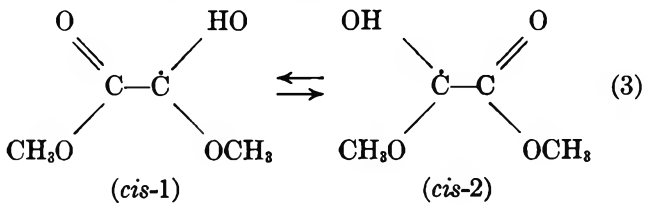

(3)

The parameters for these two isomers are in Table I. The lines in spectrum (c) are some of the lines of $(CH_3)_2\dot{C}OH$. They arise from components of the central (20-strength) line of a pattern resulting from six equivalent protons which is split by second-order effects into lines with intensities 1-5-9-5 (in order, from low field to high field) and then further split in two by the small hydroxyl hydrogen coupling. Isopropyl alcohol solutions containing reduced dimethyl oxalate and acetone were also examined at 15° in an effort to find line broadening in spectrum (b) at the somewhat lower temperature as evidence for a slowing of the tautomeric exchange. Line broadening was not found.

The trans neutral isomer of reduced dimethyl oxalate is expected by analogy with the trans protonated semidione derived from biacetyl[4,7,8] to undergo acid-catalyzed exchange between tautomeric forms through a very short-lived symmetrical intermediate

With an intermediate rate of exchange line shape effects would be seen, and with fast enough exchange the trans spectrum of Figure 1a (nonexchanging) would be transformed to a sharp-lined spectrum lacking the coupling to the unique hydrogen and having coupling to protons of two equivalent rather than nonequivalent methyl groups. It was found that just the addition of water to the isopropyl alcohol solution provided enough acid to bring about these changes. As water was added the spectrum of the cis isomer (Figure 1b) became stronger. The trans spectrum (Figure 1a) underwent changes which could not be followed in detail, because the signal was weak, line spacings were small, and other lines interfered. Nonetheless, it was apparent that the lines underwent width and shape changes which are characteristic of exchange. The lines broadened to the point of being very difficult to see, and there then emerged a second 1-6-15-20-15-6-1 spectrum partly resolved from that of the cis isomer. Figure 2 shows the

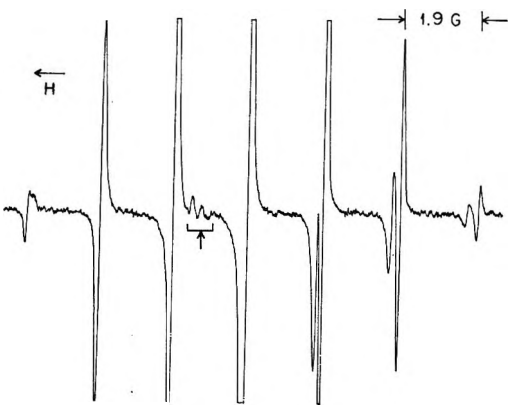

Figure 2. Spectrum during photolysis of an isopropyl alcohol solution containing 24 g of dimethyl oxalate, 81 ml of acetone, and 206 ml of H_2O per liter at 31°. The stronger lines are from two partially resolved 1-6-15-20-15-6-1 spectra from two isomers of reduced dimethyl oxalate. There are weak lines present (arrow) from $(CH_3)_2\dot{C}OH$.

spectrum after 206 ml of water per liter had been introduced. Two partially resolved 1-6-15-20-15-6-1 spectra are present. The one with smaller line heights (probably with broader lines) is from the neutral trans isomer. It has the smaller g value and coupling. Much weaker lines (arrow) from $(CH_3)_2\dot{C}OH$ are also present. Figure 3 shows the spectrum for a solution which was mainly aqueous. The radical $(CH_3)_2\dot{C}OH$ was not detected. This solution contained monoester as well as diester because of hydrolysis. The 1-3-3-1 stick spectrum labels lines from the reduced monoester showing splittings from

$$CH_3O(OH)\dot{C}COOCH_3 + H^+ \underset{\text{fast}}{\overset{k}{\rightleftharpoons}} [CH_3OC(OH)C(OH)OCH_3]^+ \quad (4)$$

$$CH_3OOC\dot{C}(OH)OCH_3 + H^+ \underset{\text{fast}}{\overset{k}{\rightleftharpoons}}$$

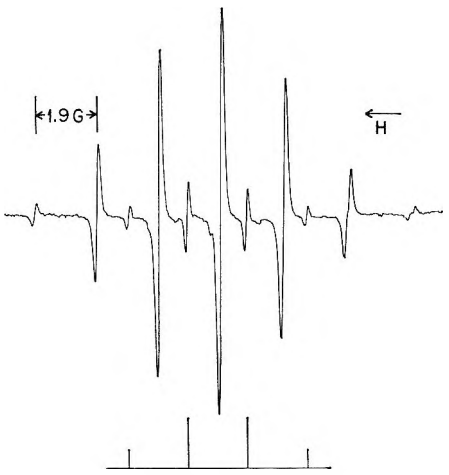

Figure 3. Spectrum during photolysis of an aqueous solution at about 33° with pH about 1.9 and made up with 20 g of dimethyl oxalate, 102 ml of acetone, and 102 ml of isopropyl alcohol per liter. The 1-3-3-1 stick spectrum identifies the lines from reduced monomethyl oxalate. The remaining lines are due to two nearly superposed 1-6-15-20-15-6-1 spectra from the cis and trans isomers of reduced dimethyl oxalate.

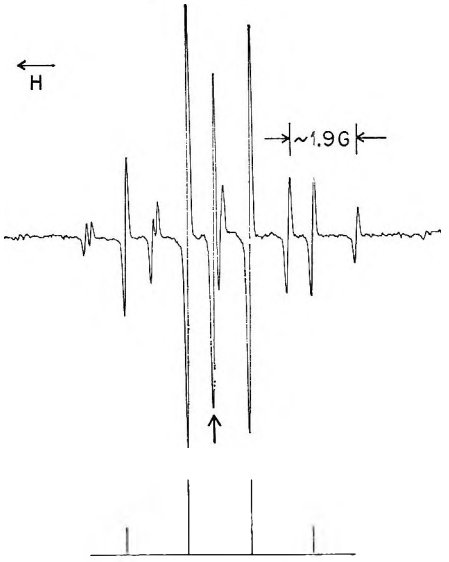

Figure 4. Spectrum during photolysis of an aqueous solution made up with 17 g of dimethyl oxalate, 86 ml of acetone, 86 ml of isopropyl alcohol, and 138 ml of concentrated HCl per liter at about 33°. The arrow points to the single line from reduced oxalic acid. The 1-3-3-1 stick spectrum identifies the lines from reduced monomethyl oxalate. The remaining lines are from two nearly superposed 1-6-15-20-15-6-1 spectra from the cis and trans isomers of reduced dimethyl oxalate.

three equivalent protons of the methyl group. The remaining lines are from the reduced neutral diester isomers. Only the two lowest field lines of the two isomers are partially resolved. Lines of the two isomers appear to have about the same height and width, and it is clear that the trans isomer is now undergoing fast exchange. Figure 4 is for an aqueous solution which was made 1.7 *N* in HCl. Hydrolysis was occurring rapidly, and oxalic acid as well as monoester was present. The stick spectrum labels lines from the reduced monoester which are relatively strong, as much hydrolysis had occurred. The arrow points to the line from reduced oxalic acid. The remaining lines are from the two isomers of neutral reduced dimethyl oxalate. The highest field lines of the isomers are resolved, whereas in the absence of HCl (Figure 3) the lowest field lines are partially resolved.

The concentration of acid needed to give a fast-exchange spectrum (characterized by six equivalent protons) in water solution depends not only upon k in eq 4 but also upon the hydroxyl proton coupling value, the difference in the two methyl group proton couplings, and upon the line width for the nonexchanging radical. A comparison of the coupling values for trans-protonated reduced dimethyl oxalate (Table I) with those[4,7] of the analogous radical derived from biacetyl show that fast exchange would occur for the oxalate radical at much higher pH, provided that the protonation rate constant is the same for both.

Isomer assignments for the neutral reduced dimethyl oxalate radicals have been made on the basis of behavior which would be expected from exchange between tautomers. The assignment may also be made from a comparison of the alkyl proton couplings of the two isomers. Assignments for the semidiones were made by Russell and Stephens[5] on the basis that larger spin densities are expected at the carbonyl carbon atom (and less at the carbonyl oxygen) for the cis isomer because of charge repulsion. For this reason the alkyl proton couplings are higher for the cis isomer. Subsequently assignments were made for both semidiones and their protonated derivatives by Norman and Pritchett,[4] who saw both by changing the pH. They too assigned higher couplings for the alkyl protons of the cis isomer. Assignments made in this way for the neutral reduced dimethyl oxalate isomers agree with the assignments we have made on the basis of exchange behavior. From Table I it is seen that in isopropyl alcohol solution the mean methyl proton coupling for the trans isomer is smaller than that for the cis isomer. After 206 ml of water per liter was introduced to this solution, the trans isomer (which then underwent fairly rapid exchange) still had the smaller coupling.

Measurements of the spectra of reduced monomethyl and reduced dimethyl oxalate were made for aqueous solutions of dimethyl oxalate containing acetone and isopropyl alcohol at three acid concentrations. This was done to learn whether the reduced esters were in the anion or the neutral monoprotonated form. The results for the reduced monoester will be discussed later. In the absence of added acid the solutions were acidic because of hydrolysis; a typical solution had a pH of 1.9. Measurements were also made at a pH of 5.1 for a solution made less acid by adding sodium acetate and also for a solution which was made 0.39 *N*

Table II: Values of g and Couplings (a) for Reduced Diethyl Oxalate[a]

Compn of soln (per l.)	Medium	pH	g	a	Radical
Equal volumes of diethyl oxalate, 2-propanol, and acetone at 37°	Nonaqueous	(Slightly acid)	2.00415	1.60	*cis*-$C_2H_5O_2C\dot{C}(OH)OC_2H_5$
50 ml of diethyl oxalate, 75 ml of acetone, 250 ml of 2-propanol, and 19 g of sodium acetate at 34°	Aqueous	5.5	2.00426 2.00418	1.57 1.50	*cis*-$C_2H_5O_2CCO_2C_2H_5\cdot^-$ *trans*-$C_2H_5O_2CCO_2C_2H_5\cdot^-$
50 ml of diethyl oxalate, 75 ml of acetone, and 250 ml of 2-propanol at 32°	Aqueous	1.9	2.00410 2.00403	1.70 1.64	*cis*-$C_2H_5O_2C\dot{C}(OH)OC_2H_5$ *trans*-$C_2H_5O_2C\dot{C}(OH)OC_2H_5$
Above soln after adding concd HCl at 32°		(0.3 *N* HCl)	2.00410 2.00403	1.71 1.65	*cis*-$C_2H_5O_2C\dot{C}(OH)OC_2H_5$ *trans*-$C_2H_5O_2C\dot{C}(OH)OC_2H_5$

[a] Couplings are in Gauss for four equivalent protons.

in HCl. The isomers of reduced dimethyl oxalate had very nearly equal concentrations for a given solution. Unfortunately, their lines were not resolved well enough to be measured separately (Figures 3 and 4). However, measurements were made which determined an average value of g and of the hyperfine coupling. This was done by measuring only the lines of the isomers which were nearly in coincidence. Parameters deduced from these measurements are in Table I. The estimated accuracy of values for the average parameters is somewhat lower than usual for a pH of 1.9 and much lower for a pH of 5.1 as shown in the table. At a pH of 5.1 the average concentration of the reduced dimethyl esters was about 3 times higher than at lower pH. Supplemental qualitative observations of strengths and couplings for spectra (including reduced monoester) at several pH values were also made for another aqueous solution. Its pH value was slowly decreasing due to hydrolysis. Increases in pH were effected by additions of sodium acetate; one addition brought the pH from 2.0 to 2.8, and a second brought it to 5.1. The poorly resolved 1-6-15-20-15-6-1 spectra from isomers of reduced dimethyl oxalate were stronger at a pH of 5.1 than at a pH of 2.8 and 2.0, and the couplings were noticeably smaller. The isomers are assuredly in the neutral form in the solution acidified with HCl. The g value and the mean proton coupling are very nearly unchanged for a pH value of 1.9. Somewhere between pH values of 2.8 and 5.1 there is a significant change in these values and in the radical concentration. At the higher pH the g value is higher, the coupling is lower, and the concentration is higher. We attribute these changes to the presence of the anion form at the higher pH. This is consistent with the semidiones and their protonated derivatives for which there is a higher g value[7] and a lower coupling[4,7] for the anion. The higher radical concentration at the higher pH is attributed to longer chemical lifetime for the anion. Our findings place the pK somewhere in the broad range of 2.8 to 5.1. For comparison, the pK of the monoprotonated semidione derived from biacetyl has the value[4] *ca.* 4.

Reduced Diethyl Oxalate. In a solution made up of equal volumes of diethyl oxalate, acetone, and isopropyl alcohol at 37° there was a 1-4-6-4-1 spectrum as well as a very strong spectrum of $(CH_3)_2\dot{C}OH$. We attribute the 1-4-6-4-1 spectrum to the cis isomer of the neutral protonated form of reduced diethyl oxalate, CH_3CH_2-$O_2C\dot{C}(OH)OCH_2CH_3$. Protonation following electron capture by the diester may have been caused by acid formed by hydrolysis due to water present as an impurity. The equivalence of the four CH_2 protons is believed to be caused by rapid interchange between two tautomeric forms analogous to eq 3. It is assumed that interchange is brought about by intramolecular proton transfer. Measurements for this radical appear in Table II. Other weak lines were present, but we could not analyze them. In a solution containing redistilled diethyl oxalate and relatively more isopropyl alcohol, the weak lines could still not be analyzed. However, the outermost weak lines were well resolved and the g value was found to be very nearly the same as that of the 1-4-6-4-1 spectrum. This solution was also examined at −31 and at −43°. With lower temperature, the lines of the 1-4-6-4-1 spectrum become broader, whereas lines of $(CH_3)_2\dot{C}OH$ become sharper. The line-broadening could reasonably result from a slowing of the intramolecular proton exchange for this cis neutral isomer. Other weaker lines were present at −31 and at −43°, but we could not analyze them.

Upon adding water to isopropyl alcohol solutions containing diethyl oxalate and acetone, the spectrum of $(CH_3)_2\dot{C}OH$ became weaker and the 1-4-6-4-1 spectrum from the cis neutral isomer became stronger. The other weak lines whose spectrum could not be analyzed in the absence of water appeared to become stronger and changed in position and width. With enough water present, they could be recognized as a second 1-4-6-4-1 spectrum with broader lines partly resolved from the spectrum of the cis isomer. With 337 ml of

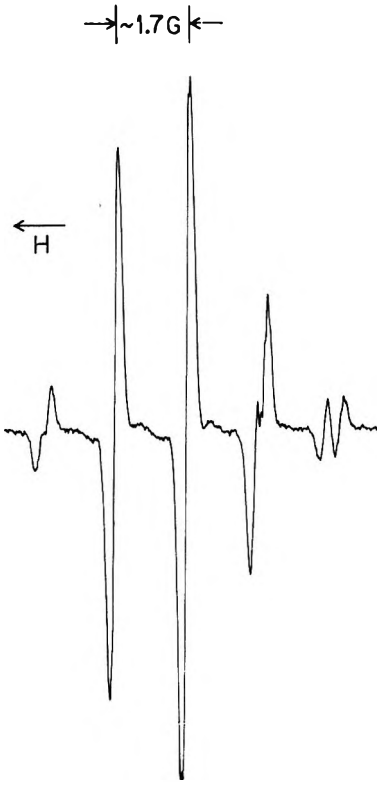

Figure 5. Central part of the spectrum during photolysis of an isopropyl alcohol solution containing 210 ml of diethyl oxalate, 320 ml of acetone, 125 ml of H_2O, and 18 ml of concentrated HCl per liter at about 35°. The spectrum is due mainly to two nearly superposed 1-4-6-4-1 spectra from the cis and trans isomers of reduced diethyl oxalate.

water per liter the lines become about as sharp and as strong as those of the cis isomer. We interpret this to be the trans isomer. The line shape effects seen after adding water are attributed to acid-catalyzed exchange between tautomeric forms analogous to eq 4. With 337 ml of water per liter present the trans isomer was seen to have a smaller g value and hyperfine coupling than the cis isomer. The relative couplings are consistent with what is expected for these isomer assignments.

The trans isomer showed the fast-exchange spectrum (characterized by couplings from four equivalent protons) in solutions containing less water provided that acid was also added. Figure 5 shows the spectrum for an acidified solution at about 35°. Not much hydrolysis of the diester had yet occurred, and there are present mainly the two partially resolved 1-4-6-4-1 spectra from the neutral reduced diester isomers. After more HCl was added and much more hydrolysis had occurred, the outermost lines became relatively much weaker, and there were two barely resolved lines in the center instead of just one. The two lines in the center and the two flanking lines were mainly from a mixture of reduced oxalic acid and reduced monoethyl oxalate. Reduced monoethyl oxalate gives a 1-2-1 spectrum due to the splittings from two equivalent CH_2 protons. This splitting is very nearly the same as the splitting for the reduced diesters, and in the spectrum just described, the 4-strength lines of the reduced diester isomers and the 1-strength lines of the reduced monoester were unresolved. For this reason this spectrum was not satisfactory for measuring the parameters of reduced monoethyl oxalate.

Solutions of diethyl oxalate which were mostly aqueous and which also contained acetone and isopropyl alcohol were examined at different acid concentrations to determine whether the reduced esters were in the anion or monoprotonated form. The solutions showed two partly resolved 1-4-6-4-1 spectra from the reduced diethyl oxalate isomers. The isomers had nearly equal strengths. The lowest field line of each was resolved, and the two lines at highest field, one from each isomer, were in coincidence (more so than shown in Figure 5). This made it possible to measure the parameters for each isomer. In the absence of added acid or base the solutions were quite acidic due to hydrolysis, typically a pH of 1.9. Measurements were also made at a pH of 5.5 in a solution to which sodium acetate had been added. Finally, a solution which was made 0.3 N in HCl was measured. The concentration of reduced diethyl oxalate was about 3 times higher at a pH of 5.5 than at the two lower pH values. The measured parameters appear in Table II, together with assignments to isomeric form and to anion or neutral radical. The isomers are assuredly neutral in the solution which was acidified with HCl. The g values and couplings are almost the same for a pH of 1.9. Somewhere between pH values of 1.9 and 5.5 there is a significant change in the parameters and in the radical concentration. At the higher pH the g value is higher, the coupling is lower, and there is a higher radical concentration. These findings are similar to those for the reduced dimethyl oxalate isomers, and here too the changes are attributed to the dissociation of neutral radicals to form anions at the higher pH. The identifications of cis and trans isomers for the aqueous solutions in Table II are based only on their couplings (see section on reduced dimethyl oxalate).

It is interesting that the related radical anions of methyl and ethyl mesoxalate, $RO_2CCOCO_2R\cdot^-$, have been prepared[12] from the mesoxalate esters and also by reduction of the *oxalate esters* by potassium in hexamethylphosphoramide. For both anions the coupling to the protons was found[12] to be 0.66 G which, as expected, is lower than values for the reduced oxalic acid diester radicals described in this manuscript.

Reduced Monoesters. A number of monoesters were reduced by electron transfer from donor radicals in aqueous solutions. Only the reduced monomethyl ester

(12) G. A. Russell and S. A. Weiner, *J. Amer. Chem. Soc.*, 89, 6623 (1967).

Table III: Values of g and Couplings ($a(n)$) (in Gauss for n Equivalent Protons) for Reduced Monoesters of Oxalic Acid in Acidified Aqueous Solutions

Compn of soln (per l.)	g	$a(n)$	n	Radical[a]
20.4 g of dimethyl oxalate, 102 ml of acetone, 102 ml of 2-propanol, and 32 ml of concd HCl at 34°	2.00406	1.79	3	$CH_3O_2C\dot{C}(OH)_2$
19 g of oxalic acid, 400 ml of ethyl alcohol, 34 ml of acetaldehyde, and 34 ml of concd HCl at 37°	2.00408	1.65	2	$CH_3CH_2O_2C\dot{C}(OH)_2$
22 g of oxalic acid, 370 ml of 2-propanol, 123 ml of acetone, and 31 ml of concd HCl at 37°	2.00408	0.90	1	$(CH_3)_2CHO_2C\dot{C}(OH)_2$
19 g of oxalic acid, 325 ml of n-propyl alcohol, 132 ml of acetone, and 26 ml of concd HCl at 37°	2.00410	1.68	2	$CH_3CH_2CH_2O_2C\dot{C}(OH)_2$
14 g of oxalic acid, 390 ml of ethylene glycol, 115 ml of acetone, and 24 ml of concd HCl at 37°	2.00410	1.78	2	$HOCH_2CH_2O_2C\dot{C}(OH)_2$

[a] Rapidly exchanging reduced monoester radicals: $RO_2C\dot{C}(OH)_2 \rightleftarrows RO(OH)\dot{C}CO_2H$.

was measured (Table I) at several pH values, as described in the section on reduced dimethyl oxalate. The other reduced monoesters were measured (Table III) in solutions acidified with HCl. To prepare reduced monoethyl oxalate a solution was made up with oxalic acid, ethyl alcohol, acetaldehyde, HCl, and H_2O. This solution contained a small equilibrium concentration of the monoester. The reducing radical was $CH_3\dot{C}HOH$ formed[7] by H-atom abstraction from CH_3CH_2OH by excited CH_3CHO. The spectrum contained a very strong sharp line from reduced oxalic acid and two very much weaker sharp lines from reduced monoethyl oxalate on either side of the strong line. The center line of the reduced monoester was obscured by the line from reduced oxalic acid. This solution also gave a spectrum of the donor radical $CH_3\dot{C}HOH$. Reduced monoesters of oxalic acid with ethylene glycol, isopropyl alcohol, and n-propyl alcohol were prepared by photolysis of acidified aqueous solutions made up with oxalic acid, the appropriate alcohol, and acetone. The donor radicals $(CH_3)_2\dot{C}OH$ and $R'R\dot{C}OH$ were produced[10] from excited acetone by H-atom abstraction from R'RCHOH. In each solution the spectrum of $(CH_3)_2\dot{C}OH$ was absent or nearly absent, because it had quickly donated an electron to the monoester. In the solution containing n-propyl alcohol, there was a spectrum from $CH_3CH_2\dot{C}HOH$ showing splittings from all protons except the hydroxyl group proton. The radical $CH_2OH\dot{C}HOH$ was not seen in the solution containing ethylene glycol. This does not necessarily mean that $CH_2OH\dot{C}HOH$ is a good donor, since it is known[9a] to disappear quickly in acid solutions. Figure 6 shows lines in the central part of the spectrum for the solution containing ethylene glycol. The strongest line is from reduced oxalic acid. In addition, there is a 1-2-1 spectrum from the reduced monoester of ethylene glycol. Very weak lines (not shown in Figure 6) from the donor $(CH_3)_2\dot{C}OH$ were also present. This solution was also examined before adding acetone, and as expected, no lines were seen. Figure 7 shows the spectrum for the solution containing isopropyl alcohol. The strong line

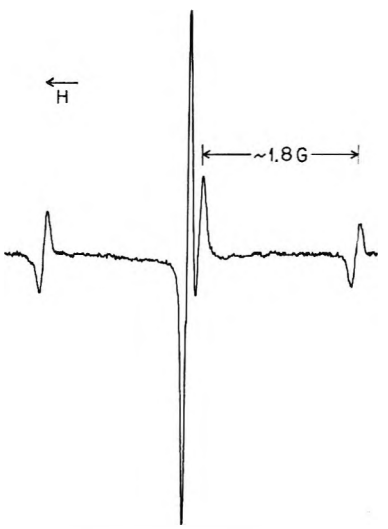

Figure 6. Central part of the spectrum during photolysis of an aqueous solution containing 2.7 g of oxalic acid, 446 ml of ethylene glycol, 115 ml of acetone, and 92 ml of concentrated HCl per liter at about 37°. The strongest line is due to reduced oxalic acid. The 1-2-1 spectrum is due to the reduced monoester of oxalic acid and ethylene glycol.

from reduced oxalic acid is stronger than for the previous solution, mainly because the oxalic acid concentration is 8 times greater. The two weak lines constitute a 1-1 spectrum from the reduced monoester of isopropyl alcohol.

The reduced monoester radicals produced in acidified aqueous solution were undoubtedly in the neutral protonated form (I) or (II) or a mixture as a result of protonation following electron capture

$$\begin{aligned} ROOCCOOH + \dot{D} &\longrightarrow ROOCCOOH\cdot^- + D^+ \\ ROOCCOOH\cdot^- + H^+ &\begin{cases} \nearrow RO(OH)\dot{C}COOH & (I) \\ \searrow ROOC\dot{C}(OH)_2 & (II) \end{cases} \end{aligned} \qquad (5)$$

Only a single spectrum of reduced monoester was seen in these acid solutions, whereas three forms are pos-

Table IV: Values of g for Reduced Oxalic Acid in Aqueous Solutions

Compn of soln (per l.)	pH	g	Radical
117 g of potassium oxalate, 75 ml of acetone, 75 ml of 2-propanol, and 15 ml of 1 *N* HCl at 32°	5.9	2.00419	$HO_2CCO_2H\cdot^-$
Above soln after adding concd HCl at 32°	5.0	2.00418	$HO_2CCO_2H\cdot^-$
0.7 g of oxalic acid, 16.2 g of potassium oxalate, 75 ml of acetone, and 75 ml of 2-propanol at 32°	4.9	2.00417	$HO_2CCO_2H\cdot^-$
Above soln after adding concd HCl at 32°	4.5	2.00416	$HO_2CCO_2H\cdot^-$
Above soln after adding concd HCl at 33°	1.7	2.00405	$HO_2C\dot{C}(OH)_2$
Above soln after adding concd HCl at 31°	1.0	2.00404	$HO_2C\dot{C}(OH)_2$
67 g of oxalic acid, 283 ml of 2-propanol, and 10 ml of H_2O_2 at 38°	0.8	2.00403	$HO_2C\dot{C}(OH)_2$
67 g of oxalic acid, 283 ml of ethyl alcohol, and 11 ml of H_2O_2 at 35°	~0.8	2.00400	$HO_2C\dot{C}(OH)_2$
67 g of oxalic acid, 140 ml of acetone, and 140 ml of 2-propanol at 34°	~0.8	2.00401	$HO_2C\dot{C}(OH)_2$
22 g of oxalic acid, 370 ml of 2-propanol, and 123 ml of acetone at 37°	(0.37 *N* HCl)	2.00402	$HO_2C\dot{C}(OH)_2$

Figure 7. Spectrum during photolysis of an aqueous solution containing 22 g of oxalic acid, 370 ml of isopropyl alcohol, 123 ml of acetone, and 31 ml of concentrated HCl per liter at about 37°. The strongest line is due to reduced oxalic acid. The two weaker lines constitute a 1-1 spectrum due to the reduced monoester of oxalic acid and isopropyl alochol.

sible, namely (II) and cis and trans isomers of (I). However, all three radical forms can be converted one to the other by acid-catalyzed hydroxyl proton transfer similar to that shown by eq 2. If the exchange rates are comparable to those for the reduced diesters, they would be fast enough to give a single averaged spectrum as was seen. It is not apparent how much of each exchanging form is present.

Measurements of reduced monomethyl oxalate at several pH values are given in Table I. At a pH of 1.9 there was only one 1-3-3-1 spectrum from reduced monomethyl oxalate, and its parameters are within experimental error the same as for the acidified solution. It too is undoubtedly from the rapidly exchanging neutral radicals I and II. At a pH of 2.8 this spectrum became so weak that its stronger lines were barely seen. At a pH of 5.1 there was present a very strong 1-3-3-1 spectrum and probably another much weaker 1-3-3-1 spectrum. The latter spectrum is somewhat suspect, as it is not entirely definite that it is a 1-3-3-1 spectrum. Its 3-strength lines were not resolved from other lines, but the 1-strength lines were resolved and measured. Both 1-3-3-1 spectra had larger g values and smaller couplings than those at lower pH's. This is similar to what was found for the reduced diesters, and as in those cases, this is attributed to dissociation of the neutral radicals to form anions. At a pH of 5.1 the 1-3-3-1 spectra are probably two of the three anion radicals $CH_3O(OH)\dot{C}CO_2^-$, $CH_3O_2CCO_2H\cdot^-$, and $CH_3O_2CCO_2\cdot^{2-}$.

Reduced Oxalic Acid. The one-line spectrum for reduced oxalic acid was only studied in aqueous solution as its spectrum was very weak or absent in the absence of water. The line was not seen at a pH of 7.7 in an aqueous solution containing 117 g of potassium oxalate, 75 ml of acetone, and 75 ml of isopropyl alcohol per liter. However, when the pH was progressively lowered by adding HCl, the signal appeared with increasing intensity. At a pH of 5.9 the signal-to-noise ratio was 3. At a pH of 5.3 the line was 10 times stronger, and at a pH of 5.0 it was stronger again by a factor of 3. Observations at still lower pH values were made on another solution containing less oxalate ion and oxalic acid (see Table IV). For pH values ranging from 4.9 to 1.0 the line-heights increased by a factor of 340. This behavior suggests that electron capture occurs for oxalic acid, but not for the oxalate ions.

Table IV gives g values for reduced oxalic acid and the pH for a number of solutions. Although the absolute g values may have errors as large as ± 0.00004, the precision with which these values were measured in a single run was about ± 0.00001. The larger error is due to uncertainty in the difference in field for the positions of the epr sample and the field probe. This difference changes from run to run. The smaller error may be used in comparing g values for the same solutions at different pH values in Table IV. At some pH values it is likely that substantial amounts of neutral and anion radicals were present at the same time. Since only a single line was observed, these radicals either have superposed lines or interconvert rapidly. The g value for a pH of 1.7 is slightly higher than at lower pH values. This may be a real difference indicating the presence of some radicals in the anion form. Measurements were not made over the pH range of 1.7 to 4.5 where a large change in g takes place. The much larger values of g at the higher pH values suggest that mainly anion radicals are present while at the lower pH values mainly the neutral radical is present.

Solutions with pH values of 1.0 or less had strong enough lines that ^{13}C signals, provided they were unbroadened, should have been seen. Although large field scans were made, we did not find lines which we can confidently attribute to ^{13}C. However, we may have seen ^{13}C in two solutions. One contained 2.9 g of oxalic acid per liter and was about 5 N in HCl. Several weak lines were near the strong line. Two of these, spaced apart by (2.6 ± 0.5) G, were equally spaced from the strong line. Each weak line had about 1/200 the height of the strong line. The weak lines seemed to be broader than the strong line, but an accurate comparison could not be made. Another solution with the same concentration of oxalic acid but about 10 N in HCl also had two weak lines equally spaced from the strong line. The spacing between the two weak lines was (2.25 ± 0.15) G, and the ratio of the line height for a weak line to that of the strong line was about 1/130.

For pH values of 1.0 or less it seems very likely that there would be rapid exchange among the various forms of reduced oxalic acid by a protonation mechanism. As in the case of the reduced diesters, fast exchange is expected between tautomeric forms. Exchange between the unsymmetrical tautomeric forms such as

$$\begin{aligned} HO_2{}^{13}C\dot{C}(OH)_2 &\overset{H^+}{\rightleftharpoons} (HO)_2{}^{13}\dot{C}CO_2H \\ -O_2{}^{13}C\dot{C}(OH)_2 &\overset{H^+}{\rightleftharpoons} (HO)_2{}^{13}\dot{C}CO_2{}^- \end{aligned} \qquad (6)$$

would cause the two carbon positions to appear equivalent in an exchange averaged spectrum. Exchange between neutral and anion forms by acid dissociation and by protonation would also be expected to be rapid at a pH of 1.0 and lower. These fast exchanges would then involve all forms of reduced oxalic acid, and if the ^{13}C coupling is only a few gauss we would expect to find a sharply averaged spectrum with two hyperfine lines from species containing one ^{13}C atom, and each line would have 1/90 the strength of the main line rather than 1/180 (isotopic abundance of ^{13}C is 1.1%). We conclude that exchange by the above protonation mechanism is not responsible for the failure to find sharp ^{13}C lines at the highest acidity.

Electron exchange between oxalic acid and reduced oxalic acid in an anion form could lead to line broadening if the rate is intermediate or to loss of ^{13}C hyperfine structure if the rate is fast

$$HO_2{}^{13}CCO_2H\cdot^- + HO_2CCO_2H \rightleftharpoons HO_2{}^{13}CCO_2H + HO_2CCO_2H\cdot^- \qquad (7)$$

Exchange for this process would be slower at high acid concentrations as less of the radical would be in the anion form (which undergoes rapid exchange with the neutral forms). It is quite conceivable that the pair of weak lines seen in solutions approximately 5 N and 10 N in HCl are ^{13}C hyperfine lines and that their line heights relative to the strong central line are less than 1/90 because of broadening due to electron exchange.

Anomalous Spectra. In previous studies of solutions undergoing photolysis, we had often seen spectra whose hyperfine lines appeared to have anomalous strengths. They did not have the expected relative heights even when the microwave power was low to avoid saturation and the 100-kHz field modulation was large to reduce the effect due to possible differences in line width. In the present work we noticed that hyperfine lines of $(CH_3)_2\dot{C}OH$ are very anomalous in aqueous solutions containing oxalic acid. For this reason, we recorded spectra at room temperature in aqueous solutions containing acetone, isopropyl alcohol, HCl, and different concentrations of oxalic acid. Excited acetone reacted

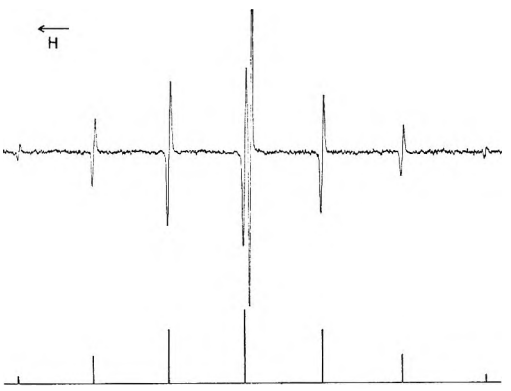

Figure 8. Spectrum during photolysis of an aqueous solution containing 1.0 g of oxalic acid, 423 ml of isopropyl alcohol, 106 ml of acetone, and 70 ml of 1 N HCl per liter at about 37°. The strongest line is due to reduced oxalic acid. The stick spectrum identifies lines of $(CH_3)_2\dot{C}OH$.

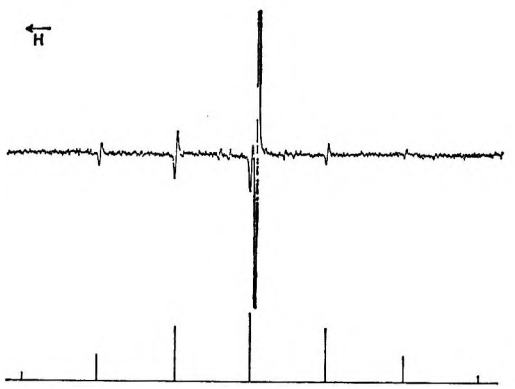

Figure 9. Spectrum during photolysis of an aqueous solution containing 11.4 g of oxalic acid, 421 ml of isopropyl alcohol, 105 ml of acetone, and 70 ml of 1 *N* HCl per liter at about 37°. The strongest line is from reduced oxalic acid. The stick spectrum identifies lines from $(CH_3)_2\dot{C}OH$.

Figure 10. Spectrum during photolysis of an aqueous solution containing 20.6 g of oxalic acid, 192 ml of isopropyl alcohol, 192 ml of acetone, and 39 ml of concentrated HCl per liter at about 37°. The strongest line is from reduced oxalic acid. The stick spectrum identifies lines from $(CH_3)_2\dot{C}OH$.

with isopropyl alcohol to form $(CH_3)_2\dot{C}OH$.[10] As the concentration of oxalic acid was increased, the steady-state concentration and lifetime of $(CH_3)_2\dot{C}OH$ decreased because of electron transfer to oxalic acid. Hydrochloric acid was incorporated in these solutions to eliminate by chemical exchange[10] the small splitting from the OH-group protons of $(CH_3)_2\dot{C}OH$. Figures 8 and 9 are for solutions which were nearly identical except for the concentration of oxalic acid. The spectrometer settings were the same in both cases. For Figure 8 there was present only 1.0 g of oxalic acid per liter. This is enough to give a very strong line from reduced oxalic acid (the strongest line present). The spectrum for $(CH_3)_2\dot{C}OH$, identified by the stick spectrum, is quite similar to the way it appears without oxalic acid, and there is a noticeable anomaly in that the low-field lines are weaker than the corresponding high-field lines. For Figure 9 there was present 11.4 g of oxalic acid per liter. The line from reduced oxalic acid is much stronger, and the lines from $(CH_3)_2\dot{C}OH$ are much weaker. Furthermore, the intensity anomaly is much greater; the ratio of high-field to low-field 6-strength or 15-strength lines differs further from unity. With even more oxalic acid present, the anomaly became even greater. In a solution containing more oxalic acid but different proportions of the other components, the low-field, 1-, 6-, and 15-strength lines were emission lines, whereas the others were absorption lines. This is shown in Figure 10.

Additions of oxalic acid were also made to acidified aqueous solutions containing acetone and ethyl alcohol which generated[6] the electron donors $(CH_3)_2\dot{C}OH$ and $CH_3\dot{C}HOH$. As before, $(CH_3)_2\dot{C}OH$ showed the intensity anomaly and it became greater as oxalic acid was added. In the absence of oxalic acid $CH_3\dot{C}HOH$ showed the intensity anomaly in a comparison of its 1-strength lines. As oxalic acid was added, the anomaly became more pronounced and quite evident in the 3-strength lines of $CH_3\dot{C}HOH$ as well; however, emission lines were not seen. It is interesting that the anomaly was seen for both radicals, as they were made in the same reaction by the transfer of hydrogen from ethyl alcohol to excited acetone.

Spectra with inverted low-field lines have been reported by Fessenden and Schuler[13] for atomic hydrogen and deuterium in liquid methane and methane–ethane mixtures during irradiation with fast electrons. Smaller, Remko, and Avery[14] saw spectra whose low-field lines were inverted or reduced in strength for all radicals they studied by pulse radiolysis. They found that emission occurs for an initial period varying from 6 to 60 μsec for different radicals. It is quite possible that this intensity anomaly is closely related to the observation[15] of nuclear magnetic resonance emission and enhanced adsorption during fast free-radical reactions.

(13) R. W. Fessenden and R. H. Schuler, *J. Chem. Phys.*, **39**, 2147 (1963).

(14) B. Smaller, J. R. Remko, and E. C. Avery, *ibid.*, **48**, 5174 (1968).

(15) (a) G. L. Closs and L. E. Closs, *J. Amer. Chem. Soc.*, **91**, 4549 (1969); (b) J. L. Closs and A. D. Trifunac, *ibid.*, **91**, 4554 (1969); (c) see references contained in a and b.

The Chemically Significant Details of Some Nuclear Reactions

by C. H. W. Jones

Chemistry Department, Simon Fraser University, Burnaby 2, British Columbia, Canada *(Received March 9, 1970)*

The chemical effects of nuclear transformations have been widely studied in solids. The aim of the present paper is to reexamine the sequence of events as they occur following thermal neutron capture in a solid. Experimental evidence recently reported in the literature is reviewed. In particular, attention is focussed on the possible existence in the γ cascade following neutron capture, of delayed states with half-lives of nanoseconds or greater, and which may be highly internally converted. The stopping time for energetic atoms recoiling from nuclear reactions in solids is also discussed, and relevant experimental evidence from Mössbauer spectroscopy and perturbed angular correlation studies is reviewed. The implications of the reported experimental work for models of the chemical reactions occurring following the (n,γ) reaction are discussed.

Introduction

Studies of the chemical effects of nuclear transformations in solids have been principally concerned in the past with investigations of the (n,γ) reaction.[1,2] A model which set out to describe the physical and chemical processes occurring during and following the recoil event was formulated by Harbottle and Sutin[3] in 1958. The purpose of the present paper is to reexamine, in the light of experimental evidence accumulated in the literature in recent years, some of the important features of the (n,γ) reactions for several specific cases. In particular, attention is focussed on the possible existence in the prompt γ cascade, following thermal neutron capture, of delayed states with half-lives of nanoseconds or greater, and which may have high internal conversion coefficients. The time over which the recoil event takes place is also examined, and relevant experimental evidence, obtained from Mössbauer spectroscopy and perturbed angular correlation measurements, is reviewed.

In the hot-zone model for recoil events in solids,[3] it was visualized that in an (n,γ) reaction the daughter atom would acquire a kinetic energy of perhaps 100's of eV as a consequence of the emission of high-energy γ rays in the γ cascade. The recoil atom was then envisaged as losing its kinetic energy in *ca.* 10^{-13} sec in collisions with surrounding substrate atoms and molecules, and in so doing the radioactive daughter atom could become chemically recombined. The recoil energy transferred to the lattice was visualized as producing 5 or 6 local "hot-spots" in the crystal surrounding the recoil atom. These hot-spots would then coalesce in *ca.* 10^{-12} sec to form a hot zone in which the crystal would be essentially molten. The hot zone was then pictured as cooling down below the melting point of the lattice in *ca.* 10^{-11} sec. During the lifetime of the hot zone it was proposed that further chemical reactions could occur involving the recoil atom. The Harbottle and Sutin model did not take account of the spectrum of recoil energies made available as a consequence of the vector cancellation of γ-ray momenta in the complex γ cascade. In one or two instances, where the main details of the γ cascade were sufficiently well established, calculations of the recoil energy spectra have been attempted.[4,5] For those specific cases, the calculations show that in a very large fraction of events the recoil kinetic energies are considerably greater than chemical bond energies, or the energy required to displace an atom in a solid lattice.

A second point, of probably greater significance, is whether the processes occurring during the recoil event are dominated simply by the kinetic energy of the recoil, or whether electronic excitation and ionization of the recoiling species will play a significant role.[6] At the recoil kinetic energies available in (n,γ) reactions, ionization will not occur through the autoionization process. However, internal conversion of γ rays in the γ cascade will result in very extensive ionization of the recoiling atom through the Auger charging process. The γ transitions which will have high internal conversion coefficients will be low-energy transitions with high multipole character. Such transitions are just those transitions which may involve delayed states with lifetimes of nanoseconds or greater.

Several authors have in the past made reference to the possible existence of relatively long-lived states with high internal conversion coefficients in the n,γ cascade, including Wexler,[5] Campbell,[4] and Wolfgang.[7] The latter author has pointed out the possibility that the recoiling atom in the (n,γ) reaction could lose its

(1) (a) L. V. Groshev, A. M. Demidov, V. I. Pelekhov, L. L. Sokolovskii, G. A. Bartholomew, A. Doveika, K. M. Eastwood, and S. Monaro, *Nucl. Data*, **A3**, 4 (1967); **A5**, 1 (1968); **A5**, 3 (1969); (b) C. M. Lederer, J. M. Hollander, and I. Perlman, Ed., "Tables of Isotopes," 6th ed, Wiley, New York, N. Y., 1967.

(2) (a) G. Harbottle, *Ann. Rev. Nucl. Sci.*, **15**, 89 (1965); (b) A. G. Maddock in "Nuclear Chemistry," Vol. II, L. Yaafe, Ed., Academic Press, New York, N. Y., 1968, p 186.

(3) G. Harbottle and N. Sutin, *J. Phys. Chem.*, **62**, 1344 (1958).

(4) I. G. Campbell, *Adv. Inorg. Chem. Radiochem.*, **5**, 135 (1963).

(5) S. Wexler, *Act. Chim. Biol. Radiat.*, **8**, 107 (1965).

(6) G. N. Walton, *Radiochim. Acta*, **2**, 108 (1964).

(7) R. Wolfgang, *Progr. React. Kinet.*, **3**, 97 (1965).

kinetic energy and become chemically bound long before the internal conversion of the long-lived state. The final chemical products incorporating the daughter radioactivity would then be greatly influenced by the Auger ionization and excitation occurring in the primary (n,γ) recoil product molecule. Müller[8] has further proposed that there may be several rounds of successive ionization and subsequent electronic relaxation following successive internal conversion of several states in the γ cascade.

In the early 1950's Wexler and Davies[9] and Yosim and Davies[10] demonstrated that iodine, bromine, and indium (n,γ) recoils acquire a positive charge in a certain fraction of events as a consequence of internal conversion. Thompson and Miller[11] subsequently investigated the charge states of In, Dy, and Mn recoils and observed that the charge state of the recoil ejected from the surface of an irradiated foil or film was independent of the chemical composition of the target. They concluded that the charge was acquired, after ejection from the surface, through internal conversion of long-lived states in the γ cascade. These experiments have been well reviewed by Wexler.[4]

The above experiments do not provide a very detailed picture of the recoil event. This can only be obtained by the direct measurement of the energy levels populated in the γ cascade, the lifetimes, and the relative number of events occurring through these states. Such information is slowly emerging from nuclear spectroscopic studies of the prompt γ cascades following thermal neutron capture and other nuclear reactions, and from related spectroscopic studies of radioactive decay processes. In addition, direct experimental evidence as to the stopping time for energetic recoil atoms in solids is becoming available from Mössbauer and angular correlation work, together with measurements on the electronic relaxation time accompanying the Auger process.

A review of information available from the literature is now presented for several nuclei of interest and the implications of the data for theories concerning the chemical effects of the (n,γ) event in solids are discussed.

Evidence for Delayed States

The data for several nuclei of interest are abbreviated in Table I and the data are discussed in detail below for each isotope.

Phosphorus-32. Phosphorus is monoisotopic and the reaction $^{31}P(n,\gamma)^{32}P$ has been one of the most widely used to produce recoil atoms in solids, and is therefore of some interest.

Mendelsohn and Carpenter[12] have recently studied the prompt γ rays emitted in the $^{31}P(d,p)^{32}P$ reaction and have determined the lifetime of the 0.077-MeV first excited state in ^{32}P to be 5×10^{-10} sec. The transition to the ground state is in all probability an M1 transition. The internal conversion coefficient will then be very small as indicated by the theoretical calculations of Sliv and Band for the internal conversion coefficient as a function of Z, the atomic number, the energy, and the multipolarity of the transition.[13] The (n,γ) cascade has been studied in some detail[14] and an examination of the intensities of the γ transitions indicates that the cascade proceeds through the 0.077-MeV level in *ca.* 45 events per 100 neutron captures.

Table I: Delayed States

Nuclide	Delayed state, MeV	Half-life, nsec	K-shell internal conversion coeff[a]	No. of events/100 neutron captures[b]	Ref for half-lives
^{32}P	0.077	0.5	Very small	45	12
^{51}Cr	0.750	10.8	Very small	72	15
^{56}Mn	0.109	5.1	(0.1–1.0)	20	18, 19
	0.023	11.0	(*ca.* 3)	25	18, 19
^{65}Zn	0.054	1600	(9)	...	22
^{80}Br	0.037	7.4	1.6	100 (Isomeric transition)	26
^{128}I	0.132	8.0	(0.5)	42	18, 27, 28
	0.030	8.6	...	...	18

[a] Values in parentheses are deduced values. [b] For the (n,γ) reactions, the values quoted are the intensities of the γ rays directly observed in the prompt spectrum.

Since the internal conversion coefficient will be small, the net effect of the delayed 0.077-MeV transition will be that the phosphorus will acquire a further recoil kinetic energy of 0.1 eV, given by

$$E_R = 537\frac{E^2\gamma}{M}$$

in eV, where E_γ is the photon energy in MeV and M is the atomic mass.

Chromium-51. Chromium has several stable isotopes, but the one reaction widely studied in recoil chemistry is the $^{50}Cr(n,\gamma)^{51}Cr$ reaction.

Bauer, *et al.*,[15] have studied the prompt γ radiation observed in the $^{51}V(p,n\gamma)^{51}Cr$ and $^{48}Ti(\alpha,n\gamma)^{51}Cr$ reac-

(8) H. Müller, Proceedings of the Symposium on Chemical Effects of Nuclear Radiations and Radioactive Transformations, International Atomic Energy Agency, Vienna, 1964, Vol. II, p 359.

(9) S. Wexler and T. H. Davies, *J. Chem. Phys.*, 20, 1688 (1952).

(10) S. Yosim and T. H. Davies, *J. Phys. Chem.*, 56, 599 (1952).

(11) J. L. Thompson and W. W. Miller, *J. Chem. Phys.*, 38, 2477 (1963).

(12) R. A. Mendelsohn and R. T. Carpenter, *Phys. Rev.*, 165, 1214 (1968).

(13) L. A. Sliv and I. M. Band, ref 1b, p 580.

(14) Reference 1a, *Nucl. Data*, A3 (1967).

(15) R. W. Bauer, J. D. Anderson, and J. L. Christensen, *Phys. Rev.*, 130, 312 (1963).

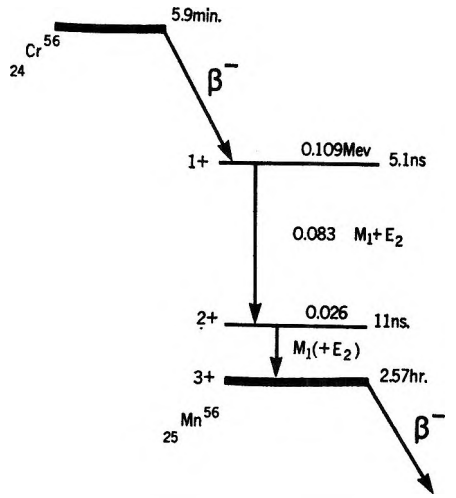

Figure 1. The decay scheme for ^{56}Cr showing the 5.1- and 11-nsec states in ^{56}Mn.[17]

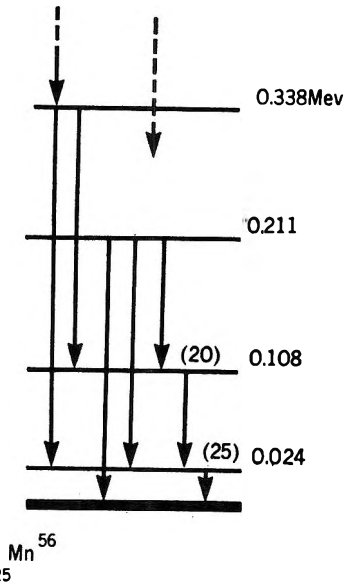

Figure 2. Part of the prompt γ cascade observed following thermal neutron capture by ^{55}Mn.[21]

tions, bombarding vanadium and titanium targets in the Livermore variable energy cyclotron. They report a 0.75-MeV state for ^{51}Cr with a half-life of 10.8 ± 0.5 nsec. They confirmed this half-life by studying the β^+ decay of 45 min ^{51}Mn which populates the 0.75-MeV state in ^{51}Cr in 0.1% of events.

The prompt γ cascade in the (n,γ) reaction has been studied by several workers.[16] The deexcitation cascade is reported to proceed through the 0.75-MeV transition in 72 events per 100 neutron captures.

The internal conversion coefficient for this high-energy transition will be very small and the net effect of the delayed state will be to impart a recoil kinetic energy to the chromium-51 atom of 5.9 eV.

Manganese-56. Manganese is again monoisotopic and the reaction of interest here is ^{55}Mn(n,γ)^{56}Mn.

The decay of ^{56}Cr allows the study of the low-lying states in ^{56}Mn as shown in Figure 1.[17] The half-life of the 109-keV level is reported[17] as 5.1 nsec while the 25-keV level is also delayed with a half-life of 11 nsec. The internal conversion coefficients for the 83-keV and 26-keV transitions have not been measured. However, the theoretical calculations of Sliv and Band,[13] together with the multipolarities reported by Dropesky, *et al.*,[17] suggest the following assignments (Table II) for the transitions.

Table II: Transitions for ^{51}Cr

Transition	Multipolarity	K-shell internal conversion coeff
0.083 MeV	$M_1 + E_2$	0.1–1.0
0.026 MeV	$M_1(+E_2)$	*ca.* 1.5

The thermal neutron capture cascade has been extensively studied. Du Toit and Bollinger[18] and D'Angelo[19] measured the lifetime of the 109-keV level directly in the γ cascade using delayed coincidence techniques. They reported values of 5.1 nsec and 11.4 nsec in good agreement with the values reported from the ^{56}Cr decay work.

Hughes, *et al.*,[20] have investigated the prompt γ-ray spectrum in detail in both the high-energy reaction, 3 MeV to 7.3 MeV, and the low-energy region 84 keV to 1 MeV. In all, some 120 γ rays were identified. This work clearly shows that the 83-keV and-26 keV levels are populated in the γ cascade in a significantly large number of events. The intensities of the γ rays per 100 neutron capture events[21] are shown in Figure 2, which also illustrates the relevant part of the γ cascade. Since the 0.026-MeV γ ray is observed in 25% of events, assuming an internal conversion coefficient of *ca.* 1.5, it follows that deexcitation through internal conversion may occur in *ca.* 36% of events. This is not inconsistent with the data available for the total number of events feeding that level.[21]

Zinc-65. Recoil studies have been concerned with two reactions ^{64}Zn(n,γ)^{65}Zn and ^{68}Zn(n,γ)^{69m}Zn.

Decay studies of ^{65}Ga have allowed a detailed investigation of the 0.054 MeV level in ^{65}Zn. The half-life measured by August and Frichtenicht[22] was found to be 1.6 μsec. The multipolarity of the 54-keV transition

(16) G. A. Bartholomew, E. D. Earle, M. R. Gunye, *Can. J. Phys.*, **44**, 2111 (1966).
(17) B. J. Dropesky, A. W. Schardt, and T. T. Shull, *Nucl. Phys.*, **16**, 357 (1960).
(18) S. J. Du Toit and L. M. Bollinger, *Phys. Rev.*, **123**, 629 (1961).
(19) N. D'Angelo, *ibid.*, **117**, 510 (1960).
(20) L. B. Hughes, T. J. Kennett, and W. V. Prestwich, *Nucl. Phys.*, **80**, 131 (1966).
(21) Reference 1a, *Nucl. Data*, **A3** (1967).
(22) L. S. August and J. F. Frictenicht, *Phys. Rev.*, **120**, 2072 (1960).

has not been assigned but the half-life is consistent with an E_2 transition based on the Weisskopf estimates[23] for γ-ray half-lives as a function of Z and the multipolarity of the transition. The K-shell internal conversion coefficient should then be *ca.* 9 (Sliv and Band).

The $^{64}Zn(d,p)^{65}Zn$ reaction has been studied by Lin and Cohen[24] and the 0.054-MeV transition observed in the prompt γ-ray spectrum. Thermal neutron capture studies for zinc have only been carried out on the naturally abundant element,[25] which contains several isotopes. In the prompt γ-ray spectrum some lines have been assigned to the $^{64}Zn(n,\gamma)^{65}Zn$ reaction and the 0.054 MeV level is populated, although the relative intensities of the γ-transition are not known in detail.

In the above work some transitions have been assigned to the $^{68}Zn(n,\gamma)^{69m}Zn$ reaction although again the work is as yet incomplete.

Bromine. There are several suitable nuclear transformations which have been thoroughly investigated for the bromine isotopes, including $^{79}Br(n,\gamma)^{80m}Br$, ^{80}Br, $^{81}Br(n,\gamma)^{82m}Br \rightarrow {}^{82}Br$ and studies, in labeled compounds, of the isomeric transition process $^{80m}Br \rightarrow {}^{80}Br$.

There is no evidence yet reported of long-lived states in the (n,γ) cascade populating ^{80m}Br or ^{80}Br. With reference to the isomeric transition studies, however, it must be pointed out that the decay of ^{80m}Br to ^{80}Br proceeds through the 37-keV level which, although it is reported to be an E_1 transition, has a half-life of 7.4 nsec.[26] The internal conversion coefficients of the 0.049-MeV and 0.037-MeV transitions are *ca.* 300 and 1.6, respectively (Figure 3).

The time taken for an Auger cascade to reach the outer valence shell of the atom, following the creation of a hole in the K shell by internal conversion is considered to be about 10^{-14} to 10^{-15} sec. Carlson and White[27] have studied the kinetic energy of the fragments observed following the explosive decomposition of molecules such as CH_3I in the gas phase as a result of an Auger cascade produced by X-ray bombardment and inner-shell hole production. Their experiments led to the conclusion that the Auger cascade reaches the valence shell in about 10^{-14} sec. Subsequent electronic rearrangements and charge neutralization will also occur fairly rapidly (see below). Thus, following internal conversion of the 0.049-MeV transition in almost every event, a rapid electronic relaxation would occur and the recoil atom may become stabilized in some chemical form before the 0.037-MeV transition takes place. In this second transition *ca.* 60% of the recoils would undergo a second Auger charging process. The recoil event would, in 60% of events, be a two-step process in effect.

Iodine-128. The $^{127}I(n,\gamma)^{128}I$ reaction has been widely studied in both inorganic and organic systems. Iodine-128 is a shielded nucleus and its energy levels cannot therefore be elucidated by decay studies. However, iodine is monoisotopic and has a large thermal neutron capture cross section. Therefore a considerable amount of work has been done on the prompt γ-ray spectrum for this element. Du Toit and Bollinger[18] first reported that the 133-keV level in ^{128}I had a half-life of 8×10^{-9} sec. This measurement has subsequently been confirmed by other workers.[28,29] Du Toit and Bollinger also inferred the existence of a 30-keV delayed state with a half-life of 8.8 nsec on the basis of experiments conducted using a thin (6 mm) NaI crystal both as the iodine target and as the γ-ray detector. This conclusion was subsequently concurred with by Cristu and Papa.[28] High-resolution γ-ray spectra taken by Archer, *et al.*,[30] and by Korteling, *et al.*,[29] show no evidence of a 30-keV γ ray, which may in turn be evidence that the transition is highly internally converted. In any event the details of the low-energy part of the γ-ray spectrum have yet to be clearly established. Archer, *et al.*, inferred the existence of an 86-keV state from their work although an 86-keV γ ray was not directly observed in that work, or in that of Korteling, *et al.*

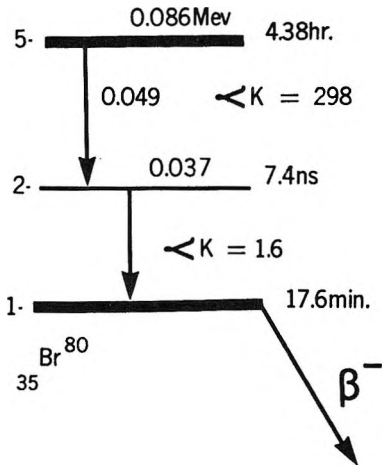

Figure 3. The decay scheme for ^{80m}Br showing the 7.4-nsec excited state.[26]

Returning to the 133-keV level whose existence and lifetime is not in question, Korteling, *et al.*, have proposed that it is an enhanced E_2 transition. This would correspond to an internal conversion coefficient of about 0.5. The 133-keV γ ray is observed in 42% of neutron capture events. It follows that thermal neutron cap-

(23) Weisskopf estimates, ref 1b, p 578.

(24) E. K. Lin and B. L. Cohen, *Phys. Rev.*, **130**, 312 (1963).

(25) Reference 1a, *Nucl. Data*, A3 (1967).

(26) W. D. Schmidt-Ott, K. W. Hoffmann, I. Y. Krause, A. Flammersfeld, *Z. Phys.*, **158**, 242 (1960).

(27) T. A. Carlson and R. M. White, *J. Chem. Phys.*, **44**, 4510 (1966); **48**, 5191 (1968).

(28) M. I. Cristu and M. S. Papa, *Rev. Roum. Phys.*, **10**, 673 (1965).

(29) R. G. Korteling, J. D'Auria, C. H. W. Jones, and T. Isenhour, *Nucl. Phys.*, in press.

(30) N. P. Archer, L. B. Hughes, T. J. Kennett, and W. A. Prestwich, *ibid.*, **83**, 241 (1966).

ture is accompanied in *ca.* 21% of events by internal conversion of the 133-keV transition.

Thus in at least *ca.* 21% of events ionization will accompany the production of ^{128}I recoil nuclei and this ionization will occur some 11 nsec on average following the primary recoil event. If the 30-keV transition exists and is highly internally converted, the fraction of events in which delayed Auger charging occurs may be even greater.

Other Nuclei. For completion, the existence of several very long-delayed states should be noted.

Chlorine-38 has a metastable isomer with a half-life of 0.74 sec and an energy of 0.67 MeV. This state has an internal conversion coefficient of 0.0005.[31] The recoil would impart a kinetic energy of 6.3 eV to the ^{38}Cl nucleus. However, cross-section measurements indicate that ^{38m}Cl is produced in only eight events for every 1000 ^{38}Cl nuclei produced.[1b]

As has been discussed in previous work, for both ^{82}Br[32] and ^{60}Co[33] there exist metastable isomers with half-lives of 6.1 min and 10.5 min, respectively. For ^{82}Br the (n,γ) reaction proceeds through the ^{82m}Br isomer in almost every event and the 0.046-MeV transition to the ground state has an internal conversion coefficient of 382.[34] For Co the cross section for the production of ^{60m}Co is 18 barns and for ^{60}Co 19 barns.[35] The internal conversion coefficient of the 0.0586-MeV transition of ^{60m}Co to the ground state is 41.[35] Thus, in these two instances the existence of the very long delayed state is readily observable. In most instances where the chemistry of ^{82}Br and ^{60}Co recoils has been investigated, the primary recoil event has been subsequently followed by Auger charging in almost every event for ^{82}Br and in approximately one-half the events for ^{60}Co. This has been taken note of in the more recent work.[32,33]

The Time of Electronic Relaxation Following K-Shell Hole Production

Direct evidence that electronic relaxation, following K-hole production and subsequent Auger processes, occurs very rapidly has been obtained for ^{57}Fe from Mössbauer spectroscopy. Trifthauser and Craig[36] performed a time differential Mössbauer emission experiment using ^{57}CoO as a source, and a single line absorber. Employing delayed coincidence techniques, the Mössbauer spectrum was taken for selected variable survival times of the 14-keV Mössbauer state following the electron capture event. The spectra exhibited a relativistic "time-filtering" effect, but there was no evidence of any change in the chemical form of the ^{57}Fe for times from 10 nsec to 200 nsec following the electron capture. This indicates that the Auger charging process and ensuing electronic rearrangements and charge neutralization processes are complete in times less than about 10^{-8} sec.

Many angular correlation experiments have been performed to study the so-called "hole-recovery effect" following production of a K-shell hole by internal conversion or electron capture.[37,38] The technique is similar to that of the experiment of Trifthauser and Craig in that a time differential experiment is performed, but now the angular correlation of the decay radiation is studied as a function of the selected variable survival time of the intermediate state in the decay. If, following the K-hole production, the subsequent electronic relaxation and rearrangement occurs over a time comparable with the lifetime of the intermediate state in the correlation study, then this will be observed as a time-dependent perturbation effect. If the relaxation is fast, but the equilibrium chemical environment of the daughter atom is very different from that of the parent because of effects resulting from the Auger cascades, then this may be observed as a static perturbation effect. The third possibility is that no perturbation effect is observed which would indicate complete and rapid recovery following the Auger cascade. For the purposes of the present discussion only examples in the first category will be discussed. The results of such experiments are generally open to interpretation and the effects of impurities and anomalous field gradients appear to confuse the issue. However, the picture emerges that in metals, as might be expected, the atomic rearrangement and recovery occurs very rapidly in times of 10^{-12} sec. In insulators, the recovery may take considerably longer and, for example, the $e_k-\gamma$ correlation in the decay of ^{197m}Hg[39,40] exhibits a perturbation for ^{197m}Hg sources embedded in insulators. This is interpreted as evidence of hole-recovery occurring during the 7-nsec lifetime of the intermediate state, following internal conversion of the 0.165-MeV transition (Figure 4). No perturbation was observed for the 0.130 MeV–0.279 MeV $\gamma-\gamma$ cascade in ^{197}Au which proceeds through the 16-psec state. This branch of the decay passes through the 0.409-MeV 7.2 sec isomer of ^{197}Au. Thus following the electron capture, complete recovery of the atomic shell may take place in less than

(31) P. Kienle, K. Wien, F. Wunderlich, and R. Haas, *Z. Phys.* **170**, 76 (1962).

(32) R. M. Iyer and J. E. Willard, *J. Amer. Chem. Soc.*, **87**, 2494 (1965).

(33) E. Lazzarini, *J. Inorg. Nucl. Chem.*, **29**, 7 (1967).

(34) J. F. Emery, *ibid.*, **27**, 903 (1965).

(35) Reference 1b, p 21.

(36) W. Trifthauser and P. P. Craig, *Phys. Rev. Lett.*, **16**, 1161 (1966).

(37) See S. Karlsson, E. Matthias, and K. Siegbahn, Ed., "Perturbed Angular Correlations," North-Holland Publishing Co., Amsterdam, 1964, p 329.

(38) S. Debenedetti, F. De Barros, and G. R. Hoy, *Ann. Rev. Nucl. Sci.*, **16**, 31 (1966).

(39) B. G. Petterson, T. R. Gerholm, J. Thun, and K. Siegbahn, *Phys. Rev. Lett.*, **6**, 14 (1961).

(40) B. G. Petterson, J. E. Thun, and T. R. Gerholm, *Nucl. Phys.*, **24**, 223 (1961).

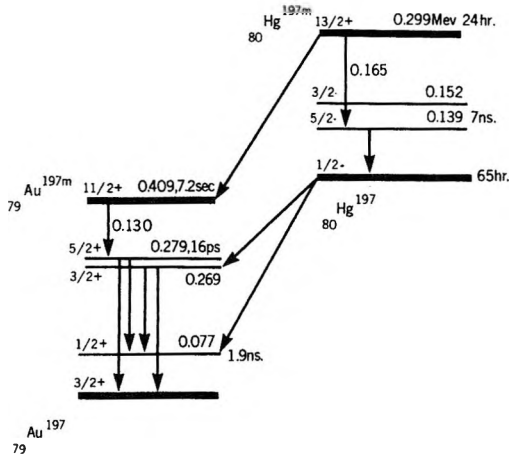

Figure 4. The decay scheme for ^{197m}Hg showing the 7-nsec perturbable state.[39]

7 sec. Alternatively, the 16-psec state may be too short-lived to couple effectively to the local electrostatic field and thus yields an unperturbed correlation.

The Stopping Time of a Recoil Atom in a Solid

The hot-zone model, proposed by Harbottle and Sutin to describe the slowing down of a recoil atom in a solid, visualized an atom recoiling, following thermal neutron capture, as losing its kinetic energy of several hundred electron volts in less than 10^{-13} sec. Several experiments have been performed in recent years which lend support to the theoretical slowing down time of the order of 10^{-13} sec. Thus Stone and Pillinger[41] investigated the 59.6-keV, 63-nsec Mössbauer transition for ^{237}Np, populated by α decay from ^{241}Am and by β^- decay from ^{237}U. In both instances the Mössbauer effect was observed, although following α decay the recoil-free fraction was lower than that following β^- decay. Kaplan[42] has examined this particular system in detail and, applying a stopping theory of high-velocity ions, concluded that the 93-keV ^{237}Np recoil produced in α decay would travel *ca.* 200 Å, stopping in a time of *ca.* 4×10^{-13} sec. Thus, following decay of the parent ^{241}Am, the recoiling ^{237}Np would come to rest long before the 59.5-keV Mössbauer transition was observed. The appreciable recoil-free fraction is evidence that a significant number of ^{237}Np nuclei come to rest and are equilibrated in strongly bonded positions in the solid lattices before the Mössbauer transition is reached.

Mullen[43] has proposed that the lower recoil-free fraction for the ^{241}Am source can be explained by local heating of the lattice due to the energy dissipated as the recoiling atom slows down. This would raise the effective temperature in the vicinity of the recoil atom above the ambient temperature. The observed recoil-free fraction corresponds to an effective temperature of 215°K, from which Mullen calculates the thermal conductivity of NpO_2 to be 1.6×10^{-5} cal cm^{-1} deg^{-1} sec^{-1}, the calculation being based on the energy deposited and on the assumption that the heat diffuses out of the recoil zone with time.

Similar Mössbauer studies have been performed using nuclear reactions to populate the Mössbauer level of interest, and observation of the recoil-free fraction, and the line width, obtained in such experiments provides evidence as to the bonding to the recoil atom at the time that the Mössbauer γ ray is emitted. Thus ^{39}K(d,p)^{40}K, ^{56}Fe(d,p)^{57}Fe, ^{39}K(n,γ)^{40}K, ^{56}Fe(n,γ)^{57}Fe, ^{155,157}Gd(n,γ)^{156,158}Gd reactions have all been studied, in addition to investigations of Coulomb excitation for ^{61}Ni, ^{57}Fe, and ^{73}Ge. In each of these experiments the procedure is essentially the same. The source in the Mössbauer experiment is the excited nucleus directly populated in the respective nuclear reaction, and the spectrum is taken against an appropriate single-line absorber. These experiments are briefly summarized in Table III.[44-51] The one important characteristic of all of these experiments is that the recoil-free fraction is substantial and that the line widths approach the theoretical values. Thus, these experiments again indicate that in these nuclear reactions the recoil atom must come to rest in the majority of events in strongly bonded positions in the solid lattice in the very short interval of time before the Mössbauer transition is observed. This was true even for the ^{61}Ni experiments where the recoil kinetic energy would be many keV and the lifetime of the Mössbauer transition is only 5.2 nsec.

Similar studies to the above have been carried out using angular correlation techniques. For particle-induced nuclear reactions, the excited states populated in the reaction may have their spins aligned with respect to the incident particle beam, and the deexcitation γ rays may then show an angular correlation with respect to the beam direction. Time differential angular correlation studies have been performed for the nuclear reactions shown in Table IV,[52-55] and again the

(41) J. A. Stone and W. L. Pillinger, *Phys. Rev. Lett.*, 13, 200 (1964).
(42) M. Kaplan, *J. Inorg. Nucl. Chem.*, 28, 331 (1966).
(43) J. G. Mullen, *Phys. Lett.*, 15, 15 (1965).
(44) S. L. Ruby and R. E. Holland, *Phys. Rev. Lett.*, 14, 591 (1965).
(45) D. W. Hafemeister, E. B. Shera, *ibid.*, 14, 593 (1965).
(46) D. A. Goldberg, P. W. Keaton, Jr., Y. K. Lee, L. Madansky, and J. C. Walker, *ibid.*, 15, 418 (1965).
(47) F. E. Obenshain and W. Berger, *Bull. Amer. Chem. Soc.*, 12, 24 (1967).
(48) J. Fink and P. Kienle, *Phys. Lett.*, 17, 326 (1965).
(49) D. Seyboth, F. E. Obenshain, and G. Czjzek, *Phys. Rev. Lett.*, 14, 954 (1965).
(50) D. A. Goldberg, Y. K. Lee, E. T. Ritter, R. R. Stevens, Jr., and J. C. Walker, *Phys. Lett.*, 20, 571 (1966).
(51) G. Czjzek, J. L. C. Ford, Jr., J. C. Love, F. E. Obenshain, and H. H. F. Wegener, *Phys. Rev. Lett.*, 18, 529 (1967).
(52) J. Schmidt, J. Morganstern, H. J. Körner, J. Braunsfurth, and S. J. Skorda, *Phys. Lett.*, 24B, 457 (1967).
(53) A. W. Sunyar and P. Thieberger, *Phys. Rev.*, 151, 910 (1966).
(54) J. Bleck, D. W. Haag, W. Leitz, and W. Ribbe, *Phys. Lett.*, 26B, 134 (1968).

Table III: Mössbauer Studies[a,b]

Nuclear transformation	Mössbauer transition populated E, keV	$t^{1/2}$, nsec	Source compd	Effect	Ref
$^{237}U\ \beta^-\ ^{237}Np$	59.6	63	Oxide	f, following β-decay	41
$^{241}Am\ \alpha\ ^{237}Np$	59.6	63	Oxide	Larger than that for α-decay	
$^{39}K(d,p)^{40}K$	29.4	3.9	Metal	Anomolously high f due to source oxidation	44
$^{39}K(n,\gamma)^{40}K$	29.4	3.9	Metal KF KCl	All f values slightly low	45
$^{56}Fe(d,p)^{57}Fe$	14.4	100	Metal	No effect	46
$^{56}Fe(n,\gamma)^{57}Fe$	14.4	100	Metal Fe_2O_3	Change in hyperfine interactions observed	47
$^{155}Gd(n,\gamma)^{156}Gd$	89.0	2.2	Oxide and metal in each case	Small effect on f with target material	48
$^{157}Gd(n,\gamma)^{158}Gd$	79.5	2.3			
^{61}Ni Coulomb excitation	67.4	5.2	Metal	f slightly low	49
^{57}Fe Coulomb excitation	14.4	100	Metal	No change in f	50
			Fe_2O_3	f slightly low	
^{73}Ge Coulomb excitation	67	1.6	Metal	f slightly low	51

[a] A table similar to this one may be found in J. F. Ullrich, Ph.D. Thesis, Department of Nuclear Engineering, University of Michigan, 1967. [b] N. A. Burgov and V. Davydov in "Chemical Applications of Mössbauer Spectroscopy," V. I. Goldanskii and R. H. Herber, Ed., Academic Press, New York, N. Y., 1968.

Table IV: Time Differential Angular Correlation Studies

Nuclear reaction	Target material	γ-Transition studied with respect to the incident particle beam E, MeV	$t^{1/2}$, nsec	Ref
$^{16}O(He^3,p)^{18}F$	$CaO_{(s)}$	1.125	221	52
$^{19}F(\alpha,n)^{22}Na$	$CaF_{2(s)}$	0.587	350	52
$^{19}F(\alpha,\alpha')^{19}F$	$CaF_{2(s)}$	0.197	126	52
$^{19}F(\alpha,n)^{22}Na$	$HF_{(soln)}$	0.587	350	53
$^{79}Br(p,n)^{79}Kr$	$KBr_{(solc)}$	0.148	112	54
$^{57}Fe(p,p')^{57}Fe$	Metal foil	0.136	8.9	55

results clearly show that the highly energetic recoil atoms stop in times short by comparison with the half-life of the isomeric state populated in the reaction. The time differential angular correlation pattern exhibits a pure precession, without any attenuation or perturbation, in the solid as well as the liquid substrates. In the case of the solid targets this indicates that the recoil comes to rest in a normal cubic lattice site in times short by comparison with the half-life of the intermediate state. The case of the recoiling Fe nuclei is of particular interest because of the comparison available with the Mössbauer work and the fact that the angular correlation study extends the time measurement down to 10 nsec or so, since the latter employs the 133-keV, 8.9-nsec state. The results, using an iron-foil as target, show that all the recoiling nuclei are present in equivalent magnetic sites 10 nsec after the recoil and that the radiation damage surrounding the recoil is negligible.

The above experiments provide only an upper estimate of the stopping time for the energetic recoil. Recent studies of the time-integral perturbed angular correlations observed in particle-induced nuclear reactions have led to the direct study of the stopping process for such recoils. This work is discussed in detail in a recent review.[56] The experiments may be briefly described as follows. A target foil of ^{70}Ge, mounted on an iron backing, is bombarded with 30 to 50-MeV ^{16}O ions. The incident heavy-ion beam is backscattered and the excited ^{70}Ge nuclei recoil with energies of 10 to 20 MeV into the iron backing. The γ ray from the 1.04-MeV, 1.3-psec C excited state of the recoiling ^{70}Ge nucleus exhibits a very large angular correlation with respect to the direction of the back-scattered ^{16}O ion beam. This correlation is perturbed by the magnetic field in the iron foil. The perturbation manifests itself as both an attenuation and a precession of the time integral angular correlation function. As discussed by Grodzins, the experimental data indicate anomalous precessions which can be explained by the presence of a time-dependent perturbation lasting less than 2 psec and which apparently has its origin in the physical phenomena accompanying the slowing down of the recoil in the metal foil. The precise origin of the transient hyperfine field observed is not well understood but it may lie in the picking up of electrons in the host ma-

(55) H. J. Köstner, J. Braunsfurth, H. F. Nesemann, S. Skorka, and B. Zeitnitz, *Compt. Rend. Cougr. Intern. Phys. Nucl., Paris, II*, 478 (1964).

(56) L. Grodzins, *Ann. Rev. Nucl. Sci.*, **18**, 291 (1968).

terial as the highly charged recoil slows down. These experiments are very important ones since they appear to provide direct physical evidence as to the time scale of the slowing down event and the nature of the processes occurring.

Discussion

In the light of the above literature review it is possible to reexamine the hot-zone model proposed by Harbottle and Sutin.

All of the experiments in which the stopping time of the recoil produced in a nuclear reaction was studied indicate that the very energetic (keV to MeV) recoiling ion produced in many of these processes stops in the lattice at an apparently normal lattice site in times less than 10^{-9} sec. The experiments discussed by Grodzins suggest that for 10–20-MeV ^{70}Ge nuclei in a metal foil the stopping time is of the order of picoseconds or less. In the latter experiment there is no evidence that the lattice at the end of the recoil track is maintained at very high temperatures for times of the order of 10^{-11} sec. However, while the recoil energy deposited in this reaction is extremely high, the very high thermal conductivity of the iron foil, into which the ions recoil, would presumably dissipate the energy very rapidly indeed. In contrast, Mullen's interpretation of Stone and Pillinger's work suggests that the AmO_2 lattice surrounding the ^{237}Np 93 keV α recoil is still above the ambient temperature some 100 nsec following the recoil event. In this instance the insulating nature of the host-lattice prevents the rapid diffusion of heat out of the recoil zone and the experimental results are consistent with the generation of high local temperatures in the recoil site.

Returning then to the case of (n,γ) recoils, the low energy of 100's of eV will undoubtedly be lost to the lattice in less than picoseconds. Whether or not this leads to very high local temperatures and melting of the crystal is not clear. The Mössbauer experiments of Table III indicate that the effects on f, the recoil-free fraction, were of a similar nature in the (n,γ) studies as for the other, more energetic, nuclear reactions. This may well indicate that the physical characteristics of the lattice site at which the recoil finally comes to rest are determined principally by the expenditure of the last several hundred eV of energy at the end of the recoil track. Notwithstanding Mullen's argument, there is no direct evidence, either from the Mössbauer or angular correlation work, that the crystal actually becomes molten around the recoil. The relatively nondefective lattice site observed in almost every instance 10^{-9} sec or so following the nuclear reaction would suggest that the crystal does not undergo any traumatic physical change as the recoiling atom slows down.

Given the fact that the recoil stops in less than picoseconds and that any hot-zone created in the process will probably have cooled to ambient temperature in less than nanoseconds, the existence of the delayed states indicated in Table I is of some importance.

For the case of ^{32}P, the 0.077-MeV delayed state will probably have little effect on the recoil product distribution. The delayed recoil of 0.1 eV will not be sufficient to lead to further bond rupture or significant excitation of the recoil. Since in the primary event the recoil will have acquired 100's of eV of kinetic energy, a further 0.1 eV will hardly be significant in influencing the final chemical form of the recoil atom.

In the case of ^{51}Cr, however, the delayed recoil event now imparts 5.9 eV to the recoil atom. This could conceivably lead to a further bond rupture event since bond strengths are generally of the order of 5–10 eV. At the very least it will create a further hot-spot at the recoil site, which may lead to further chemical reactions of the recoil atom. The sequence of events occurring, then, will be primary recoil accompanying the prompt γ cascade, initial bond rupture for compound ions, and subsequent slowing down and stopping of the chromium. In the latter processes the chromium fragment may react with a substrate lattice ion and, on cooling of the recoil zone, the radioactive ^{51}Cr may become stabilized in the lattice in a chemical form different from that of the parent ion. The delayed recoil event may then produce a further bond rupture in the primary recoil molecule. This latter event will be characterized by the very low kinetic energy available in the process and, if bond rupture were to occur, the secondary chromium recoil would probably not even escape the primary fragment lattice site. Nevertheless, this second event could influence the final chemical form of the ^{51}Cr atom in the lattice and this may not be the same chemical form as resulted in the relatively high energy primary event.

The existence of the delayed states in the γ cascades for ^{56}Mn, ^{65}Zn, and ^{128}I are of great significance since in these instances the delayed transitions may be internally converted. In those instances where the recoil event is accompanied by internal conversion of the delayed state, the attendant Auger charging, ionization and excitation may be expected to play a significant role in determining the final chemical form and physical environment of the recoil atom in the solid. In addition to the gross rearrangement of the valence shell of the recoil atom, the radiolysis of the immediately surrounding lattice by the low-energy Auger electrons, and X-rays emitted in the Auger cascade, must be expected to have some effect on the final chemical form observed. In these events kinetic energy will clearly not be the only factor of importance. (It should perhaps also be noted that for nuclei with large neutron capture cross-section, the self-radiolysis of the surroundings by neutron-capture γ rays themselves cannot be neglected.)

In the cases of ^{56}Mn and ^{128}I the possibility exists for a double Auger cascade. Following the primary recoil

event, the first delayed state may undergo internal conversion to be followed by relaxation and charge neutralization in a time of *ca.* 10^{-8} sec or less. (The Mössbauer work of Trifthauser and Craig indicates a time less than *ca.* 10 nsec in CoO, while the angular correlation measurements appear to indicate that relaxation is still occurring during the lifetime of the 7-nsec state in the decay of ^{197m}Hg in insulators.) The second delayed event, with accompanying Auger charging, would then trigger a second round of ionization and subsequent charge neutralization. A similar sequence of events with respect to Auger charging may be anticipated for ^{80m}Br → ^{80}Br as discussed above.

The possibility of internal conversion occurring some considerable time after the primary recoil event in the (n,γ) reaction was not considered in Harbottle and Sutin's original paper. In the specific instances discussed above, and presumably in many other instances still to be identified, these processes must be considered where a detailed description of the reactions occurring during the recoil event is attempted.

Conclusion

The experimental evidence reviewed sheds some light on the nature of the recoil event occurring in a solid following a nuclear reaction. The recoil atom undoubtedly stops in a very short period of time, probably of the order of picoseconds. There is no conclusive evidence, for a wide variety of nuclear reactions and simple chemical substrates, that the lattice becomes molten surrounding the recoil atom. In almost all instances the recoil atom finds itself, in less than nanoseconds, in a well-ordered lattice site. No studies have been made of the slowing down and stopping of a recoil atom in a complex lattice containing compound ions.

For several nuclear reactions of interest there is evidence that the reaction occurs through a delayed state in a significant number of events and that internal conversion of those states may occur in the cases noted. The chemical effects associated with the internal conversion must be considered, in describing the recoil event in detail.

Acknowledgment. The author thanks the National Research Council of Canada for a research grant.

Trapped Hydrogen Atoms Produced by γ Rays in Alcohol–Water Mixtures at 77°K

by Hirotomo Hase[1a] and Larry Kevan[1b]

Department of Chemistry, Wayne State University, Detroit, Michigan 48202 *(Received May 14, 1970)*

Small H_t yields ($G_{max} \sim 0.1$) are observed in γ-irradiated MeOH–H_2O, EtOH–H_2O, and *n*-PrOH–H_2O mixtures at 77°K although H_t is not observed in either pure component at 77°K. The H_t yield shows a maximum at 0.1 to 0.3 mole fraction alcohol; the maximum occurs at lower mole fraction for longer chain alcohols. Electrons are also trapped in the mixtures and when they are photobleached the H_t yield increases. The H_t yields show a striking correlation with the excess enthalpy of mixing of alcohol–water mixtures; both effects seem to be related to alcohol–water complex formation. Epr line widths in deuterated mixtures give information on the trapping site structure, and the H_t yields in deuterated mixtures suggest that most of the H_t comes from the water molecules.

Introduction

Radiolysis of water produces a small yield of primary hydrogen atoms. This is indirectly deduced from scavenging effects of solutes.[2] Recently, a transient absorption spectrum near 200 nm has been interpreted as the direct observation of hydrogen atoms in pulse-irradiated water.[3] Radiolysis of ice also produces hydrogen atoms which are trapped at 4°K and can be directly observed by epr.[4] However, in irradiated ice at 77°K no hydrogen atoms are trapped, although they are presumably formed. In liquid alcohols there is

(1) (a) Research Reactor Institute, Kyoto University, Osaka, Japan. (b) To whom correspondence should be addressed.

(2) E. Hayon in "Radiation Chemistry of Aqueous Systems," G. Stein, Ed., Interscience, New York, N. Y., 1968, pp 157–209.

(3) P. Pagsberg, H. Christensen, J. Rabani, G. Nilsson, J. Fenger, and S. O. Nielsen, *J. Phys. Chem.*, **73**, 1029 (1969).

(4) H. S. Judeikis, J. M. Fluornoy, and S. Siegal, *J. Chem. Phys.*, **37**, 2272 (1962).

also much indirect evidence based on solute reactions that hydrogen atoms are produced during radiolysis,[5] but in ethanol irradiated at 4°K no trapped hydrogen atoms are detected by epr,[6] nor are they found at any higher temperature. Recent work on irradiated solid alkanes has shown that H atom trapping is dependent on subtle characteristics of the matrix.[7]

Even though neither irradiated water or alcohol traps hydrogen atoms at 77°K we find that trapped H atoms, H_t, are observed in irradiated water–alcohol mixtures at 77°K.[8] The H_t yield *vs.* mixture composition seems to correlate with some thermodynamic properties of alcohol–water mixtures and suggests that the H atoms are trapped in a specifically structured environment. Deuterated mixtures have been used to probe the structural requirements for trapping and to determine the molecular source of the H atoms that are trapped.

Experimental Section

Reagent grade 1-propanol, methanol, and ethanol were used without further purification. Methanol-d_4 was obtained from Stohler Isotope Chemicals and D_2O was obtained from Matheson Coleman and Bell Co.

Spherical samples were prepared as described previously;[9] this avoids the use of any sample container. ^{60}Co γ irradiation was carried out at 77°K at a dose rate of 0.34 Mrad/hr. The total dose was 0.34 Mrad for each sample. The H_t yields appeared to be linear with dose to at least 0.5 Mrad; higher doses were not studied.

The epr spectra were recorded on a Varian V4502 epr spectrometer with a field modulation frequency of 100 kHz and a modulation amplitude of 0.6 G at low microwave power. Measurements were generally taken at a microwave magnetic field, $H_1 = 0.006$ G, low enough to avoid saturation of H_t in 7.0 *M* H_2SO_4. It was assumed that there was no significant saturation of H_t in the alcohol–water mixtures under this condition and extensive studies were not carried out. The number of trapped spins was determined by comparison with the H_t yield in γ-irradiated 7.0 *M* H_2SO_4 at 77°K. The 100-eV yield (*G* value) of the H_t spectrum in 7.0 *M* H_2SO_4 at 77°K was taken as 1.2.[10]

Results and Discussion

H_t is identified by its 505-G doublet epr spectrum[8] and is easily measured quantitatively. Figure 1 shows the H_t yield *vs.* mole fraction of the alcohols. Note that the absolute *G* value is small compared to $G(e_t^-)$ in alcohol. The maximum H_t yield was obtained at the mole fraction of 0.16, 0.20, and 0.30 for 1-propanol–water, ethanol–water, and methanol–water mixtures, respectively. The maximum H_t yield obtained here is about 5% of the H_t yield in 7.0 *M* H_2SO_4 at 77°K.[10] In the case of 1-propanol–water and ethanol–water mixtures, the samples were opaque near the mole fraction of the alcohols that gave the maximum H_t yield, while the samples were glassy (*i.e.*, transparent) in the case of methanol–water mixtures.

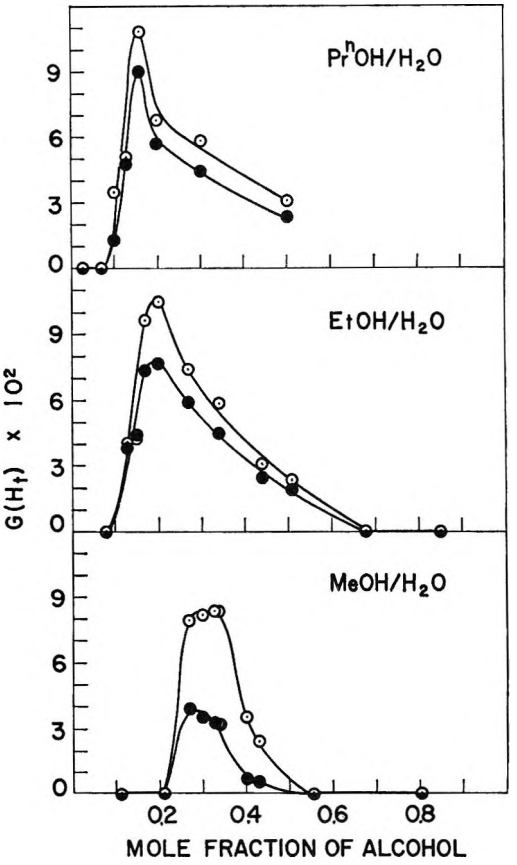

Figure 1. H_t yields per 100 eV of radiation energy absorbed (*G*) *vs.* alcohol mole fraction in γ-irradiated (0.34 Mrad) alcohol–water mixtures at 77°K: ●, yield after irradiation; ⊙, yield after irradiation and bleaching with visible light.

The center of the epr spectrum near $g = 2$ consists of overlapping spectra due to trapped electrons (e_t^-), OH radicals, and alcohol radicals.[11] Most of the irradiated samples were also colored blue, which color is associated with the e_t^- optical band. The color could be bleached with visible light from a tungsten bulb. The H_t yield and the alcohol radical yield were increased after complete photobleaching of e_t^-; the OH yield could not be followed because of spectral overlap. The increase in the H_t yield is shown in Figure 1; it is most dramatic in the methanol mixtures. This may be due to a larger e_t^- yield in the glassy methanol–water mixtures com-

(5) G. R. Freeman, *Actions Chim. Biol. Radiat.*, in press.
(6) D. R. Smith and J. J. Pieroni, *Can. J. Chem.*, **45**, 2723 (1967).
(7) M. Long and J. E. Willard, *J. Phys. Chem.*, **74**, 1207 (1970).
(8) A similar observation has been made by R. Chandra, personal communication.
(9) J. Zimbrick and L. Kevan, *J. Chem. Phys.*, **47**, 2364 (1967).
(10) R. Livingston and A. J. Weinberger, *ibid.*, **33**, 499 (1960).
(11) For a review see L. Kevan, *Actions Chim. Biol. Radiat.*, **13**, 57 (1969).

pared to the opaque ethanol–water and 1-propanol–water mixtures.

The increase in H_t on photobleaching suggests that mobile electrons (e_m^-) are precursors of at least some H_t. Possible reactions for forming H_t during photobleaching of e_t^- are (1) to (3) and perhaps (4). Irradiation of pure ethanol at 4°K produces e_t^-, but

$$e_t^- + CH_3OH_2^+ \xrightarrow[vis]{h\nu} CH_3OH + H_t \quad (1)$$

$$e_t^- + CH_3OH \xrightarrow[vis]{h\nu} CH_3O^- + H_t \quad (2)$$

$$e_t^- + H_3O^+ \xrightarrow[vis]{h\nu} H_2O + H_t \quad (3)$$

$$e_t^- + H_2O \xrightarrow[vis]{h\nu} OH^- + H_t \quad (4)$$

bleaching e_t^- at 4°K does not produce H_t.[6] This result suggests that H is not trapped in pure ethanol at 4°K or that reactions 1 and 2 do not occur.

To investigate the molecular origin of the H atoms, H_t and D_t yields were measured in deuterated mixtures containing 0.33 mole fraction methanol and are given in Table I. Some exchange between the hydroxyl protons of water and alcohol will occur, but one is still able to make some relevant conclusions. No exchange occurs to the hydrogens of the methyl group in methanol. The fraction of H_t out of the total hydrogen trapped in CD_3OD–D_2O mixtures was 0.10. Since the solutions were 99% deuterated it is clear that some sort of energy transfer occurs to preferentially form H_t with respect to D_t. Such effects have been observed before,[4] but they are not of primary concern here. If the preferential formation of H_t is taken into account, the H_t and D_t yields found do indicate that most of the trapped hydrogen atoms come from water and not alcohol. This is best shown by the observation of only H_t in CD_3OD–H_2O mixtures. Similar results are obtained after photobleaching of e_t^- which therefore suggest that reaction 3 and perhaps 4 occur and predominate over reactions 1 or 2. D_t from methanol should arise primarily from the methyl group since CH_2OH radicals are observed in pure methanol; so some hydroxyl proton exchange does not change our conclusions. The difference in total relative yields may indicate an isotope effect on the H_t trapping probability but its nature is not obvious.

Table I: Relative Yields and Line Widths of H_t and D_t in γ-Irradiated Methanol–Water Mixtures at 77°K[a]

	CH_3OH–H_2O	CH_3OH–D_2O	CD_3OD–H_2O	CD_3OD–D_2O
Relative total yield	1.00	0.61	1.70	0.90
Fraction H_t	1.0	0.45	1.0	0.10
Fraction D_t	0	0.55	0	0.90
ΔH_{pp} (H_t),[b] G	3.9	2.3	3.2	1.7
ΔH_{pp} (D_t),[b] G	...	2.3	...	1.7
Calcd[c] ΔH_{pp} (H_t),[b] G				
For D–H and H–D = 2		2.6	3.3	
For D–H and H–D = 3		2.4	3.5	
For D–H and H–D = 4		2.3	3.6	

[a] Mole fraction of methanol is 0.33 for all mixtures. [b] Line width between peaks of first derivative curves. [c] See text for explanation.

The line widths of H_t and D_t in the deuterated mixtures are also given in Table I. In the same matrix the H_t and D_t line widths are equal. However, the line width does decrease as the matrix is deuterated, from which one infers that a major contribution to the line width is unresolved hyperfine interaction with the matrix protons. We have analyzed the line width as a root-mean-square sum of unresolved hyperfine interactions and intrinsic line width as has been done previously for e_t^- line widths.[12] In completely deuterated mixtures the theoretical hyperfine contribution is four times smaller than in completely protiated mixtures. Using this fact and the observed line widths, we obtain the intrinsic contribution and can then calculate the line widths for specific site models for the CH_3OH–D_2O and CD_3OD–H_2O mixtures. In Table I we tabulate the results for H trapping sites which have D–H in CH_3OH–D_2O and H–D in CD_3OD–H_2O mixtures equal to the ratios 2, 3, and 4 for the matrix hydrogens that interact with H_t (*i.e.*, hydroxyl protons). Exchange between hydroxyl protons will not significantly change the D/H ratio. For each ratio the calculated values agree well with the experimental values, but the calculated values for CH_3OH–D_2O *vs.* CD_3OD–H_2O mixtures change in opposite directions as the D–H and H–D ratios increase. The best balanced agreement between the model calculations and experiment occurs for ratios between 2 and 3. The ratio of 2 is the molecular ratio of deuterated and protiated molecules in the mixtures. Thus we tentatively consider that one hydrogen from each molecule constituting the trapping site, presumably the hydroxyl hydrogen on the alcohol molecules, interacts with the trapped atom. The simplest trap structure in methanol–water mixtures would be a hydrogen-bonded trimer of one methanol and two water molecules. Such a structure must introduce some extra stability into the matrix to constitute an effective trap for H_t.

Perhaps surprisingly, thermodynamic properties of methanol–water liquid mixtures give strong support to the picture. The excess enthalpy of mixing of methanol and water at 25° is negative and has a minimum at 0.3 mole fraction methanol.[13,14] This has been interpreted as preferential hydrogen bonding between meth-

(12) L. Kevan, *J. Amer. Chem. Soc.*, **87**, 1481 (1967).

anol and water to form well defined complexes. The composition dependence of sound absorption coefficients in alcohol–water mixtures has also been interpreted as due to alcohol–water complex formation in the same composition range as suggested by the thermodynamic data. Furthermore, ethanol–water and 1-propanol–water mixtures have negative excess enthalpies of mixing with minima at about 0.2 and 0.1 mole fraction alcohol. These compositions strikingly correlate with the compositions for the maximum H_t yields in the frozen mixtures. In fact, the 1-propanol experiments were done specifically to test this correlation. It clearly appears that whatever structure is present in the alcohol–water liquid mixtures at 25° is frozen in on rapid freezing to 77°K and constitutes a trapping site for hydrogen atoms produced by radiolysis. The negative excess enthalpies become slightly more negative as the temperature is lowered below 25°, but the curve shape does not change much. Thus we expect the structure to be readily frozen-in. It also follows that precooling the matrix before freezing will not give much new information about the correlation.

Detailed knowledge of the structure of the inferred alcohol–water complexes is lacking. We have found no published spectroscopic studies that provide concrete structural details. If such studies could be done they would provide important insight into the interactions that stabilize the H atoms and affect the mixing enthalpies.

Acknowledgment. This research was supported by the Air Force Office of Scientific Research under Grant No. AFOSR-70-1852 and by the Atomic Energy Commission under Contract No. AT(11-1)-2086.

(13) F. Franks in "Physico-Chemical Processes in Mixed Aqueous Solvents," F. Franks, Ed., American Elsevier, New York, N. Y., 1967, pp 50–70; see especially pp 54–56.

(14) F. Franks and D. J. G. Ives, *Quart. Rev. Chem. Soc.*, **20**, 1 (1966).

Scavenger Effects on Electrons Produced by γ Rays and Photoionization in Alkaline Ices at 77°K

by Hirotomo Hase and Larry Kevan*

Department of Chemistry, Wayne State University, Detroit, Michigan 48202 *(Received April 16, 1970)*

Acrylamide is used as an electron scavenger in the radiolysis and ferrocyanide photoionization of 5 and 10 *M* NaOH ices. The concentration of acrylamide required to reduce the e_t^- yield to one-half its initial value is higher for γ radiolysis than for ferrocyanide photoionization by a factor of about 3.5. This difference is shown to be due to the spatial nonuniformity of e_m^- generated by γ rays. Within the framework of a simple model the average travel distance of e_m^- is 56 Å and 44 Å in 5 and 10 *M* NaOH ices, respectively, for both photoionization-produced and radiation-produced electrons. A kinetic analysis suggests that a high concentration of solute molecules tends to destroy trapping sites in the ices.

Introduction

The initial deposition of ionizing radiation in condensed media is not uniform. The ultimate trapped radicals and ions in irradiated solids may or may not reflect this nonuniform energy deposition depending on how far they move before being trapped. Information about the spatial distribution of trapped electrons (e_t^-) in frozen solutions can be obtained by (a) epr observation of spin–spin interactions, (b) dependence of e_t^- yield on scavenger concentration, and (c) thermal-decay kinetics.[1] Electrons are trapped efficiently in 10 *M* NaOH glassy alkaline ice at 77°K. Paramagnetic relaxation studies of spin–spin interactions have shown that spatially nonuniform distributions of trapped electrons exist in γ[2] and β[3] irradiated alkaline ice. A nonuniform distribution of e_t^- implies that the initially produced mobile electrons (e_m^-) do not travel far enough before being trapped to randomize. If electrons are produced in alkaline ice by photoionization of ferrocyanide, paramagnetic relaxation studies show that their spatial distribution is uniform.[4] This does

* To whom correspondence should be addressed.

(1) L. Kevan in "Radiation Chemistry of Aqueous Systems," G. Stein, Ed., Wiley-Interscience, New York, N. Y., 1968, pp 21–72.

(2) J. Zimbrick and L. Kevan, *J. Chem. Phys.*, **47**, 2364 (1967).

(3) H. Hase and L. Kevan, *ibid.*, **52**, 3183 (1970).

not mean that photoionization-produced e_m^- travel farther before being trapped than radiation-produced e_m^-; it simply reflects the fact that photoionization produces e_m^- singly.

Here, we have studied the comparative effects of acrylamide scavenger on e_m^- produced by γ radiolysis and by photoionization in alkaline ice. We find a significant difference which can only be reasonably explained by considering the difference in the initial spatial distributions of e_m^- produced by the two methods. We conclude that the travel distance of e_m^- in alkaline ice is similar for photoionization and for radiolysis. Also, we relate our results to e_m^- scavenger data for radiolysis and photoionization in nonpolar organic glasses.

In addition to relative travel distance, the dependence of e_t^- yield on the concentration of an e_m^- scavenger should give semiquantitative information about how far e_m^- travels before being trapped. A number of studies of the effect of e_m^- scavengers in γ-irradiated alkaline ice have been made.[5-10] However, several assumptions are necessary to derive an e_m^- travel distance from the scavenger concentration data. An analysis by Seddon and Smith[10] in which acrylamide was used as the scavenger led to 170 Å as the e_m^- travel distance in 8 *M* NaOH at 0.2 Mrad radiation dose. At this dose the average distance between e_t^- is 180 Å (assuming spherical volumes). If the above derived e_m^- travel distance is about correct a nearly uniform distribution of e_t^- is indicated. This conflicts with the paramagnetic relaxation data[2] and also with an analysis of thermal decay data.[11] We show that a simple analysis of e_m^- scavenger data gives e_m^- travel distances that are in agreement with other types of experimental data.

Experimental Section

Reagent grade NaOH and acrylamide were used without further purification; 5×10^{-3} *M* reagent grade potassium ferrocyanide was dissolved in 5 *M* and 10 *M* NaOH for the photoionization experiments. Different concentrations of acrylamide were added to the alkaline solutions. Spherical samples were prepared as described previously.[2] ^{60}Co γ irradiation was carried out at 77°K at a dose rate of 0.3 Mrad/hr. The total dose was 0.15 Mrad for each sample. Photoionization was carried out as described previously.[4]

Epr spectra were recorded on a Varian V 4502 epr spectrometer with a field modulation frequency of 100 kHz and a modulation amplitude of 0.6 G at low microwave power. Pure acrylamide radical spectra were obtained after complete photobleaching of e_t^-. Trapped electron signals were obtained by manually subtracting the pure acrylamide radical spectrum normalized to either side of the total spectrum in which region only the radical contributes. This normalization compensated for the increase in the radical spectrum intensity upon photobleaching. The number of the trapped spins was determined by doubly integrating the epr spectrum and by comparison with the e_t^- yield in γ irradiated 10 *M* NaOH at 77°K. The 100-eV yield (*G* value) of the uncorrected e_t^- spectrum in 10 *M* NaOH at 77°K was taken as 2.1.[1]

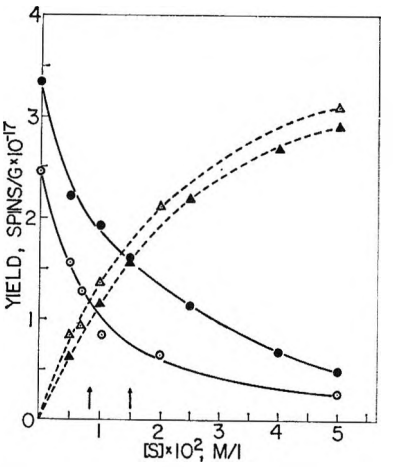

Figure 1. Effect of acrylamide concentration on the yield of e_t^-(○) and acrylamide radical (△) in 5 *M* NaOH ice, and e_t^-(●) and acrylamide radical (▲) in 10 *M* NaOH ice irradiated by γ rays at 77°K. Total γ dose was 0.15 Mrad for each sample. The arrows show the position of C_1 in 5 and 10 *M* NaOH ices (see text).

Results and Discussion

The epr spectrum obtained after γ radiolysis of the alkaline solution of acrylamide had the same structure as one after photolysis of the solution containing ferrocyanide ion and acrylamide. The spectrum consisted of a quintet and a singlet, both with $g \sim 2.000$. Seddon and Smith[10] attributed the quintet with a 25-G splitting and a binomial intensity distribution to the radical having the structure $CH_3CHCONH_2$. This radical is plausibly produced by reaction of mobile electrons with acrylamide molecules followed by proton transfer from the matrix. However, in this work the exact identity of the radical is not critical. The singlet, which is also correlated with the blue color of the irradiated sample, is attributed to e_t^-.

Radicals and e_t^- yields *vs.* acrylamide concentration in γ-irradiated or photolyzed 5 and 10 *M* NaOH solu-

(4) H. Hase and L. Kevan, *J. Amer. Chem. Soc.*, 90, 6875 (1968).

(5) P. N. Moorthy and J. J. Weiss, *Phil. Mag.*, 10, 659 (1964).

(6) L. Kevan in "Progress in Solid-State Chemistry," Vol. 2, H. Reiss, Ed., Pergamon Press, New York, N. Y., 1965, pp 304-329.

(7) B. G. Ershov, A. K. Pikaev, P. I. Glazunov, and Y. Spitsyne, *Dokl. Akad. Nauk SSSR*, 149, 363 (1963).

(8) B. G. Ershov, E. Lyu, and A. K. Pikaev, *High Energy Chem.*, 1, 478 (1967).

(9) K. Eiben and D. Schulte-Frohlinde, *Z. Phys. Chem.*, 45, 20 (1965).

(10) W. A. Seddon and D. R. Smith, *Can. J. Chem.*, 45, 3083 (1967).

(11) F. S. Dainton and C. Gopinathan, *Trans. Faraday Soc.*, 65, 151 (1969).

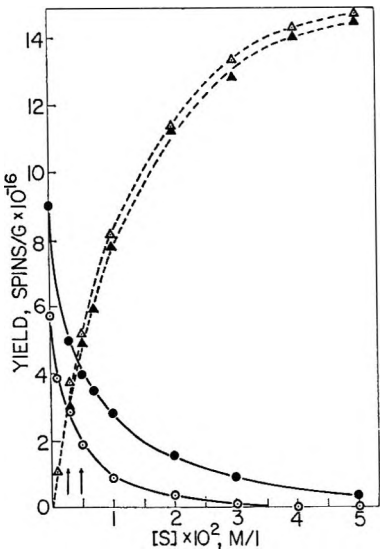

Figure 2. Effect of acrylamide concentration on the yield of e_t^-(⊙) and acrylamide radical (△) in 5 M NaOH ice, and e_t^-(●) and acrylamide radical (▲) in 10 M NaOH ice photolyzed by uv light at 77°K. Each sample contained 5×10^{-3} M of potassium ferrocyanide. The arrows show the position of C_1 in 5 and 10 M NaOH ices (see text).

tions are plotted in Figure 1 and Figure 2. The decrease in e_t^- yield and concomitant increase in the radical yield with increasing concentration of acrylamide is clearly shown. This is expected when a competition process for e_m^- occurs between acrylamide and trapping sites in which e_m^- is converted to e_t^-. The figures show that the acrylamide concentrations (C_1) at which the e_t^- yield is decreased to one-half its initial yield are larger for the γ-irradiated systems than for the photoionized systems by a factor of about 3.5. This is a significant and striking difference. The difference is not caused by the higher initial e_t^- yield that obtains in the γ-irradiated systems because C_1 is independent of the initial e_t^- yield at doses below 1 Mrad.

Relation of Scavenger to e_m^- Travel Distance

Let us consider how C_1 is related to the average distance that e_m^- travels before being trapped as e_t^-. Qualitatively, the smaller C_1 is, the greater e_m^- travel distance it infers. An approximate quantitative treatment is to equate half the average distance between scavenger molecules at scavenger concentration C_1 to the average linear distance e_m^- moves before trapping.[1] This treatment assumes (a) e_m^- is uniformly distributed when it reacts with scavenger, (b) e_m^- reacts with the scavenger on every "encounter" (*i.e.*, the scavenger is very efficient), and (c) if e_m^- travels a linear distance r, it will scatter enough to "encounter" a scavenger molecule if one is present within the spherical volume of radius r.

By photoionization e_m^- is produced uniformly. Acrylamide is a very efficient scavenger for e_m^- in ice[10] (see also Table III in ref 1). Application of the above simple model to the data in Figure 2 gives 44 Å ($C_1 = 4.7 \times 10^{-3}$ M) and 56 Å ($C_1 = 2.3 \times 10^{-3}$ M) for the average travel distances of e_m^- in 10 and 5 M NaOH, respectively. If cubic volumes of edge $2r$ are used instead of spherical volumes the calculated distances are about 10 Å less. Spherical volumes are used to compare with spherical spur sizes later in the discussion. If assumption (b) in the model is not justified, the calculated travel distances are too short. Likewise, if (c) is not satisfied, the calculated distances are too short. Thus, the model gives a lower limit to the e_m^- travel distance. A more detailed model has been described[12] and used;[10] it requires several assumptions about parameters including scattering cross sections and gives travel distances 4–5 times larger than the simple model used above. This is consistent with the fact that the simple model gives lower limits to e_m^- travel distances. For quantitative comparison between photoionization and radiolysis data it is more convenient and just as reliable to use the simple model. It is of interest that e_m^- travels farther in 5 M NaOH than in 10 M NaOH. This conclusion is valid regardless of the quantitative validity of the assumptions made in the model. If we make the reasonable assumption that the capture cross sections of the trapping sites and of the acrylamide are the same at both NaOH concentrations, then the number of trapping sites is greater in 10 M than in 5 M NaOH. This implies that there are definite concentrations of trapping sites or potential trapping sites in these matrices which depend on the matrix structure. However, the results do not appear to distinguish between trapping sites existing prior to radiolysis and trapping sites produced as a consequence of e_m^- formation (*i.e.*, potential trapping sites).

In Figure 1 in which e_m^- is generated by γ radiolysis the C_1 values are greater than for e_m^- generated by photoionization. If the same simple model is applied we would conclude that e_m^- travels a shorter distance when produced by γ radiolysis than when produced by photoionization. This seems physically unreasonable since the photoionization-produced e_m^- presumably have the lower average energy. Furthermore, assumption (a) is not valid for e_m^- in alkaline ice since the e_t^- are trapped in spurs to give a nonuniform spatial distribution.[2] For the sake of definiteness, let us postulate that there are $G(e_t^-)$ electrons per spur; this is equivalent to the common assumption that an average of 100 eV of radiation energy is deposited per spur. If one scavenger molecule were within the volume of a spur only one e_m^- could react with it. Thus to estimate the e_m^- travel distance we want the scavenger concentration that reduces the effective number of uniformly distributed e_m^- by 50% where this effective number is one e_m^- per spur. For a nonuniform distribution of e_m^- produced in spurs we therefore define

(12) P. J. Dyne and O. A. Miller, *Can. J. Chem.*, **43**, 2696 (1965).

C_1' as the scavenger concentration sufficient to reduce $[e_t^-]^0$ by 50% of $[e_t^-]^0/G(e_t^-)$. For $G(e_t^-) = 2$[1] we find from Figure 1 that $C_1' = 2.6 \times 10^{-3}$ and 4.0×10^{-3} M for γ-irradiated 5 and 10 M NaOH, respectively. These values are very close to the C_1 values from Figure 2 for photoionization and correspond to the same e_m^- travel distances.

We conclude that a nonuniform spatial distribution of e_m^- gives a larger C_1 value than does a uniform distribution of e_m^- in alkaline ices. Consequently, C_1 values determined for photoionization-produced electrons can be used to assess the spatial uniformity of radiation-produced electrons. It is remarkable and perhaps fortuitous that the e_m^- travel distance of 44 Å for 10 M NaOH obtained here is close to the 42 Å spur radius for e_t^- in 10 M NaOH deduced from paramagnetic relaxation measurements.[13] The spur radius of e_t^- should roughly correspond to the average distance e_m^- travels before being trapped.

In nonpolar organic glassy matrices like 3-methylpentane (3MP), mobile electrons probably travel farther before being trapped than in polar matrices. This is suggested by results from paramagnetic relaxation experiments.[13] Thus radiation-produced electrons in a nonpolar organic glass may approximately satisfy assumption (a) in the above model and react with scavenger with a nearly uniform spatial distribution. If so, there should be little difference between C_1 values for photoionization-produced and radiation-produced electrons in 3MP. Detailed results as in Figure 1 exist for biphenyl scavenger in irradiated 3MP which give $C_1 = 2.4 \times 10^{-3}$ M.[14] The same investigators have reported e_t^- yields for two biphenyl concentrations in 3MP in which e_m^- was produced by photoionization of tetramethylphenylenediamine (TMPD).[15] From these two points we estimate that $C_1 = 3 \times 10^{-3}$ M. Thus, the two C_1 values do seem to be similar and support the above picture.

Trapping Site Concentrations

When competition for uniformly distributed e_m^- occurs between trapping sites (T) and acrylamide (S) in alkaline ice and the stationary-state assumption is applied to $[e_m^-]$ the ratio of the radical yield to e_t^- yield, R, is given by

$$R = \frac{K_s S}{K_t[\mathrm{T}]} \tag{1}$$

where K_s and K_t are the rate constants for scavenging by acrylamide and by trapping sites respectively. C_1 is given by

$$C_1 = \frac{K_t}{K_s}[\mathrm{T}] \tag{2}$$

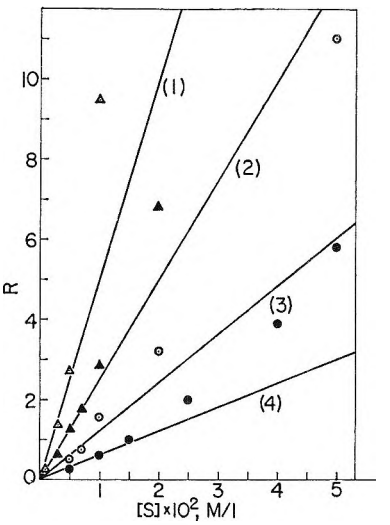

Figure 3. The ratio of radical yield to e_t^- yield *vs.* acrylamide concentration in photolyzed 5 M (△) and 10 M (▲) NaOH solutions and γ-irradiated 5 M (○) and 10 M (●) NaOH solutions. The straight lines were drawn through the points at lower acrylamide concentration.

Lower limits to the initial number of trapping sites in 5 and 10 M NaOH ices can be estimated as 2.5×10^{18}/g and 5.0×10^{18}/g, respectively. This lower limit is the number of e_t^- at the plateau in a yield–radiation dose curve.[1] At the maximum e_t^- yield of 3.3×10^{17} spins/g in our results here, more than 90% of the trapping sites are still available for trapping. We may conclude that C_1 is approximately proportional to the initial concentration of trapping sites. This is confirmed by the result that C_1 for 10 M NaOH is larger than that for 5 M NaOH by a factor of about 2 in both γ-radiolysis and photoionization cases.

Figure 3 shows a plot of R *vs.* S for γ radiolysis and photolysis in 5 and 10 M NaOH ices. Solid straight lines are drawn through the points at low acrylamide concentration. However, the points at higher acrylamide concentration fall above these straight lines. This would be the case if [T] decreased at higher solute concentrations. It seems possible that a high concentration of solute molecules destroys some trapping sites in alkaline ices.

Acknowledgment. This research was supported by the Air Force Office of Scientific Research under Grant No. AFOSR-70-1852 and the Atomic Energy Commission under Contract No. AT(11-1)-2086.

(13) D. H. Chen and L. Kevan, *Mol. Crystallogr.*, **6**, 183 (1969); *J. Chem. Phys.*, **49**, 1970 (1968).

(14) J. B. Gallivan and W. H. Hamill, *J. Chem. Phys.*, **44**, 1279 (1966).

(15) J. B. Gallivan and W. H. Hamill, *ibid.*, **44**, 2378 (1966).

Reaction of Nitriles with Hydrated Electrons and Hydrogen Atoms in Aqueous Solution as Studied by Electron Spin Resonance[1]

by P. Neta and Richard W. Fessenden*

Mellon Institute Radiation Research Laboratories and Department of Chemistry, Carnegie-Mellon University, Pittsburgh, Pennsylvania 15213 *(Received May 4, 1970)*

The radicals produced by reaction of hydrated electrons and hydrogen atoms with nitriles in irradiated aqueous solutions have been studied by esr. Irradiation with high-energy electrons was carried out directly in the esr cavity. Radicals of the type RCH=N· were observed; their esr spectra are characterized by an 80-G proton doublet splitting and a 10-G nitrogen splitting. These radicals are formed from nitriles both by reaction with hydrated electrons followed by protonation and directly by reaction with hydrogen atoms. Only about 10% of the hydrated electrons form CN^- as an additional product. No electron transfer from CO_2^- to nitriles was found to take place. Some of the radicals formed by OH reactions or by secondary reactions have also been identified.

Introduction

Although nitriles are expected to be moderately reactive toward the primary radicals of water radiolysis, little has been reported regarding the radiolysis of aqueous solutions of nitriles. A few rate constants have been determined for the reactions of OH and e_{aq}^- with acetonitrile, propionitrile, cyanoacetate ion, and benzonitrile;[2] however, no products have been determined. Esr studies of the reactions of photolytically generated OH radicals with nitriles have shown[3] that OH reacts by abstracting hydrogen from the position α to the CN group. The reaction of hydrated electrons with nitriles is not expected to yield cyanide ions by a detachment reaction similar to that occurring with halides, because of the high C–CN bond strength and the relatively low solvation energy of cyanide ions. It has been suggested,[4] therefore, that the initially formed $(RCN)^-$ would subsequently protonate to RCH=N. No chemical evidence has yet been presented to support this suggestion. That radicals of this structure can exist is shown by the observation of the esr spectrum of $H_2C{=}N\cdot$. This radical, first observed by Adrian, *et al.*,[5] in an argon matrix, has a proton coupling constant of 87.4 G (91.2 G reported more recently for the radical in CN^- doped KCl[6a]) and except for $\dot{H}CO$ has the largest proton coupling constant of any organic radical. It is to be expected that the spectra of other radicals of this type will also display a large splitting and will thus be very distinctive. Recently, Wood, *et al.*,[6b] have produced radicals of the type $R_2C{=}\dot{N}$ as discussed here by photolysis of $R_2\dot{C}NH_2$ in an adamantane matrix.

Esr spectroscopy has been used very effectively for the identification of radicals during continuous *in situ* radiolysis of aqueous nitroalkane solutions[7] and aqueous solutions of carboxylic acids and benzene derivatives.[8] It seemed interesting therefore to follow in a similar way the reaction of nitriles with e_{aq}^- and with H. A similar study of the reaction of amino acids with hydrated electrons has been recently completed.[9]

Experimental Section

Solutions of aliphatic nitriles (purest grade commercially available from Baker, Eastman Kodak, and Aldrich) were prepared in doubly distilled water[7] at concentrations of 0.01 to 0.1 *M*. Sodium formate or methanol (both Baker Analyzed Reagents) were added to certain solutions at concentrations high enough to scavenge most of the OH radicals. The pH was adjusted using potassium hydroxide, perchloric acid, sodium phosphates, and sodium tetraborate (all Baker Analyzed Reagents). Solutions were deoxygenated by bubbling with nitrogen. The irradiation was carried out in the esr cavity as previously described.[7,8] A flat silica cell of 0.5 mm internal spacing was used and during irradiation the solution was driven through the cell at a flow rate of 1 cm^3/sec. No effect of flow rate on the spectrum could be observed at rates between 0.5 and 3 cm^3/sec. The solution was cooled slightly before entering the cell and all measurements pertain to about 15°. The total electron beam current was 8 μA and

* To whom all correspondence should be addressed.

(1) Supported in part by the U. S. Atomic Energy Commission.

(2) M. Anbar and P. Neta, *Int. J. Appl. Radiat. Isotopes*, **18**, 493 (1967).

(3) R. Livingston and H. Zeldes, *J. Magnetic Resonance*, **1**, 169 (1969).

(4) M. Anbar, *Advan. Phys. Org. Chem.*, **7**, 115 (1969).

(5) F. J. Adrian, E. L. Cochran, and V. A. Bowers, *J. Chem. Phys.*, **36**, 1938 (1962).

(6) (a) J. A. Brivati, K. D. J. Root, M. C. R. Symons, and D. J. A. Tinling, *J. Chem. Soc. A*, 1942 (1969); (b) D. E. Wood, R. V. Lloyd, and D. W. Pratt, *J. Amer. Chem. Soc.*, **92**, 4115 (1970).

(7) K. Eiben and R. W. Fessenden, *J. Phys. Chem.*, **72**, 3387 (1968).

(8) K. Eiben and R. W. Fessenden, to be published.

(9) P. Neta and R. W. Fessenden, *J. Phys. Chem.*, **74**, 2263 (1970).

Table I: Structure and Coupling Constants of Radicals Produced by Reaction of e_{aq}^- with Nitriles[a,b]

Radical	g factor	a^N	a_β^H	a_γ^H	a_δ^H	a_ϵ^H
$CH_3CH{=}N\cdot$	2.00283	10.20	81.98	2.49		
$^-OOCCH_2CH{=}N\cdot$	2.00280	10.15	80.89	2.88		
$HOCH_2CH{=}N\cdot$	2.00300	9.95	82.54	2.33	0.31	
$CH_3OCH_2CH{=}N\cdot$	2.00295	9.94	83.16	2.17		0.59
$(CH_3)_3CCH{=}N\cdot$		~10.00	~82.00		~0.5	
$H_2C{=}N\cdot$[6]	2.0031	9.5	91.2			

[a] Hyperfine constants are given in gauss and are accurate to ±0.03 G. The g factors are measured relative to the peak from the silica cell and are accurate to about ±0.00005. Second-order corrections have been made [R. W. Fessenden, *J. Chem. Phys.*, **37**, 747 (1962)]. [b] The skeleton positions are labeled $\overset{\epsilon}{C}—\overset{\delta}{C}—\overset{\gamma}{C}—\overset{\beta}{C}{=}\overset{\alpha}{N}\cdot$ starting with the nitrogen as the α position. Protons bear the same label as the atom to which they are attached. This notation is consistent with that used for alkyl radicals.

that collected at an electrode in the solution was 1 μA. Second-derivative spectra were recorded by use of two modulation frequencies. This method helps to minimize the interference by the signal from the silica cell so that only the region from 3 G to 10 G above the center of the radical spectrum is obscured.

Results and Discussion

Spectra of the radicals produced in aqueous solution by reaction of e_{aq}^- with acetonitrile and cyanoacetate are shown in Figures 1 and 2. These spectra are characterized by an 80-G proton doublet splitting and a 10-G nitrogen splitting. The similarity of the proton and nitrogen coupling constants to those in $H_2C{=}N\cdot$[5,6a] together with the chemical arguments below make it clear that these radicals are of the structure $RCH{=}N\cdot$. Three other nitriles gave detectable spectra of the same type. The parameters for the five radicals are listed in Table I and are all very similar. The values for $H_2C{=}N\cdot$ are given for comparison. The β-proton hyperfine splitting is large because of the geometry with the C—H bond parallel to the p orbital containing the unpaired electron and the short C—N double bond. A discussion of this point together with an analysis of the anisotropic nitrogen hyperfine coupling (suggesting a π-spin density on the nitrogen of 0.73) has been given.[6a] It is interesting that the splittings for protons in the γ positions are large somewhat paralleling the β splittings. More distant splittings are also seen. The spectrum obtained with $(CH_3)_3CCN$ could not be fully analyzed because of the weakness of the signals. This effect is caused in part by the large number of splittings (here from δ protons) which spread the intensity over more lines. Presumably a similar explanation applies to CH_3CH_2CN, H_2NCH_2CN, NH_2COCH_2CN, and $(CH_3)_2CHCN$ where no lines of sufficient intensity to be measured could be found.

The primary species produced by the reaction of nitriles with hydrated electrons

$$RCN + e_{aq}^- \longrightarrow RCN^-$$

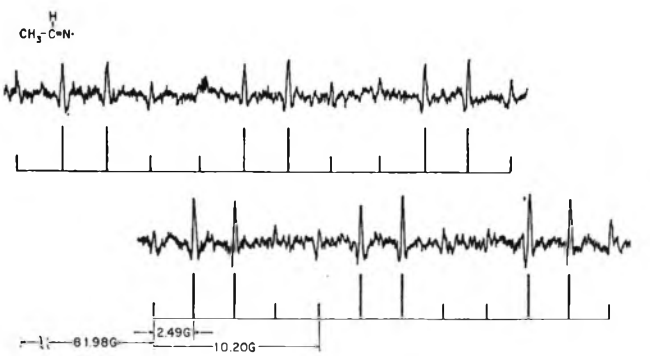

Figure 1. Second derivative esr spectrum of an aqueous solution of acetonitrile (0.1 M) at pH 9 (borax buffered) during irradiation with 2.8-MeV electrons. Magnetic field increases to the right. Two segments of the spectrum are shown which include all the lines of the $CH_3CH{=}N\cdot$ radical; the separation between them is given. The continuous scan could not be reproduced but it contains only the additional signal from the silica cell. The stick spectrum shows the relationship of the lines.

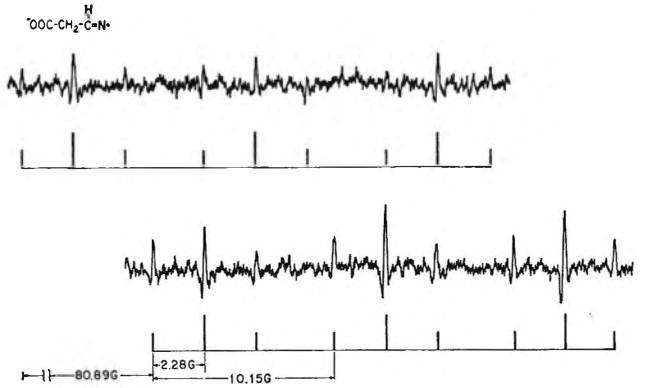

Figure 2. Esr spectrum of an aqueous solution of cyanoacetate (0.1 M) containing formate (0.1 M) at pH 6 (phosphate buffered) during irradiation. Only two portions of the spectrum, with all the lines from $^-OOCCH_2CH{=}N\cdot$, are shown. Weak lines from $\cdot CH_2COO^-$ are present in the central portion not shown.

was not observed under our experimental conditions. This radical ion most probably undergoes protonation

$$RCN^- + H_2O \longrightarrow R{-}\overset{H}{\overset{|}{C}}{=}N\cdot + OH^-$$

to give the radical observed in the esr spectrum.

To support the suggested mechanism of formation of R—CH=N· aqueous solutions of acetonitrile were irradiated under several different conditions. The spectrum of Figure 1 was obtained between pH 7 and 13 with solutions containing no other scavenger. In the presence of N_2O as a scavenger of e_{aq}^- the spectrum essentially disappeared showing that e_{aq}^- is a major precursor. Although (as pointed out in the Introduction) OH is known to produce $\cdot CH_2CN$, it could conceivably also contribute to the formation of $CH_3CH{=}N\cdot$. Elimination of >95% of the OH reaction with CH_3CN by the addition of formate or methanol did not have any effect on the observed spectrum of the radical CH_3-$CH{=}N\cdot$. In acetonitrile and glycolonitrile solutions at pH 1, where all the hydrated electrons are converted into H atoms, spectra similar to those obtained at high pH could be observed, suggesting the reaction

$$R{-}C{\equiv}N + H \longrightarrow R{-}\overset{H}{\overset{|}{C}}{=}N\cdot$$

This reaction is also supported by the recent observation[10] that the rate constants for the reaction of hydrogen atoms with acetonitrile and cyanoacetic acid are about an order of magnitude higher than the rate expected for hydrogen abstraction.

To check whether CO_2^- could transfer an electron to a nitrile to form $RCH{=}N\cdot$, solutions of acetonitrile and of cyanoacetate were irradiated either in the presence of CO_2 as a scavenger for e_{aq}^-

$$CO_2 + e_{aq}^- \longrightarrow CO_2^-$$

or in the presence of $HCOO^- + N_2O$ to convert all the primary radicals of water radiolysis into CO_2^-

$$N_2O + e_{aq}^- \longrightarrow N_2 + OH^- + OH$$

$$HCOO^- + OH \text{ or } H \longrightarrow CO_2^- + H_2O \text{ or } H_2$$

No spectrum for $RCH{=}N\cdot$ radicals could be observed under these conditions, thus eliminating the possibility of this electron transfer.

Although the mechanism of reaction of hydrated electrons with nitriles seems clearly to be leading to the formation of $RCH{=}N\cdot$ radicals, the possible formation of cyanide through

$$RCN + e_{aq}^- \longrightarrow R\cdot + CN^-$$

has to be investigated. This reaction is suggested by the observation of a weak spectrum of $\dot{C}H_2COO^-$ in solutions of cyanoacetate. To support this observation the yields of CN^- from γ-irradiated solutions of cyanoacetate and acetonitrile at pH 12 have been measured (using Orion Research cyanide ion selective electrode) and found to be $G = 0.3$ and 0.2, respectively. Thus only ~10% of the electrons form cyanide; the majority form $RCH{=}N\cdot$ which probably disproportionates and hydrolyzes to form an aldehyde.

In the absence of a competing OH scavenger some radicals could be observed as a result of hydrogen abstraction by OH radicals from the α position of nitriles (Table II). The coupling constants for $^-OOC\dot{C}HCN$, $HO\dot{C}HCN$, and $CH_3\dot{C}HCN$ are in good agreement with those determined by Livingston and Zeldes.[3] The spectrum of $\dot{C}H_2CN$ was not detected by us probably as a result of the 0.7 G line width.[3] In the case of glycolonitrile the radical $CN\dot{C}HOH$, could be observed at pH 1 to 3. However, at pH 5 to 12 the radical $CN\dot{C}HO^-$ was observed. This suggests a pK value of about 4 for the $CN\dot{C}HOH$ radical, considerably lower than pK = 8.8 for the hydroxyl group in $^-OOC\dot{C}HOH$[11] and pK = 10.7 for $\cdot CH_2OH$.[12]

In solutions of propionitrile the product of the e_{aq}^- reaction could not be observed (as mentioned above), although the product of OH reaction, $CH_3\dot{C}HCN$, could. In the presence of methanol as an OH scavenger only the spectrum of the $\cdot CH_2OH$ radical was found. When formate was added instead, a spectrum was observed which could be assigned to the radical $CH_3\dot{C}(COO^-)CN$ (Table I). Higher yields of this radical could be formed by irradiating a solution of propionitrile and CO_2. The mechanism of formation of this radical probably involves the combination of $CH_3\dot{C}HCN$ and CO_2^- to form $CH_3CH(COO^-)CN$,[13] which then competes effectively for the OH radicals

$$CH_3{-}\underset{\underset{COO^-}{|}}{CH}{-}CN + OH \longrightarrow CH_3{-}\overset{\overset{COO^-}{|}}{\dot{C}}{-}CN + H_2O$$

An attempt to produce a similar reaction in a solution of cyanoacetate was not successful, probably due to the different relative rates of the competing reactions.

It is necessary to comment here upon the spectra of two radicals found in irradiated solids which also display a proton-coupling constant of about 80 G. Radicals formed from malonamide[14] and cyanoacetylurea[15] both show $a^H \cong 80$ G and $a^N = 12$–14 G. Single crystal studies have been made and the radicals suggested in both cases are of the type $RCO\dot{N}H$ with the unpaired electron in a σ orbital much as in $H\dot{C}O$. Al-

(10) P. Neta, R. W. Fessenden, and R. H. Schuler, to be published.

(11) M. Simic, P. Neta, and E. Hayon, *J. Phys. Chem.*, **73**, 4214 (1969).

(12) K.-D. Asmus, A. Henglein, A. Wigger, and G. Beck, *Ber. Bunsenges. Phys. Chem.*, **70**, 756 (1966).

(13) See, for example: A. Appleby, J. Holian, G. Scholes, M. Simic, and J. J. Weiss, *Proc. 2nd Int. Congr. Radiat. Res.*, (1962) and F. Gütbauer and N. Getoff, *Int. J. Appl. Radiat. Isotopes*, **16**, 673 (1965).

(14) N. Cyr and W. C. Lin, *J. Chem. Phys.*, **50**, 3701 (1969).

(15) P. W. Lau and W. C. Lin, *ibid.*, **51**, 5139 (1969).

Table II: Structure and Coupling Constants of Radicals Produced in Irradiated Aqueous Solutions of Nitriles[a]

Reaction		Radical	g factor	a^N	a_α^H	a_β^H
$CNCH_2COO^- + OH$	→	$^-OOC\dot{C}HCN$	2.00325	3.16	19.78	
$CNCH_2COO^- - e_{aq}^-$ (10%)	→	$\cdot CH_2COO^-$	2.00322		21.18	
$CNCH_2OH + OH$	→	$HO\dot{C}HCN$ (pH 1–3)	2.00330	3.39	18.20	1.95
		$\downarrow\uparrow$				
		$^-O\dot{C}HCN$ (pH 5–12)	2.00362	3.31	15.32	
$CH_3CH_2CN + OH$	→	$CH_3\dot{C}HCN$	2.00292	3.51	20.31	23.27
$CH_3\dot{C}HCN + CO_2^-$						
$\downarrow$						
$CH_3\dot{C}HCN + OH$	→	$CH_3\dot{C}CN$	2.00296	3.47		20.21
$\vert$		$\vert$				
COO^-		COO^-				

[a] Hyperfine constants in gauss; see Table I for accuracy.

though it may be that the structures are of the suggested type we would like to point out that the single crystal data are more in accord with a radical structure like that found here (RCH=N·). In particular the isotropic nitrogen splitting seems too small to be that of a radical related to $H\dot{C}O$ which has $a^C = 135$ G.[16] Also, the anisotropic part of proton-coupling tensors (3.0, −1.7, −1.3) and (1.3, −0.3, −0.9) (in gauss) are much closer to those of a β proton (see the results for $CH_3\dot{C}HCOO^-$)[17] than an α proton. The approximate tensor for the proton in $H\dot{C}O$ is (5.0, −0.8, −4.2)[18] and is considerably larger. The second of the two compounds is a nitrile and therefore formation of a radical of the type RCH=N· is not surprising. It is not clear how this type of radical could be formed in malonamide.

In this paper esr spectroscopy of aqueous solutions of nitriles during irradiation has been described. Through the qualitative effect of various scavengers on the steady-state concentrations of radicals it has been possible to determine some details of the reactions of nitriles. The reactions of both e_{aq}^- and H with nitriles have been shown to lead to radicals of the type RCH=N·. The esr method has been particularly useful here because of the distinctive spectrum of these radicals with an 80-G proton doublet splitting.

(16) E. L. Cochran, F. J. Adrian, and V. A. Bowers, *J. Chem. Phys.*, **44**, 4626 (1966).

(17) I. Mayagawa and K. Itoh, *ibid.*, **36**, 2157 (1962).

(18) F. J. Adrian, E. L. Cochran, and V. A. Bowers, *ibid.*, **36**, 1661 (1962).

Radicals Formed by Electron Attachment to Peptides[1,2]

by Michael D. Sevilla

Atomics International Division, North American Rockwell Corporation, Canoga Park, California 91304
(Received April 15, 1970)

The reactions of electrons with a number of peptides, N-acetylamino acids, and N-acetyl peptides in an alkaline D_2O glass have been investigated by use of electron spin resonance (esr) spectroscopy. Results found for dipeptides show that at 77°K reaction with the electron forms a dianion. Warming to 180°K results in esr spectra which are consistent with radicals of the structure $\cdot CHRCONHCHRCO_2^-$ where R = H or an alkyl group. These radicals are formed by deamination of the primary or N-terminal amine group. Further warming to the softening point of the glass results in the appearance of a third radical species whose spectra are in most cases consistent with the radical $NH_2\dot{C}RCONHCHRCO_2^-$ or $NH_2CHRCONH\dot{C}RCO_2^-$ formed by an abstraction reaction between the parent peptide and the deaminated radical. An analogous reaction mechanism to that for dipeptides was found for the tripeptide L-alanylglycylglycine. Electron attachment to N-acetylamino acids results in localization of the electron in the peptide linkage (—CO—NH—). At 180°K the results show that the dianion of the acetylamino acids undergo deamination of the secondary amine group to produce radicals of the structure $\cdot CHRCO_2^-$. For N-acetyl dipeptides the electron is found to localize predominantly in the N-terminal peptide linkage; however, some localization at the second peptide linkage may also occur. Deamination of a secondary amine group and subsequent abstraction from the parent peptide are found upon warming. The results found here are compared to those found for electron reactions in aqueous solution at pH 7, and radiolysis of the solid state.

Introduction

The electron is an important radical intermediate in the radiolysis of water[3] and the radiolysis of solids such as amino acids[4-7] and peptides.[8] Consequently, an investigation of the isolated reactions of electrons with amino acids and peptides should aid the analyses of radiolysis experiments in aqueous media and perhaps in the solid state as well.

The reaction of electrons with amino acids in an aqueous medium (an alkaline glass) have been previously studied by use of electron spin resonance (esr) spectroscopy.[4] It was found that the electron upon reaction with an amino acid initiated a series of radical producing steps. Radical intermediates were identified which were consistent with the following mechanism

$$NH_2CRHCO_2^- + e^- \xrightarrow{77°K} NH_2CRHCO_2^{2-} \quad (1)$$

$$NH_2CRHCO_2^{2-} \xrightarrow{\geq 180°K} \cdot CRHCO_2^- + NH_2^- \quad (2)$$

$$\cdot CRHCO_2^- + NH_2CRHCO_2^- \xrightarrow{>190°K} CH_2RCO_2^- + NH_2\dot{C}RCO_2^- \quad (3)$$

where R = H or an alkyl group.

This mechanism was found to be in agreement with that proposed for the reaction of amino acids and the electron from reaction rate studies and product analysis of the radiolysis of amino acids in aqueous solution.[9a,b] Recent pulse radiolysis experiments have given evidence that the deaminated radical is a product of electron attachment to glycine and alanine.[9c] The first two steps of the reaction mechanism are also in agreement with those proposed from electron spin resonance studies of the radiolysis of solid amino acids.[10] With these encouraging results it was considered of interest to investigate the reactions of electrons with peptides.

In previous work, Willix and Garrison have found through product analysis and reaction rate studies that in oxygen-free aqueous solutions reaction of the electron with glycine dipeptides and tripeptides essentially quantitatively cleaves the N–C bond of the primary (terminal) amine group.[9b] These workers suggest that electron attachment to the carbonyl linkage next to the terminal amine group precedes deamination.

In this work a study of a number of peptides and acetyl peptides has been performed. This work veri-

(1) This work was supported by the Division of Biology and Medicine of the U. S. Atomic Energy Commission.

(2) This work was presented in part at the 158th National Meeting of the American Chemical Society, New York, N.Y., Sept 9, 1969.

(3) E. Hayon in "Radiation Chemistry of Aqueous Systems," Stein and Gabriel, Ed., Wiley, New York, N. Y., 1968, pp 157–209.

(4) M. D. Sevilla, *J. Phys. Chem.*, **74**, 2096 (1970).

(5) J. Sinclair and M. W. Hanna, *ibid.*, **71**, 84 (1967).

(6) (a) H. C. Box, E. E. Budzinski, and H. G. Freund, *J. Chem. Phys.*, **50**, 2880 (1969); (b) H. C. Box, H. G. Freund, K. T. Lilga, and E. E. Budzinski, *J. Phys. Chem.*, **74**, 40 (1970).

(7) P. B. Ayscough and A. K. Roy, *Trans. Faraday Soc.*, **64**, 582 (1968).

(8) R. C. Drew and W. Gordy, *Radiat. Res.*, **18**, 552 (1963).

(9) (a) D. B. Peterson, J. Holian, and W. M. Garrison, *J. Phys. Chem.*, **73**, 1568 (1969); (b) R. L. S. Willix and W. M. Garrison, *Radiat. Res.*, **32**, 452 (1967); (c) P. Neta, M. Simic, and E. Hayon, *J. Phys. Chem.*, **74**, 1214 (1970).

(10) An abstraction step is also found in solid amino acids; however, it differs from abstraction in aqueous media (see ref 4 for a discussion).

fies the conclusion of Willix and Garrison that deamination of primary amine groups occurs andfur ther shows that it extends to peptides composed of glycine and amino acids with alkyl side groups. Results are found which confirm the suggestion that electron localization occurs at the peptide linkage for dipeptides and predominantly at the N-terminal peptide linkage in tripeptides. In addition, evidence for an abstraction step analogous to that found in amino acids (reaction 3) is found.

Experimental Section

The peptides used in this work were obtained from Cyclo Chemical Co. and were the highest grade available.

The experimental procedure employed has been described previously.[4,11,12] In this procedure a deoxygenated 8 *N* NaOD (92% D_2O) solution containing 5 m*M* $K_4Fe(CN)_6$ and *ca.* 50 m*M* solute (peptide) is cooled to 77°K to form a glass. The glass formed is photolyzed with 2537 Å uv light at 77°K for approximately 1 min. The photolysis produces a dark blue color due to the electron by photoionization of the $K_4Fe(CN)_6$. At this point, an esr spectrum is taken of the sample to ensure that photolysis of the organic solute is minimal.[13] The sample is then photobleached at 77°K with light from an infrared lamp for approximately 4 min. The electrons become mobile and react with the solute. An esr spectrum is then taken of the sample. The solutions were prepared with D_2O since this results in improved resolution of the esr signal.

To prevent hydrolysis of the peptides the solutions were prepared when necessary by addition of the peptide dissolved in a small amount of D_2O to the cooled (<0°) alkaline solution. The sample is then quickly (<20 sec) prepared and cooled to 77°K.

A Varian V4500-10 esr spectrometer equipped with a dual cavity, Fieldial magnetic field regulator, and variable temperature accessory was employed in this work. Measurements of hyperfine splittings and *g* values were made *vs.* potassium peroxylamine disulfonate (A_N = 13.0 G, g = 2.0056).

Results and Discussion

1. Electron Reactions with Dipeptides. The reactions of electrons with dipeptides were investigated to determine whether primary or secondary deamination results from electron attachment. For this reason dipeptides of the form

$$NH_2CHRC(=O)NHCHR'CO_2^-$$

where R ≠ R′ were principally investigated. The differing side groups ease the identification of the resulting radical species and consequently the deamination process.

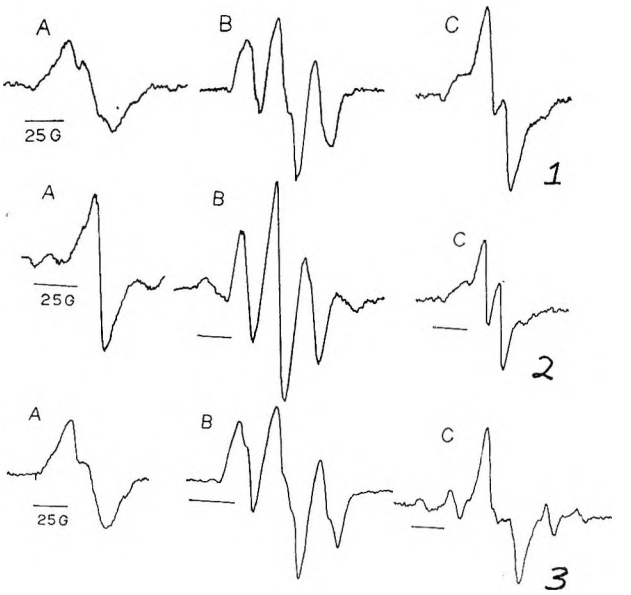

Figures 1–3. Electron spin resonance spectra of radical species produced by reaction of electrons with glycyl-L-alanine (Figure 1), L-alanylglycine (Figure 2), and glycyl-L-leucine (Figure 3) in a deuterated alkaline glass. A. The dianion species formed by electron attachment at 77°K. B. The second radical species, $\cdot CHRC(=O)NHCHRCO_2^-$, produced by deamination of the primary amine group upon warming to 180°K. C. The third radical species at 190°K produced by hydrogen abstraction from an α-carbon. The third spectrum of glycyl-L-leucine shows evidence of abstraction from the leucine side group as well (see text for a discussion). The magnetic field increases from left to right for each spectrum in these figures and subsequent figures.

a. Glycyl-L-Alanine, L-Alanylglycine, and Glycylglycine. At 77°K electron attachment to the dipeptides gly-ala, ala-gly, and gyl-gly results in esr spectra which are associated with the dianion radicals (reaction 4).

$$NH_2CRHC(=O)—NHCRHCO_2^- + e^- \longrightarrow NH_2CRHC(=O)—NHCRHCO_2^- \quad (4)$$

The spectra for gly-ala and ala-gly (Figures 1A and 2A) show little resolution of structure. The spectrum of gly-gly shows a 22-G doublet.[14] Warming the samples

(11) P. B. Ayscough, R. G. Collins, and F. S. Dainton, *Nature*, (London), **205**, 965 (1965).

(12) R. A. Holroyd and J. W. Glass, *Int. J. Rad. Biol.*, **14**, 445 (1968).

(13) Photolysis of solid peptides has been found to produce radicals (see A. Meybeck and J. J. Windle, *Photochem. Photobiol.*, **10**, 1 (1969)). The short photolysis time, the relatively low concentration of the peptide, and the absorbance of the $K_4Fe(CN)_6$ in the uv prevented any significant photolysis in this work.

containing the dianion radicals to 180°K results in esr spectra which are indicative of primary deamination reaction 5.

$$\mathrm{NH_2CRHC(O^-)NHCRHCO_2^- \longrightarrow \cdot CRHC(O)NHCRHCO_2^- + NH_2^-} \quad (5)$$

Thus for gly-ala a three-line spectrum of 22-G separation in the intensity ratio *ca.* 1:2:1 (Figure 1B) is found which is expected from the $\cdot CH_2CONH\sim$ radical.[4] In the case of ala-gly a spectrum (Figure 2B) consisting of five lines separated by 24 G is found as expected for the $\cdot CH(CH_3)CONH\sim$ radical.[4,8,15-17]

The evidence for the N-terminal or primary deamination step for gly-ala and ala-gly is made stronger by a consideration of the other possible deamination site, that is deamination of the secondary amine group. If this reaction took place a spectrum of the $\cdot CH_2CO_2^-$ radical would be found for ala-gly and a spectrum of the $\cdot CHCH_3CO_2^-$ radical would be found for gly-ala. It should be first noted that the spectra in Figures 1B and 2B are not in agreement with the structure of these radicals. In addition the esr spectra of these radical species were found to show well resolved anisotropic hyperfine components;[4,18] consequently, if they were formed in significant concentrations they would be easily detected. The spectra in Figures 1B and 2B show no evidence of these radicals; thus very little, if any, secondary deamination occurs.

Results for gly-gly are also in agreement with the primary deamination mechanism. The spectrum found at 180°K is nearly identical with that found for gly-ala (Figure 1B). If secondary deamination occurred the anisotropic components of the $\cdot CH_2CO_2^-$ radical would be observed. Since no such components are observed, it is evident that only primary deamination occurs.

Further warming of the sample containing the deaminated radical species and the parent dipeptide to 190°K where the glass softens results in a third esr spectrum. This final spectrum consists of a 14-G doublet for gly-ala (Figure 1C), a 13.5-G doublet for ala-gly (Figure 2C), and a 14-G doublet for gly-gly.[19] A similar doublet of 13.5 G was found for the third radical species of glycine produced by the abstraction reaction (reaction 3). It is therefore considered likely that an abstraction step like that found for the individual amino acids occurs for the dipeptides as well. This abstraction is shown in reaction 6 for gly-gly.

A radical of the form

$$\mathrm{NH_2\dot{C}HC(O)NHCH_2CO_2^-}$$

would result in a similar spectrum and may be produced as well.

$$\mathrm{NH_2CH_2C(O)NHCH_2CO_2^- + \cdot CH_2C(O)NHCH_2CO_2^- \longrightarrow NH_2CH_2C(O)NH\dot{C}HCO_2^- + CH_3C(O)NHCH_2CO_2^-} \quad (6)$$

The results for gly-ala and ala-gly are somewhat more complex since α-carbon radicals may be produced on either the glycyl or alanyl residues. Since a quartet would be expected for the alanyl α-carbon radical,[8,16,17] the spectra found suggest the predominant radical formed is that on the glycyl residue; however, for these dipeptides the small end components may be indicative of some abstraction from the alanyl residue.[20]

Further warming of the sample or long standing at 190°K results in a loss of the esr signal due to the final radical species. This is most likely a result of radical–radical recombination.

b. Glycyl-L-leucine and Glycyl-L-valine. The spectra found for gly-leu and gly-val after electron attachment and warming to 180°K are essentially the same as those found for gly-ala. At 90°K a partially resolved spectrum due to the dianion is found (Figure 3A). Warming to 180°K results in a 1:2:1 triplet of 22 G separation (Figure 3B) for both molecules. No evidence is found for either leucyl or valyl radicals in this step;[4] consequently evidence for significant secondary deamination is not found. Thus primary deamination as in reaction 5 occurs for these dipeptides as well.

(14) The splitting for gly-gly presumably arises from the interaction of the unpaired electron localized in the peptide linkage (see section 3) with a proton at the N terminal α-carbon position. The lack of structure in the spectra found for gly-ala and ala-gly is most likely due to the orientation of the protons to produce only a small β-proton hyperfine splitting.

(15) F. G. Liming, *Radiat. Res.*, **39**, 252 (1969).

(16) A. Meybeck and J. Windle, *ibid.*, **40**, 263 (1969).

(17) H. C. Box, H. G. Freund, and K. Lilga in "Free Radicals in Biological Systems," M. S. Blois, Ed., Academic Press, New York, N. Y., 1961, pp 239–248.

(18) The lack of resolution of anisotropic components in the $\cdot CHRCO—NH\sim$ radicals may be due to broadening of hyperfine components due to unresolved nitrogen splittings.

(19) These results compare favorably with the radiolysis of glycine peptides in their solid state. For these peptides 16-17-G doublet spectra are found which are attributed to α-carbon radicals (see ref 8, 16, 17, and R. S. Mangiaracina, *Radiat. Res.*, **32**, 27 (1967)).

(20) It should be noted that these components may also arise from anisotropic nitrogen hyperfine couplings. Such components are observed from the amino acid α-carbon radicals (ref 4), but have not been previously observed in polycrystalline peptides.

Warming the gly-leu sample to 190°K where the the glass softens and then recooling to 180°K resulted in a spectrum (Figure 3C) which consists of six resolved components. The total width of the spectrum (120 G), the regularity of spacing (24 G), and the relatively narrow line widths of the outer four lines (7 G) suggest a radical with a number of equivalent β protons. Such a radical has been observed previously in irradiated solid leucine,[21] as well as hydrogen bombarded solid leucine,[22] and poly-DL-leucine.[15] For the amino acid, the radical has been assigned the structure

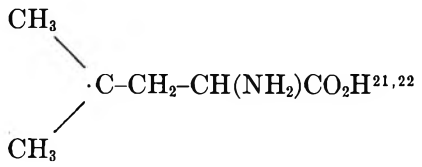

At 77°K this radical shows an eight-line spectrum due to equal coupling with the methyl protons and one of the methylene protons. The intensity ratios are theoretically 1:7:21:35:35:21:7:1 and the hyperfine splitting is in the range 23 to 25 G. The intensity ratios of the lines with the expected ratio 7:21 are in the ratio of *ca.* 7:18. The hyperfine splitting of 24 G is also in good agreement with such a radical. The intensities of the central pair of lines are greater than expected from the above radical species alone. Another species is present which has a doublet splitting. This species is most likely that produced by abstraction of an α-carbon hydrogen atom.

Rewarming the glass to its softening point for a few minutes results in a loss of the spectrum of the leucyl alkyl radical. A partially resolved doublet of *ca.* 15 G remains and is increased in intensity. This suggests a further reaction, *i.e.*, abstraction of an α-carbon hydrogen atom by the leucyl alkyl radical.

The abstraction of the tertiary hydrogen atom from the alkyl group of the leucyl residue is a somewhat surprising result. This is because (1) abstraction from the α-carbon not the alkyl side group was found for amino acids,[4] and (2) the alkyl radical evidently later abstracts from the α-carbon position. A possible explanation for these results is that the tertiary radical is formed by intramolecular abstraction (reaction 7) just

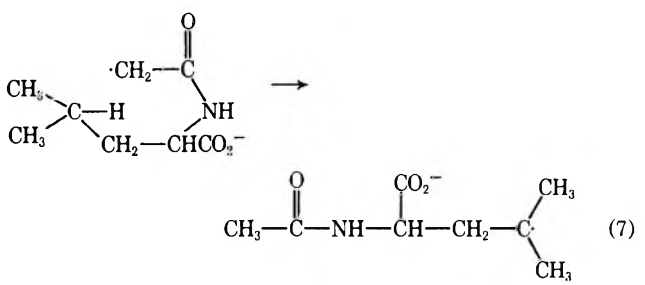

(7)

as the glass softens but before diffusion through the glass occurs. Rewarming the glass so that appreciable diffusion takes place allows the alkyl radical to abstract from an α-carbon position.

It should be noted that in the case of the amino acid leucine, the leucyl α-carbon radical produces a 13-G doublet esr spectrum due to interaction of one of the β-protons on the alkyl side group.[4] In irradiated polyleucine a 21-G doublet is found due to the analogous radical, (–NH–ĊR—CO–).[8] The 15 G doublet found in this case is in the range expected for an α-carbon radical on the leucyl residue. It is expected that the spectrum consists of an overlap of both the leucyl and glycyl α-carbon radicals. Since the spectra expected for the two radicals are so similar, no estimate can be made of the relative amounts of each present.

2. Reaction of Electrons with a Tripeptide. L-*Alanylglycylglycine.* Electron attachment to ala-gly-gly at 77°K results in a broad partially resolved singlet esr spectrum which is attributed to the dianion. Warming to 180°K results in a spectrum similar to that found for ala-gly with the exception that the central component is more intense than expected. The deamination step is slow and the large intensity of the central peak is probably due to unreacted dianion. Further warming to 190°K results in a well resolved doublet of 13 G similar in line shape to that found for ala-gly.

These results suggest that the reaction mechanisms found for dipeptides apply to tripeptides as well.

3. Reaction of Electrons with N-Acetylamino Acids and N-Acetyl Peptides. The reactions of electrons with N-acetylamino acids and peptides were investigated to determine whether electron localization on the peptide occurs. If localization does occur it is of interest to determine on which peptide unit the electron localizes. The acetyl methyl group at the peptide end should aid in this determination since it should act as a probe to ascertain the unpaired electron density at the terminal peptide linkage. Since the possibility of primary deamination is eliminated for acetylamino acids and peptides, it is also of interest to determine whether secondary deamination occurs.

a. N-Acetylamino Acids. Electron attachment to N-acetylglycine, N-acetyl-L-alanine, and N-acetyl-L-valine produce esr spectra which show 30 to 32-G doublets at 90°K. The spectra are shown in Figures 4A, 5A, and 6A. Warming the samples to 170°K results in a quartet of *ca.* 13.5-G separation for each of the dianions (Figures 4B, 5B, and 6B). This process is reversible, that is, cooling to 90°K results in the original doublet. The reversibility shows that no chemical reaction has taken place and suggests the change in spectra is due to a change in the configuration of the acetyl methyl group. A similar phenomenon has been found to occur for the acetamide anion.[23] At 85°K

(21) F. Patten and W. Gordy, *Radiat. Res.*, **14**, 573 (1961).
(22) W. Snipes and J. Schmidt, *ibid.*, **29**, 194 (1966).
(23) M. D. Sevilla, *J. Phys. Chem.*, **74**, 669 (1970).

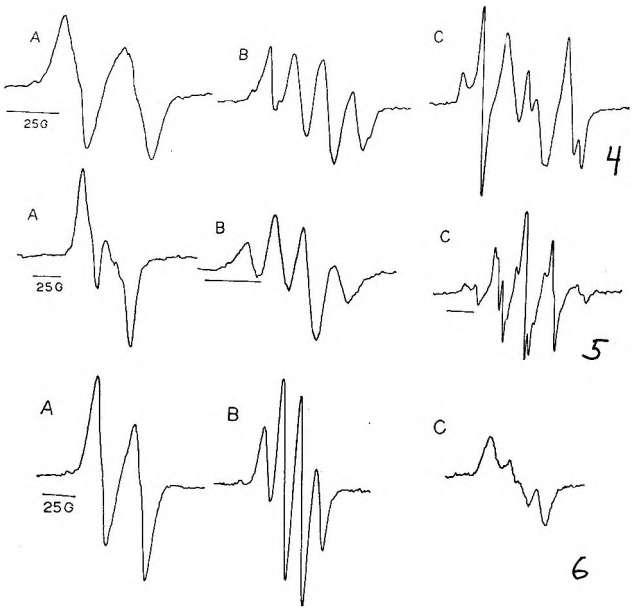

Figures 4–6. Esr spectra of radical species produced by reaction of electrons with N-acetylglycine (Figure 4), N-acetyl-L-alanine (Figure 5), and N-acetyl-L-valine (Figure 6). A. The dianion species at 90°K produced by electron attachment to the peptide linkage. The doublet spectra arise from interaction of one of the acetyl methyl group protons. B. Same radical species as in A at 170°K. These spectra show evidence of a more freely rotating methyl group. The conversion from A to B is reversible. C. The radical species, $\cdot CHRCO_2^-$ produced by deamination of the secondary amine group at *ca.* 180°K.

the esr spectrum of this species consists of a 30.8-G doublet. Upon warming to 180°K the doublet reversibly converts to a 1:3:3:1 quartet of 13.5-G separation. This phenomenon was interpreted on the basis that the methyl group was freely rotating at 180°K and locked in a particular conformation at the lower temperature so as to produce one large hyperfine splitting. Since the structure of acetamide is that of the end portion of the acetyl peptides, the nearly identical hyperfine splittings found for the locked conformation and the more freely rotating case can only be explained if the unpaired electron is localized at the acetyl peptide linkage (CH_3–CO–NH–).

The spin densities found to agree with the hyperfine splittings in acetamide anion place 0.69 of the unpaired spin at the carbonyl carbon, 0.23 at the oxygen, and 0.06 at the nitrogen.[23] The similarity in hyperfine splittings suggest these densities apply to the acetylamino acid dianions as well.

As can be seen in Figures 4B, 5B, and 6B spectra found for the quartet in some cases differ significantly from the 1:3:3:1 intensity ratio expected for a freely rotating methyl group. This is not unexpected since similar intensity ratios are found for acetamide anion at temperatures below 170°K.[23]

Warming the acetylamino acid anions to 185°K results in the spectra shown in Figures 4C, 5C, and 6C. These spectra are identical with those found for the corresponding deaminated amino acids; that is, the spectra in Figures 5C and 6C for acetylalanine and acetylvaline are identical with those found for deaminated alanine and valine. The spectrum (Figure 4C) found for acetylglycine shows some evidence of unreacted dianion; otherwise it is identical with that found for deaminated glycine. These results present convincing evidence that secondary deamination occurs *via* the reaction

$$CH_3\text{—}\overset{\overset{O^-}{\|}}{C}\text{—}NH\text{—}CHRCO_2^- \longrightarrow CH_3\text{—}\overset{\overset{O}{\|}}{C}\text{—}NH^- + \cdot CHRCO_2^- \quad (8)$$

Further warming to the softening point of the glass resulted in third radical species in the cases of acetylglycine and acetylvaline.

b. N-Acetyl Dipeptides. The results for the acetylamino acids show that electron localization occurs at the peptide bond in preference to a carboxyl group. It is of interest to determine where electron localization occurs when there is a choice of peptide bonds. For this reason two acetyl dipeptides were studied. They are acetylglycyl-L-leucine and acetylglycylglycine. The spectra found after electron attachment to the former is shown in Figure 7. The results expected for localization at the end peptide bond are found. The 27-G doublet spectrum at 90°K reversibly converts to the quartet of 13-G separation at 165°K. The intensities of the individual components of the quartet are far from the 1:3:3:1 expected for a freely rotating methyl group. This suggests considerable hindrance to rotation at

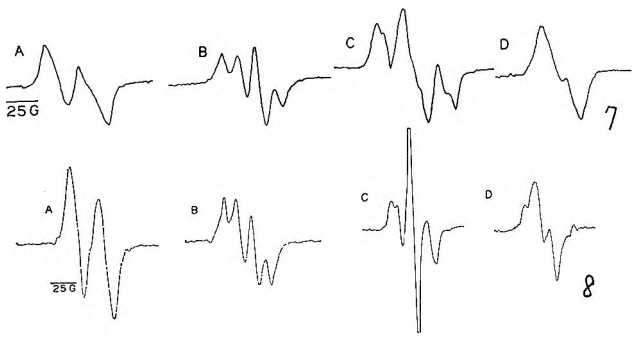

Figures 7 and 8. Esr spectra of radical species produced by reaction of electrons with N-acetylglycyl-L-leucine (Figure 7) and N-acetylglycylglycine methyl ester (Figure 8). A. The dianions at 90°K. B. Same species at 170°K. The conversion from the doublets in Figures A to the quartet in Figures B is reversible. This shows that the electron is predominantly localized in N-terminal peptide linkage. C. Radicals produced by further warming. Figure 7C (180°K) indicates N-terminal deamination and Figure 8C (185°K) suggests a radical of structure $\cdot CH_2OC(O)\sim$ is produced. D. Third radical species at 190°K. These spectra are indicative of abstraction from an α-carbon position.

165°K. It should also be noted that due to the poor resolution the possibility of a significant amount of localization at the second peptide bond cannot be eliminated.

Warming the sample to 180°K results in a spectrum which consists of three major components separated by 22 G in a *ca.* 1:2:1 intensity ratio. This spectrum is good evidence that radical formed in this step is a glycyl-like radical and that secondary deamination of the acetyl peptide unit occurs. The radical formed in this process should be the same as that formed by the primary deamination of gly-leu. The spectra found for the two cases (Figure 7C and Figure 3B) are quite similar but not identical. This is probably a result of the fact that in this case the deamination step was slow to occur and a small amount of the dianion remains. It is also possible that a small amount of secondary deamination at the gly-leu bond occurs; however, the radical produced in this process (deaminated leucine radical) has a spectral width of 88 G. Therefore if it were formed in significant amounts it would have components outside those of the glycyl radical and it would be easily observable. The spectrum shows no evidence of this species.

Further warming to 190°K results in a 13-G doublet (Figure 7D) characteristic of abstraction from an α-carbon position.

Somewhat different results are found for N-acetyl-gly-gly. At 90°K a 26-G doublet is found which converts reversibly to a quartet whose components are separated by 13.4 G at 170°K. The spectrum found at 170°K is less resolved than that found for the acetyl-amino acids and may indicate some localization at the second peptide bond. Warming the sample to 180°K gives evidence for only partial deamination. The line shapes of the deaminated species resemble that of $\cdot CH_2CO_2^-$ (Figure 4C) rather than $\cdot CH_2CONH\sim$ (Figures 1B, 3B, 7C). This indicates at least some secondary deamination of the C-terminal group. Complete deamination does not occur until temperatures are reached where the glass softens. At these temperatures (190°K) a 13.2-G doublet with components due to an anisotropic nitrogen is found which is indicative of abstraction of a hydrogen atom from an α carbon.

Although the results for the acetyl dipeptides may suggest some localization at the C-terminal peptide bond, the spectra give good evidence that the predominant localization is at the N-terminal.

c. N-Acetylglycylglycine Methyl Ester. The localization of the free electron at the N-terminal peptide bond can be explained by either of two hypotheses. First it may be due to simple charge repulsion. This is because in 8 *N* NaOH the carboxyl group is unprotonated and carries a negative charge. Therefore avoidance of the charge on the carboxyl group may result in localization of the electron at the N-terminal peptide linkage. Second, the N-terminal peptide linkage may form a deeper potential energy well than the other linkages and thus preferentially trap the electron.

To test the first hypothesis acetyl-gly-gly methyl ester was reacted with the electron. Esterification of the carboxyl group removes the charge on the group without greatly changing the electronic structure of the peptide. The spectra found after electron attachment are shown in Figure 8. The conversion from the 27-G doublet in Figure 8A to the quartet of 13.5-G separation in Figure 8B is reversible. These results demonstrate electron localization at the N-terminal bond is not a result of charge repulsion. This suggests an inherent property of the electronic structure of the peptide causes localization at the N-terminal peptide bond.

The results found on warming the anion to 185°K are somewhat unexpected (see Figure 8C). The spectrum found consists of a triplet in the intensity ratio 1:2:1 with a 15-G separation.

The 15-G splitting and the narrow central component are not consistent with radicals of structure

Results found for the reaction of electrons with glycine methyl ester suggest that the radical formed has the structure $\sim C(O)OCH_2\cdot$.[24] The formation of this species could be a result of intra- or intermolecular abstraction after deamination.

Further warming of the sample results in a spectrum (Figure 8D) associated with abstraction from an α-carbon position in the parent peptide. This may indicate that the abstraction reaction which produced the $\sim C(O)OCH_2\cdot$ radical was intramolecular in nature.

Comparison to Other Work and Conclusions

In previous work it has been found by Willix and Garrison through product analysis and reaction rate studies that electron attachment to gly-gly and gly-gly-gly in dilute aqueous solutions at pH 7 results in deamination of the primary amine group.[9b] These workers suggest that electron attachment to the peptide linkage adjacent to the primary amine group precedes deamination. The results found here confirm those of the previous work and show that

(24) The reaction of electrons with glycine methyl ester results in deamination at ≤ 170°K to produce a radical structure $\cdot CH_2C(O)OCH_3$. This species yields a spectrum showing distinct anisotropic components very similar to that found for $\cdot CH_2CO_2^-$. However, warming to 185°K results in a new spectrum virtually identical with that found in Figure 8C. Since cooling does not result in the original spectrum and since the isotropic and anisotropic hyperfine splittings are so different for the two spectra, it is concluded that a new radical has been produced. The methoxy methyl group is the only possible site of abstraction which would produce a spectrum due to two equivalent protons. It is therefore considered likely that this new radical has the structure $\cdot CH_2OC(O)\sim$ (the complete structure depends on whether the abstraction is intra- or intermolecular). This interpretation is supported by the fact that a reduced hyperfine splitting would be expected for a radical of the above structure. For example a 17.4-G splitting is found for the $\cdot CH_2OH$ radical (R. Livingston and H. Zeldes, *J. Chem. Phys.*, **44**, 1245 (1966)).

primary deamination extends to other peptides composed of glycine and amino acids with alkyl side groups. The suggestion of electron attachment to the N-terminal peptide linkage is in good agreement with results found for the N-acetylamino acids, although the acetyl peptides may suggest some localization of the electron at the second peptide bond.

The localization of the electrons at the N-terminal peptide linkage is most likely due to a deeper potential well for the end linkage. However, the potential energy difference between peptide linkages cannot be very large. One should therefore expect the effects of electron migration between the various peptide units at higher temperatures. Thus the preferential deamination of the one amine group over another may be more due to the competitive rates of deamination rather than simply localization itself. This is clearly indicated by the fact that the primary amine group deaminates in dipeptides even though the electron is localized at the peptide linkage. This extends to the acetyl dipeptides where the "weakest" bond would be expected to rupture even though the electron is "localized" at the N-terminal linkage.

Rodgers, Sokol, and Garrison have studied the reactions of electrons produced by radiolysis with N-acetyl peptides in H_2O solution at pH 7.[25] In dilute solutions reaction of the electron with N-acetylalanine is shown to lead to liberation of the free amino acid alanine. This is not in accord with the mechanism found here in 8 *N* NaOH (reaction 8). An explanation may be that in this case the mechanism for product formation is pH dependent.

There are a number of studies of the radiolysis of peptides in the solid state.[8,16,17,26-29] Several of these studies give evidence that radicals of the type $\cdot$CHRCONH$\sim$ are formed by cleavage of primary or secondary amine linkages and that these species further react probably by abstraction to form the usual α-carbon radical.[8,16] It is interesting to note that the first species could be a result of primary or secondary deamination caused by the electrons produced during radiolysis. However, the reactions of positive ions,[8] excited molecules,[30] and hydrogen atoms[15,31,32] must be considered as well.[33]

Acknowledgment. The author wishes to thank R. A. Holroyd of Brookhaven National Laboratory as well as L. S. Myers and J. Ward at the Laboratory of Nuclear Medicine and Radiation Biology, UCLA, for helpful discussions. The author also wishes to thank the Division of Biology and Medicine of the U. S. Atomic Energy Commission for support of this work.

(25) M. A. J. Rodgers, H. A. Sokol, and W. M. Garrison, *J. Amer. Chem. Soc.*, **90**, 795 (1968).

(26) W. C. Lin and C. A. McDowell, *Mol. Phys.*, **4**, 333 (1961).

(27) M. Katayamaand and W. Gordy, *J. Chem. Phys.*, **35**, 117 (1961).

(28) R. S. Mangiaracina, *Radiat. Res.*, **32**, 27 (1967).

(29) A. F. Usatyi, V. I. Panin, M. A. Ponomareva-Stepnaya, and L. A. Molodov, *Khim. Vys. Energ.*, **2**, 444 (1968).

(30) M. A. J. Rodgers and W. M. Garrison, *J. Phys. Chem.*, **72**, 758 (1968); *Int. J. Radiat. Phys. Chem.*, **1**, 541 (1969).

(31) R. Braams, *Nature* (London), **200**, 752 (1966).

(32) R. A. Holroyd, J. W. Glass, and P. Riesz, *Radiat. Res.*, in press.

(33) NOTE ADDED IN PROOF. Neta and Fessenden have recently reported an esr study of the deamination reaction for several amino acids, model compounds, and glycylglycine (P. Neta and R. W. Fessenden, *J. Phys. Chem.*, **74**, 2263 (1970)). These workers observe the deaminated radicals in neutral aqueous solution at room temperature and find that deamination takes place to a somewhat lesser extent in alkaline solutions. Primary deamination is found for gly-gly as is found in this work. The experimental technique used by Neta and Fessenden involves continuous electron irradiation of liquid solutions. This enables a greatly increased resolution of hyperfine components and in the case of gly-gly results in a complete assignment of hyperfine splittings to each magnetic nucleus in the deaminated radical.

Tetracyanomethane as a Pseudo-(carbon tetrahalide)

by R. E. Hester,* K. M. Lee,

Department of Chemistry, University of York, York, England

and E. Mayer

Institut für Anorganische und Analytische Chemie, Universität Innsbruck, Innsbruck, Austria (Received February 16, 1970)

The infrared spectrum from 4000 to 50 cm^{-1} and the Raman spectrum have been obtained for tetracyanomethane, $C(CN)_4$. Raman polarization data have been determined from acetonitrile and acetone solutions, and vapor phase infrared data obtained at 170° are reported and compared with both infrared and Raman data from the solid compound at room temperature. The spectra are shown to be compatible with T_d molecular symmetry, and the C–CN bond force constant is consistent with the treatment of the CN group as a pseudohalogen. The $C(CN)_4$ reactivity is attributed to the pseudohalogen groups, rather than the C–C bonds, and is justified by the high stability of the $C(CN)_3^-$ reaction product.

Introduction

The recent synthesis of tetracyanomethane, $C(CN)_4$, and investigation of some of its chemical properties revealed a number of similarities with the carbon tetrahalides.[1] However, there also are apparent inconsistencies in the treatment of $C(CN)_4$ as a pseudotetrahalide such as its ready hydrolysis under both acidic and basic conditions and its occurrence as a crystalline solid at normal room temperature. CF_4 is a gas, and CCl_4 is a volatile liquid at room temperature. Both are stable towards hydrolytic reagents. Its mass would place $C(CN)_4$ between these two compounds, so that it becomes interesting to ask whether the inconsistencies observed result from the inherent reactivity of the pseudohalogen group or from the carbon–pseudohalogen bonding differing significantly (presumably being weaker) from that of the normal carbon tetrahalides. A vibrational analysis, leading to force constant determinations, can help to provide an answer to this question.

Experimental Section

Tetracyanomethane was prepared by treating cyanogen chloride with silver tricyanomethanide ($ClCN + AgC(CN)_3 \rightarrow C(CN)_4 + AgCl$), as reported earlier.[1] All transfers of the compound, for loading Raman cells or making up mulls or solutions, were carried out in a dry nitrogen-filled glove bag. Analytical reagent grade acetonitrile and acetone were thoroughly dried and redistilled before use as solvents.

Infrared spectra were obtained in the region 4000 to 200 cm^{-1} using a Perkin-Elmer Model 621 spectrometer equipped with a dry air purging unit. CsI plates were used for containing hydrocarbon and halocarbon mulls of the compound, and a heated 5-cm path length gas cell, fitted with AgCl windows, was used at 170° for a vapor-phase study. The vapor reacted with alkali metal salt windows, as detailed in an earlier publication,[1] but AgCl proved inert and was used for deposition of sublimed crystalline material as well as for containing the vapor. Far-infrared spectra of petroleum jelly smears containing the powdered solid were obtained from a Grubb-Parsons Cube Interferometer, using standard polyethylene disks to contain the samples. Raman spectra were obtained with a modified Perkin-Elmer spectrophotometer, using a Spectra Physics Model 125 He–Ne laser, and with a Coderg PH1 instrument. Raman frequencies were determined to ± 2 cm^{-1}, and infrared frequencies to ± 1 cm^{-1}.

Results and Discussion

The infrared and Raman band frequencies found for $C(CN)_4$ as a solid at room temperature, as a vapor at 170°, and as a solute in acetonitrile and acetone solutions, are listed in Table I. Infrared spectra obtained from a Nujol mull of $C(CN)_4$ and from $C(CN)_4$ vapor at 170° are reproduced in Figure 1. Halocarbon mull spectra and sublimed $C(CN)_4$ crystal spectra showed that there are no $C(CN)_4$ bands in coincidence with Nujol bands. The solubility of the compound was low, so that reliable Raman polarization data were obtained only for the strongest bands. PQR structures were apparent in each of the strong infrared bands of the gas-phase spectrum, but no absorptions were present in the 550-cm^{-1} region, in contrast with the infrared spectrum of the solid compound.

By analogy with the normal carbon tetrahalides and with tetracyanometallate complex ions, it is reasonable to expect the overall symmetry of the $C(CN)_4$ molecule to be tetrahedral. The normal modes for T_d molecules of the general form $X(YZ)_4$ have been determined by a number of authors,[2-4] and the forms of these modes for

* To whom correspondence should be addressed.

(1) E. Mayer, *Monatsh.*, **100**, 462 (1969).
(2) B. L. Crawford and P. C. Cross, *J. Chem. Phys.*, **32**, 1482 (1938).
(3) H. Murata and K. Kawai, *J. Chem. Phys.*, **26**, 1355 (1957).

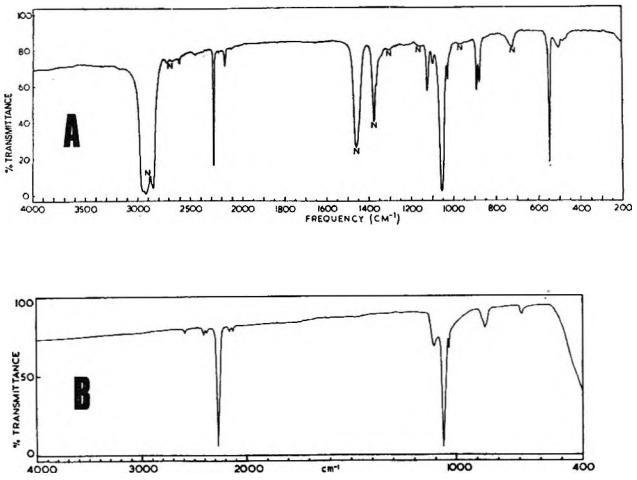

Figure 1. Infrared spectra of $C(CN)_4$: A, solid in Nujol mull (N indicates Nujol band); B, vapor at 170°.

Table I: Principal Infrared and Raman Bands of $C(CN)_4$[a]

Infrared		Raman	
Solid	Vapor	Solid	Soln polarization data
116, vw		115, vs	
156, s		154, vw	
178, s		178, vw	
		190, s	
503, w, b			
550, s			
560, vw, sh		560, s	Polarized
		573, w	
876, m	863 m(PQR)		
889, m			
1025, w, sp	1034, w		
1056, vs, b	1061, vs(PQR)	1056, m	Depolarized
1095, w	1104, w		
1123, m		1130 vw	
2276, vs, sp	2270, s(PQR)		
		2288, vs, b	Polarized

[a] All frequencies in cm^{-1}. Relative intensity designations: w = weak, m = medium, s = strong, v = very, sh = shoulder, sp = sharp, b = broad, PQR = band with P, Q, and R branch structures clearly defined.

the $Ni(CO)_4$ molecule are displayed in at least one textbook.[5] The modes are distributed amongst the T_d symmetry species with the following activities: $2A_1(R) + 2E(R) + T_1$ (inactive) $+ 4T_2(R,IR)$, where R and IR signify Raman and infrared activities, respectively. However, treating the CN group as a pseudohalide, X, it becomes interesting to consider the CX_4 skeletal modes independently and to look for simple analogies with the normal carbon tetrahalide modes, it being anticipated that this will represent a good approximation for the bond stretching modes, but a rather poor one for the angle deformations. While but little mixing of C–N stretching in with the C–C bond stretching mode is expected, by analogy with $Ni(CO)_4$,[6] the δ(CCC) and δ(CCN) deformations can be expected to have similar force constants, leading to strong coupling in the normal modes.

A plot of the $\nu_1(A_1)$ symmetric stretching mode frequencies of the normal carbon tetrahalides as a function of the mass of the halogen produces a smooth curve, from which CN group mass of 26 then leads to a prediction that the symmetric C–C stretching mode should occur at around 580 cm^{-1} if CN can be treated as a pseudohalogen. Table I shows a very strong and polarized Raman band at 562 cm^{-1} which can confidently be assigned to this C–C mode. The occurrence of a weak band at 560 cm^{-1} in the infrared spectrum from the solid $C(CN)_4$ probably is due to relaxation of the T_d selection rules, whereby this A_1 mode is infrared forbidden. The $C(CN)_4$ molecule occupying a site of lower symmetry than T_d within the crystal lattice could produce this effect. However, there is a stronger infrared band at 550 cm^{-1} which remains unaccounted for. This band, though strong in the spectrum of the solid, is completely absent from the spectrum of the vapor. This fact suggests that this also arises from a crystal lattice effect (relaxation of selection rules or, more likely, in view of the lack of a Raman coincidence, a correlation field splitting of the symmetric CC_4 stretching mode), the same effect being responsible for the appearance of the 573-cm^{-1} component adjacent to the CC_4 fundamental in the Raman spectrum.

The PQR band structures found in the vapor phase spectrum provide further evidence for a regular tetrahedral structure. Spherical top molecules conform with the rotational selection rules $\Delta J = 0, \pm 1$ for all vibrational modes. The principal vapor phase infrared bands can be assigned to asymmetric C–C and C–N bond stretching modes. The 1061-cm^{-1} band corresponds with a depolarized Raman band and falls between the 776 and 1265-cm^{-1} $\nu_3(T_2)$ bands of CCl_4 and CF_4, respectively. The 2270-cm^{-1} band can only be due to the T_2 C–N stretching mode. The 2288-cm^{-1} polarized Raman band is assigned to the A_1 totally symmetric C–N stretching mode, which is close to the 2262-cm^{-1} band previously assigned to the A_1 symmetric C–N stretch of the Cl $C(CN)_3$ molecule.[7] This 2288-cm^{-1} band was sufficiently broad to encompass the 2276-cm^{-1} band found in the infrared region, though no obvious band asymmetry was detectable.

The assignment of deformation modes is less readily achieved, due to the complexity which undoubtedly arises from coupling of CC_4 and CCN modes. Distortions due to solid state coupling effects also cloud the picture here, though it is possible to make some further

(4) L. H. Jones, *J. Mol. Spectrosc.*, **5**, 133 (1960).

(5) D. M. Adams, "Metal-Ligand and Related Vibrations," Edward Arnold Ltd., London, 1967, p 85.

(6) L. H. Jones, R. S. McDowell, and M. Goldblatt, *J. Chem. Phys.*, **48**, 2663 (1968).

(7) F. A. Miller and W. K. Baer, *Spectrochim. Acta*, **19**, 73 (1963).

tentative assignments on the basis of the data given in Table I and Figure 1. In the region below 200 cm^{-1} there are two strong Raman bands, at 115 cm^{-1} and 190 cm^{-1}, the former having a very weak infrared equivalent and the latter no infrared equivalent. Conversely, strong infrared bands at 156 cm^{-1} and 178 cm^{-1} have only weak corresponding Raman bands. The selection rules listed earlier suggest assignments as follows: E-type CC_4 deformation at 115 cm^{-1}; T_2-type CC_4 deformation at 156 cm^{-1}; T_2-type CCN deformation at 178 cm^{-1}; and E-type CCN deformation at 190 cm^{-1}. Two extremely weak infrared bands at 62 cm^{-1} and 138 cm^{-1} and a similarly feeble Raman band at 75 cm^{-1} all can be assigned as lattice modes. The 863-cm^{-1} band in the infrared spectrum of the vapor, which splits to a doublet in the solid, can be assigned either to a combination of $560(A_1) + 178(T_2) + 115(E)$ cm^{-1} fundamentals or to the difference tone $1056(T_2) - 190(E)$ cm^{-1}. At 1025 cm^{-1} (solid-spectrum) we have the possibility of either a ^{13}C isotope component of the strong 1056-cm^{-1} band, or a combination of $1056(T_2)$ with $156(T_2) - 178(T_2)$ cm^{-1}. Either combination $1056(T_2) + 190(E) - 156(T_2)$ cm^{-1} or $1056(T_2) + 154(T_2) - 115(E)$ cm^{-1} could account for the observed band at 1095 cm^{-1}, while an overtone of the $560(A_1)$ cm^{-1} fundamental produces a reasonable fit with the observed 1123-cm^{-1} band which also is detectable in the Raman spectrum. Numerous very weak bands were apparent in infrared spectra from strong mulls, particularly in the region above 2000 cm^{-1}. Suggested assignments for these are as follows: 660 $cm^{-1} \sim 1056(T_2) - 560(A_1) + 178(T_2)$; 1208 $cm^{-1} \sim 1056(T_2) + 156(T_2)$; 1230 $cm^{-1} \sim 2288(A_1) - 1056(T_2)$ or $1057(T_2) + 178(T_2)$; 1380 $cm^{-1} \sim 1056(T_2) + 178(T_2) + 156(T_2)$; 1945 $cm^{-1} \sim 2288(A_1) - 190(E) - 156(T_2)$; 2104 $cm^{-1} \sim 2 \times 1056(T_2)$ or $2278(T_2) - 178(T_2)$; 2165 $cm^{-1} \sim 2278(T_2) - 115(E)$; 2225 $cm^{-1} \sim 2288(A_1) - 176(T_2) + 115(E)$; 2245 $cm^{-1} \sim$ ^{13}C satellite of $2278(T_2)$; 2425 $cm^{-1} \sim 2278(T_2) + 156(T_2)$; 2450 $cm^{-1} \sim 2278(T_2) + 178(T_2)$ or $2288(A_1) + 156(T_2)$; 2602 $cm^{-1} \sim 2278(T_2) + 156(T_2) + 178(T_2)$; 2832 $cm^{-1} \sim 566(A_1) + 2278(T_2)$; 3332 $cm^{-1} \sim 1056(T_2) + 2278(T_2)$. Some of the foregoing assignments are necessarily somewhat speculative, but a high degree of confidence can be placed in the assignment of the bond stretching fundamentals, where interaction between C–C and C–N modes is expected to be but slight. The separability of stretching modes can therefore be justified, and the assignments summarized in Table II can be quoted with confidence.

The X–Y bond force constant for a T_d molecule XY_4 can be determined from the relationship $f = m_y 4\pi^2 \nu_1^2$, where m_y is the mass of the atom Y, and ν_1 is the XY_4 symmetric stretching frequency[8] (neglecting interactions between XY bonds). Taking Y as the CN group, this leads to a value of 4.86×10^5 dyn cm^{-1} for the C–C bond force constant in $C(CN)_4$. The corresponding

Table II: Assignments of Bond Stretching Fundamentals for $C(CN)_4$

Mode	Description	Frequency, cm^{-1}
$\nu_1(A_1)$	symm C≡N stretch	2288
$\nu_2(A_1)$	symm CC_4 stretch	562
$\nu_5(T_2)$	asymm C≡N stretch	2270
$\nu_6(T_2)$	asymm CC_4 stretch	1061

values for the normal carbon tetrahalides are as follows: CF_4, 9.14; CCl_4, 4.38; CBr_4, 3.36; CI_4, 2.38. It is seen that the reactivity of $C(CN)_4$ cannot be attributed to an unusually weak C–CN bond, since the force constants show that this lies between the C–F and C–Cl bond values. Carbon–carbon single bond strengths in other molecules are seen from the following values also to be of the same order as that in $C(CN)_4$ (Table III)

Table III

Molecule	ν_s(C—C), cm^{-1}	f(C–C), dyn cm^{-1}
CH_3–CH_3[8]	993	4.50
$C(CH_3)_4$[a]	734	4.94
CH_3–CN[8]	918	5.18

[a] K. A. Taylor and L. A. Woodward, *Proc. Roy. Soc., Ser. A*, **264** 558 (1961).

It is significant that the anion $C(CN)_3^-$ appears to be a common product of $C(CN)_4$ reactions. For example, the acid and base hydrolysis reactions may be described by the equations[1]

$$C(CN)_4 + 2H_2O \xrightarrow{H^+} C(CN)_3^- + NH_4^+ + CO_2$$

and

$$C(CN)_4 + 2OH^- \longrightarrow C(CN)_3^- + OCN^- + H_2O$$

The high acid strength of $HC(CN)_3$ has been attributed to the resonance stabilization of the anion,[9] which is specially favored in a trigonal planar configuration.[7] Using the 657-cm^{-1} band assigned to the $\nu_2(A_1')$ symmetric CC_3 stretch of the planar (D_{3h}) $C(CN)_3^-$ ion,[7] the value 6.63×10^5 dyn cm^{-1} for the C–C bond force constant may be calculated from a similar relationship to that used for $C(CN)_4$.[8] This value is significantly higher than that found for the parent $C(CN)_4$ molecule, suggesting a good thermodynamic reason for the $C(CN)_4$ reactivity. Of course, chemical reactivity is associated

(8) G. Herzberg, "Infrared and Raman Spectra of Polyatomic Molecules," Van Nostrand, Princeton, N. J., 1945.

(9) R. H. Boyd, *J. Amer. Chem. Soc.*, **83**, 4288 (1961).

more with kinetic factors, and mechanistic considerations are of importance. From the comparison made with the carbon tetrahalide series, however, it is clear that neither a dissociative SN1 mechanism nor an SN2 mechanism involving attack by a nucleophile (H_2O or OH^- in the hydrolysis reaction) at the central carbon atom in $C(CN)_4$ is likely. The reactivity must therefore be attributed to the pseudohalogen groups themselves.

Acknowledgments. We thank Dr. E. Ernstbrunner and M. J. Taylor of this department for helpful discussions on the substance of this paper, and Dr. J. A. Creighton of the University of Kent for a Raman spectrum obtained with the Coderg spectrometer. The laser and interferometer used in the work were purchased with grants from the Science Research Council. Collaboration between the Universities of York and Innsbruck was aided by a Royal Society grant.

Nuclear Magnetic Resonance Study of the Exchange Rates of the Peptide Protons of Glycylglycine and Triglycine in Water and Aqueous Urea[1a]

by Charles A. Swenson[1b] and Lynn Koob

Department of Biochemistry, University of Iowa, Iowa City, Iowa 52240 *(Received April 14, 1970)*

The rates of exchange for the peptide protons of glycylglycine and triglycine were measured in water and aqueous urea solutions as a function of pH using nmr techniques. In contrast to the composite exchange rates reported for proteins, the rates for some of the peptide protons in these model peptides are slower in aqueous urea than in water and are markedly affected by their neighboring groups. The nmr spectra of glycyl-^{15}N-glycine and triglycine are also reported.

Hydrogen–deuterium exchange has long been used as a tool for studying protein conformation.[2] Peptide proton exchange rates are generally slower than the rates for protons on acidic or basic groups and can be measured by conventional techniques.[2] The rationale for conformational studies is that peptide protons exchange relatively more slowly when they are on the inside of the protein and possibly involved in specific interactions than when exposed to the solvent. Furthermore, the variation of any parameter which would cause a change in the conformation would be reflected in the exchange rate. For large molecules, such as proteins, the exchange rates cannot be interpreted without ambiguity as they are affected by a number of environmental factors. A first step to the understanding of exchange in proteins would be knowledge of the factors affecting exchange in small molecule models.[3-6]

Hydrogen–deuterium exchange rates of proteins are known to increase in concentrated aqueous solutions of a protein denaturant, such as urea. This observation can, of course, be attributed to the exposure of additional groups to the solvent, but there is also the possibility of specific interactions of urea with the peptide group and/or the alteration of bulk solvent effects which may modify the exchange rate of exposed and possibly buried groups. In order to understand more fully proton exchange in proteins and specifically the effects of aqueous urea, we have measured the rates of exchange for the peptide protons of glycylglycine and triglycine in water and in aqueous urea as a function of pH using nmr techniques.[7,8] These peptides were

(1) (a) This research was supported by a grant from the Division of Molecular Biology, National Science Foundation, GB-7167; (b) Research Career Development Awardee, 1-K04-GM42384-01 of the National Institutes of Health. To whom correspondence should be directed.

(2) A. Hvidt and S. O. Nielsen, *Advan. Protein Chem.*, **21**, 287 (1966).

(3) (a) I. M. Klotz and B. H. Frank, *J. Amer. Chem. Soc.*, **87**, 2721 (1965); (b) I. M. Klotz and P. L. Feidelseit, *ibid.*, **88**, 5103 (1966).

(4) B. H. Leichting and I. M. Klotz, *Biochemistry*, **5**, 4026 (1966).

(5) I. M. Klotz and D. D. Mueller, *ibid.*, **8**, 12 (1969).

(6) C. Y. S. Chen and C. A. Swenson, *J. Amer. Chem. Soc.*, **91**, 234 (1969).

(7) E. Grunwald, A. Lowenstein, and S. Meiboom, *J. Chem. Phys.*, **27**, 630 (1957).

chosen since their spectra are relatively simple, and furthermore, band assignments[9] and rate studies in water were available for glycylglycine.[9,10]

Experimental Section

Materials. Glycylglycine and triglycine were obtained from Fisher and Cyclo Chemical Co., respectively, and were used without purification after verifying that no contaminants were present by paper chromatography. The concentrations of the peptide solutions were ~1.0 *M* for glycylglycine and 0.5 *M* for triglycine. The desired pH's, which were measured before and after the nmr measurement on a radiometer pH meter, were achieved by adding concentrated acid or base as needed. For deuterium oxide solutions the pH was adjusted by the addition of concentrated DCl or NaOD and the appropriate correction applied.[11] The heavy water and concentrated solutions of DCl and NaOD were obtained from Stohler Isotope Chemicals. Recrystallized urea was used for all the aqueous urea solutions.

Carbobenzoxyglycine *p*-nitrophenyl ester and ^{15}N-glycine, which were obtained from Sigma Chemical Co. and Bio-rad Laboratories, respectively, were used without further purification. Carbobenzoxyglycyl-^{15}N-glycine was synthesized from the reaction of carbobenzoxyglycine *p*-nitrophenyl ester and ^{15}N-glycine according to the illustrative procedure of Greenstein and Winitz.[12] The heating time was extented to approximately 1 hr at a reaction temperature of about 100°. The recrystallized product (dioxane:water, 7:1) melted at 174–175°. Glycyl-^{15}N-glycine was prepared from carbobenzoxyglycyl ^{15}N-glycine by catalytic hydrogenation over paladium in methanol–water (1:1) at atmospheric pressure. The product was separated from the reaction mixture on a Dowex-50 column, which was equilibrated with sodium citrate buffer at pH 3.25. Desalting was also achieved on a column of Dowex-50.

Methods. The spectra were measured on a Varian A-60 spectrometer at a temperature of 40°. Chemical shifts were measured from the resonance line in the reference compound, 3-(trimethyl silyl)-propane sulfonic acid sodium salt. The mean lifetime, τ, of the peptide proton was calculated from the line shape of the theoretical curves for the methylene doublet or triplet.[7,8] The effective spin–spin relaxation time, T_2, used in the calculation of the rates, was for the aqueous solution since the main contribution to line width is field inhomogeneity. The effective T_2 was 0.7 to 1.0 sec from our measurements. The theoretical curves for the broadened doublet were used at the slower exchange rates, and the curves for the collapsed doublet were used at the higher exchange rates. Although the values from both methods form a continuous curve of rate *vs.* pH, the latter method is less accurate. Almost all the results reported are from the former method.

Results and Discussion

Spectra of Glycylglycine. The spectrum of glycylglycine in water contains four lines which in order of increasing magnetic field are (a) the peptide proton, (b) water plus rapidly exchanging amino protons, and (c) two peaks arising from the methylene hydrogens. The assignment of the two methylene peaks to the α and β hydrogens was made by Sheinblatt[9] with a spin-decoupling experiment and the pH dependence of the two resonances. We have also observed the spectrum in deuterium oxide, which serves as a further proof of the assignment. The β-methylene group which is attached to the rapidly exchanging amino protons shows a single narrow line at all pH's. The α-methylene hydrogens which are spin-coupled to the peptide deuterium show either a singlet or a triplet, depending on the pH.

In addition, we measured the spectrum of glycyl-^{15}N-glycine wherein the resonance of the NH proton is a sharp triplet since it is no longer broadened by quadrupole relaxation. From this absorption we obtained a first-order splitting constant of 5.9 ± 0.1 cps which is what we observed for the methylene-splitting constant in both glycyl-^{15}N-glycine and glycylglycine. These coupling constants represent the mean with their respective standard deviations. Spectra of glycyl-^{15}N-glycine at two pH's are shown in Figure 1. Substitution of ^{15}N for ^{14}N in glycylglycine enables one to observe the strong coupling of the peptide proton to the nitrogen nucleus, and thus, we observed two triplets which are separated by the coupling constant, 93 cps. A splitting of each component of the α-methylene doublet (Figure 1b) into two peaks arises because of coupling of these protons with a nitrogen nucleus for which the coupling constant was measured to be 1.1 cps. Figure 1a, which shows a spectrum of glycyl-^{15}N-glycine at a higher pH, illustrates the difficulty encountered due to overlapping lines when one tries to measure exchange rates from the broadening of the α-methylene doublet. An accurate measurement of the same rate can be made using the peptide proton triplet of glycyl-^{15}N-glycine.

Spectra of Triglcyine. Triglycine in aqueous solution shows six resonances in addition to the water resonance when the peptide and amino protons are undergoing fast exchange. As with glycylglycine, the resonances of the rapidly exchanging amino protons are averaged with the water resonance. The other observed resonances at pH 4.7 are (a) three methylene resonances at

(8) A. Lowenstein and S. Meiboom, *J. Chem. Phys.*, **27**, 1067 (1957).

(9) M. Sheinblatt, *J. Amer. Chem. Soc.*, **87**, 572 (1965).

(10) S. O. Nielsen, W. P. Bryan, and K. Mikkelsen, *Biochem. Biophys. Acta*, **42**, 550 (1960).

(11) P. K. Glascoe and F. A. Long, *J. Phys. Chem.*, **64**, 188 (1960).

(12) J. P. Greenstein and M. Winitz, "Chemistry of the Amino Acids," Vol. 2, Wiley, New York, N. Y., 1961, p 1034.

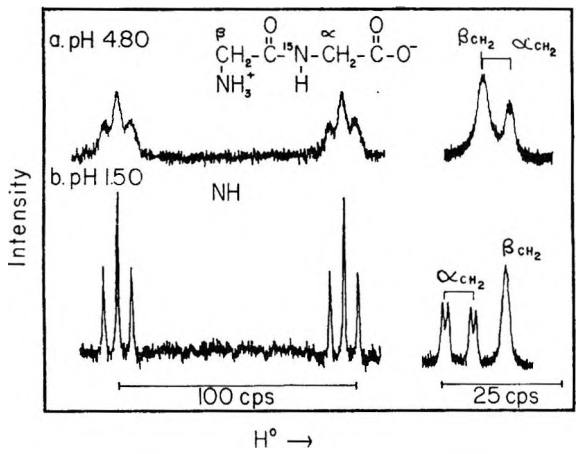

Figure 1. Spectrum of glycyl-^{15}N-glycine in water. (a) pH 4.80; (b) pH 1.50.

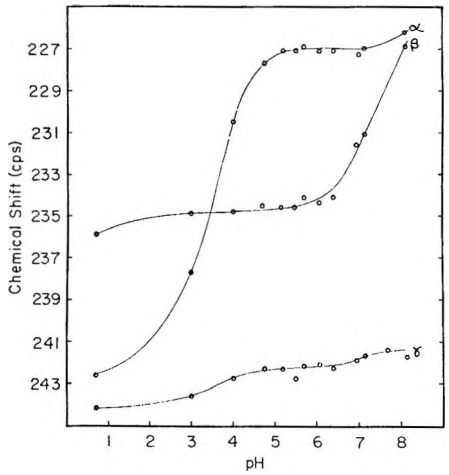

Figure 2. pH dependence of chemical shift of methylene protons of triglycine in water.

3.83, 3.92, and 4.03 ppm (δ) and (b) two NH resonances at 8.10 and 8.59 ppm (δ).

Assignment of the resonances due to the α-, β-, and γ-methylene protons was made on the basis of pH shifts measured in the study. The peaks at 3.83, 3.92, and 4.03 ppm (δ) are assigned to the α-, β-, and γ-methylene protons, respectively. Ionization of the carboxyl group shifts the resonance of the adjacent α-methylene group to a higher field due to the smaller inductive effect of the carboxylate ion as compared to the carboxyl group as is well known.[9] The γ- and β-methylene protons would be expected to show analogous but smaller shifts as their distance from the carboxyl group is larger. The resonance which shifts to higher field in the pH range where the amino group is neutralized was assigned to the adjacent β-methylene protons. This is expected from the relative shielding effects of NH_2 and NH_3^+ groups. Neither ionization significantly affected the position of the third methylene resonance which was assigned to the γ protons. The behavior of these resonances as a function of pH is shown in Figure 2. The sigmoidal shape of the plot of chemical shift of α-methylene protons as a function of pH indicates the titration of the carboxyl group, and the pK can be obtained from the inflection. Complete agreement is observed between the present assignments and those of the cationic, zwitterionic, and anionic forms as made by Nakamura and Jardetsky[13] on the basis of selective deuteration.

Assignment of the resonance at 8.10 ppm (δ) to the α-peptide proton results from its shift from 8.30 to 8.10 as the carboxyl group ionizes. The second peak at 8.59 ppm (δ) which does not shift in this pH range was assigned to the γ-peptide proton. An analogous behavior was noted for the α-peptide proton of glycylglycine.

Exchange Rates. The average lifetime, τ, is related to the specific rate of exchange by the equation

$$\frac{1}{\tau} = k' = \frac{\mathrm{d} \ln c_A}{\mathrm{d}t} = \frac{1}{c_A}\frac{\mathrm{d}c_A}{\mathrm{d}t}$$

where c_A is the concentration of the peptide proton and k' is the specific exchange rate (this is the number of exchanges per second). The mechanism of exchange of the peptide proton of glycylglycine, for example (same for triglycine), involves the following reactions.[14]

$$NH_3^+CH_2CONHCH_2COO^- + H_3O^+ \underset{}{\overset{k_{H^+}}{\rightleftharpoons}} NH_3^+CH_2CONH_2^+CH_2COO^- + H_2O$$

$$NH_3^+CH_2CONHCH_2COO^- + H_2O \overset{k_{H_2O}}{\rightleftharpoons} NH_3^+CH_2CO{-}NCH_2COO^- + H_3O^+$$

$$NH_3^+CH_2CONHCH_2COO^- + OH^- \overset{k_{OH^-}}{\rightleftharpoons} NH_3^+CH_2CO{-}NCH_2COO^- + H_2O$$

Measurements were not possible below a pH of 4.0 as the rates were too slow for the nmr technique ($\tau > 0.2$ sec). Experiments were attempted in the pH range 0.5 to 4.0, but no discernible rate increase was noted, which indicates that the catalysis by hydrogen ion is negligible in agreement with the work of Sheinblatt.[9] The specific exchange rate can thus be expressed as

$$k' = k_{OH^-}\frac{K_w}{[H^+]} + k_{H_2O}[H_2O]$$

The measured exchange rates for glycylglycine in water and 6 M urea are shown as a function of the reciprocal of hydrogen ion activity in Figure 3. Base catalytic constants for the exchange in water and 6 M urea, which were evaluated from the measured slope of the plots of k' *vs.* the reciprocal of hydrogen activity, are presented in Table I. The value used for pK_w in 6 M urea was 14.26.[15] Our value of $1.0 \times 10^{+9}$ (M sec)$^{-1}$ for the base

(13) A. Nakamura and O. Jardetsky, *Biochemistry*, **7**, 1226 (1968).

(14) A. Berger, A. Lowenstein, and S. Meiboom, *J. Amer. Chem. Soc.*, **81**, 62 (1959).

(15) H. B. Bull, K. Breeze, G. L. Ferguson, and C. A. Swenson, *Arch. Biochem. Biophys.*, **104**, 297 (1964).

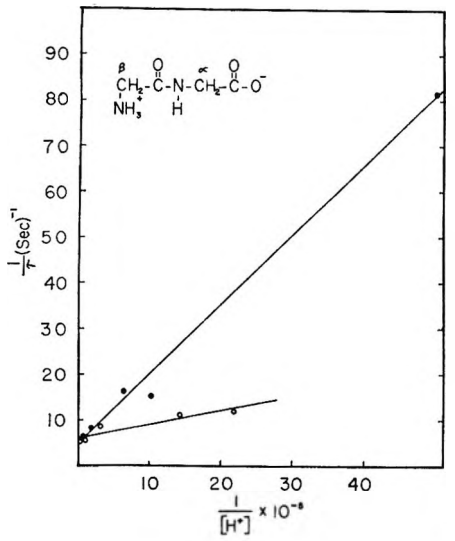

Figure 3. Exchange rate *vs.* pH for glycylglycine: —●—, in water; –O–, in 6 *M* urea.

Table I: Base Catalytic Constants, k_{OH^-}, $(M \text{ sec})^{-1}$

	Water	6 *M* Urea
Glycylglycine	1.0×10^9	5.7×10^8
Triglycine α	6.0×10^7	1.4×10^8
γ	9.2×10^9	3.7×10^9

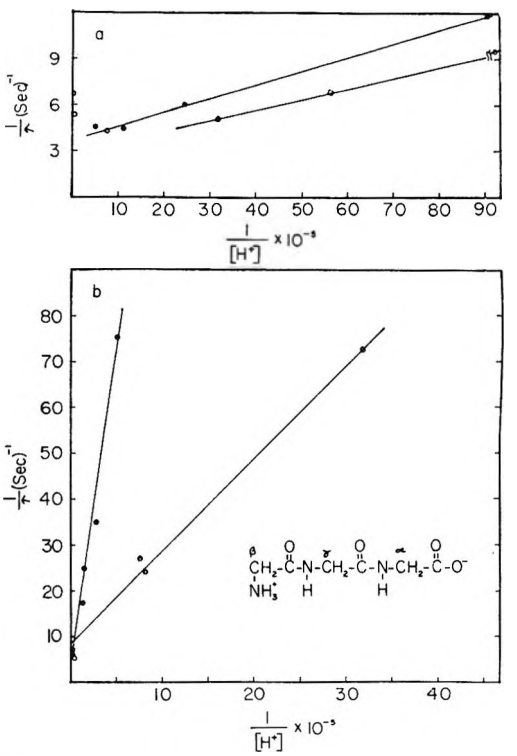

Figure 4. Exchange rate *vs.* pH for triglycine. (a) α proton: —●—, in water; –O–, in 6 *M* urea. (b) γ proton: —●—, in water; –O–, in 6 *M* urea.

catalytic constant in water at 40° is higher than the value of $7.8 \times 10^{+8}$ $(M \text{ sec})^{-1}$ reported by Sheinblatt[9] at 23°. We consider these results to be in agreement in view of the different temperatures used for the two experiments and the standard error for the rate measurements which ranged from 10 to 15%. Instrumental factors which affect the measured rates make a quantitative comparison of the rates from two different instruments difficult. However, it should be feasible to compare relative rates as we have done.

Similar data are presented for the α and γ protons of triglycine in Figures 4a and 4b, respectively, and in Table I.

Several interesting points can be made concerning these constants. For the peptide protons of glycylglycine and triglycine in water catalysis by OH^- seems to be dominated by the charged groups on the molecule. In glycylglycine where the peptide proton is located between the positively charged α amino and the negatively charged carboxylate ion the value for the basic catalytic constant is 1.0×10^9 which is intermediate to the values found for the γ and α protons of triglycine. The exchange rates of the γ peptide proton of triglycine and the peptide proton of glycylglycine show no catalysis by hydrogen ion down to a pH of approximately 0.5 where our measurements concluded. In contrast, the rates for the α proton of triglycine which are catalyzed to a much smaller extent by base are catalyzed by hydrogen ion, which is similar to the case of *N*-methyl acetamide[3] and lactams.[3,6] The charged amino group thus seems to suppress catalysis by hydrogen ion at the adjacent peptide linkage. The relatively small value of the base catalytic constant for the α proton of triglycine also reflects the presence of the carboxylate ion in the immediate environment. It is clear that the charged groups in the vicinity of the exchanging peptide protons have a marked effect on the observed rates.

In aqueous urea the peptide protons all show a longer mean lifetime compared to water even though the relationships between the lifetimes of the various protons are the same. Furthermore, the γ-peptide proton of triglycine and the peptide proton of glycylglycine have slightly reduced base catalytic constants in aqueous urea. The α-peptide proton of triglycine, however, shows a higher base catalytic constant in urea. For the long lifetimes measured here the experimental error may be larger than the 10 to 15% estimated, and probably one could consider these two rates to be identical.

Certainly the effect of urea on these compounds is not to change the exposure of groups to solvent as in the unfolding of a protein. Its effect must be mediated either through a specific interaction with the peptide group or through a change in bulk solvent.

At the pH's used for our measurement the urea protons are exchanging rapidly with the water protons and are averaged with the water resonance. Urea might

then be a reactant in the exchange just as water. Further insight into the role of urea in the exchange mechanism can be obtained by consideration of intercepts of the lines in Figures 3 and 4. The intercept on the ordinate for the exchange in water is equal to $k_{H_2O}[H_2O]$. In the aqueous urea solution it is $k_{H_2O}[H_2O] + k_u[\text{urea}]$ where k_u is the catalytic constant for urea. For each of the peptide protons of glycylglycine and triglycine the intercept in water and aqueous urea is identical within experimental error. This is possible if the catalytic constant for urea is the same as that for water and urea would then substitute for water in the exchange in the aqueous urea solutions.

Urea may decrease the base-catalyzed rate by specifically interacting with the peptide hydrogen *via* a hydrogen bond which is stronger than that formed between the peptide hydrogen and water. In an unfolded protein in aqueous urea the observed rate would then be the sum of two components: (1) an increase in the rate due to an increase in accessibility as compared to the folded protein and (2) a decrease in rate due to the specific interaction of urea with peptide hydrogen *via* hydrogen bonding which decreases the rate *via* the base catalytic constant. It is our opinion that urea does not enter into the exchange reaction as a charged species in a manner analogous to water as it would then need to be protonated or lose a proton—which urea does not do readily as it results in a loss of 37 kcal/mol of resonance energy. It does, however, as indicated above participate in an exchange reaction as H_2O does with a very small catalytic constant. In any case, exchange measurements, which are used to assess conformation or conformational changes in proteins in water and aqueous urea solutions, are likely to contain ambiguities due to the local environment and to the solvent interactions which are different for each peptide group. Appropriate consideration should be given these environmental effects.

Proton Magnetic Resonance Study of Counterion and Solvent Effects on Nitrogen-14 Quadrupole Relaxation in Tetraalkylammonium Ions

by David W. Larsen

Department of Chemistry, University of Missouri-St. Louis, St. Louis, Missouri 63121 *(Received December 23, 1969)*

Nuclear magnetic resonance line shapes for α-methyl protons in $(CH_3)_4N^+$ and $(CH_3)_3NCH_2CH_3^+$ salts are presented. The dependence of the line shapes on salt concentration, added electrolyte concentration, solvent, and temperature was studied. The observed effects are caused by the ^{14}N quadrupole relaxation rate, which is governed by the nature of fluctuating field gradients at the ^{14}N nucleus. Electric field gradients and correlation times are discussed in terms of structure of the cations, solvent interactions, and ion pairing. The small temperature dependence of the line shapes suggests that the correlation decay mechanism is rotation of the cation. The results are interpreted in terms of contact ion pairs in dimethyl sulfoxide solution and solvent-separated ion pairs in aqueous solution. The present results for $R_4N^+X^-$ ion pairs are in agreement with previous results for $R_4N^+MX_n^{3-}$ ion pairs from studies of nmr pseudocontact effects.

Introduction

Nmr studies of ion pairs of the type $R_4N^+MX_n^{3-}$, where M = Fe and Cr, have been reported.[1-3] These studies indicate that the ion pairs are of the solvent-separated type in aqueous solution and of the contact type in dimethyl sulfoxide solution. Interionic separations were calculated from the observed pseudocontact effects on the proton resonance of the R_4N^+ ions caused by the paramagnetic MX_n^{3-} ions. These calculated distances depend somewhat upon the model used for the ion pair geometry, and the results apply only to the large, triply charged MX_n^{3-} ions.

The present studies were made to determine whether or not solvent-separated ion pairs are formed between

(1) D. W. Larsen and A. C. Wahl, *Inorg. Chem.*, **4**, 1281 (1965).
(2) D. W. Larsen, *ibid.*, **5**, 1109 (1966).
(3) D. W. Larsen, *J. Amer. Chem. Soc.*, **91**, 2920 (1969).

R_4N^+ and a wide variety of anions in aqueous solution, and also to test the validity of the geometric model used in the previous calculations.[1-3]

Proton magnetic resonance spectra of tetraalkylammonium ions in general exhibit spin coupling between ^{14}N and both α and β protons.[4,5] The proton line shape (triplet from coupling with ^{14}N) depends upon the rate of the ^{14}N quadrupole relaxation.[6,7] The quadrupole relaxation rate depends upon the magnitude and frequency of fluctuating electric field gradients[8-10] at the ^{14}N nucleus. This fact suggests that studies of the proton line shapes of diamagnetic salts of R_4N^+ would be informative since the field gradients reflect such things as structure of the cation, solvent interactions, ion association, and motions affecting correlation. Study of the proton resonance is more useful than study of the ^{14}N resonance would be since the former may be done directly in dilute solution whereas the latter could only be done directly in very concentrated solution.

Experimental Section

Nmr Measurements. Solutions approximately 0.05 *M* in tetraalkylammonium iodide were prepared. Solvents used in the studies were deuterium oxide, dimethyl sulfoxide-d_6 (DMSO-d_6), and nitrobenzene. The proton magnetic resonance spectra of the solutions were recorded using a Perkin-Elmer R-20 nmr spectrometer operating at 60 MHz. The resolution was adjusted with extreme care before recording each separate spectrum. An average of 15 spectra were recorded for each sample to obtain optimum nmr line shapes for the study. It was found that neither degassing nor bubbling of nitrogen through the solution had an observable effect on the recorded spectra. The temperature of the samples was varied between 12 and 200°.

Results

Our approach was to choose a tetraalkylammonium ion in which the rate of ^{14}N quadrupole relaxation is of the correct magnitude to cause partial collapse of the proton triplet, so that changes in the proton line shape as a function of temperature, solvent, and added electrolyte could then be studied. It was found, after a wide variety of tetraalkylammonium ions had been studied, that the only protons exhibiting nmr spectra in which the ^{14}N coupling is in a state of partial collapse for dilute aqueous solutions at 35° are those in *N*-methyl groups. The methyl protons in *N*-ethyl groups, for example, exhibit completely resolved ^{14}N splittings, which are not affected by solvent variation, temperature change, etc. In this case, no spectral changes are observed because the variation of the experimental parameters does not increase the quadrupole relaxation rate beyond the "slow limit" case. The *N*-methyl spectra of the ions $(CH_3)_4N^+$ and $(CH_3)_3NCH_2CH_3^+$ were found to be the most informative for the focus of the present study. The observed line shapes for the iodide salts in D_2O are illustrated in Figure 1. As shown in the figure the methyl spectra of these two ions are different, indicating different rates of ^{14}N quadrupole relaxation. It can also be seen that the temperature dependence of the line shapes is quite small (roughly $1/T$). The variation of the $(CH_3)_4N^+$ line shapes with temperature is enhanced when DMSO-d_6 is used as the solvent. The observed line shapes for $(CH_3)_4N^+I^-$ in DMSO-d_6 solution over the temperature range 12 to 75° are illustrated in Figure 2. It was observed that the line shapes for $(CH_3)_3NCH_2CH_3^+$ are independent of solvent at a given temperature and that they exhibit a temperature dependence of $\sim 1/T$. The temperature dependence of the nmr spectra was studied for the solvents D_2O, DMSO-d_6, and nitrobenzene; in the latter solvent the $1/T$ dependence was observed over the range 35 to 200°.

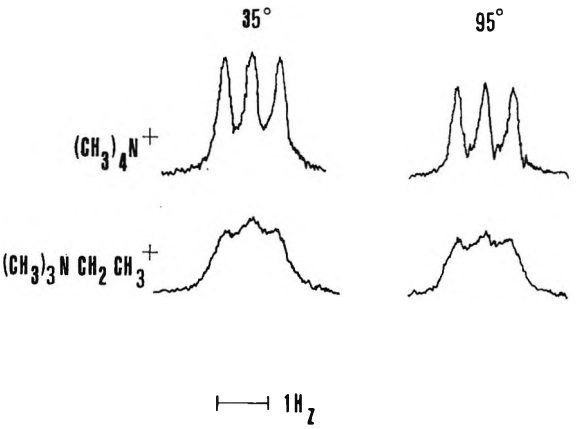

Figure 1. Observed methyl proton magnetic resonance spectra for $(CH_3)_4N^+I^-$ and $(CH_3)_3NCH_2CH_3^+I^-$ at two temperatures in D_2O solution. The value of J_{N-CH_3} is 0.56 Hz and the value of the line width at half-maximum is 0.12 Hz for $(CH_3)_4N^+$.

The aqueous solutions of $(CH_3)_4N^+I^-$ and $(CH_3)_3NCH_2CH_3^+I^-$ were studied as functions both of concentration of tetraalkylammonium salt and of concentration of added electrolyte. It was found that the proton nmr spectra are independent of both these parameters. The concentration range of tetraalkylammonium salts studied was from 0.05 *M* up to the solubility limit of the salt (several molar). The following electrolytes were added to samples which were 0.05 *M* in $(CH_3)_3NR^+I^-$, potassium salts: fluoride, chloride, bromide, iodide, cyanide, thiocyanate, sulfate, and perchlorate; sodium salts: nitrate, acetate, benzoate,

(4) H. C. Hertz and W. Spalthoff, *Z. Elektrochem.*, **63**, 1105 (1959).
(5) M. Franck-Neumann and J. M. Lehn, *Mol. Phys.*, **7**, 197 (1964).
(6) J. M. Anderson, J. D. Baldeschwieler, D. C. Dittmer, and W. D. Phillips, *J. Chem. Phys.*, **38**, 1260 (1963).
(7) A. G. Massey, E. W. Randall, and D. Shaw, *Spectrochim. Acta*, **20**, 379 (1964).
(8) J. A. Pople, *Mol. Phys.*, **1**, 168 (1958).
(9) R. A. Sack, *ibid.*, **1**, 163 (1958).
(10) M. Suzuki and R. Kubo, *ibid.*, **7**, 201 (1964).

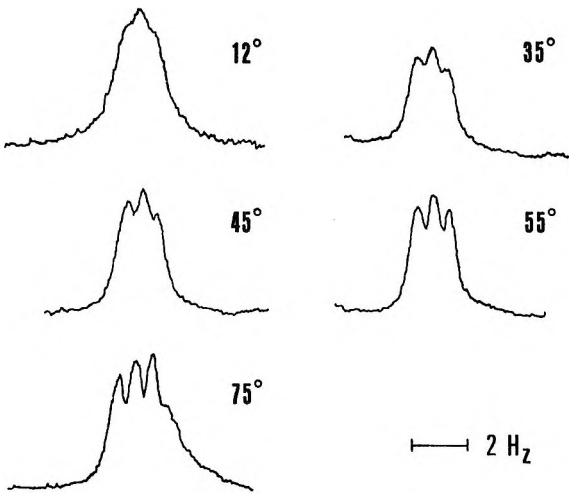

Figure 2. Observed proton magnetic resonance spectra for $(CH_3)_4N^+I^-$ in DMSO-d_6 over a range of temperatures. The slight asymmetry in the 75° spectrum is due to the superposition of the small, highly temperature sensitive residual water peak.

citrate, phosphate, and pyrophosphate. Successive additions of each electrolyte were made up to the solubility limit.

Discussion

Pople[8] gives the transition probability, p, for transitions between adjacent spin states of an $I = 1$ nucleus

$$p = \frac{3}{40}\left(\frac{e^2Qq}{\hbar}\right)^2 \tau_c \qquad (1)$$

where eq is the electric field gradient, eQ is the nuclear electric quadrupole moment, and τ_c is the correlation time (*i.e.*, the time characterizing the process which causes the field gradient to fluctuate). Theoretical line shapes for protons coupled to an $I = 1$ nucleus are given by the Pople–Sack[8,9] equations. These line shapes as a function of p were simulated using an IBM 1130 computer. Comparison of the observed line shapes for $(CH_3)_3NR^+I^-$ salts with the simulated line shapes gives the approximate values for p (Table I).

Table I

Ion	Approximate p value: D_2O (35°)	DMSO-d_6 (12°)	DMSO-d_6 (75°)
$(CH_3)_4N^+$	<0.1	0.5	0.1
$(CH_3)_3NCH_2CH_3^+$	0.5	0.5	0.5

The p values obtained in this way are approximate since there are qualitative differences between the observed and calculated line shapes. This is due to neglect of effects such as proton natural line width. The problem is presently being studied in our laboratories and preliminary computer simulations gave exact fits of the observed line shapes from modified Pople–Sack equations using p values somewhat smaller than those given above. However, the approximate values of p are sufficient for the focus of the present study.

Aqueous Solution Spectra. According to eq 1, the strength of the interaction (p) depends upon eq, eQ, and τ_c. Since eQ is independent of experimental variables, changes in p must be due to changes in eq and/or τ_c. Correlation decay is usually assumed to arise from rotation and/or translation. Correlation times have been estimated from the Stokes–Einstein equation,[11,12] *i.e.*, $\tau_c \propto \eta/T$, where η is the viscosity. However, the general use of the Stokes–Einstein equation for nmr correlation times in aqueous electrolyte solutions has been criticized in a recent discussion of this question,[13] and it was concluded that a proportionality between τ_c and η/T is unlikely to be generally valid, especially when the ions involved have a marked effect on the structural equilibrium of the water. The temperature dependence of quadrupole relaxation rates has also been rationalized by use of an Arrhenius type expression.[14] The calculation of reliable nmr correlation times is as yet an unsettled question; however, the observed small temperature dependence of the lineshapes (roughly $1/T$) is indicative of a low activation energy process. One such process is suggested by the spherical nature of the cation; rotational tumbling[15] of the cation could contribute to correlation decay and is expected to be characterized by a low activation energy.[16] Also, a highly concerted (low activation energy) reorientation of solvent dipoles in the solvation sheath could conceivably contribute to correlation decay. Effects such as rotation of functional groups[17] in the cation and exchange of solvent or anions, which could possibly contribute to correlation decay, would be expected to exhibit larger temperature dependences than are observed. A study of proton relaxation times in aqueous solutions of tetraalkylammonium salts has been reported.[18] The results of the study indicate that there is increased water structure around the cation as compared to the pure solvent and that the cations with short alkyl groups (such as those in the present study) "reorient themselves relatively quickly in their hydrate

(11) N. Bloembergen, E. M. Purcell, and R. V. Pound, *Phys. Rev.*, **73**, 679 (1948).

(12) H. G. Hertz and M. D. Zeidler, *Ber. Bunsenges. Phys. Chem.*, **67**, 774 (1963).

(13) M. S. Arnold and K. J. Packer, *Mol. Phys.*, **14**, 241 (1968).

(14) S. Alexander and A. Tzalmona, *Phys. Rev. Lett.*, **13**, 546 (1964).

(15) W. B. Moniz, W. A. Steele, and J. A. Dixon, *J. Chem. Phys.*, **38**, 2418 (1963).

(16) M. Davies, Ed., "Molecular Relaxation Processes," Chemical Society Special Publication No. 20, Academic Press, New York, N. Y., 1966.

(17) E. O. Stejskal, D. E. Woessner, T. C. Farrar, and H. S. Gutowsky, *J. Chem. Phys.*, **31**, 55 (1959).

(18) H. G. Hertz and M. D. Zeidler, *Ber. Bunsenges. Phys. Chem.*, **68**, 821 (1964).

cage." Although the mechanism for proton relaxation is of course different from that for quadrupole relaxation, the conclusions as to the increased structure in the solvent sheath would suggest that the presently observed lack of proportionality between τ_c and η/T is to be expected.[13] Also, the conclusion as to the rapid reorientation of the cation in the hydrate cage is in agreement with the presently proposed low activation energy reorientation of the cation. The study[18] also suggests that two ions as similar as $(CH_3)_4N^+$ and $(CH_3)_3NCH_2CH_3^+$ would not be expected to have τ_c values which differ by as much as a factor of 5. Thus the difference in p values for the two ions in aqueous solution must be due primarily to a difference in *eq*.

There are at least three different factors which influence the distribution of charge about the ^{14}N nucleus: the nature of the N–R bonds, solvent dipoles surrounding the ion, and ion pairing. Observations made in this laboratory and by others suggest that ion pairing has relatively little influence upon the quadrupole relaxation rate of R_4N^+ in aqueous solution. The spectra are independent of R_4N^+ concentration[7,19] and of added electrolyte (containing ions of varying size and charge) up to concentrations of several molar. These observations indicate that ion pairing in aqueous solution is not an important factor as far as the spectral line shapes are concerned. By use of experimental equilibrium constants[1] for ion pairs of the type in this study, we estimate that there is a negligibly small fraction of ion pairs in aqueous 0.05 M $R_4N^+I^-$, and that the fraction is increased essentially to unity when a large excess of electrolyte is added to the solution. Since line shapes are independent of added electrolyte, the contribution to *eq* from ion pairs must therefore be small. It should be particularly noted that addition of the electrolytes sodium citrate and sodium pyrophosphate to aqueous tetramethylammonium solutions caused no detectable change in the line shape. Citrate and pyrophosphate have both been observed[20] to strongly affect ^{23}Na line shapes in aqueous solution. The line shapes were also found to be independent of pH.

If the difference in p for $(CH_3)_4N^+$ and $(CH_3)_3NCH_2CH_3^+$ in aqueous solutions is due exclusively to a difference in *eq* and if ion pairing effects are negligible, then the remaining two factors to be considered are the effects of the N–R bonds and solvent dipoles. If solvent dipoles surrounding the cation are the major source of the field gradient, then the difference in interaction strengths could be rationalized in terms of the arrangement of solvent dipoles as dictated by the shape of the cation. The $(CH_3)_4N^+$ ion has approximate spherical symmetry (small *eq*), and substitution of one CH_2CH_3 for one CH_3 should cause a distortion of the sphere (large *eq*). However, it was observed that the $(CH_3)_3NCH_2CH_3^+$ spectra are essentially identical in three solvents, D_2O, DMSO-d_6, and nitrobenzene. If the field gradient is caused by the solvent dipole alignment, the spectra should exhibit a strong solvent dependence. Only in the case of $(CH_3)_4N^+$ are the spectra solvent dependent.

Conversely, if the field gradient for the aqueous solutions is determined by the N–R bonds, the difference in p values may be explained on the basis of variation of C–N–C bond angles.[21] In the solid state, the bond angle is exactly tetrahedral[22] for $(CH_3)_4N^+$. The bond angles depart markedly from tetrahedral when R groups other than CH_3 are present.[23,24] The tetrahedral bond angle in $(CH_3)_4N^+$ gives rise to a small *eq*, and bond angles other than the tetrahedral angle in $(CH_3)_3NCH_2CH_3^+$ would give rise to a larger *eq*.

Dimethyl Sulfoxide Solution Spectra. The solvent dependence of $(CH_3)_4N^+$ p values can be attributed to the small contribution to *eq* from the N–R bonds, which allows the effects of electric fields from sources external to the cation to be seen in the spectra. The small value of p for $(CH_3)_4N^+$ in aqueous solutions indicates that there is no distortion of the electrical field in the vicinity of the cation which is long-lived enough to affect p. This is consistent with the previous proposal[1-3] of solvent-separated ion pairs in aqueous solution. In contrast, the spectra of $(CH_3)_4N^+$ in DMSO-d_6 solution indicate that there is a distortion of the electric field in the vicinity of the cation which is long-lived enough to affect p. The larger temperature dependence of p in this case could be due to either a larger temperature dependence of τ_c or to a temperature-dependent variation of the fraction of ion pairs present. In the latter case, the larger low-temperature p value would indicate either contact ion pairs or considerable realignment of solvent dipoles within the ion pair relative to the free ion. If the p value variation is due to an ion-pair effect rather than a τ_c effect, a mass-action effect should be observed by addition of electrolyte to the solution. Unfortunately, the amount of additional electrolyte which is soluble in the DMSO solutions is negligible for most electrolytes. However, appreciable amounts of additional electrolyte are soluble in the mixed solvent water–DMSO, and it was possible to observe an increase in p from $\simeq 0.1$ to $\simeq 0.4$ upon addition of either NaCl or LiCl to a solution of 0.1 M $(CH_3)_4NCl$ in 40% H_2O–60% DMSO. Thus, the changes in p caused by changes in temperature and addition of electrolyte agree qualitatively with the dictates of equilibrium considerations for ion pairs.

(19) E. Bullock, D. G. Tuck, and E. J. Woodhouse, *J. Chem. Phys.*, **38**, 2318 (1963).

(20) O. Jardetzky and J. E. Wertz, *J. Amer. Chem. Soc.*, **82**, 318 (1960).

(21) C. T. O'Konski and Tae-Kyn Ha, *J. Chem. Phys.*, **49**, 5354 (1968).

(22) J. D. McCullough, *Acta Crystallogr.*, **17**, 1067 (1964).

(23) L. M. Trefonas and J. Couvillion, *Acta Crystallogr.*, **16**, 576 (1963).

(24) A. Zalkin, *ibid.*, **10**, 557 (1957).

Since the variation in p values for $(CH_3)_4N^+$ in DMSO solution can be accounted for by variation in the fraction of ion pairs, this indicates that the temperature variation of τ_c is small. Since eq is determined by particles external to the cation, rotation of the cation within the hydration sheath does not necessarily change either the direction or the magnitude of eq relative to the quadrupole axis of quantization (the applied magnetic field). Thus rotation of the cation might not be effective in causing correlation decay. Only to the extent of the interaction between the alkyl chains in the cation and the solvent dipoles (DMSO) will rotation of the cation modulate eq. If there is sufficient interaction between alkyl groups and solvent dipoles, the correlation time could correspond to the cation rotation time even though it is solvent dipole reorientation which changes eq. An alternate possibility for a correlation decay mechanism in this case is a concerted reorientation of solvent dipoles and anion motion. This could be a low activation energy process which would change eq.

The fact that τ_c values and thus cation rotation times are essentially independent of solvent for $(CH_3)_3NCH_2CH_3^+$ suggests that cation rotation times are identical for $(CH_3)_4N^+$ in D_2O and in DMSO-d_6. If the correlation time is assumed to be the cation rotation time for $(CH_3)_4N^+$, then τ_c values are also identical for the D_2O and for the DMSO-d_6 solutions, and the observed differences in p are due to differences in eq. The large eq for the DMSO-d_6 solutions has been related (in this study) experimentally to the presence of ion pairs, by both temperature and mass-action effects. It is also known from previous nmr studies[1] and from conductivity data[25] for aqueous solutions of $R_4N^+X^-$ salts that the R_4N^+ ions are essentially completely ion paired in the presence of a large excess of electrolyte. The conclusion to be drawn is that the eq values for $(CH_3)_4N^+$ are different for aqueous and for DMSO ion pairs. The large eq value for ion paired $(CH_3)_4N^+$ in DMSO may be due to one of two things, (a) "contact" ion pairs or (b) substantial realignment of solvent dipoles within "solvent-separated" ion pairs. The small eq value for ion paired $(CH_3)_4N^+$ in aqueous solution is undoubtedly due to the presence of "solvent-separated" ion pairs. The alternate explanation that anion field effects are exactly balanced by water dipole realignment is unlikely, since this behavior should be a function of anion parameters (size, shape, charge, etc.).

A more detailed knowledge of the electric field gradients in ion pairs is needed to distinguish between the two possible origins of the large eq values in DMSO. However, one may easily make crude estimates of field gradients by assuming point charges for anions and neglecting the effects of solvent dipoles.[26] These field gradients and a typical value[12] for τ_c (same for both solvents) were used in eq 1 to give ion pairing distances $\sim$3 Å in DMSO-d_6 and >5 Å in D_2O. This indicates that the large eq values for DMSO solutions are due to "contact" ion pairs. The results of this study thus provide additional evidence in support of the previous observations[1-3] of solvent separated and contact ion pairs.

Acknowledgment. Support of the Office of Water Resources Research through Grant A-022-MO is gratefully acknowledged.

(25) B. Pesce, Ed., "Electrolytes," Pergamon Press, New York, N. Y., 1962.

(26) M. S. Arnold and K. J. Packer, *Mol. Phys.*, **10**, 141 (1966). Their calculation suggests counterions are more effective than solvent dipoles in producing the field gradient.

Preparation, Raman and Nuclear Quadrupole Resonance Data for the Complex $SCl_3^+AlCl_4^-$

by H. E. Doorenbos, J. C. Evans, and R. O. Kagel*

The Dow Chemical Company, Midland, Michigan 48640 *(Received March 5, 1970)*

$SCl_3^+AlCl_4^-$, the suspected chlorinating agent in SO_2Cl_2 solutions containing S_2Cl_2 and $AlCl_3$, was prepared from SCl_4 and $AlCl_3$ at low temperature. The white crystalline material is stable at room temperature when kept dry. Raman spectra of the solid (25°) and of the molten material (125°) showed that in both phases the structure is ionic, $SCl_3^+AlCl_4^-$. Depolarization measurements, made on the molten material, enabled a complete vibrational assignment to be made for both ions, pyramidal SCl_3^+ and tetrahedral $AlCl_4^-$. Four ^{35}Cl nqr lines were detected near 10.5 MHz for the solid (28°); these were assigned to the four chemically equivalent but physically inequivalent Cl atoms of $AlCl_4^-$ located at a lattice site of low symmetry.

Introduction

Preparative aromatic-chlorination studies using Ballester's[1] chlorinating system, $AlCl_3$ and S_2Cl_2 in large excess of SO_2Cl_2, led us to hypothesize that the effective chlorinating agent is the complex, $SCl_3^+ \cdot AlCl_4^-$, which is formed *via*

$$S_2Cl_2 + SO_2Cl_2 \longrightarrow 2SCl_2 + SO_2$$

$$SCl_2 + SO_2Cl_2 \longrightarrow SCl_4 + SO_2$$

$$SCl_4 + AlCl_3 \longrightarrow SCl_4 \cdot AlCl_3 \text{ or } SCl_3^+ \cdot AlCl_4^-$$

Substantiation required an independent preparation of the complex and a qualitative understanding of its structure. Ruff and Golla,[2] who first prepared the material, used the formulation $AlCl_3 \cdot SCl_4$, and the organic sulfonium halides, which are also effective nuclear-halogenating agents,[3] appear to have covalent or charge-transfer structures.[4] On the other hand, Raman studies of related inorganic complexes indicate a general preference for ionic structures: $SeCl_3^+ \cdot AlCl_4^-$ and $TeCl_3^+ \cdot AlCl_4^-$;[5] $SCl_3^+ \cdot AsF_6^-$;[6] $MCl_3^+ \cdot SbCl_6^-$ (M = S, Se, Te).[7] Reported here are our Raman studies of the solid and molten complex which demonstrate its ionic structure in both phases, and a partial ^{35}Cl nqr spectrum of the solid which is in accord with this structure. After this work was completed a Raman spectrum for solid $SCl_4 \cdot AlCl_3$ at −90° was reported;[8] although the structural conclusions are the same, the data presented here include additional, essential depolarization measurements and several spectral features which were not resolved by Gerding and Stufkens.

Experimental Section

A. Preparation of $SCl_3^+AlCl_4^-$. A three-necked, 500-ml round-bottom flask, fitted with a Dry Ice cold-finger condenser and a Teflon mechanical stirrer, was maintained under dry nitrogen as it was cooled to −78° in a Dry Ice–methylene chloride bath. To the cold flask was added 52 g (0.5 mol) of sulfur dichloride and stirring was begun. Chlorine gas was passed slowly into the flask whereupon the orange SCl_2 gradually changed to a yellow solid, sulfur tetrachloride. A large excess of chlorine was added to give an easily stirred, yellow-green slurry which was stirred for 1 hr.

To the stirring suspension, 66 g (0.49 mol) of anhydrous aluminum chloride was slowly added in 2–4-g portions. After addition of all $AlCl_3$, the slurry was stirred for 4 hr at −78°. The reaction mixture was allowed to warm slowly to room temperature, and the cold finger condenser was removed allowing excess chlorine to boil away. To the remaining white solid was added 250 ml of thionyl chloride with stirring to give a slurry of $SCl_3^+AlCl_4^-$ in the solvent. The slurry was warmed to 60° where much of the complex dissolved and then cooled to −25° where it was filtered under dry nitrogen. After washing with anhydrous carbon tetrachloride and drying under vacuum, 145 g of analytically pure $SCl_3^+AlCl_4^-$ was recovered, mp 118–120°.

Anal. Calcd for $AlCl_7S$: Al, 8.8; Cl, 80.8; S, 10.4. Found: Al, 9.1; Cl, 80.4; S, 10.6.

The density of this material as determined by a Beckman Air Comparison Pycnometer (Model 930) in a drybox was found to be 1.95 g/cm^3. Raman spectra were recorded with a Spex Ramalog System using for

* To whom correspondence should be addressed.

(1) M. Ballester, J. Castaner, and J. Riera, *J. Amer. Chem. Soc.*, **82**, 4254 (1960).

(2) O. Ruff and H. Golla, *Z. Anorg. Allgem. Chem.*, **138**, 17 (1924).

(3) G. H. Bing and R. A. Krieger, Australian Patent No. 230,337 (1960); *Chem. Abstr.*, **55**, 27214 (1961).

(4) G. C. Hayward and P. J. Hendra, *J. Chem. Soc. A*, 1760 (1969).

(5) H. Gerding and H. Houtgraaf, *Rec. Trav. Chim.*, **73**, 759 (1954).

(6) W. Sawodny and K. Dehnicke, *Z. Anorg. Allgem. Chem.*, **349**, 169 (1967).

(7) I. R. Beattie and H. Chudzynska, *J. Chem. Soc. A*, 1119 (1967).

(8) H. Gerding and D. J. Stufkens, *Rec. Chim. Min.*, **6**, 795 (1969).

excitation a Spectra Physics 125 helium–neon laser emitting approximately 70 mW at 6328 Å. Spectra of the powder were obtained on samples sealed in Pyrex capillaries (~1.5 mm o.d.). Spectra of the melt were obtained by heating the powdered sample (sealed in a capillary) in a small furnace to ~125°. After slight initial decomposition the material appeared to be stable at the melting point in the sealed capillary system. The furnace consisted of a thick-walled capillary tube (>1.5 mm i.d.) warmed with nichrome heating wire: the central portion of the tube was not obstructed by the windings and transverse–transverse excitation-viewing geometry was used.

All attempts to obtain satisfactory mid- and far-infrared spectra were unsuccessful. The complex proved to be highly reactive towards both mulling agents and window materials.

For the ^{35}Cl nuclear quadrupole resonance studies, samples, sealed in glass tubes under vacuum, were examined over the frequency range, 9–50 MHz, using a super-regenerative spectrometer constructed in this laboratory after the Petersen and Bridenbaugh design;[9] scans were made with samples held at 77, 195, and 301°K. Frequencies of the observed resonances were measured using a calibrated radio receiver (Collins Radio Co., Type 5IJ-4).

Results

The Raman spectra of crystalline $SCl_3^+AlCl_4^-$ and of the melt are shown in Figure 1. The observed Raman bands are summarized in Table I. The coincidence between the band positions in the solid and melt indicates that the complex has essentially the same structure in both phases.

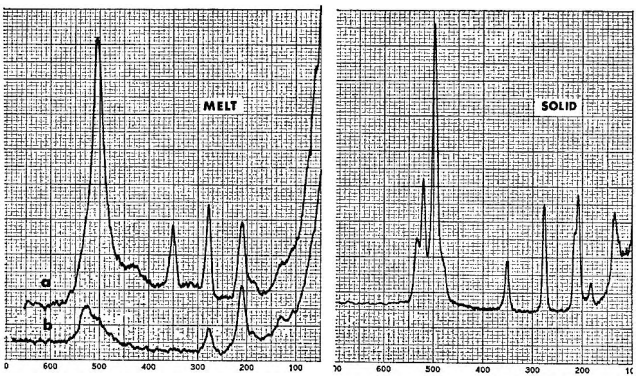

Figure 1. Raman spectra of $SCl_3^+AlCl_4^-$; melt (125°), (a) $I_{||}$, (b) $I_\perp(\rho = I_\perp/I_{||})$ and crystalline solid in the region 50–700 cm^{-1}.

Nuclear quadrupole resonances were detected only at 301°K; four resonances of approximately equal intensities (S/N about 4) were observed near 10.5 MHz (Table II). A lower sample coil filling factor necessarily required by the lower-temperature experimental arrangement may explain the failure to detect resonances. Adequate annealing periods (several weeks) were allowed the samples at these temperatures but this did not induce the appearance of the expected resonances.

Table II: Observed ^{35}Cl Nqr Lines for $SCl_3^+AlCl_4^+$ at 301°K

ν, MHz	Uncertainty, MHz[a]	Assignment
9.91	±0.03	Cl bonded to Al
10.18	±0.03	Cl bonded to Al
10.46	±0.03	Cl bonded to Al
11.04	±0.03	Cl bonded to Al

[a] The uncertainty quoted is approximately the quench frequency employed.

Table I

SCl_3^+, cm^{-1}

	This work: Melt	This work: Solid	Solid[a]	Solid[b]	Solid[c]
ν_1 (A_1)	504 vs,p	498 vs	519 vs	494 ws	525 m
ν_2 (A_1)	278 m,p	276 m	284 m	271 s	280 m
ν_3 (E)	522 m,dp	521 m 533 mw	543 s	516 vs 530 m	502 v
ν_4 (E)	210 m,dp	208 m 215 mw	214 s	206 s	...

$AlCl_4^-$, cm^{-1}

	This work: Melt	This work: Solid	Solid[d]	Melt[e]
ν_1 (A_1)	349 m,p	352 m	350 w	351 vs,p[f]
ν_2 (E)	130 w,dp	138 m	174 m	121 s,dp
ν_3 (F_2)	Obscured	480 w,sh	481 vw	490 m,dp
ν_4 (F_2)	186 w,dp	185 w	174 m	186 s,dp

[a] SCl_3^+ in $SCl_3^+\cdot AsF_6^-$ (ref 6). [b] SCl_3^+ in $SCl_3^+\cdot AlCl_4^-$ (ref 8). [c] SCl_3^+ in $SCl_3^+\cdot SbCl_6^-$ (infrared spectrum ref 7). [d] $AlCl_4^-$ in $SCl_3^+\cdot AlCl_4^-$ (ref 8). [e] $AlCl_4^-$ in $Na^+\cdot AlCl_4^-$ (G. Torsi, G. Mamantov, and G. M. Begun, *Inorg. Nucl. Chem. Lett.*, in press). [f] Key: v = very; s = strong; m = medium; w = weak; p = polarized; dp = depolarized; sh = shoulder.

Discussion

Pyramidal SCl_3^+ should show two polarized (A_1) and two depolarized (E) Raman bands in its liquid-phase spectrum, and these expectations are realized (Table I). Listed for comparison in the table are some previous assignments for SCl_3^+ which were made without the benefit of depolarization measurements; the assignments in ref 7 for ν_1 and ν_3 should be reversed. Both E modes are split into two components in the solid-phase spectrum of $SCl_3^+\cdot AlCl_4^-$; Gerding and Stufkens observed this for ν_3 but not for ν_4.

(9) G. E. Petersen and P. M. Bridenbaugh, *Rev. Sci. Instrum.*, **35**, 698 (1964).

Tetrahedral $AlCl_4^-$ should show in the Raman spectrum of the melt one polarized (A_1) and three depolarized bands. Three are observed, ν_1, ν_2, and ν_4, while ν_3 is obscured by the stronger bands of SCl_3^+ near 500 cm^{-1}. In the solid-phase spectrum a weak shoulder at 480 cm^{-1} may well be ν_3. Gerding and Stufkens'[8] Raman spectrum in the low-frequency region did not allow these authors to separate ν_2 and ν_4.

Turning to the nqr data we find that previous nqr studies have established that chlorine atoms covalently bonded to aluminum show resonances in the 11-MHz region. Several studies were of $AlCl_4^-$ salts[10,11] and one was of the complex, $AlCl_3 \cdot O(CH_2CH_3)_2$.[12] The occurrence of four equally intense resonances in this same region demonstrates the presence of similarly bonded Cl in the solid $SCl_3^+ \cdot AlCl_4^-$. The simplest interpretation is that there are four chemically equivalent but physically inequivalent Cl atoms attached to Al in the unit cell, *i.e.*, the $AlCl_4^-$ ion located at an asymmetric site. The mean of the four frequencies (10.40 MHz) and the total frequency spread (1.13 MHz) are very similar to the values reported for $GaAlCl_4$ (10.61 and 1.01 MHz). Alternative interpretation may be made but in view of the fact that the vibrational data clearly confirm the occurrence of the $AlCl_4^-$ ion we shall not discuss these. It is unfortunate that, due presumably to unfavorable lattice-relaxation times, the Cl atoms attached to S were not detected in the nqr spectrum; these are expected to arise in the 40-MHz region.

Acknowledgment. The authors wish to acknowledge the help of Dr. R. Nunemaker who performed the elemental analysis and Dr. R. R. Stevens who performed certain parts of the synthesis. This work was performed under Contract AF 33(615)-3495 with the Aerospace Research Laboratories, Wright-Patterson Air Force Base, Ohio.

(10) J. C. Evans and G. Y-S. Lo, *Inorg. Chem.*, **6**, 836 (1967).
(11) S. L. Segal and R. G. Barnes, U.S. A.E.C. Report IS-520 (1962).
(12) H. Dehmelt, *J. Chem. Phys.*, **21**, 380 (1953).

The Kinetics of Some Oxidation–Reduction Reactions Involving Cobalt(III) in Aqueous Perchloric Acid[1]

by Geoffrey Davies[2] and Kay O. Watkins[3]

Chemistry Department, Brookhaven National Laboratory, Upton, New York 11973 *(Received January 14, 1970)*

The stoichiometries and kinetics of the reactions of cobalt(III) with hydrogen peroxide, nitrous acid, hydroquinone, bromide, iodide, and thiocyanate have been investigated in aqueous perchloric acid solution over wide concentration ranges. Stoichiometries were determined using standard analytical procedures and kinetic data were obtained from conventional and stopped-flow spectrophotometry. The reactions were all found to be first order in each reactant and intermediate complex formation could not be detected either kinetically or by spectrophotometric means. The second-order rate constants generally obey the relationship $k_{obsd} = a + b/(H^+)$, where a and b are interpreted as referring to the reactions of Co_{aq}^{3+} and $CoOH_{aq}^{2+}$, respectively, with the predominant reductant species. The mechanisms of these reactions are discussed and a comparison is drawn between the rates of oxidation and complexation reactions of cobalt(III) and the rates of complexation reactions of iron(III). It is concluded that the rate-determining steps in the reactions between $CoOH_{aq}^{2+}$ and H_2O_2, HNO_2, Br^-, and SCN^- involve the replacement of water molecules in the inner sphere of the oxidant. The faster reactions with hydroquinone and iodide evidently proceed by a different mechanism in which the OH^- ligand may be involved as a bridging group between the reactants.

Introduction

The instability of perchloric acid solutions of cobalt(III) has limited the number of investigations involving Co_{aq}^{3+} and $CoOH_{aq}^{2+}$ ions. Some systems which have been studied previously are the reactions of cobalt(III) with water,[4-8] chloride ions,[9] malic acid,[10] iron(II),[11] and cerium(III).[12] These studies have led to conflicting conclusions[13] concerning the nature of the oxidizing species. We have investigated a series of oxidations by Co_{aq}^{3+} ions in perchloric acid solution in an attempt to obtain additional information concerning the extent of hydrolysis of Co_{aq}^{3+},[9,10,12] the existence of polymeric species,[6-8,13] and the mechanisms of reactions of cobalt(III) under weakly complexing conditions. In this paper we report on the stoichiometry and kinetics of the oxidation of hydrogen peroxide, hydroquinone, nitrous acid, and bromide, iodide, and thiocyanate ions by cobalt(III).

Experimental Section

Materials. Stock solutions approximately 7 M in sodium perchlorate were prepared by neutralizing sodium carbonate with perchloric acid and were standardized gravimetrically. The stock solutions of cobalt(III) were prepared as described previously,[9] using cobalt(II) perchlorate hexahydrate as starting material. Spectrophotometric measurements were used to determine the cobalt(III) and cobalt(II) concentrations (ϵ_{605} 35.3 and ϵ_{509} 4.84, respectively). The concentration of cobalt(III) was also checked by adding an aliquot to an excess of standardized iron(II) solution and titrating the excess iron(II) with standard chromium(VI) solution, using diphenylamine as indicator.

All other reagents were of analytical grade and triply distilled water was used throughout. Hydrogen peroxide solutions (prepared by dilution of 30% wt/vol hydrogen peroxide) were standardized either by titration with cerium(IV) using ferroin as indicator, or by estimation as the titanium(IV) complex (ϵ_{415} 731).[14] Sodium nitrite solutions were standardized either by addition of excess standard manganese(VII), followed by addition of excess iodide and titration of the resulting iodine with standard thiosulfate solution, or spectrophotometrically as nitrous acid (ϵ_{328} 13.7, ϵ_{337} 23.3, ϵ_{347} 36.7, ϵ_{358} 50.3, ϵ_{372} 52.0, and ϵ_{386} 30.6). Bromine was determined gravimetrically as AgBr and iodide as AgI. Hydroquinone stock solutions were always

(1) Research performed under the auspices of the U. S. Atomic Energy Commission.

(2) Address inquiries to University Chemical Laboratory, University of Kent, Canterbury, Kent, England.

(3) On sabbatical leave from Adams State College, Alamosa, Colorado.

(4) C. E. H. Bawn and A. G. White, *J. Chem. Soc.*, 331 (1951).

(5) D. W. Weiser, Ph.D. Thesis, University of Chicago, 1956.

(6) J. H. Baxendale and C. F. Wells, *Trans. Faraday Soc.*, **53**, 800 (1957).

(7) H. Taube, *J. Gen. Physiol.*, **29**, 49 (1966).

(8) M. Anbar and I. Pecht, *J. Amer. Chem. Soc.*, **89**, 2553 (1967).

(9) T. J. Conocchioli, G. H. Nancollas, and N. Sutin, *Inorg. Chem.*, **5**, 1 (1966).

(10) J. Hill and A. McAuley, *J. Chem. Soc. A*, 1169, 2405 (1968).

(11) L. E. Bennett and J. C. Sheppard, *J. Phys. Chem.*, **66**, 1275 (1962).

(12) L. H. Sutcliffe and J. R. Weber, *Trans. Faraday Soc.*, **52**, 1225 (1956).

(13) C. F. Wells, *Discuss. Faraday Soc.*, **46**, 197 (1968), and references therein.

(14) R. Bailey and D. F. Boltz, *Anal. Chem.*, **31**, 117 (1959).

freshly prepared in darkened flasks using deoxygenated water and were standardized by titration with cerium(IV) immediately before use. Thiocyanate was determined by the Volhard procedure.

Stoichiometry Measurements. Most stoichiometry measurements were made by adding a solution of cobalt(III) to an excess of reductant. In some cases the concentration of the reductant remaining after reaction was determined, while in others the concentration of the oxidation product was estimated spectrophotometrically.

The stoichiometry of the reaction with hydrogen peroxide was determined by estimating the remaining reductant, as described above. The concentration ranges used were $(Co^{III}) = 0.62–6.7 \times 10^{-3}$ *M*, $(H_2O_2) = 2.322 \times 10^{-2}$ *M*, and $(H^+) = 0.15–1.50$ *M*. The reaction with nitrous acid was studied by titrating the remaining oxidant or estimating the remaining nitrous acid spectrophotometrically, as described above. The concentration ranges used were $(Co^{III}) = 9.93 \times 10^{-5}$ to 1.19×10^{-2} *M*, $(HNO_2) = 1.06–11.1 \times 10^{-3}$ *M*, and $(H^+) = 0.15–3.10$ *M*. Bromine formed in the oxidation of excess bromide was determined by adding the product solution to an excess of iodide and titrating the iodine formed with standard thiosulfate solution (starch end point) or by spectrophotometric measurements as Br_3^-, (ϵ_{400} 4.28×10^2 at $(Br^-) = 1.84 \times 10^{-1}$ *M*). The concentration ranges used were $(Co^{III}) = 1.7–7.1 \times 10^{-3}$ *M*, $(Br^-) = 1.00–1.84 \times 10^{-1}$ *M*, and $(H^+) = 0.30–1.50$ *M*. Iodine formed in the reaction with iodide was determined as described above. The concentration ranges used were $(Co^{III}) = 0.35–10.4 \times 10^{-3}$ *M*, $(I^-) = 0.2–0.4$ *M*, and $(H^+) = 0.30–1.80$ *M*. The product *p*-benzoquinone formed in the oxidation of *p*-hydroquinone, H_2Q, was determined spectrophotometrically (ϵ_{240} 1.82×10^4, ϵ_{250} 2.11×10^4, ϵ_{260} 0.88×10^4)[15] in the range $(Co^{III}) = 5.44–43.5 \times 10^{-4}$ *M*, $(H_2Q) = 2.44 \times 10^{-3}$ *M*, and $(H^+) = 0.12–0.96$ *M*. The stoichiometry in the presence of an excess of thiocyanate was determined in a three-chamber mixing apparatus as follows. Various measured volumes of a standardized cobalt(III) solution in 3 *M* perchloric acid were added to 10 ml of 1.114 *M* sodium thiocyanate solution, and after vigorous stirring the mixture was rapidly added to 10 ml of 5 *M* sodium iodide solution.[16] After dilution to about 200 ml, the iodine formed was titrated as described above. The concentration ranges used were $(Co^{III}) = 2.46–6.82 \times 10^{-3}$ *M*, $(SCN^-) = 0.28–0.56$ *M*, $(I^-) = 1.0–2.5$ *M*, and $(H^+) = 0.6–1.5$ *M*. Variation of the thiocyanate and iodide concentrations had no observable effect on the stoichiometric results. The product of oxidation was identified as follows. Cobalt(III) solution (25 ml) (2.51×10^{-2} *M* in 3 *M* $HClO_4$) was added to 10 ml of 1.11 *M* sodium thiocyanate solution in a separatory funnel. Diethyl ether (25 ml) was then added and the mixture was shaken for 5 min. After standing a further 10 min the yellow solid which had formed at the interface was filtered off. The combined products from repeated experiments were washed several times with water followed by ether and were then dried overnight *in vacuo* over calcium chloride.[17] The yellow-orange solid was then analyzed for carbon, nitrogen, and sulfur, with the following results.[18]

Anal. Calcd for $(CNS)_x$: C, 1; N, 1.17; S, 2.67. Found: C, 1; N, 1.26; S, 2.71.

Kinetic Measurements. Most of the kinetic measurements were performed using the stopped-flow apparatus described previously.[19] The Cary Model 14 spectrophotometer was used for some of the slower runs. In all cases the reductant was present in sufficient excess to ensure pseudo-first-order conditions. Each rate constant is the average of at least six independent measurements.

The reactions with hydrogen peroxide, nitrous acid, and thiocyanate were followed by measuring the rate of disappearance of cobalt(III) in the wavelength range 240–605 nm. The choice of wavelength depended on the initial cobalt(III) concentration employed. In the reaction with bromide the appearance of tribromide ion was monitored in the wavelength range 250–325 nm. At lower bromide ion concentrations the disappearance of cobalt(III) was followed at 240–250 nm. The reaction with iodide was followed by measuring the rate of appearance of triiodide ion at 288–330 nm. The rate of appearance of *p*-benzoquinone was measured at 247–250 nm in the reaction with hydroquinone.

Results

The stoichiometric measurements established that the following reactions occurred under the experimental conditions used.[20]

$$2Co^{III} + H_2O_2 \longrightarrow 2Co^{II} + O_2 + 2H^+ \quad (1)$$

$$2Co^{III} + HNO_2 + H_2O \longrightarrow 2Co^{II} + NO_3^- + 3H^+ \quad (2)$$

$$2Co^{III} + p\text{-}C_6H_4(OH)_2 \longrightarrow 2Co^{II} + p\text{-}C_6H_4O_2 + 2H^+ \quad (3)$$

$$2Co^{III} + 3Br^- \longrightarrow 2Co^{II} + Br_3^- \quad (4)$$

$$2Co^{III} + 3I^- \longrightarrow 2Co^{II} + I_3^- \quad (5)$$

$$2Co^{III} + 2SCN^- \longrightarrow 2Co^{II} + (SCN)_2 \quad (6)$$

(15) G. Davies and K. Kustin, *Trans. Faraday Soc.*, **65**, 1630 (1969).

(16) C. E. Vanderzee and A. S. Quist, *Inorg. Chem.*, **5**, 1238 (1966).

(17) Control experiments showed that no solid material appeared in the absence of cobalt(III) under the experimental conditions.

(18) Only the relative composition is presented since the solid product was contaminated with sodium thiocyanate and water. The carbon, nitrogen, and sulfur accounted for about 70% of the material.

(19) G. Dulz and N. Sutin, *Inorg. Chem.*, **2**, 917 (1963).

(20) The upper limit of uncertainty is 2% of the given stoichiometry in all cases.

The ultraviolet and visible spectra of the immediate products of the reaction of cobalt(III) with hydroquinone, bromide, and iodide ions were identical with those of *p*-benzoquinone (λ_{max} 247 nm),[15] tribromide ion (λ_{max} 265 nm), and triiodide ion (maxima at 288 and 348 nm), respectively. The kinetic data[21] indicate that each reaction is accurately first order in each reactant.[22-24] The observed second order rate constants are independent of (Co^{III}), (Co^{II}),[25] and wavelength of measurement.[26] The latter observation suggests that competing photochemical reactions play only a minor role and that the slow formation of appreciable concentrations of cobalt(III)–reductant complexes, such as those found in the reactions with chloride[9] and malic acid,[10] does not occur during the course of the reactions studied in this work. The rate law for each reaction is thus

$$-\frac{1}{n}\frac{d(Co^{III})}{dt} = \frac{d(\text{product})}{dt} = k_{obsd}(Co^{III}))(B) \quad (7)$$

where

$$k_{obsd} = a + b/(H^+) \quad (8)$$

In these equations B is the reductant, n is the appropriate stoichiometric factor, and (H^+) is assumed equal to ($HClO_4$). The parameters a and b may be obtained from the intercept and slope, respectively, of plots of k_{obsd} *vs.* $1/(HClO_4)$. Examples of plots of eq 8 for reactions at 25.0° are given in Figure 1, which illustrates the point that for some reactions the intercepts of plots of k_{obsd} *vs.* $1/(H^+)$ are very uncertain (*e.g.*, for H_2O_2 and Br^-), while for others the intercept is much better established (*e.g.*, for SCN^- and H_2Q). Thus, only upper limits could be obtained for a in the reactions with hydrogen peroxide and bromide.

The following mechanism is consistent with the observed rate law

$$Co_{aq}^{3+} + H_2O \rightleftharpoons CoOH_{aq}^{2+} + H_3O^+ \qquad K_h \quad (9)$$

$$Co^{3+} + B \xrightarrow{k_0} Co^{II} + B\cdot \quad (10)$$

$$CoOH^{2+} + B \xrightarrow{k_{-1}} Co^{II} + B\cdot \quad (11)$$

$$Co^{III} + B\cdot \xrightarrow{fast} \text{products} \quad (12)$$

$$2B\cdot \xrightarrow{fast} B_2 \quad (13)$$

in which steps 10 and 11 are rate-determining and B· is a radical species. The observed rate law (eq 7) is predicted by this mechanism if $K_h/(H^+) \ll 1$. Under these conditions $a = k_0$ and $b = k_{-1}K_h$, where K_h is the acid-dissociation constant of Co_{aq}^{3+}, eq 9. Evidently, values of k_{-1} can only be obtained from a knowledge of K_h under the experimental conditions. Although this parameter is believed[27] to be about 2×10^{-3} M^{-1} at 25°, there is no accurate value available. We have

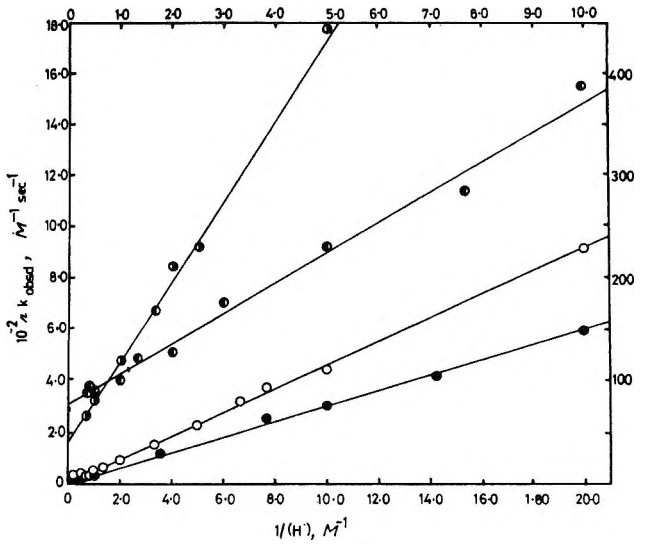

Figure 1. Examples of plots of $10^{-2}n$ k_{obsd} *vs.* $1/(H^+)$ for the following reactions at 25.0° and ionic strength 3.0 *M*: ○, H_2O_2, (n = 2); ●, Br^-, (n = 1); ◑, SCN^-, (n = 2), (left and bottom scales); ◐, I^-, (n = 1), (right and top scales).

collected values of k_0 and the product $k_{-1}K_h$ together with their apparent activation parameters in Table I.[28]

Discussion

The second-order rate law which has been found over a range of cobalt(III) concentrations in this series of reactions supports the conclusion[27,29] that the predominant cobalt(III) species at equilibrium under our experimental conditions[25] are monomeric Co_{aq}^{3+} and $CoOH_{aq}^{2+}$ cations. An upper limit of 5×10^{-3} *M* for the acid-dissociation constant of Co_{aq}^{3+} is suggested from the exact rate law $k_{obsd} = (k_0 + k_{-1}K_h/(H^+))/(1 + K_h/(H^+))$ if $K_h/(H^+) \leq 0.1$ at the lowest acidity in our experimental range. Unfortunately, the reduction of cobalt(III) by water is very rapid at the low acidities which would be required to obtain a direct estimate of this parameter.[5,6,27,30] Davies and Warnqvist[27] have recently proposed a value of $(2 \pm 1) \times 10^{-3}$

(21) G. Davies and K. O. Watkins, unpublished data.

(22) In the reactions with hydrogen peroxide, hydroquinone, and nitrous acid the reductant is assumed to be the predominant molecular species, *i.e.*, H_2O_2, *p*-$C_6H_4(OH)_2$, and HNO_2, respectively.[23,24] See text.

(23) N. Sutin, *Ann. Rev. Phys. Chem.*, **17**, 119 (1966).

(24) G. Davies, *Coord. Chem. Revs.*, **4**, 199 (1969).

(25) The concentrations of cobalt(III) and cobalt(II) were varied between extremes of 0.20–55.5 $\times 10^{-4}$ *M* and 0.2–874 $\times 10^{-4}$ *M*, respectively.

(26) A direct proportionality between the initial cobalt(III) concentrations and the corresponding absorbances at zero time was observed in those reactions in which the disappearance of cobalt(III) was followed.

(27) G. Davies and B. Warnqvist, *Coord. Chem. Rev.*, in press.

(28) The kinetic data from this study have been combined with those of ref 6 in the calculation of the activation parameters for the reaction with hydrogen peroxide.

(29) B. Warnqvist, *Inorg. Chem.*, **9**, 682 (1970).

(30) P. Carrington and L. H. Sutcliffe, private communication.

Table I: Kinetic Data for Some Oxidation Reactions Involving Co_{aq}^{3+} and $CoOH_{aq}^{2+}$ in Aqueous Acid Perchlorate Mixtures at Ionic Strength 3.0 *M*

Reductant	k_0,[a] M^{-1} sec^{-1}	$k_{-1}K_h$,[a] sec^{-1}	$\Delta H_0^{\ddagger}$, kcal mol^{-1}	$\Delta S_0^{\ddagger}$, cal deg^{-1} mol^{-1}	$\Delta H_{-1}^{\ddagger}$,[b] kcal mol^{-1}	$\Delta S_{-1}^{\ddagger}$,[b] cal deg^{-1} mol^{-1}	Ref
Malic acid[c]	4.6	58	...	...	...	...	*d*
Thiomalic acid[c]	$\lesssim$6	15.2	...	...	...	...	*d*
Cl^-[c]	3	24.6	...	...	...	...	*e*
Thiourea	...	52	...	...	15.7	+3	*f*
H_2O_2[g]	$\lesssim$2	23.0	...	...	23.5	+25	*h*
HNO_2	18	17.2	18.3	+9	21.7	+19	*h*
HN_3[g]	$\lesssim$2	35.2	...	...	23.1	+15	*i*
ClO_2[g]	$\lesssim$1	59.6	...	...	21.8	+23	*j*
Br^-[g]	$\lesssim$5	30.4	...	...	26.1	+37	*h*
SCN^-	86.5	79.6	20.6	+20	25.6	+37	*h*
H_2Q	2200	1280	18.2	+18	18.6	+17	*h*
I^-	8000	2860	19.4	+25	21.5	+30	*h*

[a] At 25.0°. [b] These are composite parameters involving the enthalpy and entropy of acid dissociation (eq 9). [c] The parameters refer to complex formation. [d] See ref 10, data at ionic strength 0.25 *M*. [e] See ref 9. [f] A. McAuley and U. D. Gomwalk, *J. Chem. Soc., A*, 977 (1969): ionic strength in the range 0.82–1.50 *M*; and ref 27. [g] It was not possible to obtain accurate activation parameters for the reactions of Co_{aq}^{3+} in these reactions. See text. [h] This work. [i] See ref 37, data at ionic strength 2.0 *M*. [j] See ref 38, data at ionic strength 2.1 *M*.

M for K_h which is also consistent with the present kinetic data as well as with previous spectrophotometric estimates.[5,6]

The kinetic dependence in this series of reactions contrasts sharply with the more complex kinetics observed, for example, in the reactions of cobalt(III) with chloride,[9] malic and thiomalic acids,[10] and cysteine,[31] where the formation and disappearance of intermediate complexes have been monitored spectrophotometrically. The kinetic and spectrophotometric observations suggest that any intermediate complexes formed are present at undetectably low concentration levels in the reactions we have studied.

Comparison of our results with other data for cobalt(III) reactions, (Table I), points to some interesting correlations. Thus, we note that a narrow range of valus of $k_{-1}K_h$ characterizes[32] the reactions of $CoOH_{aq}^{2+}$ with all the reductants except QH_2 and I^-, which react at considerably higher rates than do the other species. Now some of the data in Table I refer to rates of complex formation in the absence of a net oxidation reaction, and so it seems reasonable to suppose that the independence of the reaction rate on the nature of the reductant is related to a common rate-determining step which depends mainly on the properties of the oxidant. This common process is evidently water exchange on the oxidant, which, to a first approximation, can be considered to be ligand independent for an inner-sphere, "dissociative interchange"[33] mechanism. A comparison of these results with the available data[23,34] for complexation reactions of $FeOH_{aq}^{2+}$ tends to support this assignment of an inner-sphere mechanism for the cobalt(III) reactions. For example, the rate of oxidation of SCN^- by $CoOH_{aq}^{2+}$ is faster than those of Br^- and HN_3 by about the same factor as is involved in the corresponding complexation reactions of $FeOH_{aq}^{2+}$. This is reasonable if both cations react *via* a water-exchange mechanism with these ligands.

The limited amount of accurate data for reactions of Co_{aq}^{3+} which is available makes definite mechanistic assignments difficult for the reactions of this species. Comparison of the ratios $k_{-1}K_h/k_0$ for reactions of iron(III)[35–39] and cobalt(III) does suggest, however, that the rates of reaction of Co_{aq}^{3+} with Br^-, Cl^-, HN_3, and SCN^- may be influenced by the rate of water exchange on the oxidant, but this cannot be proven in the absence of more extensive data for complexation reactions. The activation parameters for the redox reactions may

(31) A. McAuley, private communication.

(32) This observation also strongly supports the assignment of HX as the reducing species in reactions involving weak acids:[22] thus, the examples in Table I cover a p*K* range of about nine units for the reductants of the weak-acid type, indicating that reactions with anionic and more highly protonated species may be neglected in the interpretation of the data.[23,24]

(33) C. H. Langford and H. B. Gray, "Ligand Substitution Processes," W. A. Benjamin, New York, N. Y., 1965.

(34) D. Seewald and N. Sutin, *Inorg. Chem.*, **2**, 643 (1963).

(35) The mechanism of reactions of the type $Fe_{aq}^{3+} + X^-$ is not firmly established:[36] thus, the rate constants for the cases where X is SCN, Br, and Cl have a ligand dependence which is not consistent with the limiting Sn1-type mechanism. In the reactions of Co_{aq}^{3+} with H_2O_2, Br^-, HN_3,[37] and ClO_2[38] the apparent acid-independent rate term could be attributable to changes in activity coefficients on replacement of H_{aq}^+ by Na_{aq}^+ or Li_{aq}^+.[37–39]

(36) F. Basolo and R. G. Pearson, "Mechanisms of Inorganic Reactions," 2nd ed, Wiley, New York, N. Y., 1967, Chapter 3.

(37) R. K. Murmann, J. C. Sullivan, and R. C. Thompson, *Inorg. Chem.*, **7**, 1876 (1968).

(38) R. C. Thompson, *J. Phys. Chem.*, **72**, 2642 (1968).

(39) A. J. Zielen and J. C. Sullivan, *ibid.*, **66**, 1065 (1962).

give further insight into the reaction mechanisms when this information becomes available.

Comparison of the rate constants for the reactions of cobalt(III) with hydroquinone and iodide with those for the other reactants suggests that water exchange in the oxidant is not rate-determining in these faster reactions. If $K_h \leq 5 \times 10^{-3}\ M$, then $k_{-1} \gtrsim 10^2 k_0$ and it is evident that the OH^- ligand has a much larger influence than might be expected for an outer-sphere reaction.[23] It seems likely that the OH^- ligand is acting preferentially as a bridge for electron transfer; some stabilization of the product might be expected for such a route, especially in the reaction with I^-.[23,36]

Acknowledgment. It is a pleasure to acknowledge helpful discussions with Dr. Norman Sutin.

Thermodynamics of Divalent Metal Sulfate Dissociation and the Structure of the Solvated Metal Sulfate Ion Pair

by John W. Larson

Department of Chemistry, Marshall University, Huntington, West Virginia 25701 *(Received March 26, 1970)*

Heat of dilution data for several divalent metal sulfates are used to calculate reliable values of $\Delta S°$ for reactions of the type MSO_4 (ion pair) = $M^{2+}(aq) + SO_4^{2-}(aq)$. The values obtained are $\Delta S° = -14.7, -15.2, -17.8, -15.6, -16.6$, and -15.7 gibbs/mol for M = Mg, Zn, Cd, Ca, Cu, and Ni, respectively. Inadequacies in the electrostatic description of ion-pair formation are pointed out. The $\Delta S°$ values are explained by assuming that the microscopic structures of the ion pairs differ in the number of water molecules the sulfate ion displaces from the primary octahedral hydration of the metal ion. There is good agreement between the extent of hydration of the ion pair assumed in order to account for the $\Delta S°$ values and the extent of hydration arrived at by spectroscopic techniques.

Ion-pair formation has long been considered to have an important place in an adequate theoretical description of electrolyte solutions. More recently, ion-pair formation has been shown to be of practical importance in that the energetics of many biological reactions are greatly affected by it.[1]

Reliable thermodynamic data are needed both to help in providing an adequate description of the extent of ion-pair formation and to provide clues to the microscopic description of the solvated ion pair, especially in connection with recent work on ultrasonic absorption and optical spectroscopy.[2-5]

In order to provide reliable data for the heats and entropies of dissociation of divalent metal sulfate ion pairs, calculations are reported here that make use of the very precise heats of dilution measured by Lange and his coworkers.[6] Although these workers were able to demonstrate that the heat of dilution data for such diverse and complex substances as Na_2SO_4, $K_3Fe(CN)_6$, and $K_4Fe(CN)_6$ obeyed the Debye–Hückel limiting law at low concentrations, no such agreement was obtained for the six divalent metal sulfates used in their investigations.[6]

Even though this discrepancy has been attributed to ion-pair formation,[7] no detailed analysis along this line has been made. From the known equilibrium constants for the dissociation of these metal sulfate ion pairs it can easily be ascertained that even at $10^{-4}\ m$, approximately 3% of these compounds are undissociated. No agreement between measured heats of dilution and the Debye–Hückel theory could, therefore, be expected at concentrations above $10^{-4}\ m$. The relevance of these heat of dilution data to the thermodynamics of ion-pair formation, therefore, seems obvious.

Nair and Nancollas[8] have reported potential measure-

(1) H. B. Clarke, D. C. Cusworth, and S. P. Datta, *Biochem. J.*, **58**, 146 (1954); **64**, 604 (1956).

(2) M. Eigen and K. Tamm, *Z. Elektrochem.*, **66**, 107 (1962).

(3) R. Larsson, *Acta Chem. Scand.*, **18**, 1923 (1964).

(4) J. M. Smithson and R. J. P. Williams, *J. Chem. Soc.*, 457 (1958).

(5) G. Atkinson and S. K. Kor, *J. Phys. Chem.*, **69**, 128 (1965).

(6) E. Lange in "The Structure of Electrolyte Solutions," W. J. Hamer, Ed., Wiley, New York, N. Y., 1959; E. Lange and J. Monheim, *Z. Phys. Chem. (Frankfurt am Main)*, **150A**, 349 (1930); E. Lange and H. Streeck, *ibid.*, **157A**, 1 (1931); E. Lange, J. Monheim, and A. L. Robinson, *J. Amer. Chem. Soc.*, **55**, 4733 (1933); E. Lange and W. Miederer, *Z. Elektrochem.*, **60**, 34 (1956).

(7) H. S. Harned and B. B. Owen, "The Physical Chemistry of Electrolyte Solutions," Reinhold, New York, N. Y., 1958.

(8) V. S. K. Nair and G. H. Nancollas, *J. Chem. Soc.*, 3934 (1959).

ments that were used in calculating the equilibrium constant for reaction 1

$$HSO_4^- + M^{2+} = H^+ + MSO_4 \qquad (1)$$

and its temperature dependence. From these data and their previously determined heat of dissociation of the bisulfate ion, they calculated ΔG°, ΔH°, and ΔS° values for reaction 2.

$$MSO_4 \text{ (ion pair)} = M^{2+}(aq) + SO_4^{2-}(aq) \qquad (2)$$

These measurements on the sulfates of Mg, Zn, Co, and Ni, while yielding good ΔG_2° values, apparently contain large systematic errors and are inadequate for the calculation of ΔH_2° and ΔS_2°. This conclusion is substantiated by recent calorimetric studies on the dissociation of the bisulfate ion.[9] Similarly, the measurements of Izatt, *et al.*,[10] on the association of SO_4^{2-} and metallic ions are inapplicable, since they were carried out at high concentrations (0.02 *m*) and require a long extrapolation to infinite dilution.

Calculations and Results

A detailed analysis of the method used here to obtain ΔH_2° and ΔS_2° values will be given for $ZnSO_4$. An identical method has been used for the other compounds.

For $ZnSO_4$, the value of the equilibrium constant for reaction 2, K_2, is taken as 4.7×10^{-3}.[8,11,12] The expression for the equilibrium constant is given by eq 3

$$K_2 = \frac{\gamma_\pm^2 \alpha^2 m}{(1 - \alpha)} \qquad (3)$$

where m is the molality of the $ZnSO_4$ solution, α is the degree of dissociation, and $\gamma_\pm$ is the mean activity coefficient of the dissociated $ZnSO_4$. The activity coefficient of the neutral associated $ZnSO_4$ is assumed to be unity at all concentrations. For a solution of the pure salt, the total ionic strength of the solution is simply $4\alpha m$. The value of $\gamma_\pm$ is estimated by using the extended Debye–Hückel equation[13] for 2–2 electrolyte solutions, eq 4

$$\log \gamma_\pm = \frac{-4.092(\alpha m)^{1/2}}{1 + 0.6582a(\alpha m)^{1/2}} + 4b(\alpha m) \qquad (4)$$

where a is the assumed distance of closest approach for the ions and b is an empirical parameter. α at any specified m may be calculated from the given a, b, K_2 values, using these equations.

The relative apparent molal heat constant ϕ_H, is assumed to be made up of two parts,[14,15] the heat of dissociation of the associated ion pair and the heat of dilution of the dissociated $ZnSO_4$, ΔH_d. This may be written as

$$\phi_H = (1 - \alpha)\Delta H_2^\circ + \alpha \Delta H_d \qquad (5)$$

Values of ϕ_H have been arrived at by Lange, *et al.*, from heats of dilution obtained with a twin adiabatic calorimeter. The values of ΔH_d are estimated by use of the extended Debye–Hückel theory for 2–2 electrolytes

$$\Delta H_d = \frac{3.776(\alpha m)^{1/2}}{1 + 0.6582(\alpha m)^{1/2}} \text{ kcal/mol}^{1/2} \qquad (6)$$

where a has the same value as used in eq 4. Although eq 5 could then be used to calculate ΔH_2° from reported values of ϕ_H, the values of ϕ_H reported contain a relatively large uncertainty associated with the extrapolation of the experimental data to $m = 0$. To eliminate this source of error, a differential form of eq 5 was therefore used, that after rearrangement results in eq 7.

$$\Delta H_2^\circ = \frac{\Delta \phi_H}{\Delta(1 - \alpha)} - \frac{\Delta(\alpha \Delta H_d)}{\Delta(1 - \alpha)} \qquad (7)$$

Values of $\Delta(1 - \alpha)$ and $\Delta(\alpha \Delta H_d)$ between any two concentrations may be calculated by the method given above and $\Delta\phi_H$ data are taken from the actual experimental determinations of Lange, *et al.*

Values of $a = 4$ Å and $b = 0.4$ were used in the calculations reported here. As reported in Table I, at concentrations below 0.01 *m*, setting $a = 0$ and $b = 0$ results in a calculated ΔH_2 only slightly different than the value obtained with $a = 4$ and $b = 0.4$. At higher concentrations, however, only values of a and b of approximately 4 and 0.4 gave results consistent with those obtained at lower concentrations.

Table I: The Enthalpy of Dissociation of $ZnSO_4$

Initial molality	Final molality	$-\Delta\phi_H$, cal/mol	ΔH_2°, kcal/mol ($a = 0$, $b = 0$)	ΔH_2°, kcal/mol ($a = 4$, $b = 0.4$)
0.01	0.0001	530	−1.43	−1.36
0.04	0.01	245	−1.12	−1.51
0.25	0.04	278	−5.69	−1.39
0.49	0.0001	1139	...	−1.40

Because ΔG_2° and K_2 for some of the salts considered here are known only with considerable uncertainty, it is necessary to consider the dependence of the calculated

(9) J. M. Readnour and J. W. Cobble, *J. Inorg. Chem.*, **8**, 2174 (1969).

(10) R. M. Izatt, D. E. Eatough, J. J. Christensen, and C. H. Bartholomew, *J. Chem. Soc. A*, 47 (1969).

(11) L. G. Sillen and A. E. Martell, "Stability Constants of Metal-ion Complexes," Special Publication 17, The Chemical Society, London, 1964.

(12) C. W. Davies, "Ion Association," Butterworths, Washington, D. C., 1962.

(13) R. A. Robinson and R. H. Stokes, "Electrolyte Solutions," 2nd ed, revised, Butterworths, London, 1965.

(14) P. Hopkins, Jr., C.-H. Wu, and L. G. Hepler, *J. Phys. Chem.*, **69**, 2244 (1965).

(15) H. P. Hopkins, Jr., and C. A. Wulff, *ibid.*, **69**, 6, 9 (1965).

$\Delta H_2°$ on the value of $\Delta G_2°$ or K used in the calculation with eq 1. In Table II, values of $\Delta H_2°$ and $\Delta S_2°$ for $ZnSO_4$ are calculated on the basis of first assuming $\Delta G_2°$ is 150 cal/mol larger than the "best" value and then assuming $\Delta G_2°$ is 150 cal/mol smaller than the "best" value. It can be seen that no independently accurate $\Delta H_2°$ can be calculated from heat of dilution data.

Table II: Dependence of $\Delta H_2°$ and $\Delta S_2°$ on Assumed $\Delta G_2°$ for $ZnSO_4$

$\Delta G_2°$, kcal/mol	$\Delta H_2°$, kcal/mol	$\Delta S_2°$, gibbs/mol
3.175	−1.36	−15.2
3.325	−1.23	−15.3
3.025	−1.52	−15.2

The minimum error in $\Delta H_2°$ is approximately equal to the error in the value used for $\Delta G_2°$. Much more important, however, is that if a low value is used for $\Delta G_2°$, the resulting $\Delta H_2°$ will be low by approximately the same amount, and thus $\Delta S_2°$ is virtually unchanged. This happens to be the quantity that is of most interest from the theoretical standpoint. No such fortuitous compensation takes place by combination of the $\Delta G_2°$ and $\Delta H_2°$ values arrived at from the equilibrium or apparently from the titration calorimetry measurements.

In principle the variation of the heat of dilution data with concentration could be used to calculate the equilibrium constant for reaction 2. In practice, the best that can be done is to restrict the value of log K to within ± 0.4 unit. Any of the more common methods[13] of determining K result in a value of K more accurate than this and, therefore, values of K from the literature are used in all of the calculations.

The results of calculations for 5 other salts for which there are adequate heat of dilution data are tabulated in Table III. The estimated maximum uncertainties reported in $\Delta H_2°$ and $\Delta S_2°$ include the uncertainty associated with choice of K_2, a, and b. Only the heat of dilution data in the concentration range below 0.01 m were used in calculating the results presented in Table III to minimize the uncertainty associated with the choice of a and b.

The values of $\Delta H_2°$ and $\Delta S_2°$ reported in Table III are in quantitative and qualitative disagreement with those reported by Nair and Nancollas.[8] Good qualitative agreement is obtained between the results presented here and those of Izatt, *et al.*,[10] but quantitatively the $\Delta H_2°$ and $\Delta S_2°$ values reported by Izatt, *et al.*,[10] are less negative by approximately 0.9 kcal/mol and 2.1 gibbs/mol, respectively. This discrepancy is of the order of magnitude expected in view of the fact that no corrections for the ionic strength of the solutions were made to the reported ΔH data.[10]

As stated by Nancollas,[16] "It is not easy to assess the limits of accuracy of heat and entropy values; those obtained from temperature coefficient data are obviously not as reliable as calorimetric values. On the other hand, the calorimetric method usually involves the use of rather high ionic strength which introduces other uncertainties." Calculation of heat and entropy values based on heat of dilution data as reported here has both the advantage of being a direct measurement of enthalpy and the advantage of being done at very low ionic strengths. Because of the demonstrated precision of the measured heat of dilution data,[17] the $\Delta H_2°$ and $\Delta S_2°$ values reported here should be more reliable than any of the previous values.[8,10]

The partial molal entropies of the aqueous divalent metal ions are listed in Table III. These have been used along with the values of $\Delta S_2°$ reported here and the $S_2°$ of $SO_4^{2-}(aq)$[18-20] to obtain the partial molal entropies of the metal sulfate ion pairs reported in Table III.

Discussion

The first theory that led to a description of the thermodynamics of ion-pair formation was due to Bjerrum.[21] This theory has been successful in many respects.[13] The Bjerrum theory nevertheless is inadequate in some respects as pointed out by Fuoss.[22] Some of these inadequacies have been eliminated by taking into account the discontinuous nature of the solvent and by considering only those ions of opposite charge in actual contact to be ion pairs.[22] Theoretical values of $\Delta G_2°$ and $\Delta S_2°$ calculated by Fuoss' theory[13,22] with a center to center distance of 4 Å are reported in Table IV along with the average experimental values from Table III. In spite of this good agreement in the magnitude of the values of $\Delta G_2°$ and $\Delta S_2°$, no agreement is observed between the predicted and observed trend of these quantities, especially $\Delta S_2°$, with the center to center distance of the ions. Instead of a generally more negative entropy change as the size of the cation decreases, as the theory predicts, just the opposite trend is observed.

The trend predicted by this theory (and other electrostatic theories[21,23]) results from assuming the trend in $\Delta S_2°$ is predominately determined by the differences in

(16) G. H. Nancollas in *Discuss. Faraday Soc.*, 24, 128 (1957).

(17) See ref 7, p 335.

(18) W. M. Latimer, "Oxidation Potentials," 2nd ed, Prentice-Hall, Englewood Cliffs, N. J., 1952.

(19) J. W. Larson, P. Cerutti, H. K. Garber, and L. G. Hepler, *J. Phys. Chem.*, 72, 2902 (1968).

(20) D. D. Wagman, W. H. Evans, V. B. Parker, I. Halow, S. M. Bailey, and R. H. Schumm, National Bureau of Standards Technical Note 270-3, U. S. Government Printing Office, Washington, D. C. 1968.

(21) N. Bjerrum, *K. Danske Vidensk, Selsk.*, 7, No. 9 (1926).

(22) R. M. Fuoss, *J. Amer. Chem. Soc.*, 80, 5059 (1958).

(23) J. T. Denison and J. B. Ramsey, *ibid.*, 77, 2615 (1955).

Table III: The Thermodynamics of Ion-Pair Dissociation

Ion pair	$\Delta G_2°$,[11,12] kcal/mol	$\Delta H_2°$, kcal/mol	$\Delta S_2°$, gibbs/mol	$\bar{S}_2°$ (M^{2+} (aq)), gibbs/mol	$\bar{S}_2°$ (ion pair), gibbs/mol
$MgSO_4$	3.15 ± 0.05	−1.27 ± 0.20	−14.7 ± 0.5	−28.2[18]	−8.7
$ZnSO_4$	3.17 ± 0.05	−1.36 ± 0.20	−15.2 ± 0.5	−26.9[19]	−6.9
$CdSO_4$	3.15 ± 0.05	−2.15 ± 0.17	−17.8 ± 0.4	−17.4[19]	+5.2
$CaSO_4$	3.15 ± 0.05	−1.50 ± 0.20	−15.6 ± 0.5	−13.2[18]	+7.2
$CuSO_4$	3.22 ± 0.07	−1.72 ± 0.20	−16.6 ± 0.5	−23.6[19]	−2.2
$NiSO_4$	3.14 ± 0.05	−1.52 ± 0.20	−15.7 ± 0.5	−31.6[19]	−11.1

Table IV: Average Values of $\Delta G°$ and $\Delta S°$ for the Dissociation of 2-2 Electrolytes

	$\Delta G_2°$, kcal/mol	$\Delta S_2°$, gibbs/mol
Fuoss theory	3.20	−15.5
Av exptl values	3.16 ± 0.05	−15.9 ± 2

the entropies of the dissociated ions, the entropies of the neutral associated ion pairs being relatively unaffected by the size of the cations. The $\bar{S}_2°$ values of the cations are expected to decrease as the cation becomes smaller. Considering only those ions that are unaffected by crystal field splitting, the trend in the $\bar{S}_2°$ values reported in Table III is Ca > Cd > Zn > Mg, the same as the trend in their ionic radii.[13] The electrostatic predictions of relatively constant $\bar{S}_2°$ values for the ion pairs, however, are shown to be incorrect by the values in Table III. These values are markedly different, so much so that the total entropy change has a trend opposite that predicted.

This theory does not take into account the electrostatic attraction of the ions for the solvent dipoles. The mutual potential energy, G, between the cation (of charge z_1) and the anion (of charge z_2) may be written

$$G = \frac{z_1 z_2}{DR}$$

where R is the distance the ions are apart and D is the dielectric constant of the medium between them. The potential energy between the oriented solvent dipole and the ion may be written as

$$G = -\frac{\mu z_1}{DR^2}$$

where μ is the dipole moment. Equating these energies, a critical distance, R_c, equal to μ/z_2 is obtained. For an anion with a point charge of 2.4 esu and a point dipole of 1.8 D, R_c = 0.7 Å. Inside this distance, displacement of the solvent dipole would result in an increase in potential energy. Cations with a radius greater than R_c might, therefore, be expected to form predominately "contact ion pairs" while cations with a radius less than R would be expected to form "solvent-separated ion pairs."[24] Although there is no easy way to take into account the finite size of the ions and solvent molecules and behavior of the latter in the very high field in the vicinity of ions, a trend towards forming contact ion pairs in preference to solvent separated ion pairs would be expected as the cation became larger.

The $MgSO_4$, $NiSO_4$, and $ZnSO_4$ ion pairs are assumed to contain an octahedrally hydrated metal ion both because of their small radii and the fact that they form crystalline heptahydrates. Only lower hydrates are known for the sulfates of Ca, Cu, and Cd. Assuming the sulfate ion does penetrate the primary octahedral hydration shell of the Ca and Cd ions, the observed $\bar{S}_2°$ for the ion pairs may be explained. From the geometry of the sulfate ion, it does not appear unreasonable to assume that the sulfate ion acts as a bidentate ligand displacing two adjacent water molecules attached to the metal ion. This would result in a large increase in entropy. The entropy of the "water of hydration" is estimated by Latimer's rules to be 9.4 gibbs/mol.[18,25] After displacement, the entropy of this water would be equal to the entropy of ligand water or 16.71 gibbs/mol.[20] The total entropy change when two molecules of the "water of hydration" are displaced by the sulfate ion is therefore about 14.6 gibbs/mol (or approximately twice the molar entropy of melting ice). This is in excellent agreement with the observed difference between the entropies of the Zn, Mg ion pairs (predominately solvent-separated ion pairs), and the Ca, Cd ion pairs (predominately contact ion pairs).

In $CuSO_4 \cdot 5H_2O$ the sulfate ion occupies the axial positions of the octahedral coordination of the copper ion.[26] The axial water molecules in the hydration of the Cu^{2+} ion are apparently easily displaced because of the Jahn–Teller effect. The axial water molecules are, however, not adjacent and therefore the sulfate ion could displace at most one. The value of the partial molal entropy of the $CuSO_4$ ion pair is therefore expected to be approximately halfway between the entropy of the solvent separated ion pair and the contact ion pairs with two displaced waters of hydration. This

(24) Contact ion pairs and solvent-separated ion pairs are often referred to as inner-sphere complexes and outer-sphere complexes.

(25) W. M. Latimer and W. L. Jolly, *J. Amer. Chem. Soc.*, 75, 1548 (1953).

(26) F. A. Cotton and G. Wilkinson, "Inorganic Chemistry," Interscience Publishers, New York, N. Y., 1966.

explanation is clearly supported by the data in Table III.

The conclusions drawn here from the entropies of the ion pairs are in at least qualitative agreement with the conclusions drawn from other work. From infrared spectroscopy, Larsson[3] has arrived at the order Cd > Cu > Zn > Ni for the tendency of the metal ion to form contact ion pairs with the sulfate ion. From the examination of the visible absorption spectrum of the $CuSO_4$ and $CoSO_4$ ion pairs, Smithson and Williams[4] concluded $CuSO_4$ forms a contact ion pair and $CoSO_4$ a solvent-separated ion pair. From data on the volume change for reaction 2, Hamann, Pearce, and Strauss[27] have concluded that $MgSO_4$ forms a solvent-separated ion pair.

Ultrasonic absorption studies on divalent metal sulfate solutions have led to equilibrium constants of the conversion to the solvent-separated ion pairs to the contact ion pairs, reaction 8.[2,5,28-30] Values of K_8 for M = Ni, Mg, and Zn have been reported as $^1/_{10}$, $^1/_8$ and $^1/_4$, respectively. Data that lead to values of K_8 for M = Cu and Ca have also been reported, but because reaction 8 is kinetically fast, the values reported are quite uncertain. For copper, values of K_8 have been reported from 10^{-2} to 10^{2+} and for calcium $K_8 > 1$.

$$M(OH_2)_nSO_4 = MSO_4 + nH_2O \quad (8)$$

Neither the spectroscopic nor the ultrasonic absorption work results in a value for the number of water molecules displaced when the contact ion pair is formed.

Acknowledgment. The author wishes to thank the Marshall University Research Board for financial support.

(27) S. D. Hamann, P. J. Pearce, and W. Strauss, *J. Phys. Chem.*, **68**, 375 (1964).

(28) R. G. Pearson, *J. Chem. Educ.*, **38**, 164 (1961).

(29) F. Basolo in "Survey of Progress in Chemistry," A. F. Scott, Ed., Academic Press, New York, N. Y., 1964.

(30) F. Fittipaldi and S. Petrucci, *J. Phys. Chem.*, **71**, 3414 (1967).

The Ionization Constant of Water to 800° and 4000 Bars[1]

by Arvin S. Quist

Reactor Chemistry Division, Oak Ridge National Laboratory, Oak Ridge, Tennessee 37830 *(Received April 22, 1970)*

Electrical conductances of dilute aqueous ammonium bromide solutions were measured to 800° and 4000 bars. The ammonium bromide underwent extensive hydrolysis at elevated temperatures. The conductance data from these solutions were evaluated and combined with results previously obtained with HBr, NH_3, KBr, and NaBr solutions, to give values for the ionization constant of water to 800° and 4000 bars. Logarithms of these ionization constants increase linearly with the logarithm of the molar concentration of water (at constant temperature) and also increase with temperature (at constant density).

Introduction

A knowledge of the thermodynamic ionization constant (K_w) of water is of fundamental importance to understanding ionic equilibria in aqueous solutions. Well established values for this quantity are available for temperatures below 100°, but at higher temperatures, particularly in the supercritical region, few values have been reported. Until recently, the only experimentally determined K_w's above 100° were those reported by Noyes and coworkers some 60 years ago.[2] This group calculated ionization constants for water to 306°, at saturation vapor pressure, from electrical conductivity measurements on ammonium acetate solutions. More recently, K_w's have been calculated to 1000° and 133 kbars from shock wave[3] and static[4] measurements of the conductance of pure water.

Although it is very difficult to make accurate conductance measurements on pure water at high temperatures and pressures, the success of the two methods[3,4] for the direct measurement of this parameter for water at high temperatures and pressures results from the

(1) (a) Research sponsored by the U. S. Atomic Energy Commission under contract with the Union Carbide Corporation. (b) Presented in part at the 158th National Meeting of the American Chemical Society, New York, N. Y., Sept 1969.

(2) (a) A. A. Noyes, *et al.*, "The Electrical Conductivity of Aqueous Solutions," Publication No. 63, Carnegie Institution of Washington, Washington, D. C., 1907; (b) A. A. Noyes, Y. Kato, and R. B. Sosman, *J. Amer. Chem. Soc.*, **32**, 159 (1910).

(3) (a) H. G. David and S. D. Haman, *Trans. Faraday Soc.*, **55**, 72 (1959); (b) S. D. Haman and M. Linton, *ibid.*, **62**, 2234 (1966); (c) S. D. Haman and M. Linton, *ibid.*, **65**, 2186 (1969).

(4) (a) W. Holzapfel and E. U. Franck, *Ber. Bunsenges. Phys. Chem.*, **70**, 1105 (1966); (b) W. B. Holzapfel, *J. Chem. Phys.*, **50**, 4424 (1969).

large increase in K_w with increasing temperature and pressure, coupled with a corresponding decrease in dissociation constants for electrolytes (such as NaCl[5]) with increasing temperature. Consequently, as the temperature increases, the total conductance of water due to self-ionization increases by several orders of magnitude while the relative contribution of ionic impurities to the total conductance decreases. Unfortunately, this method is not very successful in the temperature region 300–800°, at low and intermediate pressures, where the conductance of small amounts of impurities usually introduced by the all-metal pressure vessel contributes substantially to the conductance of water. For this region, a more suitable method is one in which conductances of solutions of a hydrolyzable salt are measured.

The results presented in the present paper, obtained from conductance measurements on aqueous ammonium bromide solutions, bridge the gap between the data available along the liquid–vapor equilibrium curve to 306° and that recently reported from measurements to 1000° and 133 kbars. Values of K_w in this intermediate region of temperature and pressure are of particular interest since these conditions encompass the temperatures and pressures at which mineral-forming processes occur in hydrothermal solutions.

Included in this paper are measured electrical conductances of dilute (0.002–0.015 *m*) aqueous ammonium bromide solutions from 0 to 800° to 4000 bars. These data, together with information obtained earlier from measurements of HBr,[6a] NaBr,[6b] NH_3,[6c] and KBr[6d] solutions under the same conditions of temperature and pressure, provide the necessary information from which ionization constants for water were calculated for the temperature range 300–800°. These results agree well with values reported previously for K_w at both higher and lower temperatures.

Experimental Section

The general experimental methods and details of the apparatus have been presented in an earlier paper.[5] Solutions of ammonium bromide were prepared gravimetrically from reagent grade salt (Baker and Adamson, Morristown, N. J.) and conductivity water. Four concentrations were studied: 0.002008, 0.00501, 0.01000, and 0.01500 *m*. Three different inner electrodes were used for these measurements. Their cell constants were 1.96, 0.509, and 0.496 cm^{-1} as determined with 0.01 and 0.1 demal KCl solutions at 25.00 ± 0.01°.

Results

Specific and equivalent conductances were calculated from the experimental data by methods described previously.[5] Typical results are shown in Figure 1, where specific conductances of 0.002008 *m* NH_4Br are plotted against pressure at the experimental temperatures.

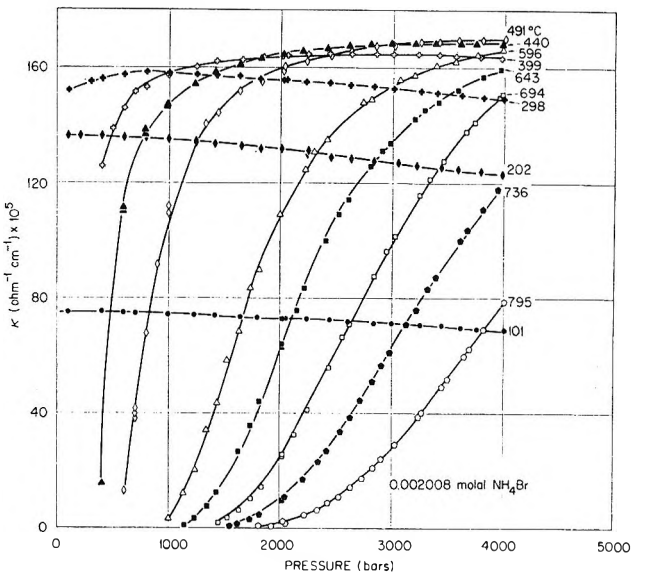

Figure 1. Specific conductances of 0.002008 *m* NH_4Br solutions as a function of pressure at several temperatures.

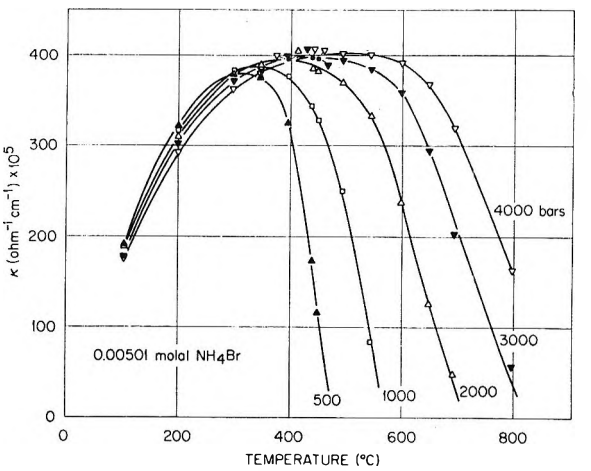

Figure 2. Isobaric variation of specific conductances of 0.00501 *m* NH_4Br solutions with temperature at pressures from 500 to 4000 bars.

Figure 2 shows the isobaric variation of specific conductance for the 0.00501 *m* solution as a function of temperature at pressures from 500 to 4000 bars. The conductances of the 0.01500 *m* solutions are given in Figure 3, where equivalent conductances are shown as a function of density, at the experimental temperatures. Equivalent conductances at integral temperatures and densities were obtained by plotting equivalent conductances, at integral densities as obtained from graphs similar to Figure 3, as a function of temperature and interpolating to integral temperatures. Table I presents equivalent conductances at integral temperatures

(5) A. S. Quist and W. L. Marshall, *J. Phys. Chem.*, **72**, 684 (1968).

(6) A. S. Quist and W. L. Marshall (a) *ibid.*, **72**, 1545 (1968); (b) *ibid.*, **72**, 2100 (1968); (c) *ibid.*, **72**, 3122 (1968); (d) *ibid.*, **73**, 978 (1969).

Table I: Equivalent Conductances (cm^2 ohm^{-1} $equiv^{-1}$) of 0.01 *m* NH_4Br Solutions at Integral Temperatures and Densities

Temp, °C	Density, g cm^{-3}											
	0.45	0.50	0.55	0.60	0.65	0.70	0.75	0.80	0.85	0.90	0.95	1.00
0												79
25												144
100												370
200										680	615	570
300							930	885	840	790	730	670
400			1000	1010	1005	990	965	925	880	835	780	
500	470	660	825	920	960	970	965	930	890			
600	230	400	585	750	850	915	935					
700	90	175	315	480	680	825						
800	36	90	185	320	480							

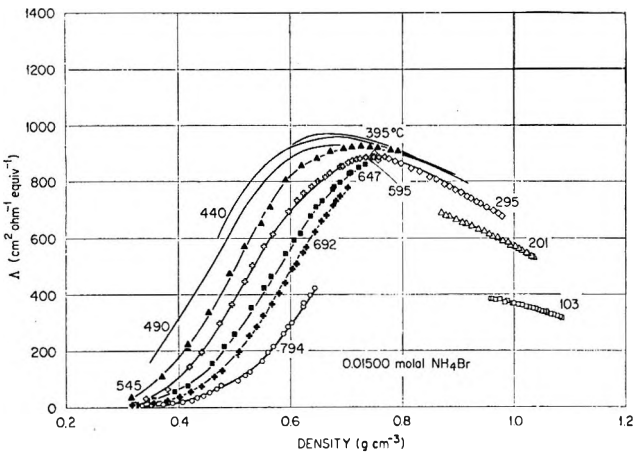

Figure 3. Equivalent conductances of 0.01500 *m* NH_4Br solutions as a function of density at several temperatures.

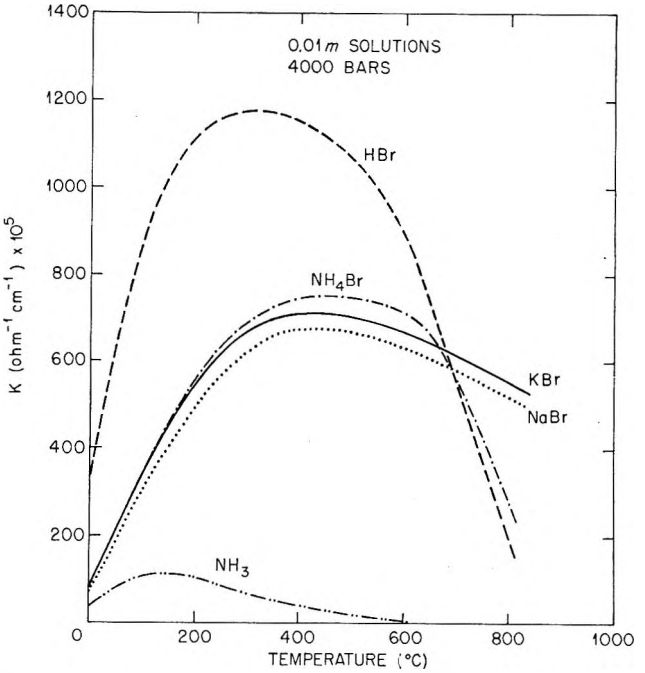

Figure 4. A comparison of the specific conductances of 0.01 *m* HBr, NH_4Br, KBr, NaBr, and NH_3 solutions as a function of temperature at 4000 bars.

and densities determined in this fashion for 0.01000 *m* NH_4Br solutions.

The conductance behavior of ammonium bromide solutions is qualitatively similar to that observed previously for salts such as NaCl,[5] NaBr,[6b] and KBr[6d] except at the higher temperatures where the conductance of ammonium bromide decreases sharply relative to the other salts. This comparative behavior is shown in Figure 4, where specific conductances of 0.01 *m* solutions of HBr,[6a] KBr,[6d] NaBr,[6b] NH_3,[6c] and NH_4Br are plotted *vs.* temperature, at a pressure of 4000 bars.

Below 100° the conductance of ammonium bromide is nearly identical with that of potassium bromide. This similarity in behavior has been observed previously at several temperatures at 1 atm pressure for limiting equivalent conductances[7] and viscosity *B* coefficients,[8] indicating that the transport properties of the ammonium and potassium ions are very similar. Previously unreported measurements in this laboratory have shown that the conductances of 0.01 *m* NH_4Br and KBr are nearly identical at pressures to 4000 bars, at 0 and 25°; this again indicates the similarity in transport properties of ammonium and potassium ions, in this case under conditions where some of the water structure has been destroyed. Considering the relative similarities in the conductance behavior of alkali metal halides to 800° and 4000 bars,[6d] it seems reasonable to assume that the mobilities of the potassium and ammonium ions will continue to be nearly identical at high temperatures and pressures.

Above 100°, at 4000 bars, the conductance of 0.01 *m* NH_4Br begins to diverge from that of KBr. The increase in conductance of NH_4Br relative to that of KBr is probably not due to any major differences in the mobilities of the potassium and ammonium ions but rather is a consequence of the hydrolysis of the ammonium ion according to the reaction

$$NH_4^+ + H_2O = NH_3 + H_3O^+ \qquad (1)$$

(7) R. A. Robinson and R. H. Stokes, "Electrolyte Solutions," 2nd revised ed, Butterworths, Ltd., London, 1965, p 465.

(8) M. Kaminsky, *Discuss. Faraday Soc.*, **24**, 171 (1957).

This hydrolysis reaction results in the replacement of ammonium ions by hydrogen ions; therefore the conductance of the NH_4Br solution becomes greater than that of the unhydrolyzed KBr solution because of the higher mobility of the hydrogen ion as compared to the mobility of the potassium ion. Since ammonia becomes a weaker electrolyte with increasing temperature,[6c] then with increasing temperature a larger fraction of the ammonium ions in the NH_4Br solution hydrolyzes and consequently the difference in conductance between NH_4Br and KBr solutions becomes greater.

A different behavior is observed above 600° (at 4000 bars) where the conductance of ammonium bromide decreases sharply. Qualitatively, this sharp decrease can be explained by comparison with the conductance of HBr solutions under the same conditions of temperature and pressure. The rapid decline in the specific conductance of HBr solutions at high temperatures, as shown in Figure 4, occurs because it becomes a weak electrolyte under these conditions.[6a] In NH_4Br solutions at these same high temperatures a significant fraction of the hydrogen ions produced by the hydrolysis of the ammonium ion (eq 1) combines with the bromide ions to form un-ionized HBr, thereby markedly reducing the conductance of these solutions also.

In potassium bromide solutions there appears to be no hydrolysis of the potassium ion to temperatures of 800°. In these solutions the hydrogen ion concentration will be determined by the self-ionization of water and will be relatively low. Therefore, in KBr solutions the concentration of un-ionized HBr will also be very low and can be neglected entirely. Consequently, the difference in conductance of an NH_4Br solution relative to that of a KBr solution of identical molality can be used to determine the concentration of the undissociated HBr present in the NH_4Br solution. The following paragraphs describe the procedure used to calculate the ionization constant for water at high temperatures and pressures from conductance measurements on NH_4Br, KBr, and HBr solutions.

Calculation of the Ionization Constant of Water

Hydrolyzed ammonium bromide solutions contain at least four different ionic species—NH_4^+, Br^-, H^+, OH^-—and, depending upon the temperature and pressure, significant concentrations of up to four un-ionized species—HBr, NH_3, NH_4Br, and H_2O. The equilibria between these ions and molecules are given by the following reactions and thermodynamic equilibrium constants

$$H_2O \rightleftarrows H^+ + OH^- \tag{2a}$$

$$K_w = [H^+][OH^-]f_\pm^2 \tag{2b}$$

$$HBr \rightleftarrows H^+ + Br^- \tag{3a}$$

$$K_a = \frac{[H^+][Br^-]}{[HBr]} f_\pm^2 \tag{3b}$$

$$NH_3 + H_2O \rightleftarrows NH_4^+ + OH^- \tag{4a}$$

$$K_b = \frac{[NH_4^+][OH^-]}{[NH_3]} f_\pm^2 \tag{4b}$$

$$NH_4Br \rightleftarrows NH_4^+ + Br^- \tag{5a}$$

$$K_s = \frac{[NH_4^+][Br^-]}{[NH_4Br]} f_\pm^2 \tag{5b}$$

where the bracketed quantities represent molar concentrations and $f_\pm$ is the mean molar ionic activity coefficient. Activity coefficients for the un-ionized species have been assumed to be unity, and for convenience the concentration of the solvent (water) has been included in the equilibrium constants. In addition to these four equilibrium constants that interrelate the concentration of the various molecular and ionic species, one can add equations of electrical charge balance

$$[NH_4^+] + [H^+] = [Br^-] + [OH^-] \tag{6}$$

and mass balance

$$C_0 = [NH_4^+] + [NH_3] + [NH_4Br] \tag{7a}$$

$$= [Br^-] + [HBr] + [NH_4Br] \tag{7b}$$

where C_0 is the stoichiometric molar concentration of NH_4Br used to prepare the solution.

Additional equations can be utilized if the electrical conductances of the solutions are measured. Thus, for every concentration of ammonium bromide there is an equation relating the measured conductance to the concentrations of the ions present in solution. For partially hydrolyzed NH_4Br solutions, the conductance equation must include the contributions of four different ions (three ions if the concentration of the hydroxide ion is neglected). Although in principle this is a straightforward process,[9,10] when this procedure is applied to calculate ion concentrations in partially hydrolyzed, partially associated, NH_4Br solutions, then high-order equations are encountered which are difficult to solve. Also, uncertainties in the experimental data and in the values for viscosities, dielectric constants, and limiting equivalent conductances necessary to calculate the theoretical parameters in the conductance equation make such a rigorous procedure of doubtful practical value.

Simpler procedures for calculating K_w from the conductance data are given below, in which conductances of 0.01 *m* solutions of NH_4Br, HBr, and KBr are compared directly. Potassium bromide is included in the comparison because it is assumed (see above) that its conductance represents that of an "unhydrolyzed" NH_4Br solution. With this assumption, the difference in conductance between 0.01 *m* NH_4Br and 0.01 *m* KBr at

(9) L. Onsager and S. K. Kim, *J. Phys. Chem.*, **61**, 215 (1957).
(10) A. S. Quist and W. L. Marshall, *ibid.*, **70**, 3714 (1966).

elevated temperatures and pressures is considered to be related to the concentration of the hydrogen ion produced by the hydrolysis of the ammonium ion (eq 1). The procedure for calculating K_w is slightly different depending on whether HBr is considered to be completely dissociated (in general, at densities of 0.80 g cm^{-3} and above) or whether significant concentrations of neutral HBr (or NH_4Br) species exist (at densities below 0.80 g cm^{-3}). These calculations are described more fully in the following paragraphs.

For electrolyte solutions, the specific conductances of the ions present in solution are additive. The specific conductance of an electrolyte (κ) is related to its equivalent conductance (Λ) and molar concentration (C) by the equation

$$\kappa = \frac{\Lambda m d}{1000} = \frac{\Lambda C}{1000} \quad (8)$$

where m is the molality and d is the solution density in g cm^{-3}. If it is assumed that no ionic association occurs and that the hydroxide ion concentration is negligible,[11] the specific conductance of a partially hydrolyzed NH_4Br solution of stoichiometric molar concentration C_0 is given by the equation

$$\kappa(\text{meas}) = \Lambda C_0/1000 = \{\Lambda(\text{HBr})[H^+] + \Lambda(NH_4Br)[NH_4^+]\}/1000 \quad (9a)$$

$$\Lambda C_0 = \Lambda(\text{HBr})[H^+] + \Lambda(NH_4Br)\{C_0 - [H^+]\} \quad (9b)$$

where Λ(HBr) and $\Lambda(NH_4Br)$ represent the conductances of completely ionized HBr and NH_4Br solutions at the ionic strength of the solution. The ionic strength may be calculated from the equation

$$I = {}^1/_2\sum_i C_i z_i^2 \quad (10)$$

In eq 10 C_i and z_i represent the molarity and electrical charge of the ith ion. When no association to form HBr or NH_4Br occurs, I is equal to ${}^1/_2C_0$. Under conditions where HBr is a strong electrolyte (the concentration of undissociated HBr is negligible) Λ(HBr) can be set equal to the measured value for an HBr solution at the ionic strength of the partially hydrolyzed NH_4Br solution.[6d] Under the same conditions the concentration of NH_4Br (and KBr) ion pairs will also be negligible and so the conductance of "unhydrolyzed" NH_4Br, $\Lambda(NH_4Br)$, can be set equal to the measured value for KBr at the same ionic strength,[6d] since the conductance of the K^+ and NH_4^+ ions are probably nearly identical (see above).

$$\Lambda C_0 = \Lambda(\text{HBr})[H^+] + \Lambda(\text{KBr})\{C_0 - [H^+]\} \quad (9c)$$

For every hydrogen ion produced by the hydrolysis reaction there will be an ammonia molecule formed; consequently, the ammonia concentration in these solutions will be equal to the hydrogen ion concentration. Equations 4b and 2b can be combined, and the values of K_b given previously[6c] can be used to calculate the ion product for water for temperatures and pressures where there is negligible ion association. In this procedure the activity coefficients in eq 2b and 4b, calculated without regard to ion-size parameters, are assumed to be equal and hence cancel out. Values of K_w given in Table II at densities of 0.80 g cm^{-3} and above correspond to these conditions.

Table II: Negative Logarithm of the Ion Product of Water, K_w ($= a_{H^+} \times a_{OH^-}$). Standard State is the Hypothetical 1 M Solution

Density, g cm^{-3}	Temp, °C					
	300	400	500	600	700	800
1.00	9.0	...	...			
0.95	9.3	8.7	...			
0.90	...	9.1	...			
0.85	...	9.4	9.0	...		
0.80	...	9.8	9.4	...		
0.75	...	10.1	9.9	9.6	...	
0.70	...	10.7	...	...	9.6	...
0.65	...	11.7	...	...	10.2	9.7
0.60	...	12.1	...	11.0	10.5	10.3
0.55		...	11.9	11.6	11.3	11.0
0.50		...	12.5	12.4	12.0	11.7
0.45		...	13.4	13.1	12.7	

At temperatures and pressures where there are significant concentrations of HBr molecules and NH_4Br ion pairs (for example, above 600° in Figure 4), the procedure for calculating K_w is somewhat different. In order to calculate the reduction in concentration of H^+, NH_4^+, and Br^- ions by the formation of un-ionized HBr or NH_4Br, values for the ionization constants for HBr and NH_4Br are necessary. Although ionization constants for HBr have been determined previously,[6a] it was not possible to use the same methods to obtain corresponding values for NH_4Br because of extensive hydrolysis of NH_4^+. However, values for the ionization constant of NaBr are known[6b] and it can be assumed that corresponding values for KBr are approximately the same, since the conductance behavior of all of the alkali metal bromides is very similar at high temperatures and pressures.[6d] Therefore, since the behavior of KBr and NH_4Br is also similar, values for the ionization constant for NH_4Br can be assumed to be approximately equal to the corresponding values for NaBr.

Under conditions where the concentrations of undissociated HBr and NH_4Br are significant, the measured conductances of HBr and KBr solutions do not represent the conductances of completely dissociated solu-

(11) For 0.01 m NH_4Br, the largest calculated hydroxide ion concentration under the conditions reported in this paper was at a density of 1.0 g cm^{-3} at 300° where this value was approximately 0.03% of the bromide ion concentration.

tions of these electrolytes. However, if the fraction (θ) of the electrolyte which is dissociated at the ionic strength of the solution is known, then the hypothetical conductance (Λ') of this electrolyte when it is completely dissociated at the same ionic strength can be calculated from the measured conductance Λ. For example

$$\Lambda'(\mathrm{HBr}) = \Lambda(\mathrm{HBr})/\theta(\mathrm{HBr}) \qquad (11a)$$

$$\Lambda'(\mathrm{NH_4Br}) = \Lambda(\mathrm{KBr})/\theta(\mathrm{NaBr}) \qquad (11b)$$

Values of θ were calculated from ionization constants and limiting equivalent conductances given previously.[6a,b] For internal consistency, the same methods[12] were used to calculate θ's as were originally used to obtain the ionization constants for HBr and NaBr.

Using these calculated conductances for completely dissociated HBr and NH_4Br, and using an initial estimate for the concentration of H^+, the concentration of NH_4^+ can be calculated from eq 9a. Since the hydroxide ion concentration in these solutions is insignificant compared to the concentrations of the other ions, eq 6 can be used to calculate the bromide ion concentration. Equation 5b can then be used to calculate the concentration of undissociated NH_4Br, where the activity coefficient is calculated by the equation

$$\log f_{\pm} = -AI^{1/2}/(1 + I^{1/2}) \qquad (12)$$

where A is the theoretical Debye–Hückel parameter and I has been defined earlier. This form of the Debye–Hückel equation is the same as was used earlier to calculate ionization constants for HBr,[6a] NaBr,[6b] and NH_3.[6c]

Continuing with this procedure, eq 7b was used to calculate the concentration of un-ionized HBr. A new estimate of the hydrogen ion concentration could then be obtained by the use of eq 3b. This value of the hydrogen ion concentration was then compared with the first estimate, and the calculations were repeated until successive values of the hydrogen ion concentration did not differ by more than 0.1%. It should be noted that convergence to the final value of the hydrogen ion concentration was rapidly achieved whether or not "maximum" or "minimum" possible values were selected for the first estimate of the hydrogen ion concentration.

Once final values of the above concentrations were established by the iterative procedure, the ammonia concentration was calculated as the sum of the hydrogen ion and the HBr molecule concentrations. Finally, eq 4b and 2b were combined as previously described to give values for the ion product of water. The values for K_w given in Table II at densities below 0.80 g cm^{-3} were calculated for conditions of incomplete dissociation of HBr and NH_4Br.

Comparison with Previous Research

In Figure 5, the logarithm of the thermodynamic ion product for water is plotted against the logarithm of the molar concentration of water. The linear relationship noted earlier for several other ionization equilibria[5,6,13] is again observed. For comparative purposes, some K_w values calculated from an empirical equation reported by Holzapfel[4b] are included in this graph. The slopes of the lines in Figure 5 were found to be 16.8; they appear to be independent of temperature. This value may be related to the change in hydration numbers of the reactants and products for the ionization of water.[13]

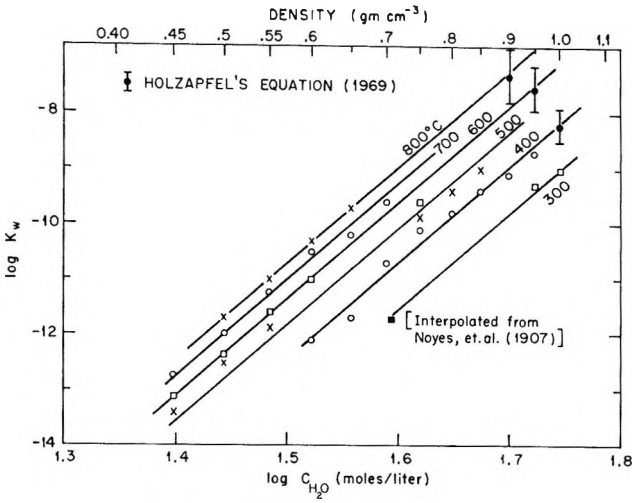

Figure 5. Log K_w (molar units) for the ion product of water as a function of the logarithm of the molar concentration of water at temperatures from 300 to 800°.

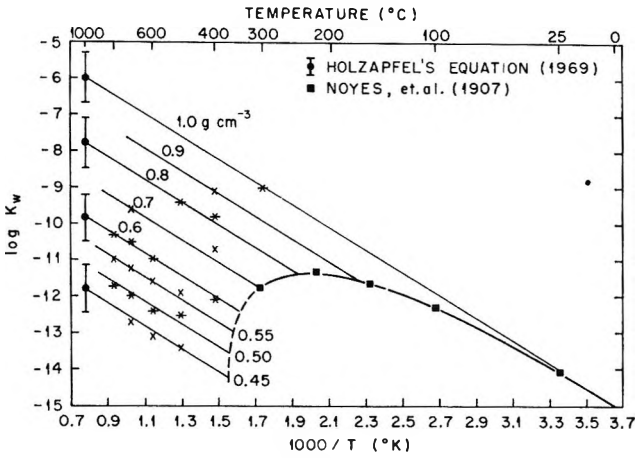

Figure 6. Log K_w (molar units) for the ion product of water as a function of $T(°K)^{-1}$ at water densities • from 045 to 1.0 g cm^{-3}.

In Figure 6, the logarithm of the ion product for water is plotted against the reciprocal of the absolute temperature, at various constant densities. The values

(12) (a) T. Shedlovsky, *J. Franklin Inst.*, 225, 739 (1938); (b) R. M. Fuoss and T. Shedlovsky, *J. Amer. Chem. Soc.*, 71, 1496 (1949).

(13) (a) W. L. Marshall and A. S. Quist, *Proc. Nat. Acad. Sci.*, 58, 901 (1967); (b) A. S. Quist and W. L. Marshall, *J. Phys. Chem.*, 72, 1536 (1968).

at 1000° were calculated from Holzapfel's equation; K_w's along the liquid–vapor equilibrium curve were taken from Noyes' work.[2] Figure 6 indicates that there is a nearly linear relationship of log K_w *vs.* T^{-1} for all densities. From the slopes of these lines, essentially the same for all densities, a value of 14.0 kg-cal/mol was calculated for the energy of ionization of water. This value is nearly the same as was used by Holzapfel in his empirical equation,[4b] and may be compared with a calorimetrically determined heat of ionization for water of 13.336 kg-cal/mol at 25° and atmospheric pressure.[14]

The uncertainties associated with the values in Table II vary, depending somewhat upon the temperature and density under consideration. At high densities and low temperatures (upper left region in Table II), where experimentally the conductances of 0.01 *M* HBr and NH_4Br solutions are always greater than those of a 0.01 *M* KBr solution, the differences between the measured conductances of the NH_4Br and KBr solutions are small (about 5–6% of the total conductance). Under these conditions, small errors in either of these conductances produce a much larger error in the calculated value of K_w. At temperatures and densities where the conductances of the KBr solution are greater than those of the NH_4Br and HBr solutions (lower right region of Table II), the differences between the measured conductances of the NH_4Br and KBr solutions are larger (20–50% or more) and so any errors associated with the conductance measurements have a lesser effect on the calculations. In addition, errors in the values of K_b produce equivalent errors in K_w. In general, an uncertainty of about 0.3–0.5 unit can be ascribed to the values in Table II. Ion products of water for the central region of the table were not reported because their uncertainties were much larger. In this region, the conductances of the 0.01 *M* NH_4Br, HBr, and KBr solutions were nearly the same and so the small uncertainties in these experimental values led to very large uncertainties in the value of K_w.

From the values of log K_w presented above, a semiempirical equation has been derived which expresses the ion product of water, within experimental error, to high temperatures and densities. This equation is obtained as follows. From Figure 5 one can obtain the equation

$$\log K_w(T) = \log K_w^0(T) + 16.8 \log C_{H_2O} \quad (13)$$

where $K_w^0(T)$ is the ion product for water at temperature T when its concentration is one mole per liter. Using the van't Hoff equation, and an energy of ionization of water of 14,000 cal/mol as obtained from Figure 6, one can write the relationship

$$\log K_w^0(T) = \log K_w^0(T_0) + \frac{14{,}000}{2.303R}\left(\frac{1}{T_0} - \frac{1}{T}\right) \quad (14)$$

where T_0 is some arbitrary reference temperature. A suitable reference temperature is 25°, where log K_w is accurately known to be −14.000 at 1 atm pressure (density = 0.9971 g cm^{-3}).[15] Using eq 13 to calculate a hypothetical log K_w^0 at 25°, this quantity can be substituted into eq 14 to give

$$\log K_w^0(T) = -33.05 - \frac{3050}{T} \quad (15)$$

Equation 15 can then be combined with eq 13 to give the final equation

$$\log K_w(T) = -33.05 - \frac{3050}{T} + 16.8 \log C_{H_2O} \quad (16)$$

Equation 16 reproduces, within experimental error, the log K_w values given in Table II to 800°. This equation also gives values of log K_w along the saturation vapor pressure curve to 306° which agree well (average deviation ±0.02 unit) with those reported earlier by Noyes.[2] [Note: for this comparison, the values reported by Noyes were all corrected by 0.09 log K_w unit to make his 25° value (14.09) agree with the currently accepted value of 14.000.] Although eq 16 seems to be adequate to express the experimental values to 1.0 g cm^{-3} at 1000°, log K_w values calculated from it at 1.5 g cm^{-3} at 1000° are about two units more negative than those reported by Holzapfel.[4b]

The values for the ion product of water as presented in this paper seem to be quite consistent with earlier values reported at both higher and lower temperatures. As a result, values for the ion product of water are now available throughout the complete range of temperature extending from 0 to 1000°, and from pressures of 1 to 133,000 bars.

Acknowledgment. The technical assistance of W. Jennings in making the conductance measurements is gratefully acknowledged. The author also wishes to thank Dr. W. L. Marshall for encouragement of this investigation.

(14) C. E. Vanderzee and J. A. Swanson, *J. Phys. Chem.*, **67**, 2608 (1963).

(15) A. K. Covington, R. A. Robinson, and R. G. Bates, *ibid.*, **70**, 3820 (1966).

Pretransition Behavior of Solid Potassium and Thallium Sulfates from Heat Content and Thermal Expansion[1]

by A. S. Dworkin* and M. A. Bredig

Chemistry Division, Oak Ridge National Laboratory, Oak Ridge, Tennessee 37830 *(Received April 6, 1970)*

In agreement with X-ray diffraction data for thermal expansion, drop calorimetric measurements of the heat contents of potassium and thallium sulfates showed these di-isomorphous salts to differ significantly with respect to the transition from an orthorhombic (pseudohexagonal) to a hexagonal crystal structure. While in potassium sulfate most of this change occurs isothermally at 584° (ΔH_{tr} = 2020 cal mol^{-1}) the corresponding change in thallium sulfate has a very small isothermal part (ΔH_{tr} = 160 cal mol^{-1} at 501°) and is predominantly a gradual pretransitional process. The difference is attributable to the high polarizability of the Tl^+ ion. The heat of fusion of thallium sulfate was found to be 5870 cal mol^{-1} at 643°.

Introduction

Majumdar and Roy[2] have reported that the enthalpy of the transition in K_2SO_4 at 584° [857°K] from the orthorhombic to the hexagonal crystal structure, as determined by means of the Clausius–Clapeyron equation $\Delta H_{tr} = (\Delta V_{tr} T_{tr})/(dT_{tr}/dp)$ = 1230 cal/mol, is only about one-half that of ΔH_{tr} = 2140 cal/mol determined calorimetrically.[3] This was explained[2] in terms of several unspecified intermediate crystal transformations in K_2SO_4 which were said to invalidate the assumption of the presence of the orthorhombic structure at 584° and thus the calculation of ΔV_{tr} (X-ray) based upon it. We felt this was highly improbable because of the great similarity in structure between the orthorhombic, pseudohexagonal structure at 25° and the hexagonal one at 600°.[4] An alternate explanation is suggested by the pretransition effect observed in the calorimetric study.[3,5] If this effect were due to an intrinsic structural characteristic of the crystal, the actual heat of the first-order transition at 584° might be as little as half of the reported calorimetric value. However, if the pretransition effect were due to the presence of a eutectoid produced by impurities as implied in the calculation of ΔH_{tr} in ref 5, then an explanation of the enthalpy discrepancy in terms of an erroneous ΔV_{tr} must be sought. In an attempt to resolve this question we have remeasured the heat content of K_2SO_4. For a comparison of K_2SO_4 with Tl_2SO_4, di-isomorphous with but chemically different from K_2SO_4, we also measured, for the first time, the heat content of Tl_2SO_4 up into the liquid range.

Experimental Section

The copper block drop calorimeter used for the measurements and the experimental procedure have been described in detail previously.[6] The salts were sealed in an inner platinum liner to prevent attack on the inconel capsules especially designed for our heat content apparatus. The heat content of the empty inconel capsules was measured in a separate series of measurements. The heat content of the platinum[7] amounted to only about 10 to 15% of that of the salt. Both the platinum and inconel capsules were welded closed in a helium drybox. Our procedure involves melting of the powdered salts before the first drop to ensure good thermal conductivity even in the solid phase. It was necessary to melt the K_2SO_4 in its sealed double container in a separate furnace prior to the first drop since our heat content furnace cannot attain the temperature of melting of K_2SO_4.

The melting and transition temperatures of both sulfates were determined by thermal analysis. The salts were held in quartz tubes with a Pt–10% Rh thermocouple extending directly into the melt. K_2SO_4 was found to melt at 1069° with a transition at 584° and Tl_2SO_4 melted at 643° with a transition at 501° in good agreement with other investigators.[2,5]

The sulfate content of our recrystallized Tl_2SO_4 was found to be 19.02 ± 0.02% (theoretical value 19.03%) and no foreign metals were found by spectrographic analysis. The K_2SO_4 was analytical reagent grade with less than 0.05% impurities. Both salts were kept in an oven at 140° for 48 hr before use.

Results

The measured heat contents are given in Table I. Smoothed values of heat content, entropy, and heat capacity are given in Table II. Figure 1 represents a

* To whom correspondence should be addressed.

(1) Research sponsored by the U. S. Atomic Energy Commission under contract with the Union Carbide Corp.

(2) A. J. Majumdar and R. Roy, *J. Phys. Chem.*, **69**, 1684 (1965).

(3) K. K. Kelley, *Bur. Mines Bull.*, 584 (1960).

(4) M. A. Bredig, *J. Phys. Chem.*, **46**, 747 (1942); **47**, 587 (1943).

(5) C. H. Shomate and B. F. Naylor, *J. Amer. Chem. Soc.*, **67**, 72 (1945).

(6) A. S. Dworkin and M. A. Bredig, *J. Phys. Chem.*, **64**, 269 (1960).

(7) D. R. Stull and G. C. Sinke, "Thermodynamic Properties of the Elements," American Chemical Society, Washington, D. C., 1956.

Table I: Measured Heat Contents of Tl_2SO_4 and K_2SO_4

Run no.	Temp, °K	$H_T - H_{298}$, kcal mol^{-1}	Run no.	Temp, °K	$H_T - H_{298}$, kcal mol^{-1}
		Tl_2SO_4			
34	400.2	3.66	29	781.6	21.16
23	428.4	4.73	30	791.5	21.59
35	460.3	5.88	18	803.7	22.12
24	486.0	7.00	6	823.7	23.08
36	512.5	8.07	7	843.9	23.96
25	534.4	8.91	8	863.0	24.87
37	559.9	9.96	9	885.0	25.83
26	584.9	11.18	10	901.1	26.66
19	620.8	12.92		Liquid	
20	644.8	14.04			
21	672.8	15.43	39	922.2	33.47
33	688.0	16.13	4	926.9	33.73
27	700.6	16.74	13	933.8	33.94
28	713.7	17.42	5	940.4	34.21
14	726.7	18.11	38	952.7	34.88
15	743.7	18.99	12	957.7	34.95
32	752.6	19.47	1	967.2	35.54
16	760.5	19.80	11	976.9	36.07
31	766.7	20.18	2	988.3	36.40
		K_2SO_4			
13	427.7	4.32	22	751.2	17.61
23	457.0	5.42	6	771.1	18.63
14	478.7	6.28	7	794.0	19.70
24	506.0	7.33	8	813.6	20.69
15	526.9	8.04	9	833.5	21.74
25	554.1	9.16	20	842.9	22.10
16	576.8	10.06	10	850.2	22.62
26	606.2	11.31	21	852.0	22.67
17	623.0	11.89	4	868.5	25.35
27	649.3	12.99	5	896.3	26.59
18	670.4	13.89	3	922.0	27.75
11	705.7	15.48	2	951.3	29.08
19	726.9	16.34	1	970.9	20.39
28	733.9	16.71			

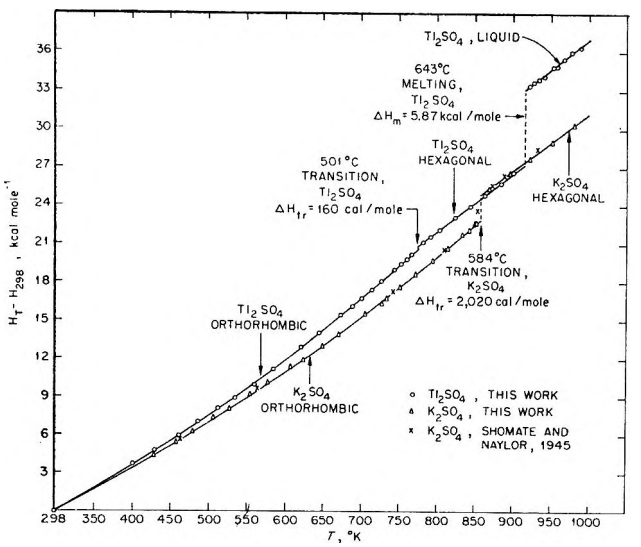

Figure 1. Heat content ($H_T - H_{298}$) of potassium sulfate and thallium sulfate.

comparison of the heat content *vs.* T for K_2SO_4 and Tl_2SO_4 and also shows the earlier calorimetric data for K_2SO_4.[5] A computer program to calculate high-temperature thermodynamic functions[8] was used to obtain the entropy and heat capacity values as well as the following equations for $H_T - H_{298}$ (cal/mol)

Tl_2SO_4. Orthorhombic

$$H_T - H_{298} = -2921 + 9.724T + 2.834 \times 10^{-2}T^2 - 7.447 \times 10^5/T(298 - 774°K) \pm 0.4\%$$

transition

$$\Delta H_{tr}\ (774°K) = 160 \pm 60\ \text{cal/mol}$$

hexagonal

$$H_T - H_{298} = -14{,}697 + 45.84T(774 - 916°K) \pm 0.1\%$$

melting

$$\Delta H_m\ (916°K) = 5870 \pm 60\ \text{cal/mol}$$

liquid

$$H_T - H_{298} = -8600 + 45.60T(916 - 1100°K) \pm 0.2\%$$

K_2SO_4. Orthorhombic

$$H_T - H_{298} = -11{,}732 + 33.95T - 5.35 \times 10^{-4}T^2 + 8.49 \times 10^{-6}T^3 + 4.27 \times 10^5/T(298 - 857) \pm 0.5\%$$

transition

$$\Delta H_{tr} = 2020 \pm 80\ \text{cal/mol}$$

hexagonal

$$H_T - H_{298} = -13{,}910 + 45.22T(857 - 1000) \pm 0.1\%$$

The fit of the data to the equations is given above. An overall accuracy of ±0.5% is estimated for the heat content measurements and the stated error for the heats of fusion and transition are estimated from the precision and accuracy of the heat content measurements. The computer program sets $\Delta H = 0$ and fixes C_p at 298°K by means of an input parameter. For K_2SO_4, the previously measured value[9] of $C_p = 31.1$ cal/deg mol^{-1} at 298°K was used. Since no low-temperature measurements for Tl_2SO_4 are available, a $C_p = 35$ cal/deg mol^{-1} at 298°K was obtained from an extrapolation of our high-temperature heat content data. The addition of a cubic term to the standard Kelley heat content equation[3] improved the fit of the data for K_2SO_4 and resulted in a heat capacity curve having the

(8) T. G. Godfrey and J. M. Leitnaker, ORNL-TM-1599 (1966).

(9) G. E. Moore and K. K. Kelley, *J. Amer. Chem. Soc.*, **64**, 2949 (1942).

Table II: Smoothed Values of Heat Content, Heat Capacity, and Entropy for Tl_2SO_4 and K_2SO_4

	Tl_2SO_4			K_2SO_4		
T, °K	C_p, cal mol^{-1} deg^{-1}	$H_T - H_{298}$, kcal mol^{-1}	$S_T - S_{298}$, cal mol^{-1} deg^{-1}	C_p, cal mol^{-1} deg^{-1}	$H_T - H_{298}$, kcal mol^{-1}	$S_T - S_{298}$, cal mol^{-1} deg^{-1}
298	35.0	0	0	31.1	0	0
400	37.1	3.64	10.5	34.9	3.37	9.7
500	41.0	7.54	19.2	38.1	7.03	17.8
600	45.8	11.88	27.1	41.3	10.99	25.1
700	50.9	16.71	34.5	44.8	15.30	31.7
774	54.8	20.62 (orth)	39.8	...	...	...
774	45.8	20.78 (hex)	40.0	...	...	...
800	45.8	21.98	41.5	48.7	19.97	37.9
857	...	...	...	51.2	22.82 (orth)	41.4
857	...	...	...	45.2	24.84 (hex)	43.7
900	45.8	26.56	46.9	45.2	26.78	45.9
916	45.8	27.30 (hex)	47.8	...	...	...
916	45.6	33.17 (liq)	54.2	...	...	...
1000	45.6	37.00	58.2	45.2	31.30	50.7
1100	45.6	41.56	62.5			

same characteristics as one obtained by adiabatic measurements and reported[10] since the completion of our experiments. This will be discussed below. The additional term neither improved the fit nor changed the C_p curve for Tl_2SO_4 and therefore was not used in that case.

Discussion

There is very little if any indication of the pretransition effect in K_2SO_4 immediately below T_{tr} = 857 (584°) as shown by our five measurements between 800°K and the transition temperature (Figure 1). Our ΔH_{tr} value of 2020 ± 80 cal/mol essentially confirms the value 1940 reported originally[5] (or 2140 presently accepted).[3] The heat content at 580° reported earlier as "pretransition"[5] actually must have reflected *partial* transition (eutectoid) caused by an impurity. (This was realized by Shomate and Naylor in arriving at ΔH_{tr} = 1940 cal/mol.) Since the effect is not intrinsic to pure K_2SO_4 and no indication of intermediate crystal transformations were found either in our work or the adiabatic measurements of Shmidt,[10] we are forced to seek another explanation of the discrepancy in ΔH_{tr} reported by Majumdar and Roy (M and R).[2]

We believe the explanation is to be found in a consideration of the difficulty involved in obtaining an accurate ΔV_{tr} by X-ray methods. One must not only use a small difference between two large numbers (*e.g.*, 74 and 73 cm^3/mol K_2SO_4 at 583°)[2] but must obtain the lower one by extrapolation in a region of strong curvature. If the absolute X-ray parameters for K_2SO_4 obtained by M and R[2,11] and other investigators[12-14] are examined, we find differences great enough to account for a variation in ΔV_{tr} of at least 50%. The difficulty of obtaining an accurate value of ΔV_{tr} by X-ray diffraction was also noted by Roy.[15] We wish to point out,

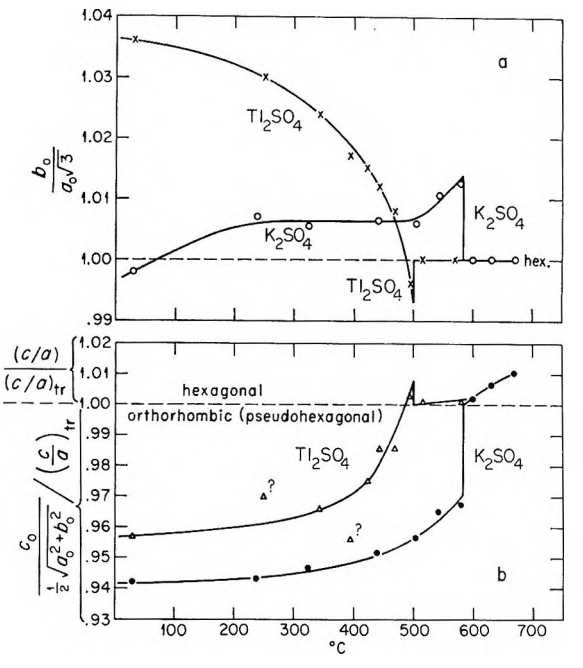

Figure 2. Continuous and discontinuous deformation of the structures of K_2SO_4 and Tl_2SO_4 with temperature (based on data from ref 2). a. Deviation from hexagonal symmetry of base plane. b. Change of pseudohexagonal $[c_0/(1/2\sqrt{a_0^2 + b_0^2}]$ and hexagonal (c/a) axial ratios relative to ratio, $(c/a)_{tr}$, at the transition temperature.

(10) N. E. Shmidt, *Russ. J. Inorg. Chem.*, **12**, No. 7, 929 (1967).

(11) A. J. Majumdar, Ph.D. Thesis, Pennsylvania State University, 1958. University Microfilms, Inc., Ann Arbor, Mich., L. C. Card. No. Mic 58-7290.

(12) M. Bernard and R. Hocart, *Bull. Soc. Fr. Mineral. Crist.*, **84**, 396 (1961).

(13) R. Moreau, *Bull. Soc. Roy. Sci. Liege*, **32**, 252 (1963).

(14) H. E. Swanson, R. K. Fuyat, and G. M. Ugrinic, National Bureau of Standards Circular 539, Vol. III, U. S. Government Printing Office, Washington, D. C., 1954, p 62-64.

(15) A. J. Majumdar and R. Roy, *J. Inorg. Nucl. Chem.*, **27**, 1961 (1965).

however, that the general nature of the increase in volume with temperature is not in question.

The calorimetric results for thallium sulfate (Figure 1) exhibit a rather significant difference from the potassium salt, in contrast to the structural similarity stressed by M and R.[2] Both the enthalpy (160 cal/mol) and the entropy (0.2 cal deg^{-1} mol^{-1}) of transition are an order of magnitude smaller than in K_2SO_4 (2030 and 2.3, respectively). This is in at least qualitative agreement with the high-temperature X-ray data[2] which suggest a much smaller volume change, $\Delta V_{tr} < 0.5$ cm^3/mol in Tl_2SO_4 than in K_2SO_4, $\Delta V_{tr} > 1.0$ cm^3/mol. Also a volume expansion in the temperature range 150° below the transition, resulting largely from an increase in the pseudohexagonal c axis of the orthorhombic structure, begins at a lower temperature and is much larger for Tl_2SO_4 than for K_2SO_4. The contrasting structural behavior may be even more readily illustrated with the dimensional deviations from the hexagonal symmetry than with the volume changes. Figure 2a demonstrates how gradual the change is in Tl_2SO_4 from the pseudohexagonal symmetry of the (001) plane of the orthorhombic structure to the truly hexagonal symmetry of the high-temperature phase. Figure 2b shows the largely isothermal change of 3% from the pseudohexagonal axial ratio $c_0/{}^1/_2(\sqrt{a_0^2 + b_0^2})$ to the hexagonal c/a for K_2SO_4 in contrast to the gradual change in Tl_2SO_4. It furthermore indicates a smaller change in c/a, above the transition temperature, for Tl_2SO_4 than for K_2SO_4.

The heat capacity behavior is also consistent with the abnormal volume expansion. The C_p of K_2SO_4 increases in the normal fashion, *i.e.*, with *de*creasing rate, up to a temperature of about 600°K where it begins to increase with *in*creasing rate. At T_{tr} the specific heat, $C_p = 51$ cal/deg mol^{-1}, is higher than that for the hexagonal solid ($C_p = 45$) or the liquid ($C_p = 47$).[5] The C_p of Tl_2SO_4 increases with an increasing rate from the lowest temperature to T_{tr} where $C_p = 55$, again much higher than the $C_p = 46$ of the hexagonal solid and the liquid. This reflects the early pretransition behavior observed in the X-ray measurements. Although the heat capacities are merely a derivative of our actual heat content measurements and as such are not highly accurate, they are essentially confirmed for K_2SO_4 by the adiabatic measurements of Shmidt.[10] His measurements over the range 298–770°K agree with ours to better than ±2% and also show an inflection at about 600°K. (Shmidt makes the unlikely claim that the point of inflection is at 505°K for all five alkali metal sulfates but the actual data seem to indicate a temperature closer to 600°K for K_2SO_4.)

The far more gradual nature of the structure change in Tl_2SO_4 may be attributed to the high polarizability of the Tl^+ ion, the most polarizable of all univalent cations. The present observations confirm those of Fischmeister,[16] who pointed out the adverse effect of increasing polarizability of the M^+ cations, especially of Tl^+, upon the sharpness of the transition in various sulfates M_2SO_4.

(16) H. F. Fischmeister, *Z. Phys. Chem.* (*Frankfurt am Main*), **7**, 91 (1956).

Polarizability of Alkali and Halide Ions, Especially Fluoride Ion

by Kasimir Fajans

Department of Chemistry, University of Michigan, Ann Arbor, Michigan 48104 *(Received October 27, 1969)*

After it was recognized, in 1924,[1] that the Lorentz–Lorenz refractivity R (proportional to dipole polarizability α) of ions in crystals depends on the electric field of oppositely charged ions, numerous attempts were made to derive values of these properties for free gaseous ions. Those proposed recently for alkali and halide ions by Wilson and Curtis (WC) differ considerably, especially for anions and particularly for F^-, from previously derived ones. On the other hand, the polarizability α of F^- obtained by WC coincides with that calculated by Cohen, applying the wave mechanical coupled Hartree–Fock approximation. It is shown in the present article how a set of α's for analogous ions can be tested for consistency, either by considering the deviations from additivity or by applying the inequalities method. Both ways lead to the conclusion that the new α for F^- (1.56 Å^3) is too large and that there is no reason to revise the value 0.95 used by the present author.

1. Introduction

Wilson and Curtis (WC) acknowledge in a recently published paper[2] our correspondence about an earlier version of their manuscript. Their work deals with the dependence of the polarizability α of ions on the field of oppositely charged ions in alkali halide crystals. In a qualitative respect the view accepted by WC in the final version of their article agrees fully with the general principle which my coworkers and I applied to an extensive experimental material since 1924: the polarizability (initially the Lorentz–Lorenz molar refractivity R_D) diminishes in the field of positive, increases in that of negative charges. Nevertheless, the same experimental polarizabilities of the crystalline alkali halides lead us to values for the free gaseous ions which differ in the following way. The ratio WC/BF is:[3] 0.79 for Na^+; on the average 0.93 ± 0.014 for K^+, Rb^+, Cs^+; 1.24 ± 0.02 for Cl^-, Br^-, I^-; for F^- it has the large value 1.635. (See the individual values of α in Tables IV and V.)[4]

We are especially concerned about the large discrepancy in the case of F^- because the α_{F^-} value of BF was used recently as the basis of our own[5a,c] and other[5b] investigations.

The reason why various investigators arrive at different α values for gaseous ions is that they attempt to satisfy different correlations. BF applied those derived by Fajans and Joos[1] (FJ) which were confirmed by further theoretical considerations relating the polarizabilities of gaseous ions to the experimental values of the noble gases as well as by extensive data involving ionic compounds in crystalline, vapor, and dissolved state. The comparison of these experimental data with the chosen values for gaseous ions led always to reasonable deviations from additivity. Therefore in order to test the new set of α values for free alkali and halide ions we shall apply to them both these methods.

2. Comparison of α for Aqueous and Crystalline Alkali Halides

First let us consider in Figure 1, as was done in Figure 1 of ref 1, the experimental differences between the alkali halides in aqueous solution and in the crystalline state. The present figure applies to the polarizabilities α in Å^3, the former one to R_D in cm^3. Numerous individual values, especially for the solutions, became more precise. Their sources in the present figure, in addition to those given in ref 2, are: for the solutions, ref 3 and 6; for the crystals, WC, Table I, column "Accept."

The general appearance of the two figures is identical, except that in the present figure of the somewhat irregular[7] values for the fluorides, namely Li −0.017, Na −0.082, K −0.096, Rb −0.085, Cs −0.051, the last two are not shown.

For the interpretation of Figure 1 one has to take into account that each $\alpha_{aq} - \alpha_{cr}$ for a given salt is the differential result of the following effects: tightening (decrease of α) of the anion in the crystal and of the

(1) K. Fajans and G. Joos, *Z. Phys.*, **23**, 1 (1924).

(2) J. N. Wilson and R. M. Curtis, *J. Phys. Chem.*, **74**, 187 (1970).

(3) The abbreviation BF refers to the paper with N. Bauer, *J. Amer. Chem. Soc.*, **64**, 3031 (1942), in which values of R_∞ were derived. We apply the relation: R (cm^3) = 2.522 α (Å^3). The values of α for free ions used here are those given by Wilson and Curtis in their Table III for Model II. The F^- value for Model I would give the still larger ratio 1.93.

(4) During the editorial treatment of the present article a still different set of α values was published by A. J. Michael, *J. Chem. Phys.*, **51**, 5730 (1969). Contrary to WC, the values of AJM are larger than those of BF for the alkali ions (AJM/BF decreases from 1.60 for Na^+ to 1.24 for Cs^+), smaller for the halide ions (AJM/BF increases from 0.80 for F^- to 0.91 for I^-). The assumed changes of α in the crystals do not show a clear regularity.

(5) (a) K. Fajans, *Struct. Bonding, (Berlin)*, **3**, 88 (1967); (b) R. A. Penneman, *Inorg. Chem.*, **8**, 1379 (1969); (c) K. Fajans, *ibid.*, **8**, 1553 (1969).

(6) K. Fajans and R. Lühdemann, *Z. Phys. Chem.*, **29B**, 152 (1935).

(7) The possible reason for the irregularity is an inaccuracy of the experimental R values of the hygroscopic crystalline RbF and CsF (see sections 3 and 6).

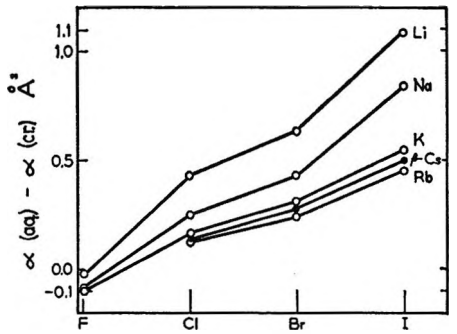

Figure 1. Polarizabilities, α_∞, which alkali halides have in dilute aqueous solution minus those in the crystal. The somewhat irregular values for RbF and CsF are omitted for the sake of clearness of the figure. See text.

water molecules in the solution due to the field of the cation; loosening of the cation in the crystal and of the water molecules in the solution, due to the field of the anion; in the case of highly polarizable ions, like I^- and perhaps Cs^+, it is possible that anions are tightened and cations are loosened also in the field of the water dipoles.

In spite of this rather complex situation there can be no doubt as to the meaning of the preponderance of positive ordinate values: the tightening of the anion by the cation in the crystals is the dominant effect. Taking into account that this effect can be expected to increase with the strength of the polarizing field of the cation and the polarizability of the anion, one understands the regular decrease of the positive ordinate values from Li^+ to Rb^+ and from I^- to Cl^-.

The line for CsCl, CsBr, CsI is above that for the Rb salts, obviously because of the different crystal structure of these three salts.[8]

Of special importance for our present discussion are in Figure 1 the negative, small values for the five fluorides. The negative sign of aq − cr can be due partly to a more pronounced tightening exerted by the cations on the water molecules in the solution than on F^- in the crystal, and also to a more pronounced loosening of the cations than of water in the field of F^-. In order to test these possibilities we shall compare the experimental α_{aq} and α_{cr} of the salts separately with the sums of the α_g of gaseous cation and anion according to BF as well as WC.

3. Comparison of Experimental α with Those for Free Ions

Starting with the aq − g values in Table I part a, one sees that they are of the same order of magnitude as the experimental values in Figure 1. Those for LiF and NaF are negative, the other three are positive; this means that in the case of Li^+ and Na^+ the tightening effects predominate, in the case of K^+, Rb^+, Cs^+ the loosening effects; even the gradation from LiF to CsF is regular. The latter is not the case for the cr − g values of RbF and CsF, which supports the assumption in ref 7. There are no evident inconsistencies in the α_g values of BF.

Table I: Change of the Sum of α (Å³) for Cation and Anion in Solution and Crystal

	LiF	NaF	KF	RbF	CsF
		a. α_g of BF			
aq − g	−0.054	−0.046	0.055	0.056	0.074
cr − g	−0.037	0.036	0.151	0.141	0.124
		b. α_g of WC			
aq − g	−0.69	−0.61	−0.47	−0.43	−0.41
cr − g	−0.675	−0.53	−0.38	−0.35	−0.36

On the other hand, the WC values in Table Ib are all negative and the absolute values are considerably (on the average 74 times) larger than the absolute experimental aq − cr values in Figure 1. The latter appear to be a small difference of much larger effects involving the gaseous ions. This does not appear to be reasonable and the situation is very different when one considers, *e.g.*, LiI, for which aq − cr is 1.09. The latter difference compares as follows with those involving gaseous ions: g − aq BF 0.25, WC 1.95; g − cr BF 1.34, WC 3.04. These values are of the same order of magnitude as 1.09, although those of WC are distinctly larger than the BF ones, because for $\alpha(I^-, \text{gas})$ the ratio WC/BF equals 1.23. Hence the great contrast for the fluorides seems to be caused by the unduly large α_{F^-} for which WC/BF is 1.69.

4. The Method of Inequalities

As the other method for testing the F^- value we shall use here that of "inequalities of quotients." It played a decisive role for the derivation of the R values for gaseous ions by FJ[1] and has been explained since on many occasions in the research literature[9a] and textbooks.[9b] The following example explains the main idea. Comparing the α values of the isoelectronic F^-, Ne, Na^+, one has to take into account that the difference of 1+ between the nuclear charges is relatively larger between Ne and F^- than between Na^+ and Ne. One has therefore to expect for the quotients Q' the inequality $\alpha_{F^-}/\alpha_{Ne} > \alpha_{Ne}/\alpha_{Na^+}$ because $10/9(1.1111) > 11/10(1.1000)$.

This idea was extended in ref 9a to the quotients Q'' and Q'''. Since in testing wave mechanical α values in

(8) K. Fajans, *Z. Phys. Chem.*, 130, 724 (1927), where the first attempt was made to treat the deviations from additivity of R_D quantitatively. See also in the WC paper ref 15–18 to investigations of Ruffa and others. The theoretical and quantitative aspects of these deviations will not be discussed in the present article.

(9) (a) See especially K. Fajans, *Z. Phys. Chem.*, 24B, 103, 114 (1934); (b) see, *e.g.*, S. Glasstone, "Text-book of Physical Chemistry," Van Nostrand, New York, N. Y., 1940, p 529; 1946, p 539.

Table II: Regularities of the Quotients for the Series 9 to 17

	9	10	11	12	13	14	15	16	17
Q'		1.1111	1.1000	1.0909	1.0833	1.0769	1.0714	1.0667	1.0625
Q''			1.0101	1.0283	1.0270	1.0260	1.0251	1.0244	1.0239
Q'''				1.0218	1.0213	1.0210	1.039	1.037	1.035
Q^{IV}					1.035	1.033	1.031 →	1.032	1.032

section 5 we shall proceed to still further quotients let us demonstrate here purely mathematically in which respect the inequalities are valid. Choosing as an example the series of the ions of neon type between the nuclear charges 9(F^-) and 17(Cl^{7+}), the results are given in Table II.

It is seen that not only Q', Q'', and Q''' decrease from left to right but that each Q'' (Q''') is smaller than both Q' (Q'') above it. The irregularity indicated by → in the series of the Q^{IV} values is caused by the insufficient accuracy due to the rounding off to four decimal places. In fact, the stated regularities apply to the further Q^n the more decimals one chooses. But even with seven decimals Q^{VIII} is somewhat larger than the smaller Q^{VII}. Finally, with eight decimals the validity of the inequalities method becomes perfect for this series $z = 9$ to 17.

Q^{VII}	1.04183	1.0586	1.041726	1.05950
		↙		
Q^{VIII}		1.0597		1.05776

5. Testing of Wave Mechanical α Values

Wilson and Curtis, comparing the α_{F^-} value derived by them with wave mechanical calculation of Cohen,[10] say: "It is therefore conceivable that even Cohen's calculated value for $\alpha(F^-)$, which agrees precisely with our extrapolated value (Model II) is too low." The inequalities method is very appropriate for testing of this assumption.

Cohen used the coupled Hartree–Fock approximation in order to calculate α for F^-, Ne, Na^+, Mg^{2+}, and Al^{3+}. His values agree closely with those of Lahiri and Mukherji[11] (LM) except that the latter include also Si^{4+}, and their value (in Å^3) for F^- (1.40) is distinctly smaller than that of WC and Cohen's (1.56). In Table III the inequalities method is applied to the LM values.

It is seen that all Q' and Q'' values are consistent with the inequalities rules and the Q''' and Q^{IV} diminish from left to right. However, the first Q''' and Q^{IV} as well as Q^V are larger than the smaller of the values above them and the same is true for the second Q^{IV}.[11a]

In order to demonstrate how sensitive this method is, let us assume that the inconsistencies indicated by the three arrows at the left side of Table III are due mainly to the F^- value 1.40 not being correct. One can achieve better consistency putting the smaller Q^{IV} equal to 1.03

Table III: Test[a] of Lahiri–Mukherji's α in Å^3

	F^- 1.40	Ne 0.350	Na^+ 0.140	Mg^{2+} 0.0697	Al^{3+} 0.0393	Si^{4+} 0.0241
Q'	4.00	2.500	2.008	1.773	1.631	
Q''		1.600	1.245	1.1325	1.087	
			↙			
Q'''			1.285	1.099	1.042	
				↙	↙	
Q^{IV}				1.169	1.055	
					↙	
Q^V					1.108	

[a] The four arrows at the bottom of the table indicate that the values involved increase in this direction instead of decreasing.

and Q^V equal to 1.02; there result as the first values on the left

$$Q^{IV}\ 1.05 \quad Q'''\ 1.15 \quad Q''\ 1.43 \quad Q'\ 3.58 \quad F^-\ 1.25$$

Accordingly the LM value 1.40 for F^- and even more the WC value 1.56 appear to be too large.

A more direct proof that the Hartree–Fock approximation is not exact enough for the derivation of the α's for ten electron systems is that the LM–Cohen value for Ne (0.350) is 11% smaller than the experimental one (0.395_3). This is not surprising because even for two electron systems the α's calculated by Cohen[10] do not agree with the precise values obtained by up to 96-term variational wave functions,[12] as the following comparison shows.

	H^-	He	Li^+
CH[12]	30.50	0.2050	0.02851
Cohen[10]	13.8	0.196	0.0280

The approximate values are smaller than the precise ones (in %) 1.8 for Li^+, 4.4 for He, and 55 for H^-. The pronounced discrepancy for H^- was first shown by Schwartz.[13a] The tremendous tightening effect ex-

(10) H. D. Cohen, *J. Chem. Phys.*, **43**, 3558 (1965); **45**, 10 (1966).

(11) J. Lahiri and A. Mukherji, *Phys. Rev.*, **153**, 386 (1967).

(11a) NOTE ADDED IN PROOF. Considering the Q' involving the α of Na^+, Mg^{2+}, Al^{3+} in Table III and those of F^-, Ne, Na^+ in Table V to be correct, the result is obtained that Q'_α is approximately equal (Q'_z).[8] A table analogous to Table II, in which $z = 9$ to 14 are replaced by 9[8] to 14,[8] shows a perfect validity of the inequalities rules down to $Q^V = 1.0_212$.

(12) K. T. Chung and R. P. Hurst, *J. Chem. Phys.*, **43**, 35 (1965) [CH].

(13) (a) C. Schwartz, *Phys. Rev.*, **123**, 1700 (1961); (b) K. Fajans, *Chimia*, **13**, 354 (1959).

erted on H^- by cations was emphasized earlier[13b] using its approximate α. The precise value is reduced from 30.5 to 2.0 in crystalline KH, to 0.8 in the H_2 ($H^- + H^+$) molecule.[14]

6. Application to α of Alkali and Halide Ions

The inequalities method can be applied to the WC and BF values in the following way. WC list in their Table III two sets of α for free alkali and halide ions. One was derived assuming that only the anions change their polarizabilities in the field of cations (Model I), the other set attempts to take into account also the less pronounced variability of the cations (Model II). For Li^+ and Na^+ the same theoretical values are listed in both sets, for the other ions the resulting α differ (in Å^3) between 0.02 for K^+ and 0.29 for Br^-. We shall test here only the set II in which α_F- is smaller than in I. Of the values given for Cs^+ (2.45–2.42) we choose the more favorable limit 2.42. The α's of the noble gases in Tables IV and V are experimental.

Table IV: Test of WC's α in Å^3

	Q'[a]		Q	
F^- 1.56	3.95	Ne 0.3953	2.67	Na^+ 0.148
Cl^- 4.41	2.687	A 1.641	2.023	K^+ 0.811
Br^- 5.84	2.350	Kr 2.485	1.815	Rb^+ 1.37
I^- 8.91	2.217	Xe 4.019	1.661	Cs^+ 2.42
Q''[b]	Ne 1.479	A 1.328	Kr 1.295	Xe 1.335
Q'''[c]	1.121	Av 1.319 ± 0.016		

[a] Q' is the ratio between two neighboring α. [b] $Q'' = Q'\left(\frac{1-}{0}\right)\Big/Q'\left(\frac{0}{1+}\right)$. [c] $Q''' = Q''(\text{Ne})/Q''(\text{av A, Kr, Xe})$.

Table V: Test of BF's α in Å^3

	Q'[a]		Q'	
F^- 0.952	2.408	Ne 0.3953	2.104	Na^+ 0.1879
Cl^- 3.475	2.118	A 1.641	1.850	K^+ 0.887
Br^- 4.821	1.940	Kr 2.485	1.673	Rb^+ 1.485
I^- 7.216	1.795	Xe 4.019	1.579	Cs^+ 2.545
Q''[a]	Ne 1.144	A 1.145	Kr 1.159	Xe 1.137

[a] The meaning of Q' and Q'' is the same as in Table IV.

The application of the inequalities method to a set of α's corresponding to those in Table IV was discussed in ref 9a. It is to be expected that both kinds of the Q' diminish distinctly, the Q'' slightly from the Ne type to the Xe type. In Table IV the Q' values fulfill this expectation but the Q'' are somewhat irregular for the A, Kr, Xe types and their average (1.319) is considerably smaller than Q'' (Ne) 1.479. This indicates that α for F^- is relatively too large. To become consistent with the other values the ratio $Q'(F^-/Ne)$ should be $1.319 \times 2.67 = 3.52$ and $\alpha(F^-)$ 1.39 instead of 1.56.

In Table V the BF values are tested the same way. The comparison of the Q'' for the Ne (1.144) and Xe (1.137) types shows the expected slight decrease, the only small irregularity is that the Kr value (1.159) is somewhat larger than both. An analogous situation was found in 1934[9a] when the method of inequalities was applied to R_D. At that time R(Kr) appeared to be somewhat uncertain and it was shown that it would be sufficient to change the latter from 6.37 to 6.44 cm^3 (1.1%) in order to avoid the irregularity. The remeasurement[15] of the refractivities of the heavy noble gases gave for R_D of Kr 6.397 and of Xe 10.435 instead of the previous 10.42, but as Table V shows, these changes do not remove completely the irregularity of Q'' for the α values. For the sake of comparison it may be said that in order to change Q'' for the Kr type from 1.159 to the regular value 1.142 it would be sufficient to change α(Kr) from 2.485 to 2.504 Å^3 (0.76%). This is out of the question but there are possibilities of small inaccuracies of the data involving some ions. For instance, it has been mentioned[7] for other reasons that R of solid RbF may not be correct. If a reinvestigation would lead to $\alpha(Rb^+)$ 1.463 instead of 1.485, Q'' for the Kr type would become 1.142.

The main result of the above discussion of Table V is that it does not contain any indication that $\alpha(F^-)$ 0.95 is considerably too small. It may also be mentioned that this value nearly coincides with the average 0.88 ± 0.09 of values obtained by Hajj, Pauling, Ruffa, and Tessman–Kahn–Shockley, as listed in a recent investigation.[16]

(14) The exceptional behavior of H^- is due to the extreme ratio 2.000 of the negative:positive charges composing it. For the anions F^- to I^- this ratio decreases only between 1.111 and 1.019. Hence it is not surprising that the inequalities regularities do not apply completely for the series H^-, He, and Li^+. For their above CH value Q'' (20.69) is much larger than the smaller Q' (7.190). More surprising is that even purely mathematically in a table analogous to Table II but for z values 1 to 4 the first Q''' (1.1852) is distinctly larger than the second Q'' (1.1250). These questions are beyond the main purpose of the present article.

(15) D. Damköhler, *Z. Phys. Chem.*, **27B**, 130 (1934).

(16) F. Hajj, *J. Chem. Phys.*, **44**, 4618 (1966).

Flow Birefringence of Real Polymer Chains. Theory

by Kazuo Nagai

Government Industrial Research Institute, Osaka, Midorigaoka 1, Ikeda, Osaka, Japan *(Received July 14, 1969)*

A theory of flow birefringence of dilute polymer solutions in the steady, laminar flow is developed on the basis of Gotlib and Svetlov's distribution function. The hydrodynamic interaction is neglected. The ratio of the intrinsic birefringence to the intrinsic viscosity, or the stress-optical coefficient, is found to be proportional to the flow-birefringence optical anisotropy of Kuhn's random link, $\Delta\Gamma_f = {}^3/_2\langle \mathrm{Tr}\, \mathbf{f}\rangle^{-1}\langle \mathrm{Tr}\, \hat{\boldsymbol{\gamma}}\mathbf{f}\rangle$, where $\mathbf{f}$ is the tensor of frictional moments, $\hat{\boldsymbol{\gamma}}$ is the optical polarizability tensor made traceless, Tr denotes the trace, and the averages refer to those on a free chain. If a polymer chain is approximated by a deformable ensemble of point frictions, we find $\langle \mathrm{Tr}\, \mathbf{f}\rangle = (\Sigma\zeta_i)^{-1}\Sigma_{i<j}\zeta_i\zeta_j\langle r_{ij}^2\rangle$ and $\langle \mathrm{Tr}\, \hat{\boldsymbol{\gamma}}\mathbf{f}\rangle = (\Sigma\zeta_i)^{-1}\Sigma_{i<j}\langle \mathrm{Tr}\, \hat{\boldsymbol{\gamma}}\, \mathbf{r}_{ij}\mathbf{r}_{ij}^{\mathrm{T}}\rangle$, where ζ_i is the friction constant of point i, $\mathbf{r}_{ij}$ is the vector connecting points i and j, r_{ij} is its magnitude, and T denotes the transpose. $\Delta\Gamma_f$ is calculated for real polymer chains with fixed bond lengths and angles and with hindered, interdependent internal rotations, on the basis of the rotational-isomeric-state approximation and the additivity principle of bond polarizabilities. It is assumed that frictions are concentrated on skeletal atoms. Expressions are derived for the two cases: finite chains of an arbitrary bond sequence and stereoregular chains of infinite length. In the latter case it is analytically verified that $\Delta\Gamma_f$ agrees with the strain-birefringence optical anisotropy of Kuhn's random link $\Delta\Gamma_s = {}^3/_2\langle r^2\rangle^{-1}\langle \mathbf{r}^{\mathrm{T}}\hat{\boldsymbol{\gamma}}\mathbf{r}\rangle$ where $\mathbf{r}$ stands for the end-to-end vector. ($\Delta\Gamma_s$ is obtained experimentally from photoelastic measurements on rubberlike materials.) Concise derivations of, and compact expressions for, $\langle r^2\rangle$, $\Delta\Gamma_s$, etc., are given for stereoregular chains of infinite length.

I. Introduction

Flow birefringence of dilute solutions of flexible polymer molecules has been theoretically treated by many authors on various models. In their pioneering work Kuhn and Kuhn[1-3] treated the simplest model, the elastic dumbbell model, *i.e.*, two beads connected by a spring. Zimm[4] discussed the multi-spring-bead model, or the Rouse model. Gotlib and Svetlov[5] examined the Kratky-Porod persistent chain model. Various effects have also been studied; the hydrodynamic interaction by Zimm[4] and Cerf,[6] the inner viscosity by Cerf,[6] the "form" anisotropy by Copic,[7] Tsvetkov,[8] and Koyama,[9] the deformation of polymer chains in a laminar flow by Peterlin,[10] and so on. Theoretical aspects were reviewed by Jerrad,[11] and theoretical as well as comprehensive experimental results by Tsvetkov[8] and Janeschitz-Kriegl.[12]

All the theories cited above were based on hypothetical models of polymer chains. Realistic models with fixed bond lengths and angles and with hindered, interdependent internal rotations have never been considered as yet. This paper concerns a general theory based on such models. The intention of the theory is to describe the flow birefringence in terms of basic, geometrical, and optical parameters of polymer chains. We have particular interest in the relation of the stress-optical coefficient $[n]/2[\eta]$ obtained from the flow birefringence, where $[n]$ and $[\eta]$ are the intrinsic birefringence and viscosity, respectively, with that from the strain birefringence. Methods for calculating the latter quantity have recently been well developed.[13-16]

In the present treatment we neglect the hydrodynamic interaction and the excluded-volume effect. For the multi-spring-bead model Cerf[6] has shown that both $[n]$ and $[\eta]$ are significantly influenced, but the ratio $[n]/2[\eta]$ is little affected, by the hydrodynamic interaction. We expect that this may be the case with our more sophisticated models.

In the course of this work we found new methods of calculations, and new expressions, for the mean-square end-to-end distance, the mean-square radius of gyration, and the stress-optical coefficient, of stereoregular polymer chains of infinite length. These results are also included here. An application of the theory to

(1) W. Kuhn and H. Kuhn, *Helv. Chim. Acta*, **26**, 1394 (1943).

(2) W. Kuhn and H. Kuhn, *ibid.*, **28**, 1355 (1945); **29**, 39, 71, 830 (1946).

(3) W. Kuhn and H. Kuhn, *J. Colloid Sci.*, **3**, 11 (1948).

(4) B. H. Zimm, *J. Chem. Phys.*, **24**, 269 (1956).

(5) Yu. Ya. Gotlib and Yu. Ye. Svetlov, *Dokl. Akad. Nauk, SSSR*, **168**, 621 (1966).

(6) R. Cerf, *J. Phys. Radium*, **19**, 122 (1958); see also ref 11, p 415.

(7) M. Copic, *J. Polymer Sci.*, **20**, 593 (1956); *J. Chem. Phys.*, **26**, 1382 (1957).

(8) V. N. Tsvetkov in "Newer Methods of Polymer Characterization," B. Ke, Ed., Interscience Publishers, New York, N. Y., 1964, Chapter 14.

(9) R. Koyama, *J. Phys. Soc. Jap.*, **16**, 1366 (1961); **19**, 1709 (1964).

(10) A. Peterlin, *J. Chem. Phys.*, **39**, 224 (1963).

(11) H. G. Jerrad, *Chem. Rev.*, **59**, 345 (1959).

(12) H. Janeshitz-Kriegl, *Advan. Polymer Sci.*, **6**, 170 (1969).

(13) K. Nagai, *J. Chem. Phys.*, **40**, 2818 (1964).

(14) (a) K. Nagai, *J. Chem. Phys.*, **47**, 2052 (1967); (b) *ibid.*, **51**, 1265 (1969).

(15) P. J. Flory, R. L. Jernigan, and A. E. Tonelli, *J. Chem. Phys.*, **48**, 3822 (1968).

(16) P. J. Flory, "Statistical Mechanics of Chain Molecules," Interscience Publishers, New York, N. Y., 1969, Chapter IX.

n-alkanes is reported in the succeeding paper.[17] Preliminary results of this work were published elsewhere.[18]

II. Flow Birefringence in the Absence of the Hydrodynamic Interaction

We consider the dynamic and optical behavior of a polymer chain in the steady, laminar flow with a velocity (Gy 0 0) in the xyz coordinate system, where G is the velocity gradient, in the absence of the hydrodynamic interaction. A polymer chain is approximated by a deformable ensemble of $n + 1$ point frictions, numbered 1, 2, ..., $n + 1$, with ζ_i being the friction constant of point i. The optical property of the chain will be introduced in a later stage. We want to calculate the intrinsic birefringence and the intrinsic viscosity. Some intermediate relations in the work of Gotlib and Svetlov,[5] which were originally derived for the persistent chain, appeared general enough to be adaptable to the present model. Use of their relations led to a minor inconsistency, indicating the presence of some errors in their treatment. We therefore decided to reexamine the problem by a different method. Our model is more general and treatments appear more elegant than theirs.

In another paper, Gotlib and Svetlov[19] derived a distribution function for a polymer chain in a laminar flow, starting with the Kirkwood[20] general diffusion equation. Their function, with an obvious generalization to the present model and with a trivial constant factor omitted, becomes

$$W_G = (1 + {}^1/_2 G f_{xy}/kT) \exp(-E_{\text{int}}/kT) \qquad (1)$$

where E_{int} is the internal conformational energy of the polymer chain, k is the Boltzmann constant, and T is the absolute temperature. f_{xy} is the xy component of the tensor of frictional moments, $\mathbf{f}$, which is expressed in a dyadic form

$$\mathbf{f} = \sum_{i=1}^{n+1} \zeta_i (\mathbf{r}_i - \mathbf{r}_{\text{cf}})(\mathbf{r}_i - \mathbf{r}_{\text{cf}})^{\text{T}} \qquad (2)$$

where $\mathbf{r}_i$ and $\mathbf{r}_{\text{cf}}$ are the coordinate vectors of point i and the center of friction, respectively, and the superscript T denotes the transpose. $\mathbf{r}_{\text{cf}}$ is given, on the analogy of the center of masses, by

$$\mathbf{r}_{\text{cf}} = (\sum \zeta_i)^{-1} \sum_i \zeta_i \mathbf{r}_i \qquad (3)$$

W_G in eq 1 is valid only up to the linear term in G. An expression analogous to eq 1 was derived in a more intuitive manner by Kramers[21] as early as 1946.

The average of the optical polarizability tensor $\boldsymbol{\gamma}$ can be obtained by averaging it over the internal and external coordinates of the polymer chain. Using eq 1 we have

$$\langle \boldsymbol{\gamma} \rangle_G = (8\pi^2)^{-1} Z_G^{-1} \int \cdots \int \boldsymbol{\gamma} (1 + {}^1/_2 G f_{xy}/kT) \times \exp(-E_{\text{int}}/kT)\, \mathrm{d}\Omega \mathrm{d}\{\theta\} \qquad (4)$$

with

$$Z_G = (8\pi^2)^{-1} \int \cdots \int (1 + {}^1/_2 G f_{xy}/kT) \times \exp(-E_{\text{int}}/kT)\, \mathrm{d}\Omega \mathrm{d}\{\theta\} \qquad (5)$$

where Ω represents a set of Eulerian angles, which specify the orientation of the polymer chain with respect to the external xyz system, and $\{\theta\}$ represents a set of internal coordinates, or, more specifically, internal-rotational angles about skeletal bonds. $\boldsymbol{\gamma}$ can be expressed

$$\boldsymbol{\gamma} = \gamma_1 \boldsymbol{\mu}_{\gamma_1} \boldsymbol{\mu}_{\gamma_1}^{\text{T}} + \gamma_2 \boldsymbol{\mu}_{\gamma_2} \boldsymbol{\mu}_{\gamma_2}^{\text{T}} + \gamma_3 \boldsymbol{\mu}_{\gamma_3} \boldsymbol{\mu}_{\gamma_3}^{\text{T}} \qquad (6)$$

$$\boldsymbol{\mu}_{\gamma_k} = \begin{bmatrix} \mu_{\gamma_k x} \\ \mu_{\gamma_k y} \\ \mu_{\gamma_k z} \end{bmatrix} \qquad k = 1, 2, 3 \qquad (7)$$

where γ_1, γ_2, and γ_3 are the three principal values of $\boldsymbol{\gamma}$, and $\boldsymbol{\mu}_{\gamma_1}$, $\boldsymbol{\mu}_{\gamma_2}$, and $\boldsymbol{\mu}_{\gamma_3}$ are the unit vectors along the corresponding principal axes. Similarly, $\mathbf{f}$ can be expressed

$$\mathbf{f} = f_1 \boldsymbol{\mu}_{f_1} \boldsymbol{\mu}_{f_1}^{\text{T}} + f_2 \boldsymbol{\mu}_{f_2} \boldsymbol{\mu}_{f_2}^{\text{T}} + f_3 \boldsymbol{\mu}_{f_3} \boldsymbol{\mu}_{f_3}^{\text{T}} \qquad (8)$$

$$\boldsymbol{\mu}_{f_k} = \begin{bmatrix} \mu_{f_k x} \\ \mu_{f_k y} \\ \mu_{f_k z} \end{bmatrix} \qquad k = 1, 2, 3 \qquad (9)$$

Substitution of the xy component of $\mathbf{f}$ in eq 8 into eq 5 and integrating over Ω yields

$$Z_G = Z_0 = \int \exp(-E_{\text{int}}/kT)\, \mathrm{d}\{\theta\} \qquad (10)$$

where Z_0 is the partition function of the polymer chain in its free state. In obtaining eq 10 use was made of

$$(8\pi^2)^{-1} \int \mathrm{d}\Omega = 1 \quad \text{and} \quad (8\pi^2)^{-1} \int \mu_{f_k x} \mu_{f_k y}\, \mathrm{d}\Omega = 0$$

Equation 10 implies that the internal free energy is not changed by the flow field up to the linear term in G. Equation 4 involves the two integrals

$$\mathbf{I}_1 = (8\pi^2)^{-1} \int \boldsymbol{\gamma}\, \mathrm{d}\Omega \qquad (11)$$

$$\mathbf{I}_2 = (8\pi^2)^{-1} \int \boldsymbol{\gamma} f_{xy}\, \mathrm{d}\Omega \qquad (12)$$

Substitution of eq 6 into eq 11 and integration yield

$$\mathbf{I}_1 = {}^1/_3 (\mathrm{Tr}\, \boldsymbol{\gamma}) \mathbf{E}_3 \qquad (13)$$

where Tr denotes the trace of a tensor and $\mathbf{E}_\nu$ is the unit matrix of order ν. In going to eq 13, use was made of

$$(8\pi^2)^{-1} \int \mu_{\gamma_k x}{}^2\, \mathrm{d}\Omega = {}^1/_3$$

$$(8\pi^2)^{-1} \int \mu_{\gamma_k x} \mu_{\gamma_k y}\, \mathrm{d}\Omega = 0 \qquad \text{etc.}$$

(17) K. Nagai, *J. Phys. Chem.*, **74**, 3422 (1970).

(18) K. Nagai, *Rep. Prog. Polymer Phys. Jap.*, **12**, 41 (1969).

(19) Yu. Ya. Gotlib and Yu. Ye. Svetlov, *Vysokomol. Soedin.*, **8**, 1517 (1966).

(20) J. G. Kirkwood, *Rec. Trav. Chim.*, **68**, 649 (1949); *J. Polymer Sci.*, **12**, 1 (1954).

(21) H. A. Kramers, *J. Chem. Phys.*, **14**, 415 (1946).

Substituting eq 6 and the xy component of $\mathbf{f}$ in eq 8 into eq 12 we obtain

$$\mathbf{I}_2 = (8\pi^2)^{-1}\int(\gamma_1\underline{\mu}_{\gamma_1}\underline{\mu}_{\gamma_1}^{\mathrm{T}} + \gamma_2\underline{\mu}_{\gamma_2}\underline{\mu}_{\gamma_2}^{\mathrm{T}} + \gamma_3\underline{\mu}_{\gamma_3}\underline{\mu}_{\gamma_3}^{\mathrm{T}})(f_1\mu_{f_1x}\mu_{f_1y} + f_2\mu_{f_2x}\mu_{f_2y} + f_3\mu_{f_3x}\mu_{f_3y})\,\mathrm{d}\Omega \quad (14)$$

Upon integration, all other than xy and yx elements vanish owing to symmetry, whereas the latter become

$$(\mathbf{I}_2)_{xy} = (\mathbf{I}_2)_{yx} = \frac{1}{30}\sum_{k,l=1,2,3}\gamma_k f_l[3(\underline{\mu}_{\gamma_k}\cdot\underline{\mu}_{f_l})^2 - 1]$$
$$= \frac{1}{30}[3\mathrm{Tr}(\boldsymbol{\gamma}\mathbf{f}) - (\mathrm{Tr}\,\boldsymbol{\gamma})(\mathrm{Tr}\,\mathbf{f})] \quad (15)$$

by utilizing

$$(8\pi^2)^{-1}\int\mu_{\gamma_k x}\mu_{\gamma_k y}\mu_{f_l x}\mu_{f_l y}\,\mathrm{d}\Omega = {}^1/_{30}\,[3(\underline{\mu}_{\gamma_k}\cdot\underline{\mu}_{f_l})^2 - 1]$$

Thus we have

$$\mathbf{I}_2 = \frac{1}{30}\begin{bmatrix} 3\mathrm{Tr}(\boldsymbol{\gamma}\mathbf{f}) - (\mathrm{Tr}\,\boldsymbol{\gamma})(\mathrm{Tr}\,\mathbf{f}) & 0 & 0 \\ 0 & 0 & 0 \\ 0 & 0 & 0 \end{bmatrix} \quad (16)$$

$$\langle\boldsymbol{\gamma}\rangle_G = \frac{1}{3}\langle\mathrm{Tr}\,\boldsymbol{\gamma}\rangle\mathbf{E}_3 + \frac{G}{60kT}\begin{bmatrix} \langle 3\mathrm{Tr}(\boldsymbol{\gamma}\mathbf{f}) - (\mathrm{Tr}\,\boldsymbol{\gamma})(\mathrm{Tr}\,\mathbf{f})\rangle & 0 & 0 \\ 0 & 0 & 0 \\ 0 & 0 & 0 \end{bmatrix} \quad (17)$$

Replacing the integrals on Ω in eq 4 with $\mathbf{I}_1$ and $\mathbf{I}_2$, eq 13 and 16, and then integrating over $\{\theta\}$, we find eq 17, where the averages without subscripts refer to those on a free chain. From eq 17 it is obvious that two of the axes of the principal polarizabilities make 45 and 135° with the positive x axis, respectively, both lying in the xy plane, while the remaining one is along the z axis. Namely, the extinction angle is 45°. The difference between the first two principal polarizabilities (45° value minus 135° value) is

$$\langle\Delta\gamma\rangle_G = 2(\langle\boldsymbol{\gamma}\rangle_G)_{xy}$$
$$= (G/30kT)\langle 3\mathrm{Tr}(\boldsymbol{\gamma}\mathbf{f}) - (\mathrm{Tr}\,\boldsymbol{\gamma})(\mathrm{Tr}\,\mathbf{f})\rangle \quad (18)$$

This $\langle\Delta\gamma\rangle_G$ can be converted to the birefringence Δn of the solution by the Lorentz–Lorenz relation. If the solution is very dilute and Δn is small, we obtain

$$\Delta n = (2\pi/9)[(n_0^2 + 2)^2/n_0]N_{\mathrm{p}}\langle\Delta\gamma\rangle_G \quad (19)$$

where n_0 is the refractive index of a solvent and N_{p} is the number of polymer molecules in 1 cm³ of the solution. The intrinsic birefringence becomes, according to eq 18 and 19

$$[n] = \lim_{\substack{c\to 0\\ G\to 0}}\Delta n/cG\eta_0$$
$$= \frac{\pi}{135kT}\frac{(n_0^2 + 2)^2}{n_0\eta_0}\frac{N_{\mathrm{A}}}{M}\langle 3\mathrm{Tr}(\boldsymbol{\gamma}\mathbf{f}) - (\mathrm{Tr}\,\boldsymbol{\gamma})(\mathrm{Tr}\,\mathbf{f})\rangle \quad (20)$$

where c is the concentration of the polymer in grams per cubic centimeter, M is the molecular weight, N_{A} is the Avogadro number, and η_0 is the viscosity of a solvent. Comparison of our results with those of Gotlib and Svetlov[5] reveals that $(N + 1)^{-1}$ is erroneously included in eq 2, and η_0^{-1} is lacking in eq 4 of ref 5.

The intrinsic viscosity can readily be obtained by generalizing the Debye[22] method. The increase in viscosity by dissolved polymer molecules is given[23] by

$$\eta - \eta_0 = {}^1/_2N_{\mathrm{p}}\left\langle\sum_i\zeta_i(y_i - y_{\mathrm{cf}})^2\right\rangle_G$$
$$= {}^1/_2N_{\mathrm{p}}(\langle\mathbf{f}\rangle_G)_{yy}$$
$$= {}^1/_6N_{\mathrm{p}}\langle\mathrm{Tr}\,\mathbf{f}\rangle \quad (21)$$

with η being the viscosity of the solution. The third equality is valid only as far as up to the linear term in G is concerned. The intrinsic viscosity becomes, therefore

$$[\eta] = \lim_{c\to 0}(\eta - \eta_0)/c\eta_0 = (N_{\mathrm{A}}/6M\eta_0)\langle\mathrm{Tr}\,\mathbf{f}\rangle \quad (22)$$

Combining eq 20 and 22 we obtain for the flow-birefringence stress-optical coefficient

$$C_{\mathrm{f}} = [n]/2[\eta] = (2\pi/45kT)[(n_0^2 + 2)^2/n_0]\Delta\Gamma_{\mathrm{f}} \quad (23)$$

with

$$\Delta\Gamma_{\mathrm{f}} = {}^1/_2\langle\mathrm{Tr}\,\mathbf{f}\rangle^{-1}\langle 3\mathrm{Tr}(\boldsymbol{\gamma}\mathbf{f}) - (\mathrm{Tr}\,\boldsymbol{\gamma})(\mathrm{Tr}\,\mathbf{f})\rangle \quad (24)$$

$\Delta\Gamma_{\mathrm{f}}$ may be called the flow-birefringence optical anisotropy of Kuhn's random link, inasmuch as, in Kuhn and Kuhn's theory,[1-3] $\Delta\Gamma_{\mathrm{f}}$ is equal to the optical anisotropy of Kuhn's random link.

The strain-birefringence stress-optical coefficient of polymeric networks is given by

$$C_{\mathrm{s}} = (2\pi/45kT)[(\bar{n}^2 + 2)^2/\bar{n}]\Delta\Gamma_{\mathrm{s}} \quad (25)$$

where $\bar{n}$ is the mean refractive index of a sample, and $\Delta\Gamma_{\mathrm{s}}$ is equal to the optical anisotropy of Kuhn's random link for the random chain,[24] while

$$\Delta\Gamma_{\mathrm{s}} = {}^1/_2\langle r^2\rangle^{-1}\langle 3\mathbf{r}^{\mathrm{T}}\boldsymbol{\gamma}\mathbf{r} - r^2\mathrm{Tr}\,\boldsymbol{\gamma}\rangle$$
$$= {}^1/_2\langle\mathrm{Tr}\,\mathbf{r}\mathbf{r}^{\mathrm{T}}\rangle^{-1}\langle 3\mathrm{Tr}(\boldsymbol{\gamma}\mathbf{r}\mathbf{r}^{\mathrm{T}}) - (\mathrm{Tr}\,\mathbf{r}\mathbf{r}^{\mathrm{T}})(\mathrm{Tr}\,\boldsymbol{\gamma})\rangle \quad (26)$$

(22) P. Debye, *J. Chem. Phys.*, **14**, 636 (1946).

(23) N. Saito, "Kobunshibutsurigaku," Shokabo, Tokyo, 1958, p 178.

(24) W. Kuhn and F. Grün, *Kolloid Z.*, **101**, 248 (1942).

for real polymer chains,[13,25] where the averages refer to those on a free chain, $\mathbf{r}$ is the end-to-end vector, and r is its magnitude. We note that eq 25 with eq 26 is valid only at the limit of infinite chain length,[13,24,25] in contrast with eq 23 with eq 24 which is valid for chains of arbitrary length. If, following Jernigan and Flory,[26] we introduce the traceless tensor

$$\hat{\boldsymbol{\gamma}} = \boldsymbol{\gamma} - {}^1/_3(\mathrm{Tr}\ \boldsymbol{\gamma})\mathbf{E}_3 \tag{27}$$

we have

$$\Delta\Gamma_f = {}^3/_2\langle \mathrm{Tr}\ \mathbf{f}\rangle^{-1}\langle \mathrm{Tr}\ \hat{\boldsymbol{\gamma}}\mathbf{f}\rangle \tag{28}$$

and[15,16]

$$\Delta\Gamma_s = {}^3/_2\langle r^2\rangle^{-1}\langle \mathbf{r}^{\mathrm{T}}\hat{\boldsymbol{\gamma}}\mathbf{r}\rangle = {}^3/_2\langle \mathrm{Tr}\ \mathbf{r}\mathbf{r}^{\mathrm{T}}\rangle^{-1}\langle \mathrm{Tr}\ \hat{\boldsymbol{\gamma}}\mathbf{r}\mathbf{r}^{\mathrm{T}}\rangle \tag{29}$$

The formal similarity of $\Delta\Gamma_f$ with $\Delta\Gamma_s$ and the formal simplicity of both are noteworthy.

For later convenience we express $\mathbf{f}$ in terms of vectors connecting pairs of friction points. By utilizing eq 3 and

$$\mathbf{r}_{cf}\mathbf{r}_{cf}^{\mathrm{T}} = (\sum \zeta_i)^{-2}\sum_{i,j}\zeta_i\zeta_j\mathbf{r}_i\mathbf{r}_j^{\mathrm{T}} \tag{30}$$

obtained therefrom, $\mathbf{f}$ in eq 2 can be rearranged successively as

$$\begin{aligned}
\mathbf{f} &= \sum_i \zeta_i\mathbf{r}_i\mathbf{r}_i^{\mathrm{T}} - (\sum \zeta_i)\mathbf{r}_{cf}\mathbf{r}_{cf}^{\mathrm{T}} \\
&= \sum_i \zeta_i\mathbf{r}_i\mathbf{r}_i^{\mathrm{T}} - (\sum \zeta_i)^{-1}\sum_{i,j}\zeta_i\zeta_j\mathbf{r}_i\mathbf{r}_j^{\mathrm{T}} \\
&= (\sum \zeta_i)^{-1}(\sum_{i,j}\zeta_i\zeta_j\mathbf{r}_i\mathbf{r}_i^{\mathrm{T}} - \sum_{i,j}\zeta_i\zeta_j\mathbf{r}_i\mathbf{r}_j^{\mathrm{T}}) \\
&= \frac{1}{2}(\sum \zeta_i)^{-1}\sum_{i,j}\zeta_i\zeta_j(\mathbf{r}_i\mathbf{r}_i^{\mathrm{T}} + \\
&\qquad \mathbf{r}_j\mathbf{r}_j^{\mathrm{T}} - \mathbf{r}_i\mathbf{r}_j^{\mathrm{T}} - \mathbf{r}_j\mathbf{r}_i^{\mathrm{T}}) \\
&= (\sum \zeta_i)^{-1}\sum_{i<j}\zeta_i\zeta_j\mathbf{r}_{ij}\mathbf{r}_{ij}^{\mathrm{T}}
\end{aligned} \tag{31}$$

where $\mathbf{r}_{ij} = \mathbf{r}_j - \mathbf{r}_i$. We therefore obtain

$$\begin{aligned}
\langle \mathrm{Tr}\ \hat{\boldsymbol{\gamma}}\mathbf{f}\rangle &= (\sum \zeta_i)^{-1}\sum_{i<j}\zeta_i\zeta_j\langle \mathrm{Tr}\ \hat{\boldsymbol{\gamma}}\mathbf{r}_{ij}\mathbf{r}_{ij}^{\mathrm{T}}\rangle \\
&= (\sum \zeta_i)^{-1}\sum_{i<j}\zeta_i\zeta_j\langle \mathbf{r}_{ij}^{\mathrm{T}}\hat{\boldsymbol{\gamma}}\mathbf{r}_{ij}\rangle
\end{aligned} \tag{32}$$

and

$$\langle \mathrm{Tr}\ \mathbf{f}\rangle = (\sum \zeta_i)^{-1}\sum_{i<j}\zeta_i\zeta_j\langle r_{ij}^2\rangle \tag{33}$$

where $r_{ij} = |\mathbf{r}_{ij}|$. It is seen that if all ζ's are equal to unity, $(n+1)^{-1}\langle \mathrm{Tr}\ \mathbf{f}\rangle$ becomes the mean-square radius of gyration. We note that $\langle \mathrm{Tr}\ \mathbf{f}\rangle$ can be related to the mean rotatory diffusion constant D_r by Einstein's relation

$$D_r = kT\langle \mathrm{Tr}\ \mathbf{f}\rangle^{-1} \tag{34}$$

III. Expression of Tr f and Tr $\hat{\boldsymbol{\gamma}}$f in Terms of Structural Parameters and Bond Polarizabilities

Both $\langle \mathrm{Tr}\ \mathbf{f}\rangle$ and $\langle \mathrm{Tr}\ \hat{\boldsymbol{\gamma}}\mathbf{f}\rangle$, and hence $\Delta\Gamma_f$, can be calculated for real polymer chains, by assuming the simple additivity principle of bond polarizabilities and the rotational isomeric state model for skeletal bond rotations. Consider a linear polymer molecule involving n skeletal bonds which are numbered 1, 2, ..., n, from one end to the other. Two terminal bonds, *e.g.*, one C–H bond in every terminal methyl group in n-alkanes, are included in these n bonds. Skeletal atoms also are numbered 1, 2, ..., $n+1$; skeletal bond i connects skeletal atoms i and $i+1$. All bond lengths and bond angles are assumed to be fixed, and chain flexibility is effected by rotation about skeletal bonds. The friction of the polymer chain is assumed to be concentrated on skeletal atoms, ζ_i being the friction constant of skeletal atom i.

We introduce a set of cartesian coordinate systems as follows.[27] Coordinate system i is attached to the plane determined by skeletal bonds $i-1$ and i in the following way. The x axis is in the direction of skeletal bond i and the y axis is in the plane of skeletal bonds $i-1$ and i, making an acute angle with skeletal bond $i-1$. The z axis is chosen so as to constitute a right-handed system together with the x and y axes. The internal-rotational angle θ_i about skeletal bond i is measured from the trans position toward the direction of the right-handed twist of the polymer chain. Two presentations $\mathbf{v}_i$ and $\mathbf{v}_{i+1}$ of components of a vector in coordinate systems i and $i+1$ are correlated by

$$\mathbf{v}_i = \mathbf{A}_i\mathbf{v}_{i+1} \tag{35}$$

$$\mathbf{A}_i = \begin{bmatrix} \alpha_i & \beta_i & 0 \\ \beta_i\cos\theta_i & -\alpha_i\cos\theta_i & \sin\theta_i \\ \beta_i\sin\theta_i & -\alpha_i\sin\theta_i & -\cos\theta_i \end{bmatrix} \tag{36}$$

where $\mathbf{A}_i$ is the transformation matrix, and $\alpha_i = \cos\omega_i$ and $\beta_i = \sin\omega_i$, with ω_i being the angle between bonds i and $i+1$, *i.e.*, the supplementary bond angle. bond vector $\mathbf{b}_i$ of skeletal bond i is now expressed in its own coordinate system as $b_i\mathbf{e}_3$, where b_i is the length of the bond and $\mathbf{e}_\gamma$ is a γ-dimensional vector defined by

$$\mathbf{e}_\gamma = (1\ 0\ 0\ \ldots\ 0)^{\mathrm{T}} \tag{37}$$

We first calculate the square end-to-end distance $r_{1,n+1}^2 \equiv r^2$ and Tr $\mathbf{f}$. Their averaging is postponed later. The former quantity can be expressed

$$\begin{aligned}
r^2 &= \sum_{i=1}^{n} b_i^2 + 2\sum_{i<j}\mathbf{b}_i\cdot\mathbf{b}_j \\
&= \sum_{i=1}^{n} b_i^2 + 2\sum_{i<j} b_ib_j\mathbf{e}_3^{\mathrm{T}}\mathbf{A}_i\mathbf{A}_{i+1}\ldots\mathbf{A}_{j-1}\mathbf{e}_3
\end{aligned} \tag{38}$$

According to a modification[14a] of Flory and Jernigan's method,[28] eq 38 can be cast into

(25) K. Nagai and T. Ishikawa, *J. Chem. Phys.*, **43**, 4508 (1965).
(26) R. L. Jernigan and P. J. Flory, *ibid.*, **47**, 1999 (1967).
(27) K. Nagai, *ibid.*, **31**, 1169 (1969).
(28) P. J. Flory and R. L. Jernigan, *ibid.*, **42**, 3509 (1965).

$$r^2 = (1\ 0\ 0)\left[\prod_{i=1}^{n}\begin{bmatrix}1 & 2b\mathbf{e}_3{}^{\mathrm{T}}\mathbf{A} & b^2\\ \mathbf{0} & \mathbf{A} & b\mathbf{e}_3\\ 0 & \mathbf{0} & 1\end{bmatrix}_i\right]\begin{bmatrix}0\\ \mathbf{0}\\ 1\end{bmatrix} \quad (39)$$

where **0**'s are null matrices whose orders are so chosen as to be consistent with other nonzero parts of matrices, and the subscript i to the bracket is implied to apply to b and **A** as subscripts. (Similar notations are used throughout this paper.) $\mathbf{A}_1$ is indefinite in θ_1 and $\mathbf{A}_n$ is so both in ω_n and θ_n. These angles can be chosen arbitrarily, as is apparent from eq 39. On the other hand

$$(\sum \zeta_i)\mathrm{Tr}\,\mathbf{f} = \sum_{i<j}\zeta_i\zeta_j r_{ij}{}^2 = \sum_{i<j}\zeta_i\zeta_j(1\ 0\ 0)\times\left[\prod_{k=i}^{j-1}\begin{bmatrix}1 & 2b\mathbf{e}_3{}^{\mathrm{T}}\mathbf{A} & b^2\\ \mathbf{0} & \mathbf{A} & b\mathbf{e}_3\\ 0 & \mathbf{0} & 1\end{bmatrix}_k\right]\begin{bmatrix}0\\ \mathbf{0}\\ 1\end{bmatrix} \quad (40)$$

which is rewritten

$$(\sum \zeta_i)\mathrm{Tr}\,\mathbf{f} = (1\ 0\ 0\ 0\ 0)\times\left[\prod_{i=1}^{n+1}\begin{bmatrix}1 & \zeta & 2\zeta b\mathbf{e}_3{}^{\mathrm{T}}\mathbf{A} & \zeta b^2 & 0\\ 0 & 1 & 2b\mathbf{e}_3{}^{\mathrm{T}}\mathbf{A} & b^2 & 0\\ \mathbf{0} & \mathbf{0} & \mathbf{A} & b\mathbf{e}_3 & \mathbf{0}\\ 0 & 0 & \mathbf{0} & 1 & \zeta\\ 0 & 0 & \mathbf{0} & 0 & 1\end{bmatrix}_i\right]\begin{bmatrix}0\\ 0\\ \mathbf{0}\\ 0\\ 1\end{bmatrix} \quad (41)$$

A similar expression (with $\zeta = 1$) was given previously in connection with the square radius of gyration.[29]

We next proceed to calculate Tr $\hat{\boldsymbol{\gamma}}\mathbf{f}$. We assume the simple additivity principle of bond polarizabilities.[30-32] According to this principle, each bond is assigned the three principal polarizabilities, α_1 in the direction of the bond and α_2 in the two directions perpendicular to the bond, and these polarizabilities are assumed independent of the conformation and environment of the molecule in which the bond exists. Polarizabilities of a whole molecule are obtained by adding tensorially polarizabilities of all bonds. As far as the anisotropy of polarizabilities is concerned, we can regard the bond as having only the longitudinal component of the magnitude $\alpha_1 - \alpha_2$. Bonds of our polymer chain are now grouped as follows. Bond $i\kappa$ is the κth bond of group i, where group i includes all bonds rigidly fixed to coordinate system i, except for skeletal bond $i - 1$. By this definition, skeletal bonds are dually indexed; skeletal bond i, or, say bond $i1$. The contribution of bond $i\kappa$ to the total polarizability $\boldsymbol{\gamma}$ is given by $(\alpha_1 - \alpha_2)_{i\kappa}\,\boldsymbol{\mu}_{i\kappa}\boldsymbol{\mu}_{i\kappa}{}^{\mathrm{T}}$, where $(\alpha_1 - \alpha_2)_{i\kappa}$ is the anisotropy of polarizabilities of the bond and $\boldsymbol{\mu}_{i\kappa}$ is the unit vector along the bond. We make $\boldsymbol{\gamma}$ traceless by so doing the tensor of polarizabilities of each bond, *i.e.*, $(\alpha_1 - \alpha_2)_{i\kappa}(\boldsymbol{\mu}_{i\kappa}\boldsymbol{\mu}_{i\kappa}{}^{\mathrm{T}} - {}^1/_3\mathbf{E}_3)$. Thus we can write

$$\hat{\boldsymbol{\gamma}} = \sum_{i=1}^{n}\hat{\boldsymbol{\gamma}}_i \quad (42)$$

$$\hat{\boldsymbol{\gamma}}_i = \sum_{\kappa}(\alpha_1 - \alpha_2)_{i\kappa}(\boldsymbol{\mu}_{i\kappa}\,\boldsymbol{\mu}_{i\kappa}{}^{\mathrm{T}} - {}^1/_3\mathbf{E}_3) \quad (43)$$

where $\hat{\boldsymbol{\gamma}}_i$ is the traceless tensor of polarizabilities of group i, and κ counts all bonds of the group. An expression of a tensor depends on a coordinate system in which its components are measured. We write the expression of $\hat{\boldsymbol{\gamma}}_i$ in coordinate system i especially as

$$\hat{\boldsymbol{\gamma}}_i = \Delta\hat{\boldsymbol{\alpha}}_i = \sum_{\kappa}(\alpha_1 - \alpha_2)_{i\kappa}(\boldsymbol{\mu}_{i\kappa}\,\boldsymbol{\mu}_{i\kappa}{}^{\mathrm{T}} - {}^1/_3\mathbf{E}_3) \quad (44)$$

where and hereafter

$$\boldsymbol{\mu}_{i\kappa} = (\mu_{i\kappa 1}\ \mu_{i\kappa 2}\ \mu_{i\kappa 3})^{\mathrm{T}} \quad (45)$$

is understood to be the expression of the unit vector in coordinate system i, though no particular indication is made.

From eq 32 and 42 we obtain

$$(\sum \zeta_i)\mathrm{Tr}\,\hat{\boldsymbol{\gamma}}\mathbf{f} = \sum_{i<j}\sum_{k}\zeta_i\zeta_j\langle\mathbf{r}_{ij}{}^{\mathrm{T}}\hat{\boldsymbol{\gamma}}_k\mathbf{r}_{ij}\rangle \quad (46)$$

For convenience we divide the sum into the three sums

$$(\sum \zeta_i)\mathrm{Tr}\,\hat{\boldsymbol{\gamma}}\mathbf{f} = S_1 + S_2 + S_3 \quad (47)$$

$$S_1 = \sum_{k<i<j} \quad (48a)$$

$$S_2 = \sum_{i\le k<j} \quad (48b)$$

$$S_3 = \sum_{i<j\le k} \quad (48c)$$

We observe that each term with specified i and j in S_2 is equivalent to $\mathbf{r}^{\mathrm{T}}\hat{\boldsymbol{\gamma}}\mathbf{r}$ in eq 29 if a subchain spanned by skeletal atoms i and j is regarded as a new chain. Therefore we can use previous results[14] for S_2. Terms in S_1 and S_3 are similar and even simpler. Important for the calculation of these quantities is the recognition of the facts that the nine components of a tensor are transformed from coordinate system $i + 1$ to coordinate system i by the direct product matrix of $\mathbf{A}_i$, *i.e.*, $\mathbf{A}_i \times \mathbf{A}_i$,[33,13-16] and this $\mathbf{A}_i \times \mathbf{A}_i$ can be reduced to the matrix $\mathbf{B}_i$ (eq 54 below) of lower order by utilizing the symmetry of $\hat{\boldsymbol{\gamma}}_k$ and $\mathbf{r}_{ij}\,\mathbf{r}_{ij}{}^{\mathrm{T}}$.[23,34] Flory and Jernigan's method[28] is also important for casting results into compact forms. Referring, for the methods of calculations, the reader to the previous papers cited above, we give only the final results

$$S_1 = \sum_{k<i<j}\Delta\hat{\boldsymbol{\alpha}}_k{}^{\dagger\mathrm{T}}\mathbf{g}\mathbf{B}_k\ \ldots\ \mathbf{B}_{i-1}(\zeta_i\mathbf{E}_6\ \mathbf{0}\ 0)\times\left[\prod_{l=i}^{j-1}\begin{bmatrix}\mathbf{B} & b\tilde{\mathbf{f}}(\mathbf{E}_3\times\mathbf{e}_2)\mathbf{A} & b^2\mathbf{e}_6\\ \mathbf{0} & \mathbf{A} & b\mathbf{e}_3\\ \mathbf{0} & \mathbf{0} & 1\end{bmatrix}_l\right]\begin{bmatrix}\mathbf{0}\\ \mathbf{0}\\ \zeta_j\end{bmatrix} \quad (49)$$

(29) K. Nagai, *J. Chem. Phys.*, **48**, 5646 (1968).
(30) E. H. L. Meyer and G. Otterbein, *Phys. Z.*, **32**, 290 (1931).
(31) S.-N. Wang, *J. Chem. Phys.*, **7**, 1012 (1939).
(32) K. G. Denbigh, *Trans. Faraday Soc.*, **36**, 936 (1940).
(33) K. Nagai, *J. Chem. Phys.*, **38**, 924 (1963).
(34) K. Nagai and T. Ishikawa, *ibid.*, **45**, 3128 (1966).

$$S_2 = \sum_{i \le k < j} \left\{ \zeta_i (\Delta\alpha_k^{\dagger T}\mathbf{g}\,0\,0) \begin{bmatrix} \prod_{l=k}^{j-1} \begin{bmatrix} \mathbf{B} & b\bar{\mathbf{f}}(\mathbf{E}_3 \times \mathbf{e}_2)\mathbf{A} & b^2\mathbf{e}_6 \\ \mathbf{0} & \mathbf{A} & b\mathbf{e}_3 \\ \mathbf{0} & \mathbf{0} & 1 \end{bmatrix}_l \end{bmatrix} \begin{bmatrix} \mathbf{0} \\ \mathbf{0} \\ \zeta_j \end{bmatrix} + (\zeta_i\,0) \begin{bmatrix} \prod_{l=i}^{k-1} \begin{bmatrix} 1 & 2b\mathbf{e}_3^T\mathbf{A} \\ \mathbf{0} & \mathbf{A} \end{bmatrix}_l \end{bmatrix} \begin{bmatrix} 0 \\ \mathbf{E}_3 \end{bmatrix} \times \right.$$

$$\left. \Delta\hat{\alpha}_k(\mathbf{E}_3\,\mathbf{0}) \begin{bmatrix} \prod_{l=k}^{j-1} \begin{bmatrix} \mathbf{A} & b\mathbf{e}_3 \\ \mathbf{0} & 1 \end{bmatrix}_l \end{bmatrix} \begin{bmatrix} \mathbf{0} \\ \zeta_j \end{bmatrix} + (\zeta_i\,0\,0) \begin{bmatrix} \prod_{l=i}^{k-1} \begin{bmatrix} 1 & 2b\mathbf{e}_3^T\mathbf{A} & b^2\mathbf{e}_6^T\mathbf{B} \\ \mathbf{0} & \mathbf{A} & b(\mathbf{E}_3 \times \mathbf{e}_2^T)\mathbf{B} \\ \mathbf{0} & \mathbf{0} & \mathbf{B} \end{bmatrix}_l \end{bmatrix} \begin{bmatrix} 0 \\ 0 \\ \Delta\alpha_k^{\dagger} \end{bmatrix} \zeta_j \right\} \quad (50)$$

$$S_3 = \sum_{i<j\le k} (\zeta_i\,0\,0) \begin{bmatrix} \prod_{l=i}^{j-1} \begin{bmatrix} 1 & 2b\mathbf{e}_3^T\mathbf{A} & b^2\mathbf{e}_6^T\mathbf{B} \\ \mathbf{0} & \mathbf{A} & b(\mathbf{E}_3 \times \mathbf{e}_2^T)\mathbf{B} \\ \mathbf{0} & \mathbf{0} & \mathbf{B} \end{bmatrix}_l \end{bmatrix} \begin{bmatrix} 0 \\ 0 \\ \zeta_j\mathbf{E}_6 \end{bmatrix} \mathbf{B}_j \cdots \mathbf{B}_{k-1}\Delta\hat{\alpha}_k^{\dagger} \quad (51)$$

$\bar{\mathbf{f}}$ is a diagonal matrix of order 6 whose first, fourth, and sixth elements are 2 and remaining ones are unity. $\mathbf{g}$ is a diagonal matrix of order 6 whose first, fourth, and sixth elements are unity and remaining ones are 2. Hence $\bar{\mathbf{f}}\mathbf{g} = 2\mathbf{E}_6$. The direct product of $\mathbf{a} = \{a_{ij}\}$ and $\mathbf{b} = \{b_{ij}\}$ is defined by

$$\mathbf{a} \times \mathbf{b} = \begin{bmatrix} \mathbf{a}b_{11} & \mathbf{a}b_{12} & \cdots \\ \mathbf{a}b_{21} & \mathbf{a}b_{22} & \cdots \\ & \cdots & \end{bmatrix} \quad (52)$$

Further

$$\Delta\hat{\alpha}_i^{\dagger} = \sum_{\kappa} (\alpha_1 - \alpha_2)_{t\kappa}(\mu_1^2 - {}^1/_3,\ \mu_1\mu_2,\ \mu_1\mu_3,\ \mu_2^2 - {}^1/_3,\ \mu_2\mu_3,\ \mu_3^2 - {}^1/_3)_{t\kappa}^T \quad (53)$$

and

$$\mathbf{B}_i = \begin{bmatrix} \alpha^2 & 2\alpha\beta & 0 & \beta^2 & 0 & 0 \\ \alpha\beta\cos\theta & (\beta^2 - \alpha^2)\cos\theta & \alpha\sin\theta & -\alpha\beta\cos\theta & \beta\sin\theta & 0 \\ \alpha\beta\sin\theta & (\beta^2 - \alpha^2)\sin\theta & -\alpha\cos\theta & -\alpha\beta\sin\theta & -\beta\cos\theta & 0 \\ \beta^2\cos^2\theta & -2\alpha\beta\cos^2\theta & 2\beta\cos\theta\sin\theta & \alpha^2\cos^2\theta & -2\alpha\cos\theta\sin\theta & \sin^2\theta \\ \beta^2\cos\theta\sin\theta & -2\alpha\beta\cos\theta\sin\theta & \beta(\sin^2\theta - \cos^2\theta) & \alpha^2\cos\theta\sin\theta & \alpha(\cos^2\theta - \sin^2\theta) & -\cos\theta\sin\theta \\ \beta^2\sin^2\theta & -2\alpha\beta\sin^2\theta & -2\beta\cos\theta\sin\theta & \alpha^2\sin^2\theta & 2\alpha\cos\theta\sin\theta & \cos^2\theta \end{bmatrix} \quad (54)$$

Adding S_1, S_2, and S_3, summing over i and j, condensing results into a single term for specified k by adjusting sizes of ensuing matrices, and finally summing over k, we reach

$$(\sum \zeta_t)\mathrm{Tr}\,\hat{\gamma}\mathbf{f} = (1\,0\,\ldots\,0)\mathbf{h}_3^{(1)}\mathbf{h}_3^{(2)}\cdots\mathbf{h}_3^{(n+1)} \begin{bmatrix} 0 \\ \cdot \\ \cdot \\ \cdot \\ 0 \\ 1 \end{bmatrix} \quad (55)$$

with

$$\mathbf{h}_3^{(k)} = \begin{bmatrix} 1 & \zeta & 2\zeta b\mathbf{e}_3^T\mathbf{A} & \zeta b^2\mathbf{e}_6^T\mathbf{B} & 0 & \Delta\hat{\alpha}^{\dagger T}\mathbf{g}\mathbf{B} & \zeta\Delta\hat{\alpha}^{\dagger T}\mathbf{g}\mathbf{B} & 2\zeta b\mathbf{e}_3^T\Delta\hat{\alpha}\mathbf{A} & \zeta b^2\mathbf{e}_3^T\Delta\hat{\alpha}\mathbf{e}_3 & 0 \\ & 1 & 2b\mathbf{e}_3^T\mathbf{A} & b^2\mathbf{e}_6^T\mathbf{B} & 0 & 0 & \Delta\hat{\alpha}^{\dagger T}\mathbf{g}\mathbf{B} & 2b\mathbf{e}_3^T\Delta\hat{\alpha}\mathbf{A} & b^2\mathbf{e}_3^T\Delta\hat{\alpha}\mathbf{e}_3 & 0 \\ & & \mathbf{A} & b(\mathbf{E}_3 \times \mathbf{e}_2^T)\mathbf{B} & 0 & 0 & 0 & \Delta\hat{\alpha}\mathbf{A} & b\Delta\hat{\alpha}\mathbf{e}_3 & 0 \\ & & & \mathbf{B} & \zeta\mathbf{B} & 0 & 0 & 0 & \Delta\hat{\alpha}^{\dagger} & \zeta\Delta\hat{\alpha}^{\dagger} \\ & & & & \mathbf{B} & 0 & 0 & 0 & 0 & \Delta\hat{\alpha}^{\dagger} \\ & & & & & \mathbf{B} & \zeta\mathbf{B} & \zeta b\bar{\mathbf{f}}(\mathbf{E}_3 \times \mathbf{e}_2)\mathbf{A} & \zeta b^2\mathbf{e}_6 & 0 \\ & & & & & & \mathbf{B} & b\bar{\mathbf{f}}(\mathbf{E}_3 \times \mathbf{e}_2)\mathbf{A} & b^2\mathbf{e}_6 & 0 \\ & & & & & & & \mathbf{A} & b\mathbf{e}_3 & 0 \\ & & \mathbf{0} & & & & & & 1 & \zeta \\ & & & & & & & & & 1 \end{bmatrix}_k \quad (56)$$

Mention must be made about quantities bearing the subscript $n + 1$. Among these, only ζ_{n+1} is significant. b_{n+1}, $\mathbf{A}_{n+1}$, and $\mathbf{B}_{n+1}$ can be arbitrarily chosen, only sizes of the matrices being significant. $\Delta\hat{\alpha}_{n+1}^{\dagger}$ must be equated to zero.

We now proceed to average Tr $\mathbf{f}$ and Tr $\hat{\gamma}\mathbf{f}$ over all internal conformations. This can be achieved by introducing the now-familiar rotational isomeric state approximation for skeletal bond rotations. It is convenient to treat the following two cases separately.

IV. Finite Chains of an Arbitrary Sequence of Bonds

According to the rotational isomeric state approximation, θ_i is assumed to be in either of s_i discrete values, or "state," $\theta_i^{(1)}, \theta_i^{(2)}, \ldots, \theta_i^{(s_i)}$. These states need not necessarily be common for different bonds in their location and in number. The conformational partition function of the molecule can be evaluated as

$$Z = \mathbf{e}_{s_1}^T\mathbf{p}_1\mathbf{p}_2\cdots\mathbf{p}_n\mathbf{e}_{s_{n-1}} \quad (57)$$

where $\mathbf{p}_i$ is the statistical-weight matrix of size $s_i \times s_{i+1}$ (except for $i = 1$, $n - 1$, and n), associated with the transition between states of skeletal bond i and $i + 1$. $\mathbf{p}$'s are constructed as follows. If only up to first-neighbor interactions are taken into account, the energy of the molecule is given by eq 58.

$$E = [E_2(\theta_2) + E_2(\theta_2, \theta_3)] + [E_3(\theta_3) + E_3(\theta_3, \theta_4)] + \ldots + [E_{n-2}(\theta_{n-2}) + E_{n-2}(\theta_{n-2}, \theta_{n-1})] + E_{n-1}(\theta_{n-1}) \quad (58)$$

This grouping of energy components leads to

$$\mathbf{p}_i = (\exp\{-[E_i(\theta_i^{(k)}) + E_i(\theta_i^{(k)}, \theta_{i+1}^{(l)})]/kT\}), \quad i = 1, 2, \ldots, n-1 \quad (59)$$

$$\mathbf{p}_n = \mathbf{E}_{s_{n-1}} \quad (60)$$

In constructing $\mathbf{p}_1$ and $\mathbf{p}_{n-1}$ according to eq 59 we assume $E_1(\theta_1) = E_1(\theta_1, \theta_2) = 0$ and $E_{n-1}(\theta_{n-1}, \theta_n) = 0$. All elements of $\mathbf{p}_1$ (or $\mathbf{p}_{n-1}$) except in the first row (or column) are arbitrary, as is apparent from eq 57. The above formulation of Z is slightly different from that previously given[14] but is equivalent and more convenient in constructing $\mathbf{p}$'s because different types of $\mathbf{p}$'s of a less number (2) suffice (*cf.* succeeding paper).

Now the required averages are obtained as

$$\langle r^2 \rangle = Z^{-1}(\mathbf{e}_{s_2}{}^T\ \mathbf{0}\ \mathbf{0})\mathbf{H}_0^{(1)}\mathbf{H}_0^{(2)} \ldots \mathbf{H}_0^{(n)} \begin{bmatrix} \mathbf{0} \\ \mathbf{0} \\ \mathbf{e}_{s_{n-1}} \end{bmatrix} \quad (61)$$

$$(\sum \zeta_i)\langle \mathrm{Tr}\ \mathbf{f} \rangle =$$

$$Z^{-1}(\mathbf{e}_{s_2}{}^T\ \mathbf{0}\ \mathbf{0}\ \mathbf{0}\ \mathbf{0})\mathbf{H}_2^{(1)}\mathbf{H}_2^{(2)} \ldots \mathbf{H}_2^{(n+1)} \begin{bmatrix} \mathbf{0} \\ \mathbf{0} \\ \mathbf{0} \\ \mathbf{0} \\ \mathbf{e}_{s_{n-1}} \end{bmatrix} \quad (62)$$

$$(\sum \zeta_i)\langle \mathrm{Tr}\ \hat{\boldsymbol{\gamma}}\mathbf{f} \rangle =$$

$$Z^{-1}(\mathbf{e}_{s_2}{}^T\ \mathbf{0}\ \ldots\ \mathbf{0})\mathbf{H}_3^{(1)}\mathbf{H}_3^{(2)} \ldots \mathbf{H}_3^{(n+1)} \begin{bmatrix} \mathbf{0} \\ \cdot \\ \cdot \\ \cdot \\ \mathbf{0} \\ \mathbf{e}_{s_{n-1}} \end{bmatrix} \quad (63)$$

with

$$\mathbf{H}_0^{(i)} = \begin{bmatrix} \mathbf{p} & 2b(\mathbf{E}_s \times \mathbf{e}_3{}^T)\tilde{\mathbf{A}} & b^2\mathbf{p} \\ \mathbf{0} & \tilde{\mathbf{A}} & b(\mathbf{p} \times \mathbf{e}_3) \\ \mathbf{0} & \mathbf{0} & \mathbf{p} \end{bmatrix}_i \quad (64)$$

$$\mathbf{H}_2^{(i)} = \begin{bmatrix} \mathbf{p} & \zeta\mathbf{p} & 2\zeta b(\mathbf{E}_s \times \mathbf{e}_3{}^T)\tilde{\mathbf{A}} & \zeta b^2\mathbf{p} & \mathbf{0} \\ \mathbf{0} & \mathbf{p} & 2b(\mathbf{E}_s \times \mathbf{e}_3{}^T)\tilde{\mathbf{A}} & b^2\mathbf{p} & \mathbf{0} \\ \mathbf{0} & \mathbf{0} & \tilde{\mathbf{A}} & b(\mathbf{p} \times \mathbf{e}_3) & \mathbf{0} \\ \mathbf{0} & \mathbf{0} & \mathbf{0} & \mathbf{p} & \zeta\mathbf{p} \\ \mathbf{0} & \mathbf{0} & \mathbf{0} & \mathbf{0} & \mathbf{p} \end{bmatrix}_i \quad (65)$$

$$\mathbf{H}_3^{(i)} = \begin{bmatrix} \mathbf{p} & \zeta\mathbf{p} & 2\zeta b(\mathbf{E}_s \times \mathbf{e}_3{}^T)\tilde{\mathbf{A}} & \zeta b^2(\mathbf{E}_s \times \mathbf{e}_6{}^T)\tilde{\mathbf{B}} & \mathbf{0} & (\mathbf{E}_s \times \Delta\hat{\boldsymbol{\alpha}}^{\dagger T})\mathbf{G}_s\tilde{\mathbf{B}} \\ & \mathbf{p} & 2b(\mathbf{E}_s \times \mathbf{e}_3{}^T)\tilde{\mathbf{A}} & b^2(\mathbf{E}_s \times \mathbf{e}_6{}^T)\tilde{\mathbf{B}} & \mathbf{0} & \mathbf{0} \\ & & \tilde{\mathbf{A}} & b(\mathbf{E}_{3s} \times \mathbf{e}_2{}^T)\tilde{\mathbf{B}} & \mathbf{0} & \mathbf{0} \\ & & & \tilde{\mathbf{B}} & \zeta\tilde{\mathbf{B}} & \mathbf{0} \\ & & & & \tilde{\mathbf{B}} & \mathbf{0} \\ & & & & & \tilde{\mathbf{B}} \\ & & \mathbf{0} & & & \end{bmatrix}$$

$$\begin{bmatrix} \zeta(\mathbf{E}_s \times \Delta\hat{\boldsymbol{\alpha}}^{\dagger T})\mathbf{G}_s\tilde{\mathbf{B}} & 2\zeta b(\mathbf{E}_s \times \mathbf{e}_3{}^T\Delta\hat{\boldsymbol{\alpha}})\tilde{\mathbf{A}} & \zeta b^2\mathbf{e}_3{}^T\Delta\hat{\boldsymbol{\alpha}}\mathbf{e}_3\mathbf{p} & \mathbf{0} \\ (\mathbf{E}_s \times \Delta\hat{\boldsymbol{\alpha}}^{\dagger T})\mathbf{G}_s\tilde{\mathbf{B}} & 2b(\mathbf{E}_s \times \mathbf{e}_3{}^T\Delta\hat{\boldsymbol{\alpha}})\tilde{\mathbf{A}} & b^2\mathbf{e}_3{}^T\Delta\hat{\boldsymbol{\alpha}}\mathbf{e}_3\mathbf{p} & \mathbf{0} \\ \mathbf{0} & (\mathbf{E}_s \times \Delta\hat{\boldsymbol{\alpha}})\tilde{\mathbf{A}} & b(\mathbf{p} \times \Delta\hat{\boldsymbol{\alpha}}\mathbf{e}_3) & \mathbf{0} \\ \mathbf{0} & \mathbf{0} & \mathbf{p} \times \Delta\hat{\boldsymbol{\alpha}}^{\dagger} & \zeta\mathbf{p} \times \Delta\hat{\boldsymbol{\alpha}}^{\dagger} \\ \mathbf{0} & \mathbf{0} & \mathbf{0} & \mathbf{p} \times \Delta\hat{\boldsymbol{\alpha}}^{\dagger} \\ \zeta\tilde{\mathbf{B}} & \zeta b\mathbf{F}_s(\mathbf{E}_{3s} \times \mathbf{e}_2)\tilde{\mathbf{A}} & \zeta b^2(\mathbf{p} \times \mathbf{e}_6) & \mathbf{0} \\ \tilde{\mathbf{B}} & b\mathbf{F}_s(\mathbf{E}_{3s} \times \mathbf{e}_2)\tilde{\mathbf{A}} & b^2(\mathbf{p} \times \mathbf{e}_6) & \mathbf{0} \\ & \tilde{\mathbf{A}} & b(\mathbf{p} \times \mathbf{e}_3) & \mathbf{0} \\ & & \mathbf{p} & \zeta\mathbf{p} \\ & & & \mathbf{p} \end{bmatrix}_i \quad (66)$$

In eq 66, $\mathbf{F}_s = \mathbf{E}_s \times \mathbf{f}$ and $\mathbf{G}_s = \mathbf{E}_s \times \mathbf{g}$. Also $\mathbf{p}_{n+1} = \mathbf{E}_{s_{n-1}}$. $\tilde{\mathbf{A}}_i$ and $\tilde{\mathbf{B}}_i$ are formed from $\mathbf{A}_i$, eq 36 and $\mathbf{B}_i$, eq 54, by replacing $\cos^p\theta_i \sin^q\theta_i$ by $\mathbf{c}_i{}^p\mathbf{s}_i{}^q\mathbf{p}_i$, where $\mathbf{c}_i$ and $\mathbf{s}_i$ are the diagonal matrices of order s_i whose kth elements are $\cos\theta_i^{(k)}$ and $\sin\theta_i^{(k)}$, respectively.

Namely

$$\tilde{\mathbf{A}}_i = \begin{bmatrix} \alpha\mathbf{p} & \beta\mathbf{p} & \mathbf{0} \\ \beta\mathbf{cp} & -\alpha\mathbf{cp} & \mathbf{sp} \\ \beta\mathbf{sp} & -\alpha\mathbf{sp} & -\mathbf{cp} \end{bmatrix}_i \quad (67)$$

$$\tilde{\mathbf{B}}_t = \begin{bmatrix} \alpha^2\mathbf{p} & 2\alpha\beta\mathbf{p} & \mathbf{0} & \beta^2\mathbf{p} & \mathbf{0} & \mathbf{0} \\ \alpha\beta\mathbf{cp} & (\beta^2 - \alpha^2)\mathbf{cp} & \alpha\mathbf{sp} & -\alpha\beta\mathbf{cp} & \beta\mathbf{sp} & \mathbf{0} \\ \alpha\beta\mathbf{sp} & (\beta^2 - \alpha^2)\mathbf{sp} & -\alpha\mathbf{cp} & -\alpha\beta\mathbf{sp} & -\beta\mathbf{cp} & \mathbf{0} \\ \beta^2\mathbf{c}^2\mathbf{p} & -2\alpha\beta\mathbf{c}^2\mathbf{p} & 2\beta\mathbf{csp} & \alpha^2\mathbf{c}^2\mathbf{p} & -2\alpha\mathbf{csp} & \mathbf{s}^2\mathbf{p} \\ \beta^2\mathbf{csp} & -2\alpha\beta\mathbf{csp} & \beta(\mathbf{s}^2 - \mathbf{c}^2)\mathbf{p} & \alpha^2\mathbf{csp} & \alpha(\mathbf{c}^2 - \mathbf{s}^2)\mathbf{p} & -\mathbf{csp} \\ \beta^2\mathbf{s}^2\mathbf{p} & -2\alpha\beta\mathbf{s}^2\mathbf{p} & -2\beta\mathbf{csp} & \alpha^2\mathbf{s}^2\mathbf{p} & 2\alpha\mathbf{csp} & \mathbf{c}^2\mathbf{p} \end{bmatrix}_t \quad (68)$$

We point out that $\langle r^2 \rangle$ can be expressed in terms of $\mathbf{H}_2$'s

$$\langle r^2 \rangle = Z^{-1}(\mathbf{0}\ \mathbf{e}_{s_2}{}^{\mathrm{T}}\ \mathbf{0}\ \mathbf{0}\ \mathbf{0})\mathbf{H}_2{}^{(1)}\mathbf{H}_2{}^{(2)} \cdots \mathbf{H}_2{}^{(n)} \begin{bmatrix} \mathbf{0} \\ \mathbf{0} \\ \mathbf{0} \\ \mathbf{e}_{s_{n-1}} \\ \mathbf{0} \end{bmatrix} \quad (69)$$

The expression for $\langle \mathbf{r}^{\mathrm{T}}\boldsymbol{\gamma}\mathbf{r} \rangle$ previously derived,[14] if the traceless tensor $\hat{\boldsymbol{\gamma}}$ is used, becomes

$$\langle \mathbf{r}^{\mathrm{T}}\hat{\boldsymbol{\gamma}}\mathbf{r} \rangle = Z^{-1}(\mathbf{e}_{s_1}{}^{\mathrm{T}}\ \mathbf{0} \cdots \mathbf{0})\mathbf{H}_1{}^{(1)}\mathbf{H}_1{}^{(2)} \cdots \mathbf{H}_1{}^{(n)} \begin{bmatrix} \mathbf{0} \\ \cdot \\ \cdot \\ \cdot \\ \mathbf{0} \\ \mathbf{e}_{s_{n-1}} \end{bmatrix} \quad (70)$$

with

$$\mathbf{H}_1{}^{(i)} = \begin{bmatrix} \mathbf{p} & 2b(\mathbf{E}_s \times \mathbf{e}_3{}^{\mathrm{T}})\tilde{\mathbf{A}} & b^2(\mathbf{E}_s \times \mathbf{e}_6{}^{\mathrm{T}})\tilde{\mathbf{B}} & (\mathbf{E}_s \times \Delta\hat{\boldsymbol{\alpha}}^{\dagger\mathrm{T}})\mathbf{G}_s\tilde{\mathbf{B}} & 2b(\mathbf{E}_s \times \mathbf{e}_3{}^{\mathrm{T}}\Delta\hat{\boldsymbol{\alpha}})\tilde{\mathbf{A}} & b^2\mathbf{e}_3{}^{\mathrm{T}}\Delta\hat{\boldsymbol{\alpha}}\mathbf{e}_3\mathbf{p} \\ & \tilde{\mathbf{A}} & b(\mathbf{E}_{3s} \times \mathbf{e}_2{}^{\mathrm{T}})\tilde{\mathbf{B}} & \mathbf{0} & (\mathbf{E}_s \times \Delta\hat{\boldsymbol{\alpha}})\tilde{\mathbf{A}} & b(\mathbf{p} \times \Delta\hat{\boldsymbol{\alpha}}\mathbf{e}_3) \\ & & \tilde{\mathbf{B}} & \mathbf{0} & \mathbf{0} & \mathbf{p} \times \Delta\hat{\boldsymbol{\alpha}}^{\dagger} \\ & \mathbf{0} & & \tilde{\mathbf{B}} & b\mathbf{F}_s(\mathbf{E}_{3s} \times \mathbf{e}_2)\tilde{\mathbf{A}} & b^2(\mathbf{p} \times \mathbf{e}_6) \\ & & & & \tilde{\mathbf{A}} & b(\mathbf{p} \times \mathbf{e}_3) \\ & & & & & \mathbf{p} \end{bmatrix}_t \quad (71)$$

Similarly, $\langle \mathbf{r}^{\mathrm{T}}\hat{\boldsymbol{\gamma}}\mathbf{r} \rangle$ can be expressed in terms of $\mathbf{H}_3$'s

$$\langle \mathbf{r}^{\mathrm{T}}\hat{\boldsymbol{\gamma}}\mathbf{r} \rangle = Z^{-1}(\mathbf{0}\ \mathbf{e}_{s_2}{}^{\mathrm{T}}\ \mathbf{0} \cdots \mathbf{0})\mathbf{H}_3{}^{(1)}\mathbf{H}_3{}^{(2)} \cdots \mathbf{H}_3{}^{(n)} \begin{bmatrix} \mathbf{0} \\ \cdot \\ \cdot \\ \cdot \\ \mathbf{0} \\ \mathbf{e}_{s_{n-1}} \\ \mathbf{0} \end{bmatrix} \quad (72)$$

Equations 69 and 72 are useful when we want both $\Delta\Gamma_t$ and $\Delta\Gamma_s$ since it suffices to construct only the two kinds of matrices, $\mathbf{H}_2{}^{(i)}$ and $\mathbf{H}_3{}^{(i)}$.

V. Stereoregular Chains of Infinite Length. Largest Eigenvalue Method

We are interested in the asymptotic behavior of $\langle r^2 \rangle$, $\langle \mathbf{r}^{\mathrm{T}}\hat{\boldsymbol{\gamma}}\mathbf{r} \rangle$, $\langle \mathrm{Tr}\ \mathbf{f} \rangle$, and $\langle \mathrm{Tr}\ \hat{\boldsymbol{\gamma}}\mathbf{f} \rangle$ for stereoregular (or multirepeat) chains at the limit of infinite chain length. Treatments of $\langle r^2 \rangle$ and $\langle \mathbf{r}^{\mathrm{T}}\hat{\boldsymbol{\gamma}}\mathbf{r} \rangle$ were given previously.[14] Calculations involved were of considerable length, but final expressions were fairly simple and systematic. In connection with treatments of $\langle \mathrm{Tr}\ \mathbf{f} \rangle$ and $\langle \mathrm{Tr}\ \hat{\boldsymbol{\gamma}}\mathbf{f} \rangle$, we have found new, more concise derivations, and the most compact expressions for all these quantities.

Consider a stereoregular chain composed of N structural units. For mathematical convenience, this chain is assumed to be a subchain of an infinite chain composed of the same structural units. Each unit is assumed to involve m skeletal bonds (an m-repeat polymer). Conformational statistics of the chain is characterized by m transition-probability matrices defined as in eq 59, $\mathbf{p}_1$, $\mathbf{p}_2$, ..., $\mathbf{p}_m$, and by the normalized, left- and right-hand eigenvectors $\mathbf{v}$ and $\mathbf{u}$ of $\mathbf{p}_1\mathbf{p}_2 \cdots \mathbf{p}_m$, associated with its largest eigenvalue. We assume $\mathbf{p}$'s to be so normalized that the largest eigenvalue of $\mathbf{p}_1\mathbf{p}_2 \cdots \mathbf{p}_m$ is unity. This is effected by dividing either (say, $\mathbf{p}_1$) of $\mathbf{p}$'s defined as in eq 59, by the largest eigenvalue of $\mathbf{p}_1\mathbf{p}_2 \cdots \mathbf{p}_m$. Thus we have

$$\mathbf{p}_1\mathbf{p}_2 \cdots \mathbf{p}_m\mathbf{u} = \mathbf{u},\ \mathbf{v}\mathbf{p}_1\mathbf{p}_2 \cdots \mathbf{p}_m = \mathbf{v},\ \text{and}\ \mathbf{v}\mathbf{u} = 1 \quad (73)$$

($\mathbf{v}$ and $\mathbf{u}$ play an important role in the following. For this reason we wish to refer to the method in this section as the largest eigenvalue method.) With thus redefined $\mathbf{p}$'s, $\langle r^2 \rangle$ for our subchain is given by

$$\langle r^2 \rangle = (\mathbf{v}\ \mathbf{0}\ \mathbf{0})\mathbf{X}_0{}^N \begin{bmatrix} \mathbf{0} \\ \mathbf{0} \\ \mathbf{u} \end{bmatrix} \quad (74)$$

with

$$\mathbf{H}_0{}^{(1)} \cdots \mathbf{H}_0{}^{(m)} = \mathbf{X}_0 = \begin{bmatrix} \mathbf{X}_{011} & \mathbf{X}_{012} & \mathbf{X}_{013} \\ \mathbf{0} & \mathbf{X}_{022} & \mathbf{X}_{023} \\ \mathbf{0} & \mathbf{0} & \mathbf{X}_{033} \end{bmatrix} \quad (75)$$

where $\mathbf{X}_0$ is divided into the submatrices $\mathbf{X}_{0ij}$ in such a manner as that of $\mathbf{H}_0{}^{(i)}$ in eq 64; $\mathbf{X}_{011}$, $\mathbf{X}_{022}$, and $\mathbf{X}_{033}$ are of the orders of s_1, $3s_1$, and s_1, respectively. Inverting the procedure by which we obtained eq 39 from eq 38, we can write eq 74 as

$$\langle r^2 \rangle = \sum_{i=1}^{N} \mathbf{v}\mathbf{X}_{011}{}^{i-1}\mathbf{X}_{013}\mathbf{X}_{033}{}^{N-i}\mathbf{u} + \sum_{1 \le i < j \le N} \mathbf{v}\mathbf{X}_{011}{}^{i-1}\mathbf{X}_{012}\mathbf{X}_{022}{}^{j-i-1}\mathbf{X}_{023}\mathbf{X}_{033}{}^{N-j}\mathbf{u} \quad (76)$$

Utilizing $\mathbf{v}\mathbf{X}_{011}{}^{i-1} = \mathbf{v}(\mathbf{p}_1 \ldots \mathbf{p}_m)^{i-1} = \mathbf{v}$ and $\mathbf{X}_{033}{}^{N-i}\mathbf{u} = (\mathbf{p}_1 \ldots \mathbf{p}_m)^{N-i}\mathbf{u} = \mathbf{u}$, and summing over i and j, we obtain

$$\langle r^2 \rangle = \mathbf{v}\{[\mathbf{X}_{013} + \mathbf{X}_{012}(\mathbf{E} - \mathbf{X}_{022})^{-1}\mathbf{X}_{023}]N - \mathbf{X}_{012}(\mathbf{E} - \mathbf{X}_{022})^{-2}(\mathbf{E} - \mathbf{X}_{022}{}^N)\mathbf{X}_{023}\}\mathbf{u} \quad (77)$$

or, in terms of $\mathbf{X}_0$

$$\langle r^2 \rangle/N = (\mathbf{v}\ 0\ 0)\left\{\mathbf{E} + \mathbf{X}_0\begin{bmatrix}\mathbf{0}\\ \mathbf{E}_{3s_1}\\ \mathbf{0}\end{bmatrix}(\mathbf{E} - \mathbf{X}_{022})^{-1} \times [\mathbf{E} - N^{-1}(\mathbf{E} - \mathbf{X}_{c22})^{-1}(\mathbf{E} - \mathbf{X}_{022}{}^N)] \times (\mathbf{0}\ \mathbf{E}_{3s_1}\ \mathbf{0})\right\}\mathbf{X}_0\begin{bmatrix}\mathbf{0}\\ \mathbf{0}\\ \mathbf{u}\end{bmatrix} \quad (78)$$

According to a method described in the Appendix, eq 78 is rewritten

$$\langle r^2 \rangle/N = -(\mathbf{v}\ 0\ 0)\begin{bmatrix}-\mathbf{E}_{s_1} & \mathbf{X}_{012} & \mathbf{X}_{013}\\ \mathbf{0} & (\mathbf{X}_{022} - \mathbf{E}_{3s_1})[\mathbf{E} - N^{-1}(\mathbf{E} - \mathbf{X}_{022})^{-1}(\mathbf{E} - \mathbf{X}_{022}{}^N)]^{-1} & \mathbf{X}_{023}\\ \mathbf{0} & & -\mathbf{E}_{s_1}\end{bmatrix}^{-1}\begin{bmatrix}\mathbf{0}\\ \mathbf{0}\\ \mathbf{u}\end{bmatrix} \quad (79)$$

The value of $\langle r^2 \rangle$ at the limit of $N \to \infty$, $\langle r^2 \rangle_*$, becomes

$$\langle r^2 \rangle_*/N = -(\mathbf{v}\ 0\ 0)\begin{bmatrix}-\mathbf{E}_{s_1} & \mathbf{X}_{012} & \mathbf{X}_{013}\\ \mathbf{0} & \mathbf{X}_{022} - \mathbf{E}_{3s_1} & \mathbf{X}_{023}\\ \mathbf{0} & \mathbf{0} & -\mathbf{E}_{s_1}\end{bmatrix}^{-1}\begin{bmatrix}\mathbf{0}\\ \mathbf{0}\\ \mathbf{u}\end{bmatrix} \quad (80)$$

Equation 78 with $N = \infty$ was derived previously[14a] by a lengthier calculation, and eq 78 itself and eq 79 and 80 are new.

We next calculate $\langle \mathrm{Tr}\ \mathbf{f} \rangle$. We have for the subchain

$$N\zeta_u\langle \mathrm{Tr}\ \mathbf{f} \rangle = (\mathbf{v}\ \mathbf{0} \ldots \mathbf{0})\mathbf{X}_2{}^N\begin{bmatrix}\mathbf{0}\\ \cdot\\ \cdot\\ \cdot\\ \mathbf{0}\\ \mathbf{u}\end{bmatrix} \quad (81)$$

where $\zeta_u = \zeta_1 + \ldots + \zeta_m$ is the total friction of a structural unit, and

$$\mathbf{H}_2{}^{(1)} \ldots \mathbf{H}_2{}^{(m)} = \mathbf{X}_2 = \begin{bmatrix}\mathbf{X}_{211} & \mathbf{X}_{212} & \mathbf{X}_{213} & \mathbf{X}_{214} & \mathbf{X}_{215}\\ & \mathbf{X}_{222} & \mathbf{X}_{223} & \mathbf{X}_{224} & \mathbf{X}_{225}\\ & & \mathbf{X}_{233} & \mathbf{X}_{234} & \mathbf{X}_{235}\\ & \mathbf{0} & & \mathbf{X}_{244} & \mathbf{X}_{245}\\ & & & & \mathbf{X}_{265}\end{bmatrix} \quad (82)$$

where the division of $\mathbf{X}_2$ into the submatrices is assumed to be made in accordance with that of $\mathbf{H}_2{}^{(i)}$, eq 65. $N\zeta_u\langle \mathrm{Tr}\ \mathbf{f} \rangle$ can be calculated by decomposing $\mathbf{X}_2{}^N$ as previously. We are interested only in the leading terms, *i.e.*, those of order N^3. Retaining only terms that contribute to the leading terms we obtain

$$N\zeta_u\langle \mathrm{Tr}\ \mathbf{f} \rangle \simeq \sum_{1 \le i_1 < i_2 < i_4 \le N} \mathbf{v}\mathbf{X}_{211}{}^{i_1-1}\mathbf{X}_{212}\mathbf{X}_{222}{}^{i_2-i_1-1}(\mathbf{X}_{224} + \mathbf{X}_{223}\sum_{i_2=i_1+1}^{i_3-1}\mathbf{X}_{233}{}^{i_3-i_2-1}\mathbf{X}_{234})\mathbf{X}_{244}{}^{i_4-i_3-1}\mathbf{X}_{245}\mathbf{X}_{255}{}^{N-i_4}\mathbf{u} \quad (83)$$

Summing over i's by utilizing $\mathbf{v}\mathbf{X}_{211}{}^{i-1}\mathbf{X}_{212} = \zeta_u\mathbf{v}$ and $\mathbf{X}_{245}\mathbf{X}_{255}{}^{N-i_4}\mathbf{u} = \zeta_u\mathbf{u}$, and discarding terms of orders lower than N^3, we obtain

$$N\zeta_u\langle \mathrm{Tr}\ \mathbf{f} \rangle \simeq {}^1/_6N^3\zeta_u{}^2\mathbf{v}[\mathbf{X}_{224} + \mathbf{X}_{223}(\mathbf{E} - \mathbf{X}_{233})^{-1}\mathbf{X}_{234}]\mathbf{u} \quad (84)$$

Therefore, we obtain for the asymptotic value of $\langle \mathrm{Tr}\ \mathbf{f} \rangle$

$$\langle \mathrm{Tr}\ \mathbf{f} \rangle_* = {}^1/_6N^2\zeta_u\mathbf{v}[\mathbf{X}_{224} + \mathbf{X}_{223}(\mathbf{E} - \mathbf{X}_{233})^{-1}\mathbf{X}_{234}]\mathbf{u} \quad (85)$$

We note that among various terms ensuing after decomposition of $\mathbf{X}_2{}^N$ in eq 81 into the submatrices only the terms of the form $\mathbf{X}_{211}{}^{i_1-1}\mathbf{X}_{212} \ldots \mathbf{X}_{245}\mathbf{X}_{255}{}^{N-i_4}$ contributed to the leading terms.

We can easily confirm $\mathbf{X}_{224} = \mathbf{X}_{013}$, $\mathbf{X}_{223} = \mathbf{X}_{012}$, $\mathbf{X}_{233} = \mathbf{X}_{022}$, and $\mathbf{X}_{234} = \mathbf{X}_{023}$, and hence obtain

$$\langle \mathrm{Tr}\ \mathbf{f} \rangle_* = {}^1/_6N\zeta_u\langle r^2 \rangle_* \quad (86)$$

It is of particular interest that $\langle \mathrm{Tr}\ \mathbf{f} \rangle_*$ is determined by the total friction of the polymer chain, $N\zeta_u$, and the mean-square radius of gyration $\langle r^2 \rangle_*/6$, and is independent of the way in which ζ_u is partitioned on skeletal atoms of a unit.

We now proceed to calculate $\langle \mathbf{r}^T\hat{\gamma}\mathbf{r} \rangle$. We have for the subchain

$$\langle \mathbf{r}^T\hat{\gamma}\mathbf{r} \rangle = (\mathbf{v}\ \mathbf{0} \ldots \mathbf{0})\mathbf{X}_1{}^N\begin{bmatrix}\mathbf{0}\\ \cdot\\ \cdot\\ \cdot\\ \mathbf{0}\\ \mathbf{u}\end{bmatrix} \quad (87)$$

with

$$\mathbf{H}_1{}^{(1)} \ldots \mathbf{H}_1{}^{(m)} = \mathbf{X}_1 = \begin{bmatrix}\mathbf{X}_{111} & \mathbf{X}_{112} & \mathbf{X}_{113} & \mathbf{X}_{114} & \mathbf{X}_{115} & \mathbf{X}_{116}\\ & \mathbf{X}_{122} & \mathbf{X}_{123} & \mathbf{0} & \mathbf{X}_{125} & \mathbf{X}_{126}\\ & & \mathbf{X}_{133} & \mathbf{0} & \mathbf{0} & \mathbf{X}_{136}\\ & & & \mathbf{X}_{144} & \mathbf{X}_{145} & \mathbf{X}_{146}\\ & \mathbf{0} & & & \mathbf{X}_{155} & \mathbf{X}_{156}\\ & & & & & \mathbf{X}_{166}\end{bmatrix} \quad (88)$$

where the division of $\mathbf{X}_1$ into the submatrices is assumed to be made in accordance with that of $\mathbf{H}_1{}^{(i)}$, eq 71. Decomposition of $\mathbf{X}_1{}^N$ in eq 87 into the submatrices yields a numerous number of terms. Among others we consider contributions from two groups of terms as involving the factors

$$\mathbf{X}_{114}\mathbf{X}_{144}{}^{k} \quad \text{and} \quad \mathbf{X}_{133}{}^{k}\mathbf{X}_{136} \qquad k \geq 1$$

Like these, $\mathbf{X}_{144}$ (or $\mathbf{X}_{133}$) appears always in pair with $\mathbf{X}_{114}$ (or $\mathbf{X}_{136}$). By a direct examination $\mathbf{X}_{133} = \mathbf{X}_{144} = \tilde{\mathbf{B}}_1\tilde{\mathbf{B}}_2 \ldots \tilde{\mathbf{B}}_m$ is found to have unity as its largest eigenvalue

$$\mathbf{v}'\tilde{\mathbf{B}}_1\tilde{\mathbf{B}}_2 \ldots \tilde{\mathbf{B}}_m = \mathbf{v}' \qquad \tilde{\mathbf{B}}_1\tilde{\mathbf{B}}_2 \ldots \tilde{\mathbf{B}}_m\mathbf{u}' = \mathbf{u}'$$
$$\text{and} \quad \mathbf{v}'\mathbf{u}' = 1 \tag{89}$$

where

$$\mathbf{u}' = \begin{bmatrix} \mathbf{u} \\ \mathbf{0} \\ \mathbf{0} \\ \mathbf{u} \\ \mathbf{0} \\ \mathbf{u} \end{bmatrix} \tag{90}$$

$$\mathbf{v}' = {}^1/_3(\mathbf{v}\ \mathbf{0}\ \mathbf{0}\ \mathbf{v}\ \mathbf{0}\ \mathbf{v}) \tag{91}$$

We divide $\mathbf{X}_{133} = \mathbf{X}_{144}$ into the two terms, $\mathbf{u}'\mathbf{v}'$ and $\mathbf{B}'$, *i.e.*

$$\mathbf{B}' = \tilde{\mathbf{B}}_1\tilde{\mathbf{B}}_2 \ldots \tilde{\mathbf{B}}_m - \mathbf{u}'\mathbf{v}' \tag{92}$$

The largest eigenvalue of $\mathbf{B}'$ thus defined must necessarily be smaller than unity.[35] Since $\mathbf{u}'\mathbf{v}'\mathbf{B}' = \mathbf{B}'\mathbf{u}'\mathbf{v}' \equiv \mathbf{0}$ and $\mathbf{u}'\mathbf{v}'\mathbf{u}'\mathbf{v}' \equiv \mathbf{u}'\mathbf{v}'$, we have

$$\mathbf{X}_{133}{}^{k} = \mathbf{X}_{144}{}^{k} = \mathbf{u}'\mathbf{v}' + \mathbf{B}'^{k} \qquad k \geq 1 \tag{93}$$

If this relation is substituted into the two factors mentioned above, terms involving $\mathbf{u}'\mathbf{v}'$ vanish on account of the relations

$$\mathbf{X}_{114}\mathbf{u}' = \sum_{k=1}^{m} \mathbf{p}_1 \ldots \mathbf{p}_{k-1}(\mathbf{E}_{s_k} \times \Delta\hat{\boldsymbol{\alpha}}_k{}^{\dagger\mathrm{T}})\mathbf{G}_{s_k}\tilde{\mathbf{B}}_k \ldots \tilde{\mathbf{B}}_m\mathbf{u}' \equiv \mathbf{0} \tag{94}$$

$$\mathbf{v}'\mathbf{X}_{136} = \sum_{k=1}^{m} \mathbf{v}'\tilde{\mathbf{B}}_1 \ldots \tilde{\mathbf{B}}_{k-1}(\mathbf{E}_{s_k} \times \Delta\hat{\boldsymbol{\alpha}}_k{}^{\dagger})\mathbf{p}_k \ldots \mathbf{p}_m \equiv 0 \tag{95}$$

which both are a consequence of our use of traceless tensors. This result indicates that $\mathbf{X}_{133}$ and $\mathbf{X}_{144}$ of $\mathbf{X}_1$ in eq 87 can be replaced by $\mathbf{B}'$ without error. If $\mathbf{X}_1$ so modified is designated $\tilde{\mathbf{X}}_1$, we have

$$\langle \mathbf{r}^{\mathrm{T}}\hat{\boldsymbol{\gamma}}\mathbf{r}\rangle = (\mathbf{v}\ \mathbf{0}\ \mathbf{0})\tilde{\mathbf{X}}_1{}^{N}\begin{bmatrix} \mathbf{0} \\ \mathbf{0} \\ \mathbf{u} \end{bmatrix} \tag{96}$$

with

$$\tilde{\mathbf{X}}_1 = \begin{bmatrix} \tilde{\mathbf{X}}_{111} & \tilde{\mathbf{X}}_{112} & \tilde{\mathbf{X}}_{113} \\ \mathbf{0} & \tilde{\mathbf{X}}_{122} & \tilde{\mathbf{X}}_{123} \\ \mathbf{0} & \mathbf{0} & \tilde{\mathbf{X}}_{133} \end{bmatrix} =$$

$$\left[\begin{array}{c|cccc|c} \mathbf{X}_{111} & \mathbf{X}_{112} & \mathbf{X}_{113} & \mathbf{X}_{114} & \mathbf{X}_{115} & \mathbf{X}_{116} \\ \hline & \mathbf{X}_{122} & \mathbf{X}_{123} & \mathbf{0} & \mathbf{X}_{125} & \mathbf{X}_{126} \\ & & \mathbf{B}' & \mathbf{0} & \mathbf{0} & \mathbf{X}_{136} \\ & & & \mathbf{B}' & \mathbf{X}_{145} & \mathbf{X}_{146} \\ & \mathbf{0} & & & \mathbf{X}_{155} & \mathbf{X}_{156} \\ \hline & & & & & \mathbf{X}_{166} \end{array}\right] \tag{97}$$

where $\tilde{\mathbf{X}}_1$ is divided into $\tilde{\mathbf{X}}_{1ij}$ as indicated by broken lines. We note that all eigenvalues of $\tilde{\mathbf{X}}_{122}$, which are identical with those of $\mathbf{X}_{122} = \mathbf{X}_{155} = \tilde{\mathbf{A}}_1\tilde{\mathbf{A}}_2 \ldots \tilde{\mathbf{A}}_m$ and $\mathbf{B}'$, are smaller than unity. Therefore we can hereafter proceed as in the case of $\langle r^2\rangle$. Thus we find

$$\langle \mathbf{r}^{\mathrm{T}}\hat{\boldsymbol{\gamma}}\mathbf{r}\rangle/N = -(\mathbf{v}\ \mathbf{0}\ \mathbf{0})\begin{bmatrix} -\mathbf{E}_{s_1} & \tilde{\mathbf{X}}_{112} & \tilde{\mathbf{X}}_{113} \\ \mathbf{0} & (\tilde{\mathbf{X}}_{122} - \mathbf{E}_{18s_1})[\mathbf{E} - N^{-1}(\mathbf{E} - \tilde{\mathbf{X}}_{122})^{-1}(\mathbf{E} - \tilde{\mathbf{X}}_{122}{}^{N})]^{-1} & \tilde{\mathbf{X}}_{123} \\ \mathbf{0} & \mathbf{0} & -\mathbf{E}_{s_1} \end{bmatrix}^{-1}\begin{bmatrix} \mathbf{0} \\ \mathbf{0} \\ \mathbf{u} \end{bmatrix} \tag{98}$$

which reduces, at the limit of $N \to \infty$

$$\langle \mathbf{r}^{\mathrm{T}}\hat{\boldsymbol{\gamma}}\mathbf{r}\rangle_*/N = -(\mathbf{v}\ \mathbf{0}\ \mathbf{0})\begin{bmatrix} -\mathbf{E}_{s_1} & \tilde{\mathbf{X}}_{112} & \tilde{\mathbf{X}}_{113} \\ \mathbf{0} & \tilde{\mathbf{X}}_{122} - \mathbf{E}_{18s_1} & \tilde{\mathbf{X}}_{123} \\ \mathbf{0} & \mathbf{0} & -\mathbf{E}_{s_1} \end{bmatrix}^{-1}\begin{bmatrix} \mathbf{0} \\ \mathbf{0} \\ \mathbf{u} \end{bmatrix} \tag{99}$$

or, in terms of $\mathbf{X}_{1ij}$

$$\langle \mathbf{r}^{\mathrm{T}}\hat{\boldsymbol{\gamma}}\mathbf{r}\rangle_*/N = -(\mathbf{v}\ \mathbf{0}\ \cdots\ \mathbf{0})\begin{bmatrix} -\mathbf{E}_{s_1} & \mathbf{X}_{112} & \mathbf{X}_{113} & \mathbf{X}_{114} & \mathbf{X}_{115} & \mathbf{X}_{116} \\ & \mathbf{X}_{122} - \mathbf{E}_{3s_1} & \mathbf{X}_{123} & \mathbf{0} & \mathbf{X}_{125} & \mathbf{X}_{126} \\ & & \mathbf{B}' - \mathbf{E}_{6s_1} & \mathbf{0} & \mathbf{0} & \mathbf{X}_{136} \\ & & & \mathbf{B}' - \mathbf{E}_{6s_1} & \mathbf{X}_{145} & \mathbf{X}_{146} \\ & & & & \mathbf{X}_{155} - \mathbf{E}_{3s_1} & \mathbf{X}_{156} \\ & \mathbf{0} & & & & -\mathbf{E}_{s_1} \end{bmatrix}^{-1}\begin{bmatrix} \mathbf{0} \\ \cdot \\ \cdot \\ \cdot \\ \mathbf{0} \\ \mathbf{u} \end{bmatrix} \tag{100}$$

We finally treat $\langle \mathrm{Tr}\ \hat{\boldsymbol{\gamma}}\mathbf{f}\rangle$. We have for the subchain

$$N\zeta_{\mathrm{u}}\langle \mathrm{Tr}\ \hat{\boldsymbol{\gamma}}\mathbf{f}\rangle = (\mathbf{v}\ \mathbf{0}\ \ldots\ \mathbf{0})\mathbf{X}_3{}^{N}\begin{bmatrix} \mathbf{0} \\ \cdot \\ \cdot \\ \cdot \\ \mathbf{0} \\ \mathbf{u} \end{bmatrix} \tag{101}$$

with

(35) K. Nagai, *J. Chem. Phys.*, **45**, 838 (1966).

$$\mathbf{H}_3^{(1)} \ldots \mathbf{H}_3^{(m)} = \mathbf{X}_3 = \begin{bmatrix} \mathbf{X}_{311} & \mathbf{X}_{312} & \mathbf{X}_{313} & \mathbf{X}_{314} & \mathbf{X}_{315} & \mathbf{X}_{316} & \mathbf{X}_{317} & \mathbf{X}_{318} & \mathbf{X}_{319} & \mathbf{X}_{31,10} \\ & \mathbf{X}_{322} & \mathbf{X}_{323} & \mathbf{X}_{324} & \mathbf{X}_{325} & \mathbf{0} & \mathbf{X}_{327} & \mathbf{X}_{328} & \mathbf{X}_{329} & \mathbf{X}_{32,10} \\ & & \mathbf{X}_{333} & \mathbf{X}_{334} & \mathbf{X}_{335} & \mathbf{0} & \mathbf{0} & \mathbf{X}_{338} & \mathbf{X}_{339} & \mathbf{X}_{33,10} \\ & & & \mathbf{X}_{344} & \mathbf{X}_{345} & \mathbf{0} & \mathbf{0} & \mathbf{0} & \mathbf{X}_{349} & \mathbf{X}_{34,10} \\ & & & & \mathbf{X}_{355} & \mathbf{0} & \mathbf{0} & \mathbf{0} & \mathbf{0} & \mathbf{X}_{35,10} \\ & & & & & \mathbf{X}_{366} & \mathbf{X}_{367} & \mathbf{X}_{368} & \mathbf{X}_{369} & \mathbf{X}_{36,10} \\ & & & & & & \mathbf{X}_{377} & \mathbf{X}_{378} & \mathbf{X}_{379} & \mathbf{X}_{37,10} \\ & & & & & & & \mathbf{X}_{388} & \mathbf{X}_{389} & \mathbf{X}_{38,10} \\ & & \mathbf{0} & & & & & & \mathbf{X}_{399} & \mathbf{X}_{39,10} \\ & & & & & & & & & \mathbf{X}_{3,10,10} \end{bmatrix} \tag{102}$$

where the division of $\mathbf{X}_3$ into the submatrices is assumed to be made in accordance with that of $\mathbf{H}_3^{(i)}$, eq 66. Decomposition of $\mathbf{X}_3{}^N$ in eq 101 yields a numerous number of terms. It is found that the leading terms of order N^3 are of the form $\mathbf{X}_{311}{}^{i_1-1}\mathbf{X}_{312} \ldots \mathbf{X}_{39,10}\mathbf{X}_{3,10,10}{}^{N-i_3}$ and hence come exclusively from the part of $\mathbf{X}_3$ as enveloped by broken lines. Therefore we have

$$N\zeta_u\langle \mathrm{Tr}\, \hat{\boldsymbol{\gamma}}\mathbf{f}\rangle \simeq \sum_{1\le i<j\le N} \zeta_u{}^2(\mathbf{v}\,\mathbf{0}\ldots\mathbf{0}) \times \begin{bmatrix} \mathbf{X}_{322} & \mathbf{X}_{323} & \mathbf{X}_{324} & \mathbf{X}_{327} & \mathbf{X}_{328} & \mathbf{X}_{329} \\ & \mathbf{X}_{333} & \mathbf{X}_{334} & \mathbf{0} & \mathbf{X}_{338} & \mathbf{X}_{339} \\ & & \mathbf{X}_{344} & \mathbf{0} & \mathbf{0} & \mathbf{X}_{349} \\ & & & \mathbf{X}_{377} & \mathbf{X}_{378} & \mathbf{X}_{379} \\ & \mathbf{0} & & & \mathbf{X}_{388} & \mathbf{X}_{389} \\ & & & & & \mathbf{X}_{399} \end{bmatrix}^{j-i-1} \begin{bmatrix} \mathbf{0} \\ \cdot \\ \cdot \\ \cdot \\ \mathbf{0} \\ \mathbf{u} \end{bmatrix} \tag{103}$$

where use was made of $\mathbf{v}\mathbf{X}_{311}{}^{i-1}\mathbf{X}_{312} = \zeta_u\mathbf{v}$ and $\mathbf{X}_{39,10}\mathbf{X}_{3,10,10}{}^{N-j}\mathbf{u} = \zeta_u\mathbf{u}$. We can easily confirm that $\mathbf{X}_{322} = \mathbf{X}_{111}$, $\mathbf{X}_{323} = \mathbf{X}_{112}$, etc., and hence the matrix in eq 103 is identical with $\mathbf{X}_1$, eq 88. Substituting eq 87 having $j - i - 1$ in place of N into eq 103 and summing over i and j by utilizing eq 100, we have for the asymptotic value of $\langle \mathrm{Tr}\, \hat{\boldsymbol{\gamma}}\mathbf{f}\rangle$

$$\langle \mathrm{Tr}\, \hat{\boldsymbol{\gamma}}\mathbf{f}\rangle_* = {}^1/_6 N\zeta_u\langle \mathbf{r}^T\hat{\boldsymbol{\gamma}}\mathbf{r}\rangle_* \tag{104}$$

and hence

$$\Delta\Gamma_f = {}^3/_2\langle \mathrm{Tr}\, \mathbf{f}\rangle_*{}^{-1}\langle \mathrm{Tr}\, \hat{\boldsymbol{\gamma}}\mathbf{f}\rangle_* = {}^3/_2\langle r^2\rangle_*{}^{-1}\langle \mathbf{r}^T\hat{\boldsymbol{\gamma}}\mathbf{r}\rangle_* = \Delta\Gamma_s \tag{105}$$

The analysis of this section has yielded several important results. We have explored concise derivations of $\langle r^2\rangle_*$, $\Delta\Gamma_s$, etc., and obtained (probably, the most) compact expressions for $\langle r^2\rangle_*$ and $\Delta\Gamma_s$.

Of particular importance is the relationship given by eq 105, which is valid for stereoregular chains of infinite length. It implies that flow birefringence gives the same molecular information as does strain birefringence. Of course, various assumptions that led to this conclusion should not be forgotten, *i.e.*, the neglect of the hydrodynamic interaction, the excluded-volume effect, and other side effects. It is interesting that friction constants ζ_t have canceled out in eq 105, and hence $\Delta\Gamma_f$ is independent of the way in which ζ_u is partitioned on skeletal atoms of a unit. From this result we speculate that eq 105 would be valid when frictions are attached to skeletal as well as nonskeletal atoms, *i.e.*, those on pendant groups. Rigorously, eq 105 is valid only for infinite chains. In practice, however, the agreement between $\Delta\Gamma_f$ and $\Delta\Gamma_s$ is reached with relatively short chains for polymers of an ordinary degree of flexibility, say, 10^3 skeletal bonds (see succeeding paper[17]).

Appendix

$\langle r^2\rangle/N$, etc., can be comprehended in a general relation

$$\langle\ \ \rangle/N = (\mathbf{v}\,\mathbf{0}\ldots\mathbf{0})\mathbf{Z}_2\mathbf{Z}_3\ldots\mathbf{Z}_{t-1}\mathbf{X}\begin{bmatrix} \mathbf{0} \\ \cdot \\ \cdot \\ \cdot \\ \mathbf{0} \\ \mathbf{u} \end{bmatrix} \tag{A1}$$

with

$$\mathbf{Z}_k = \mathbf{E} + \mathbf{X}\begin{bmatrix} \mathbf{0} \\ \cdot \\ \cdot \\ \cdot \\ \mathbf{0} \\ \mathbf{E} \\ \mathbf{0} \\ \cdot \\ \cdot \\ \cdot \\ \mathbf{0} \end{bmatrix}(\mathbf{E} - \mathbf{Y}_k)^{-1}(\mathbf{0}\ldots\mathbf{0}\,\mathbf{E}\,\mathbf{0}\ldots\mathbf{0}) \tag{A2}$$

$$\mathbf{X} = \begin{bmatrix} \mathbf{X}_{11} & \mathbf{X}_{12} & \ldots & \mathbf{X}_{1t} \\ & \mathbf{X}_{12} & \ldots & \mathbf{X}_{2t} \\ & & \ldots & \\ \mathbf{0} & & & \mathbf{X}_{tt} \end{bmatrix} \tag{A3}$$

In eq A2, it is assumed that the second and fourth $\mathbf{E}$'s are both preceded by $k - 1$ $\mathbf{0}$'s of appropriate sizes. If we introduce t matrices, $\xi_1, \xi_2, \ldots, \xi_t$, defined by

$$\langle\ \ \rangle/N = \mathbf{v}(\xi_1\,\xi_2\ldots\xi_{j-1}\,\mathbf{0}\ldots\mathbf{0})\mathbf{Z}_j\mathbf{Z}_{j+1}\ldots\mathbf{Z}_{t-1}\mathbf{X}\begin{bmatrix} \mathbf{0} \\ \cdot \\ \cdot \\ \cdot \\ \mathbf{0} \\ \mathbf{u} \end{bmatrix} \tag{A4}$$

then we find

$$\langle\ \rangle/N = \mathbf{v}\xi_t\mathbf{u} \tag{A5}$$

with

$$\begin{aligned} -\mathbf{E} &= -\xi_1 \\ \mathbf{0} &= \xi_1\mathbf{X}_{1j} + \xi_2\mathbf{X}_{2j} + \ldots + \xi_{j-1}\mathbf{X}_{j-1,j} + \xi_j(\mathbf{Y}_j - \mathbf{E}), \quad j = 2, 3, \ldots, t-1 \\ &= \xi_1\mathbf{X}_{1t} + \xi_2\mathbf{X}_{2t} + \ldots + \xi_{t-1}\mathbf{X}_{t-1,t} - \xi_t \end{aligned} \tag{A6}$$

Solving this set of linear simultaneous matrix equations with respect to ξ's, and substituting ξ_t into eq A5 we obtain

$$\langle\ \rangle/N = -(\mathbf{v}\ \mathbf{0}\ \ldots\ \mathbf{0}) \begin{bmatrix} -\mathbf{E} & \mathbf{X}_{12} & \mathbf{X}_{13} & & \mathbf{X}_{1t} \\ & \mathbf{Y}_2 - \mathbf{E} & \mathbf{X}_{23} & & \mathbf{X}_{2t} \\ & & \mathbf{Y}_3 - \mathbf{E} & & \mathbf{X}_{3t} \\ & & & \ddots & \\ & \mathbf{0} & & \mathbf{Y}_{t-1} - \mathbf{E} & \mathbf{X}_{t-1,t} \\ & & & & -\mathbf{E} \end{bmatrix}^{-1} \begin{bmatrix} \mathbf{0} \\ \cdot \\ \cdot \\ \cdot \\ \mathbf{0} \\ \mathbf{u} \end{bmatrix} \tag{A7}$$

Putting $t = 3$, $\mathbf{X} = \mathbf{X}_0$, and

$$(\mathbf{E} - \mathbf{Y}_2)^{-1} = (\mathbf{E} - \mathbf{X}_{022})^{-1}[\mathbf{E} - N^{-1}(\mathbf{E} - \mathbf{X}_{022})^{-1}(\mathbf{E} - \mathbf{X}_{022^N})] \tag{A8}$$

we obtain eq 79.

We note that the recurrence relation eq A5 and A6 is less elegant but more effective than eq A7, for the computational purpose both in computational speed and in less occupation of computer memories. $\langle \mathbf{r}^T\hat{\gamma}\mathbf{r}\rangle_*/N$, eq 100, etc., can be expressed in the form of eq A5 with eq A6, if t, $\mathbf{X}$, and $\mathbf{Y}_k$'s are appropriately chosen.

Flow Birefringence of Real Polymer Chains. Application to *n*-Alkanes

by Kazuo Nagai

Government Industrial Research Institute, Osaka, Midorigaoka 1, Ikeda, Osaka, Japan *(Received July 14, 1969)*

The flow-birefringence optical anisotropy $\Delta\Gamma_f$ of Kuhn's random link, together with related quantities, is calculated for *n*-alkanes, on the basis of the theory developed in the preceding paper. The model employed is the familiar rotational-isomeric, three-state (trans T, gauche G, and gauche prime G′) model. The bond angles are assumed to be tetrahedral and the GG′ conformation for a pair of neighboring bonds is eliminated. The agreement of $\Delta\Gamma_f$ with $\Delta\Gamma_s$, the strain-birefringence optical anisotropy of Kuhn's random link, at the limit of infinite chain length, as predicted in the preceding paper, is numerically confirmed. The theory is compared with experimental results on *n*-alkane liquids reported by Champion and his coworkers. In comparison of theoretical results obtained for isolated chains with observed values for pure liquids, the isolated-chain approximation is employed, which was suggested by Bueche and discussed by Fox and Allen, in the theoretical interpretation of bulk viscosity of polymers. The agreement between theory and experiment is rather poor. Various aspects of the isolated-chain approximation are examined, and the short-range orientational order among chain segments is suggested to be one of mechanisms responsible for the discrepancy.

I. Introduction

This paper is concerned with an application to *n*-alkanes of the theory developed in the preceding paper.[1] One aim is to confirm numerically the agreement of the stress-optical coefficient obtained from flow birefringence with that from strain birefringence, or of $\Delta\Gamma_f$ with $\Delta\Gamma_s$, at the limit of infinite chain length, a result predicted in the preceding paper.[1] If this is the

(1) K. Nagai, *J. Phys. Chem.*, **74**, 3411 (1970).

case, it is also of great interest how rapidly the former converges to the latter with increasing chain length.

We attempt to make comparisons with experiment. Champion and his coworkers[2,3] reported flow-birefringence measurements on a series of n-alkanes as pure liquids over a temperature range. They analyzed their data by regarding a n-alkane molecule as a rigid ellipsoid of revolution, on the basis of the Raman–Krishnan theory.[4] Obviously, a rigid ellipsoid of revolution is a rather poor model for n-alkanes; even the lowest members such as butane and pentane are reasonably deformable by rotation about skeletal bonds[5] and lack the assumed symmetry for most conformations. The Raman–Krishnan theory[4] is of dubious validity. We analyze the data of Champion, *et al.*,[2,3] by means of the present theory which is based on more realistic models for n-alkanes.

The preceding paper[1] is hereafter referred to as I and eq ab of it as eq I-ab. Most of symbols which retain their previous meanings are used without definition. Preliminary results of this work were published elsewhere.[6]

II. Model and Procedure of Calculations

The model employed is the now-familiar three-state [trans ($\theta^{(T)} = 0°$), gauche ($\theta^{(G)} = 120°$), and gauche prime ($\theta^{(G')} = -120°$)] rotational-isomeric model.[7-9] Bond lengths and angles are both assumed to be fixed, the latter being taken as the tetrahedral angle. In n-alkanes the T, G, and G′ rotations about terminal C–C bonds do not produce distinguishable conformations. For this reason we regard n-alkane molecules as composed of skeletal C–C bonds alone, in constructing the partition function, etc. The partition function Z_n for the n-alkane chain comprising n C–C bonds is expressed, according to eq I-57 and I-59, as [10]

$$Z_n = \mathbf{e}_3^T \mathbf{q}^{n-1} \mathbf{e}_3 \tag{1}$$

$$\mathbf{q} = \begin{bmatrix} 1 & 1 & 1 \\ \sigma & \sigma & \epsilon \\ \sigma & \epsilon & \sigma \end{bmatrix} \tag{2}$$

where σ is the statistical weight of a gauche bond neighboring to a trans bond or a gauche bond of the same sense, and ϵ, which we set equal to zero throughout, is that of a gauche bond neighboring to a gauche bond of the opposite sense.

According to a previous formulation (ref 14 of I), Z_4 is given by

$$Z_4 = (1\ 1\ 1)\begin{bmatrix} 1 & 0 & 0 \\ 0 & 1 & 0 \\ 0 & 0 & 1 \end{bmatrix}\begin{bmatrix} 1 & 1 & 1 \\ \sigma & \sigma & \epsilon \\ \sigma & \epsilon & \sigma \end{bmatrix}\begin{bmatrix} 1 & 0 & 0 \\ 0 & \sigma & 0 \\ 0 & 0 & \sigma \end{bmatrix}\begin{bmatrix} 1 \\ 1 \\ 1 \end{bmatrix} \tag{3}$$

whereas the present formulation, eq 1 or eq I-57, yields

$$Z_4 = (1\ 0\ 0)\begin{bmatrix} 1 & 1 & 1 \\ \sigma & \sigma & \epsilon \\ \sigma & \epsilon & \sigma \end{bmatrix}\begin{bmatrix} 1 & 1 & 1 \\ \sigma & \sigma & \epsilon \\ \sigma & \epsilon & \sigma \end{bmatrix}\begin{bmatrix} 1 & 1 & 1 \\ \sigma & \sigma & \epsilon \\ \sigma & \epsilon & \sigma \end{bmatrix}\begin{bmatrix} 1 \\ 0 \\ 0 \end{bmatrix} \tag{4}$$

In eq 4, the second and third rows of the first matrix and the second and third columns of the last matrix are arbitrary but are chosen as above in order to express Z_4 in terms of the single matrix $\mathbf{q}$. The equivalence of eq 3 and 4, and the advantages of the latter, are obvious.

We normalize $\mathbf{q}$ by dividing by its largest eigenvalue

$$\lambda = {}^1/_2\{1 + \sigma + \epsilon + [(1 + \sigma + \epsilon)^2 + 4(\sigma - \epsilon)]^{1/2}\}$$

as suggested previously,[1,10] *i.e.*

$$\mathbf{p} = \lambda^{-1}\mathbf{q} \tag{5}$$

and thus have

$$Z_n = \lambda^{n-1}\mathbf{e}_3^T\mathbf{p}^{n-1}\mathbf{e}_3 \tag{6}$$

The advantage of using $\mathbf{p}$ instead of $\mathbf{q}$ lies in that it prevents elements of various matrices to become extraordinarily large numbers when matrices are raised to high powers.

As far as anisotropies of polarizabilities are concerned, we can regard, with the assumption of the tetrahedral bond angles, that each C–C bond possesses the effective bond anisotropy

$$\Delta\alpha_e = (\alpha_1 - \alpha_2)_{C-C} - 2(\alpha_1 - \alpha_2)_{C-H} \tag{7}$$

and C–H bonds no anisotropy, where $(\alpha_1 - \alpha_2)_{C-C}$ and $(\alpha_1 - \alpha_2)_{C-H}$ are the anisotropies of the C–C and C–H bonds, respectively.[11] Remembering that the unit vector along a C–C bond is given by $(1\ 0\ 0)^T$ in the coordinate system defined with respect to this and preceding C–C bonds,[1] we find for the traceless tensor of each group

$$\Delta\hat{\alpha} = \Delta\alpha_e\begin{bmatrix} {}^2/_3 & 0 & 0 \\ 0 & -{}^1/_3 & 0 \\ 0 & 0 & -{}^1/_3 \end{bmatrix} \tag{8}$$

and hence

$$\Delta\hat{\alpha}^\dagger = \Delta\alpha_e({}^2/_3\ 0\ 0\ -{}^1/_3\ 0\ -{}^1/_3)^T \tag{9}$$

Concerning the hydrodynamic property of the chain, we assume all carbon atoms to have an identical friction constant ζ.

(2) J. V. Champion and G. H. Meeten, *Trans. Faraday Soc.*, **64**, 238 (1968).
(3) J. V. Champion and P. F. North, *ibid.*, **64**, 2287 (1968).
(4) C. V. Raman and K. S. Krishnan, *Phil. Mag.*, **5**, 769 (1928).
(5) G. J. Szasz, N. Sheppard, and D. H. Rank, *J. Chem. Phys.*, **16**, 704 (1948); N. Sheppard and G. J. Szasz, *ibid.*, **17**, 86 (1949); S. Mizushima and H. Okazaki, *J. Amer. Chem. Soc.*, **71**, 3411 (1949); K. Kuchitsu, *Bull. Chem. Soc. Jap.*, **32**, 748 (1959); L. S. Bartell and D. A. Kohl, *J. Chem. Phys.*, **39**, 3097 (1963).
(6) K. Nagai, *Rep. Prog. Polym. Phys. Jap.*, **12**, 41 (1969).
(7) C. A. J. Hoeve, *J. Chem. Phys.*, **35**, 1266 (1961).
(8) K. Nagai and T. Ishikawa, *ibid.*, **37**, 496 (1962).
(9) A. Abe, R. L. Jernigan, and P. J. Flory, *J. Amer. Chem. Soc.*, **88**, 631 (1966).
(10) K. Nagai, *J. Chem. Phys.*, **45**, 838 (1966).
(11) R. A. Sack, *ibid.*, **25**, 1087 (1956).

We have now defined all quantities in terms of which to express $\langle r^2 \rangle$, etc. We have for $\langle r^2 \rangle$

$$\langle r^2 \rangle = Z_n^{-1}\lambda^{n-1}(\mathbf{0}\ \mathbf{e}_3^T\ \mathbf{0}\ \mathbf{0}\ \mathbf{0})\mathbf{H}_2^{n-1}\mathbf{H}_2^{(n)}\begin{bmatrix}\mathbf{0}\\ \mathbf{0}\\ \mathbf{0}\\ \mathbf{e}_3\\ \mathbf{0}\end{bmatrix} \quad (10)$$

where $\mathbf{H}_2$ is given by eq I-65 and $\mathbf{H}_2^{(n)}$ is equal to $\mathbf{H}_2$ with $\mathbf{E}_3$ in place of $\mathbf{p}$. For the computational purpose it is more convenient to arrange eq 10 as

$$\langle r^2 \rangle = Z_n^{-1}\lambda^{n-1}(\mathbf{0}\ \mathbf{e}_3^T\ \mathbf{0}\ \mathbf{0}\ \mathbf{0})\mathbf{H}_2^{n}\begin{bmatrix}\mathbf{0}\\ \mathbf{0}\\ \mathbf{0}\\ \mathbf{p}^{-1}\mathbf{e}_3\\ \mathbf{0}\end{bmatrix} \quad (11)$$

with

$$\mathbf{p}^{-1}\mathbf{e}_3 = \lambda(\sigma - \epsilon)^{-1}[-(\sigma + \epsilon)\ \sigma\ \sigma]^T \quad (12)$$

Similarly, we have

$$(n+1)\zeta\langle \mathrm{Tr}\ \mathbf{f} \rangle = Z_n^{-1}\lambda^{n-1}(\mathbf{e}_3^T\ \mathbf{0}\ldots\mathbf{0})\mathbf{H}_2^{n}\begin{bmatrix}\mathbf{0}\\ \mathbf{0}\\ \mathbf{0}\\ \zeta\mathbf{p}^{-1}\mathbf{e}_3\\ \mathbf{p}^{-1}\mathbf{e}_3\end{bmatrix} \quad (13)$$

$$\langle \mathbf{r}^T\hat{\boldsymbol{\gamma}}\mathbf{r} \rangle = Z_n^{-1}\lambda^{n-1}(\mathbf{0}\ \mathbf{e}_3^T\ \mathbf{0}\ldots\mathbf{0})\mathbf{H}_3^{n}\begin{bmatrix}\mathbf{0}\\ \cdot\\ \cdot\\ \cdot\\ \mathbf{0}\\ \mathbf{p}^{-1}\mathbf{e}_3\\ \mathbf{0}\end{bmatrix} \quad (14)$$

$$(n+1)\zeta\langle \mathrm{Tr}\ \hat{\boldsymbol{\gamma}}\mathbf{f} \rangle = Z_n^{-1}\lambda^{n-1}(\mathbf{e}_3^T\ \mathbf{0}\ldots\mathbf{0})\mathbf{H}_3^{n}\begin{bmatrix}\mathbf{0}\\ \cdot\\ \cdot\\ \cdot\\ \mathbf{0}\\ \zeta\mathbf{p}^{-1}\mathbf{e}_3\\ \mathbf{p}^{-1}\mathbf{e}_3\end{bmatrix} \quad (15)$$

The flow-birefringence and strain-birefringence optical anisotropies of Kuhn's random link are then expressed, respectively, as

$$\Delta\Gamma_f = {}^3/_2\langle \mathrm{Tr}\ \mathbf{f} \rangle^{-1}\langle \mathrm{Tr}\ \hat{\boldsymbol{\gamma}}\mathbf{f} \rangle \quad (16)$$

$$\Delta\Gamma_s = {}^3/_2\langle r^2 \rangle^{-1}\langle \mathbf{r}^T\hat{\boldsymbol{\gamma}}\mathbf{r} \rangle \quad (17)$$

Computations are carried out in the following way. We (i) construct $\mathbf{H}_2$, $\mathbf{H}_3$, and the column vectors at the for right in eq 11 and 13–15, (ii) multiply $\mathbf{H}_2$ or $\mathbf{H}_3$ to the vectors to yield new vectors, (iii) obtain the required averages by making the scalar product of the left, row vectors in eq 11 etc., with the ensuing column vectors and by dividing it by Z_n, and (iv) repeat the procedures (ii) and (iii) to obtain the averages for larger n. Separate calculation of Z_n is unnecessary; it is obtained as the scalar product of $\mathbf{e}_3^T$ with the last symbolic element of the ensuing column vectors. λ^{n-1} is totally omitted in the computations.

III. Numerical Results

We put $\epsilon = 0$, thereby eliminating the GG′ conformation for every pair of neighboring bonds, and assume the Boltzmann relation

$$\sigma = \exp(-E_G/RT) \quad (18)$$

where E_G is the energy of the gauche conformation, relative to that of the trans, R is the gas constant, and T is the absolute temperature. Numerical results of $\Delta\Gamma_f/\Delta\alpha_e$ are plotted against n, the chain length, for various values of E_G in Figure 1. In these calculations $R = 1.987$ cal/deg and $T = 298.16$°K were used. Values of $\Delta\Gamma_f$ for other temperatures and energies, T' and E_G', can be obtained by interpolation; seek $\Delta\Gamma_f$ for $E_G = 298.16\ E_G'/T'$.

We have examined the asymptotic behavior of various quantities for large n. From the analysis for stereoregular polymers of infinite length, given in I, we expect the following relations

$$\langle r^2 \rangle = a_0 n + b_0 \quad (19)$$

$$\langle \mathbf{r}^T\hat{\boldsymbol{\gamma}}\mathbf{r} \rangle = a_1 n + b_1 \quad (20)$$

$$(n+1)\langle \mathrm{Tr}\ \mathbf{f} \rangle = a_2 n^3 + b_2 n^2 + c_2 n + d_2 \quad (21)$$

$$(n+1)\langle \mathrm{Tr}\ \hat{\boldsymbol{\gamma}}\mathbf{f} \rangle = a_3 n^3 + b_3 n^2 + c_3 n + d_3 \quad (22)$$

where we have put b (bond length) $= 1$, $\zeta = 1$, and $\Delta\alpha_e = 1$, without any loss of generality. If these relations are reached, the coefficients determined by the relations should converge

$$a = \Delta y_n \text{ and } b = y_n - na \quad (23)$$

for $\langle r^2 \rangle$ and $\langle \mathbf{r}^T\hat{\boldsymbol{\gamma}}\mathbf{r} \rangle$, and

$$a = {}^1/_6\Delta^3 y_n,\ b = {}^1/_2[\Delta^2 y_n - 6(n-1)a]$$
$$c = \Delta y_n - (2n-1)b - (3n^2 - 3n + 1)a$$

and

$$d = y_n - an^3 - bn^2 - cn \quad (24)$$

for $\langle \mathrm{Tr}\ \mathbf{f} \rangle$ and $\langle \mathrm{Tr}\ \hat{\boldsymbol{\gamma}}\mathbf{f} \rangle$, where y_n stands for $\langle r^2 \rangle$ etc. for n, and $\Delta^k y_n = \Delta^{k-1} y_n - \Delta^{k-1} y_{n-1}$ with $\Delta^0 y_n \equiv y_n$.

The asymptotic expressions eq 19–22 were actually borne out with numerical data; the convergence was reached with $n = 100 \sim 120$, though with considerable fluctuations. As a result it is confirmed that $a_2 = a_0/6$ and $a_3 = a_1/6$, or $(\mathrm{Tr}\ \mathbf{f})_* = n\langle r^2 \rangle_*/6$ and $\langle \mathrm{Tr}\ \hat{\boldsymbol{\gamma}}\mathbf{f} \rangle_* = n\langle \mathbf{r}^T\hat{\boldsymbol{\gamma}}\mathbf{f} \rangle_*/6$, and hence

$$\Delta\Gamma_f = {}^3/_2\langle \mathrm{Tr}\ \mathbf{f} \rangle_*^{-1}\langle \mathrm{Tr}\ \hat{\boldsymbol{\gamma}}\mathbf{f} \rangle_* = {}^3/_2\langle r^2 \rangle_*^{-1}\langle \mathbf{r}^T\hat{\boldsymbol{\gamma}}\mathbf{r} \rangle_* = \Delta\Gamma_s \quad (25)$$

Table I: Coefficients in (eq 19–22) for Selected Values of E_G, (R = 1.987 cal/deg and T = 298.16°K were used)

	E_G, kcal/mol				
	0	0.4	0.5	0.6	0.8
a_0	5.575 973 99	6.886 045 42	7.395 777 75	7.997 369 98	9.537 064 83
b_0	−26.342 331	−37.455 056	−42.725 974	−49.501 924	−69.452 860
a_1	9.820 530 58	17.877 608 6	21.289 216 1	25.608 086 4	38.208 443 9
b_1	−78.292 74	−165.529 236	−209.734 4	−270.790 9	−477.102 1
a_2	0.929 328 999	1.147 674 24	1.232 629 63	1.332 895 00	1.589 510 81
b_2	−9.980 9	−14.911	−17.306	−20.411	−29.656
c_2	100.2	168.0	205.9	259.1	439.4
d_2	−482	−923	−1 190	−1 620	−3 210
a_3	1.636 755 10	2.979 601 44	3.548 202 68	4.268 014 40	6.368 073 99
b_3	−33.011	−69.202	−87.734	−113.40	−200.37
c_3	426.3	1 010	1 353	1 866	3 843
d_3	−2 570	−6 960	−9 880	−14 560	−35 100

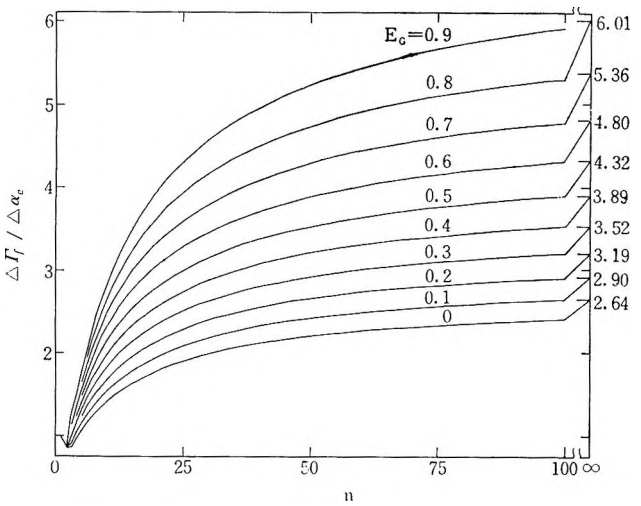

Figure 1. $\Delta\Gamma_f/\Delta\alpha_e$ *vs.* n, the chain length, for various values of E_G (kcal/mol). R = 1.987 cal/deg and T = 298.16°K were used (*cf.* eq 18).

in accordance with the theoretical prediction,[1] where the asterisked average is the limiting value at the limit of infinite chain length.

Fluctuations in coefficients with varying n arise from the fact that coefficients are obtained as small differences among large quantities. About five significant digits are lost in a_2 and a_3, and these errors introduce more exaggerated errors in b, c, and d. Fluctuations are considerably reduced by utilizing $a_2 = a_0/6$ and $a_3 = a_1/6$ instead of $a = {}^1/_6\Delta^3 y$ in eq 24, and by using values of a_0 and a_1 obtained by the largest eigenvalue method.[12] Coefficients for selected values of E_G, determined in this way by using consecutive y_n's ending at n = 100 (for the first four) or at n = 120, are given in Table I. It is found that eq 19–22 for $\langle r^2\rangle$ etc., with coefficients thus determined, reproduce values directly calculated according to eq 11 and 13–15, with an accuracy of 10^{-6} or better, for $n > 100$. Obviously the accuracy should increase with increasing n. Thus the direct calculation of $\langle r^2\rangle$ etc., through $n \simeq 100$, together with the n-dependence analysis described above permits us to cover the entire range of n, thereby obviating the time-consuming process of raising matrices of considerable sizes to very high powers.

Temperature coefficients of $\Delta\Gamma_f$ are plotted against n in Figure 2. These values are calculated from values of $\Delta\Gamma_f$ at two temperatures in a close proximity of $0.01 \sim 0.1°$.

Figure 3 indicates that $\Delta\Gamma_f/\Delta\alpha_e$ (solid curves) and $\Delta\Gamma_s/\Delta\alpha_e$ (broken) converge to a common limit, but the former does more slowly. In this figure, circles are values of $\Delta\Gamma_f$ for the hypothetical m-repeat chain which differs from the previous one only in that the first and every subsequent mth carbons alone bear a constant, nonzero friction. By the n-dependence analysis it is confirmed that $\Delta\Gamma_f$ for this model also tends to the same limit at the limit of $n \to \infty$, irrespective of m.

Ratios of values of $\langle r^2\rangle$ etc. to respective limiting values for E_G = 0.8 kcal/mol are plotted against n in Figure 4. The characteristic ratio $\langle r^2\rangle_*/n$ = 9.537 and hence the flexibility, for this value of E_G, are typical of those for most synthetic polymers. We therefore examine the degree of convergence of various quantities to respective limiting values, using this parameter. Percentage attainments at n = 200, 500, 1000, and 1500, respectively, are: $\Delta\Gamma_f$ (93.8, 97.5, 98.7, 99.2); $\Delta\Gamma_s$ (97.3, 98.9, 99.5, 99.7); $\langle r^2\rangle$ (96.4, 98.5, 99.3, 99.5); $\langle \mathbf{r}^T\hat{\boldsymbol{\gamma}}\mathbf{r}\rangle$ (93.8, 97.6, 98.8, 99.2); $(n+1)\langle \mathrm{Tr}\,\mathbf{f}\rangle$ (91.3, 96.4, 98.2, 98.8); $(n+1)\langle \mathrm{Tr}\,\hat{\boldsymbol{\gamma}}\mathbf{f}\rangle$ (85.7, 93.9, 96.9, 97.9). We thus see that lengths of about 10^3 skeletal bonds are sufficient to make $\Delta\Gamma_f$ practically indistinguishable from its limiting value.

IV. Comparison with Experiment

Some additional assumptions are needed to apply the present theory to data on pure liquids of n-alkanes, because the theory was formulated for isolated chains. It seems prohibitively difficult to develop a theory

(12) K. Nagai, *J. Chem. Phys.*, **40**, 2818 (1964).

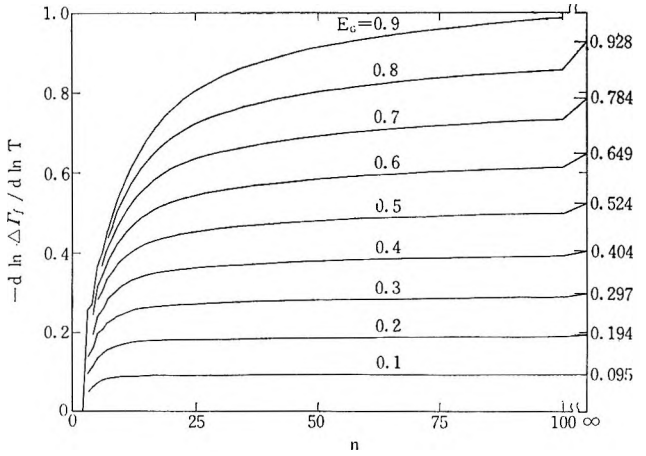

Figure 2. $-d \ln \Delta\Gamma_f/d \ln T$ *vs.* n, the chain length, for various values of E_G(kcal/mol). R = 1.987 cal/deg and T = 298.16°K were used.

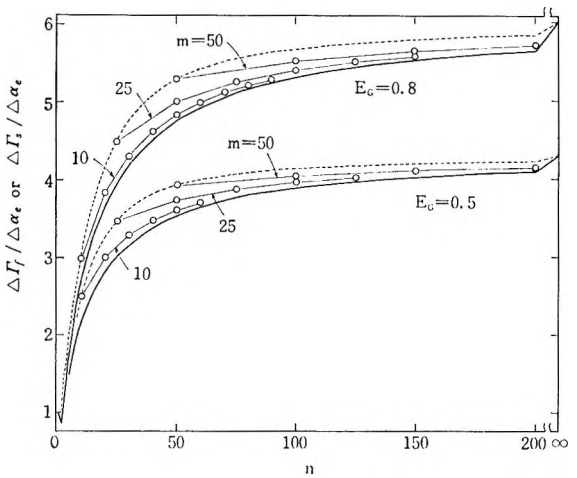

Figure 3. $\Delta\Gamma_f/\Delta\alpha_e$ (solid curves) and $\Delta\Gamma_s/\Delta\alpha_e$ (broken) *vs.* n, the chain length. Circles and lines connecting them are $\Delta\Gamma_f$ for a hypothetical m-repeat polymer, that is, the n-alkane chain whose first and every subsequent mth carbons alone bear a nonzero friction. Other parameters: E_G (kcal/mol) as indicated, R = 1.987 cal/deg, and T = 298.16°K.

which takes into account complicated interactions among chains which may occur in pure liquids in flow. According to Fox and Allen,[13-15] the chain-length dependence of bulk viscosity of most polymers can be well interpreted by a theory originally developed (by Debye[16]) for isolated chains, provided chain lengths do not exceed some critical values n_c. This result was explained as follows.[13,15] For polymers of chains shorter than n_c, chain entanglements could be neglected, and hence, for an individual chain, the rest of polymer could be regarded as acting as a continuum medium with an enhanced viscosity. This idea, which is widely accepted at present,[15] was first put forward by Bueche.[17] We follow this idea as the first approximation. n-Alkanes we are here interested in are much shorter than the critical length n_c = 270 for polyethylene.[18]

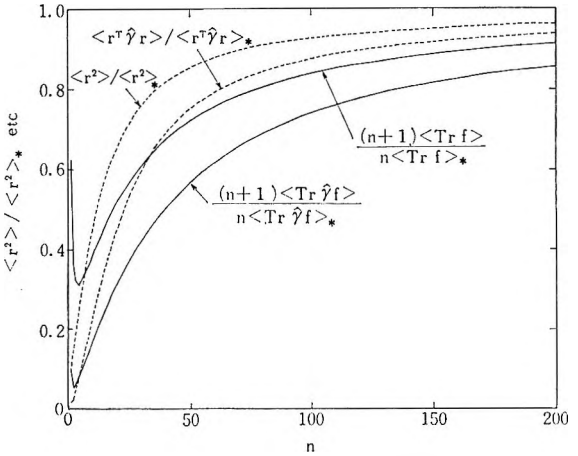

Figure 4. Ratios of $\langle r^2\rangle$ etc., to respective limiting values, *vs.* n, the chain length. Parameters: E_G = 0.8 kcal/mol, R = 1.987 cal/deg, and T = 298.16°K.

With this isolated-chain approximation, most relations given in I remain valid with minor changes. The birefringence Δn is given by eq I-19 with n the refractive index of pure liquids instead of n_0.

$$\Delta n = (\pi/45kT)[(n^2 + 2)^2/n]GN_p\langle \mathrm{Tr}\, \hat{\boldsymbol{\gamma}}\mathbf{f}\rangle \quad (26)$$

(Do not confuse this n with the chain length; n in the Lorentz–Lorenz factor is the refractive index.) The viscosity is given by eq I-21 with the η_0 term omitted

$$\eta = {}^1/_6 N_p\langle \mathrm{Tr}\, \mathbf{f}\rangle \quad (27)$$

Thus we find for the stress-optical coefficient

$$C_f = \Delta n/2\eta G = (2\pi/45kT)[(n^2 + 2)^2/n]\Delta\Gamma_f \quad (28)$$

Champion and Meeten[2] and Champion and North[3] recently reported experimental values of the stress-optical coefficient and its temperature coefficient of n-alkane liquids with n = 8~19 over a temperature range 15~50°. Some of their results are reproduced in Table II. We include there values of $\Delta\Gamma_{f,obsd}$ which are calculated from C_f according to eq 28 by using 1.422 throughout for the refractive index, the value for n-dodecane (n = 11) at 20°. Champion, *et al.*,[2,3] used Vuks' modification[19] of the Lorentz–Lorenz internal field, instead of the original L–L (used in this work). With this modification, C_f in eq 28 is smaller by a factor of $(n^2 + 2)/3$ = 1.341, and therefore values of $\Delta\Gamma_{f,obsd}$ are greater by this factor than those in Table II. Champion, *et al.*,[2,3] analyzed their data by approximating an n-alkane chain by a rigid ellipsoid of revolution, on the basis of the Raman–Krishnan[4] (R–K) as

(13) T. G Fox and V. R. Allen, *J. Chem. Phys.*, **41**, 344 (1964).
(14) V. R. Allen and T. G Fox, *ibid.*, **41**, 337 (1964).
(15) G. C. Berry and T. G Fox, *Advan. Polym. Sci.*, **5**, 261 (1968).
(16) P. Debye, *J. Chem. Phys.*, **14**, 636 (1946).
(17) F. Bueche, *ibid.*, **20**, 1959 (1952).
(18) See ref 15, p 269, Table I.
(19) M. F. Vuks, *Opt. Spectrosc.*, **20**, 361 (1966).

Table II: Observed Values of the Stress-Optical Coefficient C_f, $\Delta\Gamma_f$, and the Temperature Coefficient of C_f, of n-Alkane Liquids, by Champion and Coworkers[2,3]

n, no. of C–C bonds	$C_f \times 10^{16}$, cm sec²/g		$\Delta\Gamma_{f,obsd} \times 10^{24}$, cm³ [a]		$[d \ln C_f/d(1/T)]_{obsd}$, deg,[b]
	At 20°	At 36°	At 20°	At 36°	At 36°
8	0.355		0.904		
9	0.415		1.057		
10	0.54		1.375		
11	0.59	0.59	1.503	1.585	689
12	0.695	0.665	1.770	1.786	575
13	0.785	0.785	1.999	2.109	417
14	0.97	0.785	2.471	2.109	866
15	1.055	0.88	2.687	2.364	884
16		1.005		2.699	880
17		1.135		3.049	901
18		1.23		3.304	883
19		1.265		3.398	878

[a] Calculated from C_f according to eq 28 by using $n = 1.422$. [b] Small temperature dependences of the refractive index were neglected.[3]

well as Peterlin–Stuart[20] (P–S) theories. They found that the chain-length dependence of C_f can be satisfactorily interpreted by the R–K theory but cannot by the P–S theory, while the temperature dependence cannot by either. A rigid ellipsoid of revolution is not a good model for n-alkanes in the liquid state, as we have pointed out. The R–K theory is of dubious validity.

If our rotational-isomeric-state model and other various assumptions are valid, the ratio of observed to calculated values of $\Delta\Gamma_f$, or $\Delta\Gamma_{f,obsd}/\Delta\Gamma_{f,cal}$, should be independent of the chain length. Values of the ratio for data at 20° (circles) and 36° (squares) are plotted against n for $E_G = 0.5$ (open), 0.8 (half-filled) and ∞ (filled) kcal/mol, in Figure 5. We see that the required constancy is not obtained with values of E_G which seem reasonable, *i.e.*, $E_G = 0.5 \sim 0.8$ kcal/mol. Even $E_G = \infty$ is not sufficient to suppress the increase in the ratio with increasing n. This value of E_G, which corresponds to the fully extended, planar zigzag conformation of n-alkanes, is obviously unacceptable. Thus, as for the chain-length dependence, the present theory yields poorer agreement with experiment than does the R–K theory employed by Champion, *et al.*[2,3]

Champion and North[3] analyzed the temperature dependence of C_f through $d \ln C_f/d(1/T)$. Observed values at 36° reported by them are included in Table II. Champion and North[3] showed that if a small temperature dependence of the refractive index is ignored the R–K theory predicts $C_f \propto T^{-1}$ for a rigid model, and therefore

$$d \ln C_f/d(1/T) = T \quad (29)$$

With the same approximation on the refractive index, our theory predicts, according to eq 28

$$d \ln C_f/d(1/T) = T(1 - d \ln \Delta\Gamma_f/d \ln T) \quad (30)$$

Observed values (circles) at 36° by Champion and North[3] are shown in Figure 6, together with theoretical values (curves) calculated according to eq 30, for various values of E_G (kcal/mol) as indicated. The curve for $E_G = 0$ or ∞ corresponds to eq 29, predicted by the R–K theory.

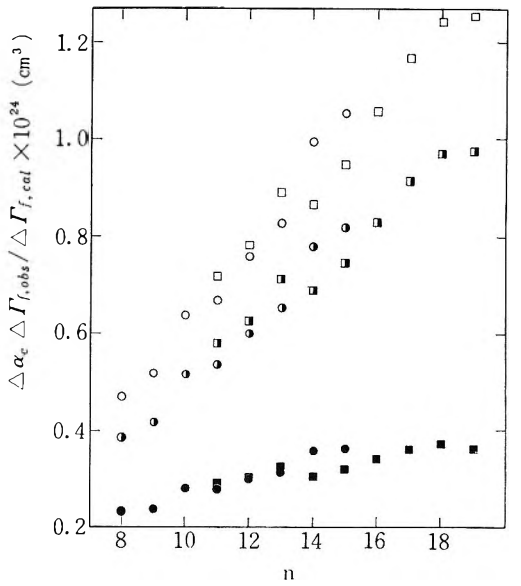

Figure 5. $\Delta\alpha_e\Delta\Gamma_{f,obsd}/\Delta\Gamma_{f,cal}$ *vs.* n, the chain length. Experimental data are those at 20° (circles)[2] and at 36° (squares).[3] Theoretical values are calculated using $E_G = 0.5$ (open), 0.8 (half-filled), and ∞ (filled) kcal/mol, and relevant temperatures.

As E_G decreases from ∞ to 0, or the chain flexibility increases, the calculated temperature coefficient first increases, then passes through a maximum around $E_G = 1.2 \sim 1.5$ kcal/mol, and thereafter decreases; it does by no means reach the observed values (except for $n = 13$). The observed values show discontinuity with respect to n. Champion and North[3] explained this by assuming that in liquids n-alkane chains with $n < 14$ are predominantly in the extended planar conformation whereas those with $n \geq 14$ are in nonextended, rotational-isomeric conformations. Such an abrupt change in flexibility does not seem reasonable, at least as far as isolated chains are concerned. The present theory, which takes into account the presence of various rotational isomers, does not predict any anomaly in the temperature coefficient.

The present theory has thus failed to interpret consistently both items of the chain-length and temperature dependences of the stress-optical coefficient, like the R–K theory employed by Champion, *et al.*[2,3] This requires reexamination of various underlying assumptions.

(20) A. Peterlin and H. A. Stuart, *Z. Phys.*, **113**, 663 (1939).

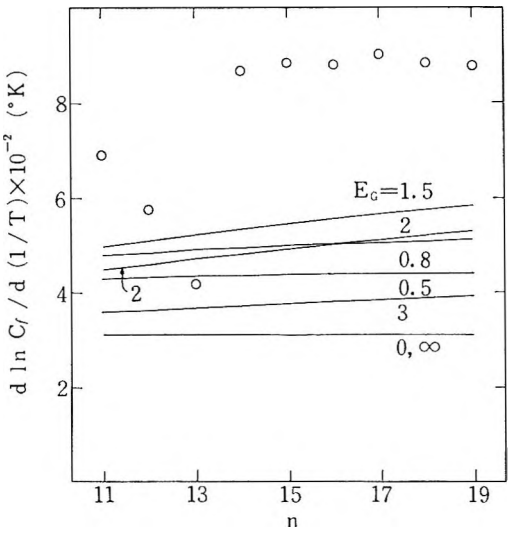

Figure 6. d ln C_f/d(1/T) *vs.* n, the chain length. Observed values (circles) by Champion and North,[3] and theoretical values for various values of E_G (kcal/mol) as indicated, both at 36°.

Attempts to improve the rotational-isomeric-state model of n-alkanes seem fruitless since the discrepancy goes far beyond any uncertainty in the model. The so-called intrachain excluded-volume effect seems negligible for chains as short as $n < 20$, and this is particularly so with our GG′-eliminated chains, as demonstrated by us[8] and by Smith.[21] The hydrodynamic interaction, which arises from a nonuniform segment density, is absent in pure liquids in which every part of liquids is equivalent and uniform at the level of segment sizes.

In the isolated-chain approximation it is implied that all dynamic and thermodynamic interchain interactions can be taken into account through friction constants ζ_i. Friction constants are known to be dependent on chain lengths for very short chains.[15] Even if this is the case, we should find the same $\Delta\Gamma_f$ as above, provided ζ_i varies by a constant factor. In the opposite case where ζ_i depends on i, or the location of a friction along the chain, we can obtain $\Delta\Gamma_f$ which may behave differently. We do not pursue further the effect because any reliable evidence is lacking at present on the location dependence of ζ_i. A separate theoretical examination of the viscosity and birefringence would be useful.

There is a thermodynamic interchain interaction which cannot be properly taken into account by the isolated-chain approximation, *i.e.*, the short-range orientation order among chain segments. n-Alkane chains in which the trans conformation is preferred are geometrically asymmetric when viewed at the level of the size of a methylene. If such chains are put in a condensed phase such as pure liquids, there would result the short-range orientational (parallel) order owing to the interchain excluded-volume effect and space-filling requirement. Both the birefringence and viscosity may be affected by the order, but, probably, the former more sensitively. The increase in chain length of n-alkanes would increase the geometrical asymmetry and the orientational order, the latter in turn increasing $\Delta\Gamma_f$ to more extent than predicted by the isolated-chain treatment, in accordance with the above observations. The rise in temperature brings about, besides the decrease in ζ which has no effect on $\Delta\Gamma_f$, the decrease in the orientational order, through the increasing chain flexibility which diminishes the geometrical asymmetry, and also through the decreasing density which makes less severe the interchain excluded-volume effect and space-filling requirement. As a result, $\Delta\Gamma_f$ decreases more rapidly than predicted by the isolated-chain treatment, again in accordance with the above observations.

We recall that similar effects were found in related properties of n-alkanes and polyethylene. The observed[22] optical anisotropy of n-alkanes as pure liquids, increases more rapidly with increasing chain length than predicted[23] by the isolated-chain treatment. The observed[24] temperature coefficient of the stress-optical coefficient of unswollen polyethylene networks is much larger than predicted.[25] These results, just in line with our observations on flow-birefringence data, were satisfactorily interpreted by the orientational order mentioned above.[23,25] The orientational order is by no means limited to n-alkanes and polyethylene. All chain molecules are necessarily geometrically asymmetric to some extent, when local portions of chains (comprising ten or so skeletal bonds) are regarded as constituent units. Frisman and her coworkers[26,27] found that for a variety of polymers $\Delta\Gamma_f$ obtained through measurements on dilute solutions strongly depends on solvents used. They ascribed these results to the short-range orientational order between solvent molecules and polymer segments, of the same nature as discussed above.[27]

On the basis of the above arguments, the orientational order may be responsible, at least in part, for the discrepancy between theory and experiment. Of course the possibility of other defects in the isolated-chain approximation, *e.g.*, the location dependence of ζ_i as mentioned above and some other mechanisms of unknown origin, cannot be ruled out at present.

(21) R. P. Smith, *J. Chem. Phys.*, **42**, 1162 (1965).

(22) C. Clément and P. Bothorel, *J. Chim. Phys.*, **61**, 878 (1964).

(23) K. Nagai, *J. Chem. Phys.*, **47**, 4690 (1967).

(24) A. N. Gent and V. V. Vickroy, Jr., *J. Polym. Sci., Part A-2*, **5**, 46 (1967).

(25) K. Nagai, *J. Chem. Phys.*, **49**, 4212 (1969).

(26) E. V. Frisman and V. Ya. Andreichenko, *Vysokomol. Soedin.*, **4**, 1559 (1962); E. V. Frisman and Ang Bao Chu, *ibid.*, **4**, 1564 (1962); E. V. Frisman, G. A. Dyuzhev, and A. K. Dadivanyan, *ibid.*, **6**, 341 (1964).

(27) E. V. Frisman, A. K. Dadivanyan, and G. A. Dyuzhev, *Dokl. Akad. Nauk USSR*, **153**, 1062 (1963); E. V. Frisman and A. K. Dadivanyan, *Vysokomol. Soedin.*, **8**, 1359 (1966); *J. Polym. Sci., Part C*, **16**, 1001 (1967).

NOTES

Volume Change during the Solvent Separation of a Tight Ion Pair in a Solvent of Low Dielectric Constant[1]

by W. J. le Noble and A. R. Das

Department of Chemistry, State University of New York at Stony Brook, Stony Brook, New York 11790
(Received April 9, 1970)

It is well known[2] that ionization in solution (unlike homolytic fission) is characterized by a volume decrease ($-\Delta V$). This decrease is largely the result of the polarization and attraction of surrounding solvent molecules by the ions (electrostriction). In ionic equilibria, ΔV can be determined from density measurements extrapolated to infinite dilution if stable solutions of the ions and of the neutral species are available; alternatively, it can be calculated from the effect of pressure on the equilibrium constant *via* the relation $\Delta V = -RT\,\partial \ln K/\partial p$. Both methods have been used for a number of weak acids in water; ΔV is generally found to be -10 to -15 cm^3/mol, which corresponds to an increase in K by roughly 50% for every thousand atmospheres. The dissociation of some ion pairs in water has also been studied at high pressure; the ΔV values for the $MnSO_4$ and $MgSO_4$ pairs are both about -7 cm^3/mol.[3] Similar considerations govern the volume changes that accompany the partial ionization accomplished as the transition state is reached in solvolytic processes; one is then dependent on the effect of pressure on the rate constant and the relation $\Delta V^* = -RT\,\partial \ln k/\partial p$. For SN1 hydrolysis, $-\Delta V^*$ is usually somewhat smaller than the $(-\Delta V)$ values characterizing weak acids since the ionization is incomplete.

The electrostriction phenomenon is described in a first approximation by the Drude–Nernst equation $\Delta V = -(q^2/2rD^2)\partial D/\partial p$. Both the q (charge) and r (radius) dependences of ΔV have been confirmed at least qualitatively; little is known, however, about solvent effects (D is the dielectric constant). Solvolysis reactions generally seem to be accelerated more by pressure if they are carried out in solvents such as alcohol or aqueous acetone than in pure water, but there is no confirmation of the very large pressure effects to be expected for ionization in nonpolar solvents. We report here the effect of pressure on the solvent separation of the tight fluorene–lithium ion pairs in tetrahydrofuran. This process has been found by Hogen-Esch and Smid[4] to be accompanied by characteristic spectral changes. We use the apparatus shown in Figure 1, so designed because of the great sensitivity of these solutions to the atmosphere. Lithium (0.1 g) and mercury (4 g) are introduced into A and fluorene (15 mg) into B; the openings are sealed and the apparatus is evacuated. The mercury is warmed slightly until amalgation occurs. THF (10 ml) is distilled from potassium into B and the solution is allowed to flow into A by tilting; remaining traces of fluorene can be transferred by distilling a little THF back to B. After 24 hr a few drops of the solution in A are allowed to flow into B; this solution is then diluted by distilling all the solvent into B. The pale yellow color indicates whether the concentration is in the proper range. The apparatus is then tilted in the opposite direction to allow the solution to flow into C. Some nitrogen is then admitted to force the solution into the Pyrex cell D (0.5-cm path). The apparatus is then tilted such that the mercury in the cell covers the sealed-in platinum tube (0.5-mm diameter; length is 2 mm inside the cell,

Table I: Effect of Pressure on the Ion Pair Equilibrium of Fluorene–Lithium in THF at 25.0 ± 0.1°

P, bars	OD at 373 nm	OD at 349 nm	K[a]
1	1.07	0.705	2.51
36	1.08	0.703	2.70
70	1.09	0.702	2.92
104	1.10	0.700	3.00
139	1.14	0.700	3.55
277	1.135	0.683	3.90
415	1.185	0.682	5.06
553	1.235	0.683	7.00
691	1.28	0.680	9.41
966	1.39	0.700	>10

[a] Calculated on the basis of ratios of $\epsilon_{373}/\epsilon_{349}$ of 2.05 and 0.178 for the solvent-separated and tight ion pairs, respectively (Figure 5, ref 4); it can readily be shown that the observed ratio is a linear function of the mole fraction of one of the ion pairs if Beer's law is obeyed by both and if both species have the same ϵ at one of the two wavelengths used (note that the OD at 349 nm is constant within 2–3% of all pressures).

(1) Paper XX in the series, "Chemical Reactions Under High Pressure."

(2) W. J. le Noble, *Progr. Phys. Org. Chem.*, **5**, 207 (1967), and reviews quoted there.

(3) F. M. Fisher and D. F. Davis, *J. Phys. Chem.*, **69**, 2595 (1965).

(4) T. E. Hogen-Esch and J. Smid, *J. Amer. Chem. Soc.*, **88**, 307 (1966).

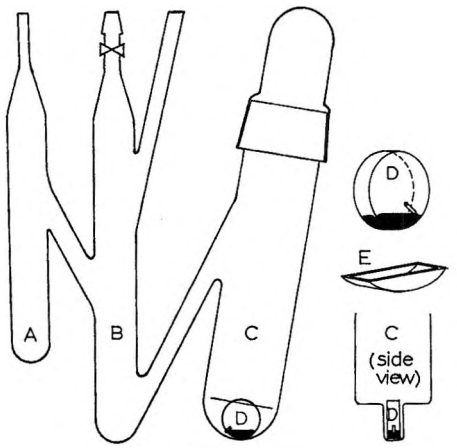

Figure 1. Apparatus for preparing and transferring THF solutions of fluorene-lithium ion pair to the high-pressure absorption cell.

0.5 mm outside); the cell can then be removed and placed in the stainless steel recepticle E, which contains a few drops of mercury and has a small indentation in the bottom to fit the platinum protrusion. The cell is washed with THF, warmed briefly with a hairdryer to expel any trace of gas remaining in the platinum tube, and entered into the cylindrical cavity of the Aminco high-pressure absorption cell. The platinum tube is wetted by the mercury; without it, oxygen apparently diffuses into the cell through the THF film between the Pyrex and the mercury.

We find that even a pressure of 1 kbar reversibly converts virtually the entire solute into solvent-separated ion pairs, and calculate ΔV to be -35 ± 5 cm^3/mol (Table I). This value—for the mere insertion of a solvent molecule—is huge even when compared to the complete ionization of most neutral species in water. If we assume ΔV for the complete dissociation in water of a monovalent ion pair to be about -2 cm^3/mol (one quarter that of the bivalent pairs of $MnSO_4$ and $MgSO_4$), we find that the volume change in THF is about twenty times as large; this difference is undoubtedly due to the greater compressibility and less rapid attenuation of electrostatic forces in low D solvents. Knowledge of these results should enable one to test mechanisms of reactions involving ions postulated for such media.

Acknowledgment. This work was generously supported by the National Science Foundation.